


1-1-2013

The Role Of Tissue Sound Speed As A Surrogate Marker Of Breast Density

Mark Sak
Wayne State University,

Follow this and additional works at: http://digitalcommons.wayne.edu/oa_dissertations

 Part of the [Bioimaging and Biomedical Optics Commons](#), and the [Medicine and Health Sciences Commons](#)

Recommended Citation

Sak, Mark, "The Role Of Tissue Sound Speed As A Surrogate Marker Of Breast Density" (2013). *Wayne State University Dissertations*. Paper 695.

This Open Access Dissertation is brought to you for free and open access by DigitalCommons@WayneState. It has been accepted for inclusion in Wayne State University Dissertations by an authorized administrator of DigitalCommons@WayneState.

**THE ROLE OF TISSUE SOUND SPEED AS A SURROGATE MARKER OF
BREAST DENSITY**

by

MARK A. SAK

DISSERTATION

Submitted to the Graduate School

of Wayne State University,

Detroit, Michigan

in partial fulfillment of the requirements

for the degree of

DOCTOR OF PHILOSOPHY

2013

MAJOR: MEDICAL PHYSICS

Approved by:

Advisor

Date

© COPYRIGHT BY

MARK A. SAK

2013

All Right Reserved

DEDICATION

To Christina, my constant source of inspiration. All our hard work and sacrifice are almost over.

To my parents, without their help and support, I could not be here.

To all the people who have helped me reach this point today.

ACKNOWLEDGEMENTS

I would like to thank my advisor, Dr. Neb Duric, for his guidance, encouragement and support. He has been incredibly important to the completion of this work. I would like to thank the rest of my dissertation committee, Dr. Michael Joiner, Dr. Michael Snyder, Dr. Norman Boyd and Dr. Gretchen Gierach for taking time to make their suggestions and comments about my work. I would also like to thank Dr. Mark Sherman for also offering new ideas and directions to take the research.

I have met many wonderful and interesting people while doing my research as a part of this lab group. I would like to thank Dr. Cuiping Li for always taking an interest in my work. I would like to thank Dr. Steven Schmidt for always being there to help me out with image reconstruction. I would like to thank Mrs. Lisa Bey-Knight and Mrs. Vivian Linke for being so vigilant with patient recruitment and scanning. I would like to thank Dr. Peter Littrup for providing me with a different perspective on life.

I would like to thank all those who helped me with my research as well. I would like to thank Lukasz Myc for helping me become familiar with working with the images. I would like to thank the other students who helped me collect data, Eric West, Muhammed Faiz, Bryan Ranger, Zack Mumm, Sarah Janner and Bryce Henney. Thanks to Yash for reviewing the finished paper as well.

TABLE OF CONTENTS

Dedication	ii
Acknowledgements	iii
List of Tables	ix
List of Figures	xi
Chapter 1 – Introduction	1
1.1 Breast Cancer Risk Models	1
1.1.1 Breast Density and Cancer Risk	2
1.1.2 Factors That Affect Breast Density	5
1.2 Screening Mammography	8
1.2.1 Qualitative Mammographic Breast Density Measurements	9
1.2.2 Quantitative Mammographic Breast Density Measurements	11
1.3 Limitations of Density Measurements Made by Mammography	12
1.4 Volume Estimation Using Mammography	16
1.5 Alternatives to Mammography	18
1.6 Dissertation Outline	28
Chapter 2 – Ultrasound Tomography	30
2.1 Measuring Breast Density Using UST	30
2.2 The UST Prototype	32
2.3 The Ultrasound Sound Speed Tomography Algorithm	34
2.3.1 Forward Modeling	35
2.3.2 The Inverse Problem	37
2.4 UST Image Reconstruction	38

2.4.1 Sound Speed Images	39
2.5 Measuring Average Sound Speed	40
2.6 K-means Clustering	46
2.7 Statistical Analysis.....	46
Chapter 3 – VASS versus MPD Study	51
3.1 Patient Recruitment for VASS versus MPD Study.....	51
3.1.1 Patient Characteristics – Type of Mammogram Received	52
3.1.2 Patient Characteristics – Menopausal Status	53
3.1.3 Patient Characteristics – Race.....	56
3.1.4 Patient Characteristics – Family History of Breast Cancer	56
3.1.5 Patient Characteristics – Parity	60
3.2 Distribution of Density Measurements	60
3.2.1 Distribution of Mammographic Imaging Characteristics	60
3.2.2 Distribution of UST Imaging Characteristics	63
3.3 Correlations of VASS and MPD.....	64
3.3.1 Correlations of VASS and MPD – Type of Mammogram	66
3.3.2 Correlations of VASS and MPD – Menopausal Status	70
3.3.3 Correlations of VASS and MPD – Race.....	73
3.3.4 Correlations of VASS and MPD – Family History of Breast Cancer.....	76
3.3.5 Correlations of VASS and MPD – Parity	76
3.4 UST Measurements Made with Different Ring Transducers	81
3.5 Association of VASS and MPD with USTPD	85
3.6 Subregion Analysis	88

3.6.1 Two-Dimensional Subregion Analysis	88
3.6.2 Three-Dimensional Subregion Analysis	92
3.6.3 Comparison of Two and Three Dimensional Segmentation.....	98
3.7 Distribution of Density within the Breast	100
3.7.1 Sound Speed Distributions across Different Average Densities.....	100
3.7.2 Image ROI Analysis.....	103
3.8 Sound Speed Inter-rater Analysis	104
3.9 Future Studies	106
Chapter 4 – The Ultrasound Study of Tamoxifen.....	107
4.1 Tamoxifen Use in the Prevention of and Treatment of Breast Cancer	107
4.1.1 Biological Effects of Tamoxifen.....	107
4.1.2 Effect of Tamoxifen on Breast Density	108
4.2 The Ultrasound Study of Tamoxifen Protocol.....	110
4.3 Measuring Breast Density.....	112
4.3.1 Measuring the Sound Speed over Time	112
4.3.2 Determining the Common Volume.....	113
4.3.3 Dark Ring Artifacts.....	115
4.4 Preliminary Results.....	119
4.4.1 Patient Characteristics – Status in the Study.....	120
4.4.2 Patient Characteristics – Menopausal Status	121
4.4.3 Patient Characteristics – Race.....	122
4.4.4 Overall Patient Characteristic Trends	123
4.5 Mammographic Measurements.....	125

4.5.1 Mammographic Percent Density and Patient Characteristic Trends	125
4.5.2 Mammographic Imaging Characteristic Trends	127
4.6 Measuring the Effects of Tamoxifen over Time.....	129
4.6.1 Overall Average Response.....	129
4.6.2 Patients Responding to Treatment	133
4.6.3 Changes in Patient Weight.....	137
4.7 Response Grouped by Baseline Sound Speed	138
4.8 Sound Speed Inter Rater Correlations.....	140
4.8.1 Whole Volume Sound Speed Inter Rater Correlation.....	140
4.8.2 Common Volume Inter Rater Correlation	141
4.8.3 Artifact Removed Inter Rater Correlation	142
4.9 Estimating the Uncertainty in the Sound Speed Measurements	143
4.10 Future Studies	145
Chapter 5 – Discussion	146
5.1 Factors that Affect Breast Density	146
5.2 Correlations Involving Breast Density.....	151
5.3 Frequency Distributions.....	163
5.4 The Ultrasound Study of Tamoxifen	164
5.5 Measurement Uncertainty.....	169
5.6 Limitations and Future Direction.....	171
Chapter 6 – Conclusions.....	174
Appendix A – ImageJ Macros Used	177
A.1 Masked Sound Speed Image Creator	177

A.2 Sound Speed Statistics Calculator Macro	180
Bibliography	182
Abstract.....	206
Autobiographical Statement.....	208

LIST OF TABLES

Table 1-1 – Factors Associated with an Increased Risk of Breast Cancer in Women ⁵	3
Table 1-2 – List of Factors that Affect the Breast Density of Women	8
Table 3-1 – Average Patient Characteristics.....	52
Table 3-2 – Patient Characteristics – Type of Mammogram.....	54
Table 3-3 – Patient Characteristics – Menopausal Status.....	55
Table 3-4 – Patient Characteristics – Race	57
Table 3-5 – Patient Characteristics – Family History of Breast Cancer	58
Table 3-6 – Patient Characteristics – Parity.....	59
Table 3-7 – VASS and MPD Correlations for All Patients	65
Table 3-8 – MPD Correlations – Type of Mammogram	67
Table 3-9 – VASS and MPD Correlations – Menopausal Status	71
Table 3-10 – VASS and MPD Correlations – Race.....	74
Table 3-11 – VASS and MPD Correlations – Family History of Breast Cancer	77
Table 3-12 – VASS and MPD Correlations – Parity	79
Table 3-13 – Calculating the Shift for Different Ring Transducers	83
Table 3-14 – Correlations for Raw and Shifted Transducer Rings.....	85
Table 3-15 – VASS and Mammography Correlations.....	88
Table 3-16 – MPD and Mammography Correlations	90
Table 3-17 – VASS and UST Volume Correlations.....	92
Table 3-18 – MPD and UST Volume Correlations	94
Table 3-19 – Area and Volume Correlations.....	100
Table 3-20 – Patients Selected and Their Average Sound Speed.....	101

Table 3-21 – Overall Imaging Characteristics of Images Analyzed.....	104
Table 3-22 – ROI Tissue Analysis.....	104
Table 4-1 – Summary of Patient Scans.....	120
Table 4-2 – Descriptive Statistics for Case and Control Groups	121
Table 4-3 – Descriptive Statistics for Menopausal Status	122
Table 4-4 – Descriptive Statistics for Racial Status.....	123
Table 4-5 – Sound Speed Correlations (n = 52)	124
Table 4-6 – Average MPD by Different Groupings	125
Table 4-7 – MPD and Patient Characteristic Correlations (n = 46).....	126
Table 4-8 – Sound Speed and MPD Correlations with Mammographic Characteristics	129
Table 4-9 – Results for Tamoxifen Cases with Two Scans (n = 20)	130
Table 4-10 – Results for Patients with Three Scans	133
Table 4-11 – Average Sound Speed of Patients Showing A Decrease.....	134
Table 4-12 – Average Changes in Patient Weight between Scans	138
Table 4-13 – Change in Sound Speed Grouped by Baseline Sound Speed.....	140
Table 4-14 – Spearman Correlation Coefficients for Inter-Rater WVSS Measurements	141
Table 4-15 – Correlation Coefficients for Inter-Rater CVSS Measurements.....	142
Table 4-16 – Correlation Coefficients for Inter-Rater DRCVSS Measurements	143
Table 4-17 – Intraclass Correlation Coefficients	143

LIST OF FIGURES

Figure 1-1 - An example of a screening mammogram. Dense breast anatomy appears as regions of white on the mammogram, while fatty tissue appears as darker regions.....	9
Figure 1-2 - Examples of the BI-RADS categories for density measurements made on mammography.	10
Figure 1-3 - X-ray characteristic curves showing differences in x-ray response of film and digital detectors ⁷⁷ . Film detectors have a sigmoidal response, while digital detectors show a linear response over many orders of magnitude. ...	14
Figure 1-4 - Coronal (Top) and transverse (Bottom) breast MRI images.	20
Figure 1-5 - (Top) Transverse, (Middle) coronal and (Bottom) sagittal breast CT scans of a breast that show a speculated mass ¹⁰⁶	22
Figure 1-6 - Breast images by DXA (left) and conventional mammography (right) ⁸⁸	24
Figure 1-7 - (a) Transverse FDG PEM image demonstrating two abnormalities. Lesion 1 represents invasive carcinoma that was depicted at conventional mammography while lesion 2 represents a noninvasive papillary carcinoma, which was not visible at conventional mammography. (b) Transverse PEM image of the left breast depicts a single focus of increased FDG activity (arrows) at the site of the mass ¹¹⁰ ...	26
Figure 2-1 - UST sound speed images showing rough estimates of the BI-RADS density categories. Top Left – Category 1; Top Right – Category 2; Bottom Left – Category 3; Bottom Right – Category 4.....	31
Figure 2-2 - (Top) Schematic diagram of the UST prototype showing patient positioning (Bottom) Actual UST prototype at the Karmanos Cancer Institute in Detroit, MI.	33
Figure 2-3 - Schematic showing the translation of the rind transducer to create UST image slices.....	34
Figure 2-4 – An example of the grid model used for the forward modeling. Rays are traced from the receiver to the transmitter ¹²¹	36
Figure 2-5 - The difference in how reflection (Rx) and transmission (Tx) ultrasound signals are collected between UST (left) and conventional ultrasound (right).	38

Figure 2-6 - An example of choosing the first slice that contains the nipple. Slice C was chosen to be the first slice with the nipple present. Slices A, B and C were therefore included in the final image stack.....41

Figure 2-7 - An example of choosing the slice to remove the chest wall from the final sound speed image. Slice C was chosen to be the first slice without any chest wall present. Slices C and D will be included in the final sound speed image stack.42

Figure 2-8 - The breast segmentation algorithm working on a sound speed image. Left: The breast/water bath interface is manually selected using 10 points Right: An ellipse is fit to the chosen points to approximate the shape of the breast in the current slice.43

Figure 2-9 - Left: The original sound speed image before the masking algorithm was applied. Right: the masked sound speed image. Bottom: The histogram obtained from the masked images showing the distribution of sound speed within the entire image stack.44

Figure 2-10 - Two examples using hypothetical data to highlight the difference between Spearman and Pearson coefficients¹⁴⁹. Left: The Spearman coefficient is less sensitive to outliers in the data. Right: Spearman coefficients are even useful on data that follows a non-linear but predictable pattern.....47

Figure 2-11 – Examples showing negatively skewed (Left) and positively skewed (Right) data using hypothetical data¹⁵¹.49

Figure 3-1 - Frequency distributions for the sound speed (VASS) and MPD measurements grouped by mammography type (bars). A normal distribution using the measured mean and standard deviation is overlaid on top of the data. For film distributions (Left), n = 166; for digital distributions (Right), n = 85.61

Figure 3-2 - Frequency distributions showing mammographic area measurements separated by mammogram type. A normal distribution is overlaid on each plot that was created by using the calculated mean and standard deviation. For film distributions (Left), n = 166; for digital distributions (Right), n = 85.....62

Figure 3-3 - Frequency distributions for the UST imaging characteristics for all patients with a normal distribution created by using the calculated mean and standard deviation. For all distributions, n = 247.....63

Figure 3-4 - Plot of volume averaged sound speed (VASS) as measured by UST compared to the mammographic percent density (MPD) as measured by mammography for all patients, n = 251.....	66
Figure 3-5 - Plots of the UST measured sound speed versus the mammographic percent density grouped according to the type of mammogram received. Top: Film, n = 166; Bottom: Digital, n = 85.....	69
Figure 3-6 - Plot of sound speed versus mammographic density grouped by menopause status. Top: Post-menopausal women, n = 86; Bottom: Pre-menopausal women, n = 154.	72
Figure 3-7 - Sound speed versus mammographic density as grouped by race. Top: African-American, n = 161; Bottom: White, n = 47.....	75
Figure 3-8 - Sound speed versus mammographic percent density for women grouped by family history of breast cancer. Top: Women with a family history of the disease, n = 52; Bottom: Women with no family history of the disease, n = 169.....	78
Figure 3-9 - Sound speed versus mammographic density comparisons grouped by parity. Top: Parous women (have given birth at least once), n = 172; Bottom: Nulliparous women (never given birth), n = 45.....	80
Figure 3-10 - The plot of sound speed versus mammographic percent density for patients that received a film mammogram separated by the ring transducer hardware that was used to create the UST image.....	82
Figure 3-11 - The VASS versus mammographic percent density for the film patients after the corrections were applied to the data from the different ring transducers.	84
Figure 3-12 - Plot of average sound speed versus ultrasound percent density for the entire population of patients, n = 247.	86
Figure 3-13 - Plots of the mammographic percent density versus the ultrasound percent density, grouped by patients receiving a film mammogram (Top, n = 163) and a digital mammogram (Bottom, n = 84).....	87
Figure 3-14 - Plots of the sound speed associated with several different mammographic characteristics grouped by mammogram type. Left: Film, n = 165; Right: Digital, n = 84.	89
Figure 3-15 - Plots of the mammographic percent density associated with several different mammographic characteristics grouped by mammogram type. Left: Film, n = 165; Right: Digital, n = 84.	91

Figure 3-16 - Plots of sound speed versus UST imaging characteristics for all patients, n = 247.	93
Figure 3-17 - Plots of mammographic percent density associated with UST imaging characteristics separated by mammogram type. Left: Film, n = 163; Right: Digital, n = 84.	95
Figure 3-18 - Plot of the average sound speed for the dense and non-dense sub-regions of the breast measured using UST, n = 247.	96
Figure 3-19 - Plot of the overall average sound speed associated with the average sound speed of the dense sub-region (Top) and the non-dense sub-region (Bottom) as measured by UST, n = 247.	97
Figure 3-20 - Correlations involving the measured sub-region volumes and areas separated by mammography type. Left: Film, n = 163; Right: Digital, n = 84.	99
Figure 3-21 – The histogram of the distribution of the sound speed voxels for the low average sound speed group. The histograms are each normalized relative to the total volume in each scan.	101
Figure 3-22 – The histogram of the distribution of the sound speed voxels for the moderate average sound speed group. The histograms are each normalized relative to the total volume in each scan.	102
Figure 3-23 – The histogram of the distribution of the sound speed voxels for the moderate average sound speed group. The histograms are each normalized relative to the total volume in each scan.	102
Figure 3-24 – The average distribution of sound speed for each group.	103
Figure 3-25 - Sound speed measurements of the same data as measured by two separate readers showing a strong intra-rater correlation ¹⁵³	105
Figure 4-1 - Observing similar landmarks in the same patient scanned at two different times. In both images, the same parenchymal patterns are apparent, indicating the slices represent the same volume is being imaged.	114
Figure 4-2 - An exaggerated example of a patient receiving three separate scans and the differences in calculating the whole volume (WV) and common volume (CV) between them.	115
Figure 4-3 - Left: Sound speed image showing the presence of the dark ring artifact near the surface of the breast. Right: Sound speed image without dark ring artifact.	116

- Figure 4-4 - The steps involved in removing the dark ring artifact from a single slice. A The original image with artifact. B An ellipse is fit tangent to part of the artifact. C The pixels outside the ellipse are cleared, removing a portion of the artifact, but leaving the remaining breast volume. D The ellipse is fit tangent to another part of the artifact where step C is repeated. E The final image with the artifact completely removed.118
- Figure 4-5 - Correlations between volume averaged sound speed and age, weight, height and BMI for all patients with a baseline scan (n = 52).124
- Figure 4-6 - Correlations between mammographic percent density and age, weight, height and BMI for all patients with a baseline scan (n = 46).126
- Figure 4-7 - Plot of volume averaged sound speed versus mammographic percent density for the patients in the UST study, n = 46.127
- Figure 4-8 - Correlations involving the mammographic imaging characteristics and the mammographic percent density (Left) and the volume averaged sound speed (Right), n = 46.128
- Figure 4-9 - The average sound speed (Top) and the average change in sound speed from baseline (Bottom) for patients with 2 scans (n = 20) using the different methods of measuring sound speed.....131
- Figure 4-10 - The average sound speed (Top) and the average change in sound speed from baseline (Bottom) for patients with 3 scans (n = 15) using the different methods of measuring sound speed.....132
- Figure 4-11 - Plots of the average change in sound speed measured using all separate measures of sound speed for patients that showed a decrease for patients with two scans (Top) and patients with three scans (Bottom).135
- Figure 4-12 - The average change in sound speed grouped by response type for patients that received two scans (Top) and three scans (Bottom).....136
- Figure 4-13 - The average sound speed (Top) and average change in sound speed (Bottom) grouped by baseline sound speed for patients that received two scans (Left) and three scans (Right).....139

CHAPTER 1

INTRODUCTION

Breast cancer is the most common type of cancer among women in North America, accounting for approximately 1 in 3 cancers diagnosed in US women. In 2013, it is estimated that approximately 230,000 women will be diagnosed with invasive breast cancer in the US and that 39,500 women will die from breast cancer¹. Currently, a woman living in the US has a 12.15%, or about 1 in 8 chance of being diagnosed with breast cancer in their lifetime. Fortunately, breast cancer death rates have decreased 2.2% per year between from 1999 to 2007 due to a combination of improvements in breast cancer treatment and early detection. Early detection is accomplished through the use of breast cancer risk models and screening mammography.

1.1 Breast Cancer Risk Models

Breast cancer typically produces no symptoms when the tumor is small and most treatable, so early detection of the disease is critical. Gail et. al² developed a model for estimating the risk of developing breast cancer in women who had no evidence of cancer at the time of their initial screening mammogram. The model was developed from case-control data from the Breast Cancer Detection Demonstration Project (BCDDP) in which more than 280,000 women volunteered to have their annual breast cancer screenings monitored for 5 years³. The Gail model used risk factors known at the time to predict the relative risk. These factors included current age, age at menarche, age at birth of first child, number of first-degree relatives with a family history of breast cancer and number of previous breast biopsy examinations. The model was modified to use during recruitment for the Breast Cancer Prevention Trial using Surveillance Epidemiology End

Results (SEER) data to update the underlying incidence rates⁴. The Gail model is useful to describe breast cancer risk in large populations, but it does not discriminate very well between individual women who will and will not develop cancer. As such, the primary use of these models is to develop power calculations for prevention trials.

However, asymptomatic women who are aware of any elevated risk factors they may possess may be more inclined to seek breast cancer screening. Screening takes on different forms for women depending on their age. For women aged 20-39, the American Cancer Society suggests a clinical breast examination every 3 years and optional breast self-examinations as a guideline for early detection of breast cancer. For women aged 40 and over, in addition to optional breast self-examinations and annual clinical breast examinations, the ACS also suggests annual screening mammograms⁵. For women with the highest lifetime risk of cancer (~20% - 25% or greater), an annual screening MRI is also suggested⁵. Yet, despite their actual level of risk, women tend to overestimate their risk of developing and dying of breast cancer^{6, 7}. It is therefore important to not only create strong predictive models of breast cancer risk, but to also inform women of the true nature of their risk to assuage their fears.

1.1.1 Breast Density and Cancer Risk

The ability to predict future occurrences of disease in individuals allows for improvements in the development of preventative strategies as well as improved clinical decision making. Yet, predictions of breast cancer risk are less well developed than risk predictions for many other diseases. The Gail model was an initial attempt to quantify a woman's risk of developing breast cancer, but it was limited by the choice of risk factors. Since the release of the Gail model, studies have shown there are other factors associated

with breast cancer risk. These include the use of hormone therapy, high body mass index (BMI), the result of previous mammographic examinations and mammographic breast density, among many other factors listed by the ACS (Table 1-1⁵). In fact, mammographic breast density is one of the strongest predictors of breast cancer risk. Women with the densest breasts are at a four- to six-fold greater risk of breast cancer when compared to women with less dense breasts. Attempts to incorporate breast density into these predictive models have shown modest improvements in risk prediction estimates⁸⁻¹⁰. However, these studies excluded young women that would benefit most from predictive models, used incomplete covariate information and qualitative measures of breast density¹¹. Despite these limitations, the studies indicate that the inclusion of breast density is an important risk factor to consider when designing a predictive model.

Table 1-1 – Factors Associated with an Increased Risk of Breast Cancer in Women⁵

Relative Risk	Factor	Relative Risk	Factor
>4.0	Age	1.1-2.0	Height (Tall)
	Biopsy-confirmed atypical hyperplasia		High socioeconomic status
	Certain inherited genetic mutations (<i>BRCA1</i> and/or <i>BRCA2</i>)		Late age at first full-term pregnancy (>30 years)
	Mammographically dense breasts		Late menopause (>55 years)
	Personal history of breast cancer		Never breastfed a child
2.1-4.0	High estrogen or testosterone levels		No full-term pregnancies
	High bone density (postmenopausal)		Obesity (postmenopausal)/adult weight gain
	High-dose radiation to the chest		One first-degree relative with breast cancer
	Two first-degree relatives with breast cancer		Personal history of endometrium, ovary or colon cancer
1.1-2.0	Alcohol consumption		Recent and long-term use of menopausal hormone therapy
	Early menarche (<12 years)		Recent oral contraceptive use

The effect breast density has, not just on predictive models, but on the actual breast cancer risk has been studied extensively and is quite strong. McCormack and dos Santos Silva¹² conducted a systematic analysis of the association between percent mammographic density and risk of breast cancer. Their data included more than 14,000 women with cancer and 226,000 women without cancer from 42 studies. They found that extensive percent mammographic density was consistently associated with an increased risk of breast cancer. Associations were stronger in studies that were conducted in general populations rather than for symptomatic women. Associations were also apparent when using both qualitative methods, such as Wolfe's parenchymal patterns or the Breast Imaging Reporting and Data System (BI-RADS) categories, and for quantitative methods, such as computer-assisted methods like Cumulus¹³. However, the associations were stronger for the quantitative measurements as opposed to the qualitative ones. The risk associated with mammographic density did not differ by age, menopausal status or ethnicity.

Many other studies have also shown that breast density is consistently associated with breast cancer risk. Boyd *et al* has investigated this relationship thoroughly over many years¹⁴⁻¹⁹. Density was primarily assessed as a percent density on mammograms through the use of a computer-assisted method. It was determined that, when compared to women with lower densities, women with the highest densities showed an increased risk of breast cancer of 4 to 6-fold. This elevated risk also persisted for at least 8 years after entry into the study and the risk due to density was greater in younger women compared to older women. In fact, for young women with more than 50% dense tissue on their mammograms, 26% of all breast cancers and 50% of cancers detected less than

12 months after a negative screening exam were attributable to their mammographic density¹⁶. Other studies done by Byrne *et al*²⁰, Byng *et al*^{21, 22}, Wolfe *et al*²³, Saftlas *et al*²⁴, Sala *et al*²⁵, Harvey *et al*²⁶ and Vachon *et al*²⁷ further highlight that no matter how mammographic breast density is measured, its presence is a strong indicator of breast cancer risk. Breast density is a risk factor that strongly correlates to breast cancer risk and may in fact account for a substantial number of breast cancers. However, of the breast cancer factors that present the greatest risk (Table 1-1), breast density is of special importance. It is a factor that can be easily influenced and altered through intervention. Breast density is therefore a key factor that can easily be monitored and modified to aid in the fight against cancer.

1.1.2 Factors That Affect Breast Density

Since breast density is a strong predictor of breast cancer risk, it is no surprise that many of the factors that affect breast cancer risk also have an effect on breast density. The average mammographic percent density (MPD) in the population decreases with increasing age^{18, 20, 24, 26, 28-32}. This should lower the risk of developing breast cancer. Yet breast cancer incidence increases with age. This apparent paradox can be explained by a model of cancer incidence proposed by Pike *et al*³³. The Pike model introduces the concept of “breast tissue aging” which is the exposure of breast tissue to hormones and growth factors. It also includes the effects that menarche, pregnancy and menopause have on these factors. Exposure is highest at the time of menarche and decreases at the time of pregnancy. It is further reduced during the perimenopausal period and is lowest after menopause. It is the cumulative effect of this aging which describes the age-

incidence for breast cancer. Women with higher exposure levels are more likely to develop breast cancer.

In a model developed by Boyd *et al*¹⁸, the average exposure to mammographically dense tissue resembles Pike's concept of breast tissue aging. We therefore expect that any factor that increases or decreases cumulative exposure to breast cancer risk will have a similar effect on breast density. Early menarche, late age at first pregnancy, nulliparity and late menopause are factors that should increase exposure to dense tissue. Late menarche, early age at first pregnancy, multiple pregnancies and early menopause are factors that should decrease cumulative exposure to mammographic density. Studies have shown that women who have given birth and women with a large number of live births show decreased density while women whose age at the birth of their first child was older have shown increased density^{26, 28, 29, 32}. As women pass through menopause, density has been shown to decline³⁴⁻³⁶.

There are many other factors that affect breast density that are not related to the concept of exposure. Higher densities have been associated with women who have a family history of breast cancer³⁷. Breast density has intrauterine roots, as reflected by increasing adult breast density with increasing birth weight and head circumference³⁸. Density has shown an inverse association with body weight and body mass index (BMI)^{26, 31, 34, 39-41} despite obesity being a known risk factor for breast cancer. Therefore, obese women with dense breasts may be at higher risk. Diet, a modifiable risk factor, has shown some correlations with breast density²⁶. In particular, a low-fat, high-carbohydrate diet has shown to decrease percent density and dense area in the breast^{34, 42}. Vitamin D intake was inversely associated with breast density^{43, 44} while intakes of protein and

animal protein were associated with higher breast densities^{44, 45}. High alcohol intake is positively correlated with breast density⁴⁶. Women with benign breast disease show higher density as well⁴⁷. The associations between race and ethnicity with breast density are conflicting and limited when comparing between African-American (AA) and white women. Some studies⁴⁸ showed that AA women have higher mammographic densities, while others^{49, 50} have shown lower densities for the AA group.

Hormonal factors can also affect breast density and breast cancer risk. Menopausal hormone therapy (MHT) slows normal breast involution⁵¹⁻⁵³ and causes an increase in MPD in 17%-73% of women⁵³⁻⁵⁸. The increase is most commonly diffuse, but breast density does appear to be very responsive to MHT. The breast responds rapidly to the treatment and the greatest change in density occurs during the 1st year of use⁵⁹. Upon the stopping of treatment, density reverts to baseline levels in as quickly as 2 to 3 weeks^{60, 61}. Examples of MHT include the use of estrogen, progesterone and progestin. Selective estrogen receptor modulators (SERM) decrease MPD presumably due to their antiestrogen effect on the breast. They are also associated with decreased breast cancer risk²⁶. Examples of SERM drugs include tamoxifen and raloxifene. Tamoxifen has been shown to reduce breast density in 44% of women and reduce breast cancer risk by half in high-risk women⁶². Since women with higher breast densities have an increased risk of breast cancer, women who experience a change in their density from either MHT or SERMs may in fact be respectively increasing or reducing their risk. It is unknown whether these risk factors that affect breast density and breast cancer risk act independent of each other or with similar mechanisms. Table 1-2 summarizes each factor described here with its effect on breast density.

1.2 Screening Mammography

Mammography is a low-dose x-ray procedure that allows visualization of the internal anatomy of the breast. Dedicated mammography devices are capable of producing high quality images with low x-ray doses. Digital systems appear to be more accurate for women under 50 with dense breasts^{63, 64}. The ACS suggests that women receive regular and annual screening mammograms beginning at age 40¹. Screening has been shown to reduce breast cancer mortality⁶⁵ in randomized trials and population-based screening evaluations. It also leads to a greater range of treatment options that include less-aggressive surgeries and therapies. A typical mammogram is shown below in Figure 1-1.

Table 1-2 – List of Factors that Affect the Breast Density of Women

Factor	Effect on Breast Density
Age	Increased age correlates to decreased density
Age at Menarche	Late age at menarche is associated with increased density
Parity	Nulliparity increases density; Multiparity decreases density
Age at First Birth	Increased age at first birth correlates to increased density
Menopause	Menopause correlates to a decrease in density
Family History	Family history of breast cancer correlates to increased density
Birth Weight	Increasing birth weight correlates to increased density
Head Size	Increasing head circumference at birth correlates to increased density
Weight	Increasing weight and BMI correlate to decreased density
Alcohol	High alcohol intake correlates to increased density
Diet	Vitamin D intake associated with decreased density; Protein correlates with increased density
Benign Disease	Benign breast diseases correlates with increased density
MHT	Menopausal hormone therapy correlates with increased density
SERM	The selective estrogen receptor modulator tamoxifen correlates with decreased density

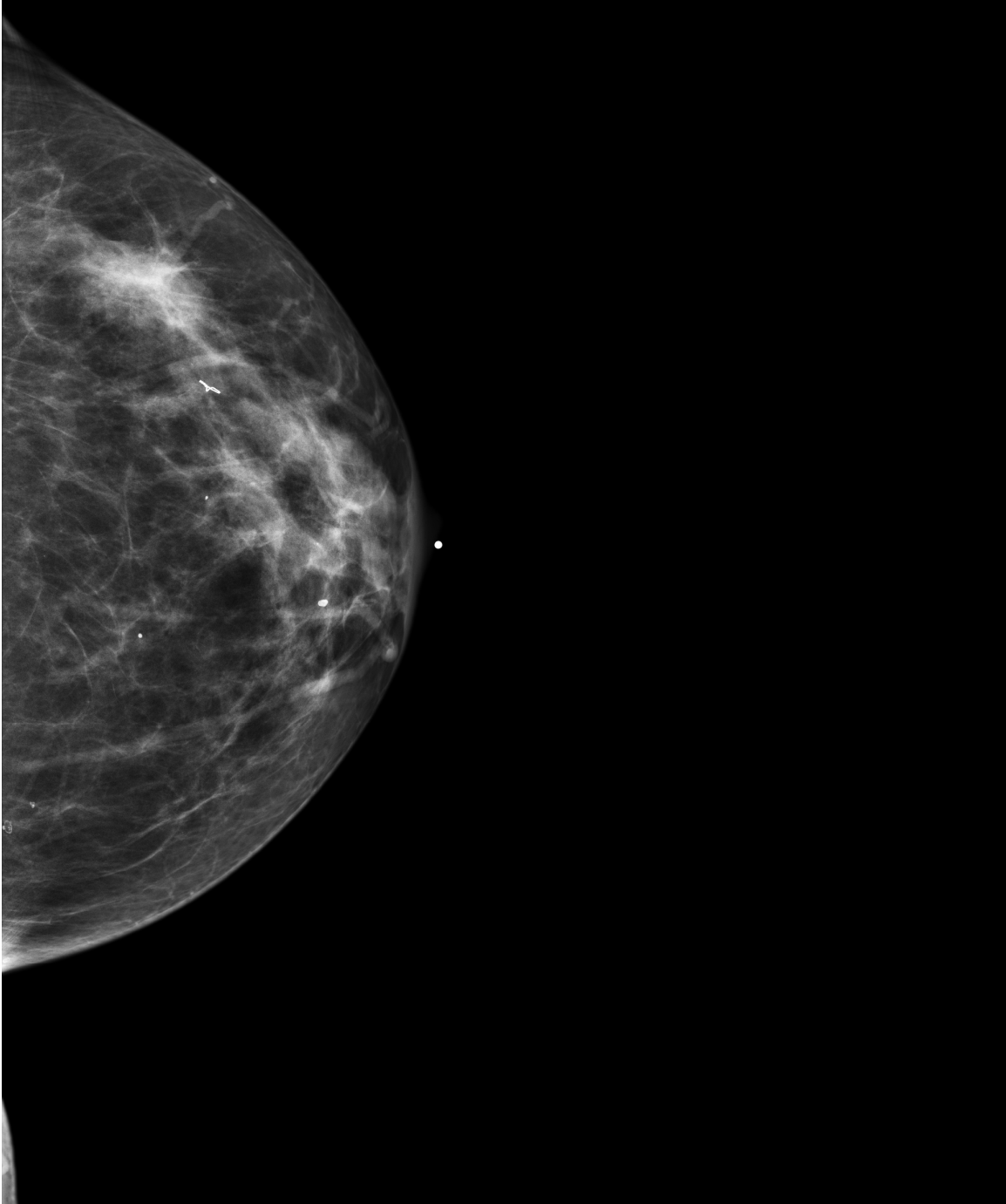
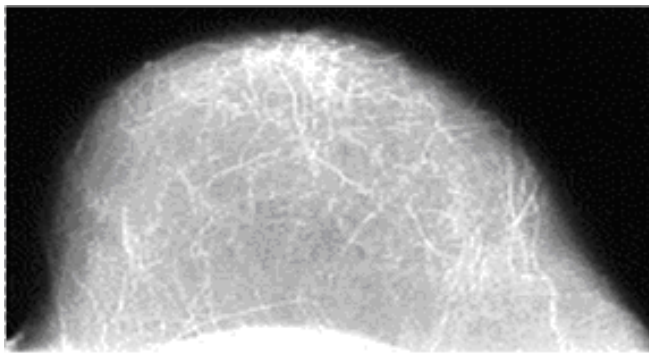


Figure 1-1 - An example of a screening mammogram. Dense breast anatomy appears as regions of white on the mammogram, while fatty tissue appears as darker regions.

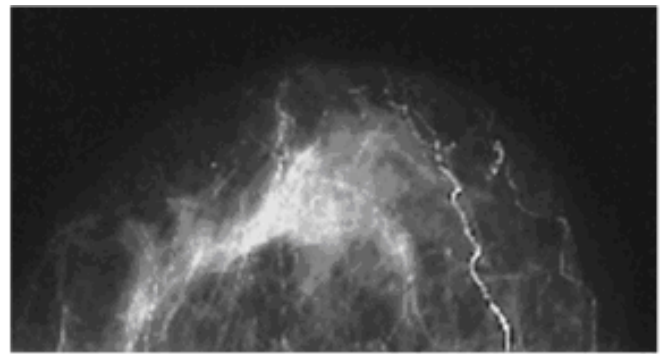
1.2.1 Qualitative Mammographic Breast Density Measurements

The radiographic appearance of the breast on mammography varies among women and reflects variations in breast tissue composition and the different x-ray

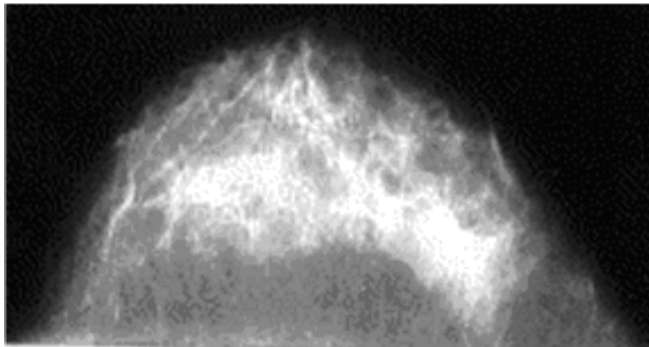
attenuation characteristics of these tissues. Fibroglandular tissue in the breast attenuates more x-rays than fat and therefore appears bright on a mammogram. Breast density is therefore a measure of these mammographic parenchymal patterns. John Wolfe was the first to propose a relationship between these patterns and breast cancer risk²³. Four classifications were used to separate women into groups according to their relative risk of developing breast cancer. Since the release of this work, many other studies have assessed the risk of breast cancer according to Wolfe's classifications⁶⁶.



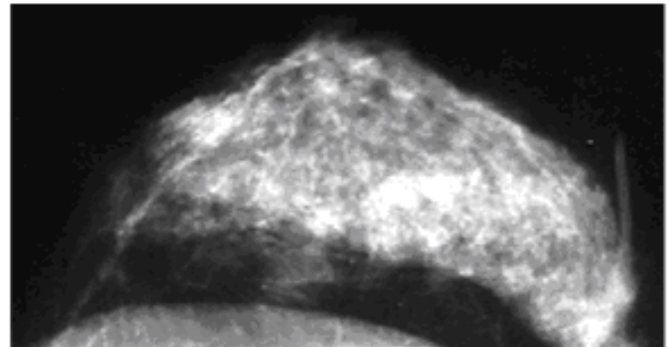
Category 1 - Fatty



Category 2 - Scattered Densities



Category 3 - Heterogeneously Dense



Category 4 - Extremely Dense

Figure 1-2 - Examples of the BI-RADS categories for density measurements made on mammography.

Currently, the Wolfe classifications have been replaced in the literature by the American College of Radiology Breast Imaging Reporting and Data System (BI-RADS) density score⁶⁷. BI-RADS is a density estimation technique that typically involves a radiologist's visual assessment of the mammogram. It is routinely included for a large

proportion of mammograms in the United States and also uses four classifications: 1 (predominately fat), 2 (scattered densities), 3 (heterogeneously dense) and 4 (extremely dense) (Figure 1-2). However, due to the subjective nature of these classifications, considerable inter- and intra- rater variability exists^{68,69}. Federal regulations⁷⁰ dictate that a report of the results of any mammography exam must be prepared by the facility where the mammogram occurred and must be sent to the patient's physician. Also, a lay summary of the results is required to be sent to the patient as well. The reporting of breast density in these reports is not yet mandated. However, several states have recently passed legislation and a bill calling for federal law has been introduced that requires the reporting of breast density in these reports⁷¹. The American College of Radiology⁷² supports the practice of patient education but warns of the possible harms this additional information can cause, including confusion, a false sense of security, undue anxiety or a loss of faith in mammography.

1.2.2 Quantitative Mammographic Breast Density Measurements

A quantitative method to measure breast density involves the use of computer-assisted programs that are based on interactive thresholding and segmentation. An example of such a program is Cumulus¹³. An observer places thresholds at the edge of the breast and at the edge of the density and the subsequent areas defined on the mammogram are recorded by the computer. Mammographic percent density can then be easily calculated by finding the ratio of fibroglandular to total breast areas. It can then be treated as either a continuous or categorical variable in subsequent analysis. Density measured in this way requires the use of trained observers and digitized film images, but

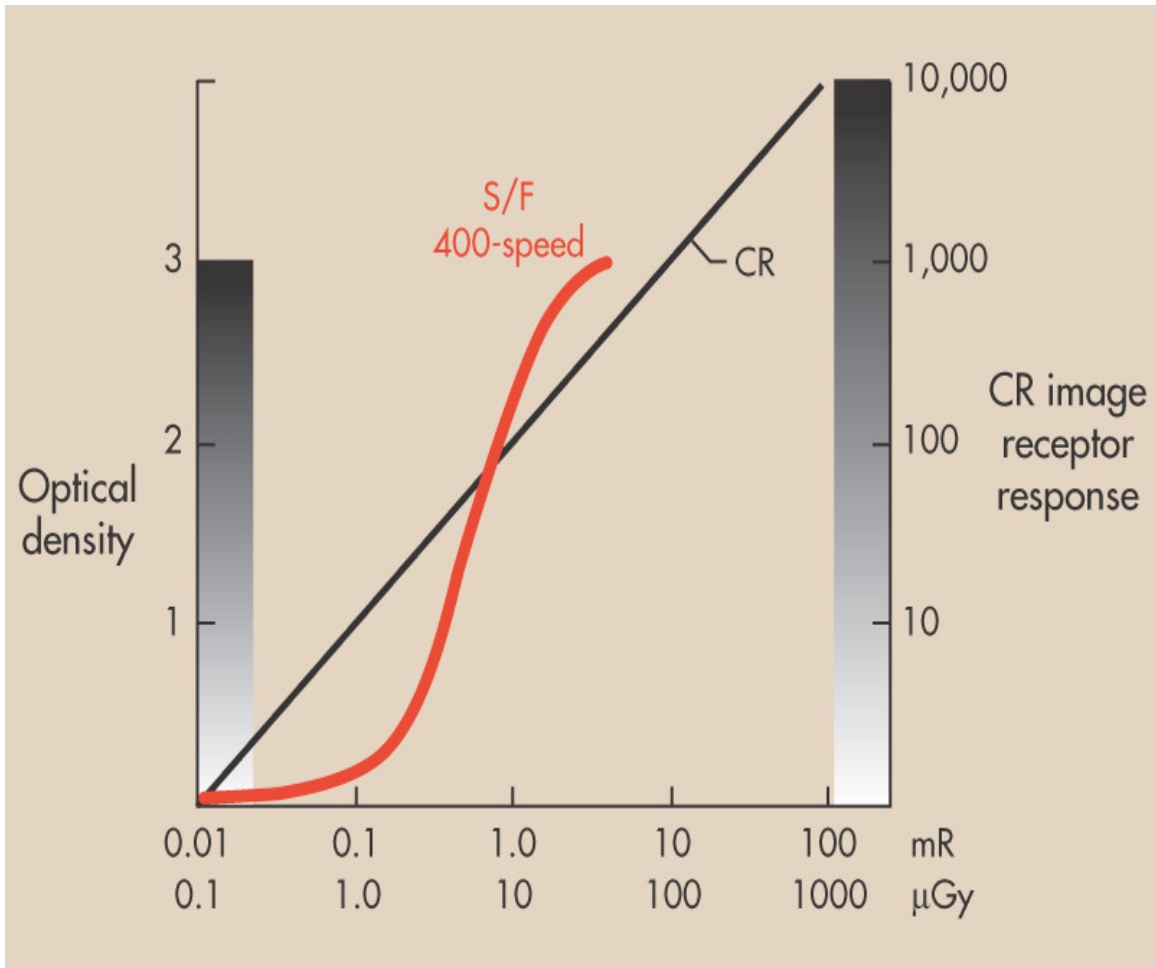
reliability between readers has been shown to be high. Observers using Cumulus have achieved an ICC of 0.9 or greater^{16, 73}.

1.3 Limitations of Density Measurements Made by Mammography

Mammography screening has been shown to reduce the mortality rate in multiple screening trials⁶⁵. However, despite being the current gold standard for breast imaging, mammography does pose some shortcomings for both cancer detection and breast density measurement. Mammographic percent density is related more towards the attenuation and absorption characteristics of the breast tissues rather than the direct density of the breast. Because of a masking bias⁷⁴, it is also the least effective for women with the densest breasts and therefore the highest risk of developing breast cancer. It uses ionizing radiation which limits its screening capabilities and can in fact lead to an increased risk of developing breast cancer⁷⁵. Diagnostic mammography also generates many abnormal findings not related to cancer which leads to costly and unnecessary procedures and biopsies⁷⁶. A mammographic image is also a two-dimensional (2D) projection of three-dimensional (3D) volume. This does not provide an accurate volumetric analysis of the density due to the variable breast thickness.

Breast density calculated by the use of mammography is dependent on the variations in breast tissue composition along with the x-ray attenuation properties of those tissues and the methods used to generate the images. Film and digital mammography interact differently with x-rays. Film has a sigmoidal response to x-rays and regions of the breast where little radiation passes through tend to be uniformly white because they fall in the flat portion of the characteristic curve. Digital mammography has a linear x-ray response and a wider dynamic range (Figure 1-3)⁷⁷, so these regions are

viewed with more shades of grey. Therefore, when using Cumulus, regions that would have appeared white on film and therefore considered dense tissue, may actually lie below the cutoff and not be counted as “density” on digital mammograms. The image processing that is applied to digital images to maximize contrast may also accentuate this effect. While this helps in detecting relevant signs of cancers, it can distort the calculation of density. Digital image processing algorithms ultimately function to spread the image more uniformly among all the possible grey levels, while film mammography tends to render most of the image towards the black or white levels with few pixels occupying the intermediate grey levels. The use of higher energy x-rays in mammography tends to flatten the grey scale and produce less contrast in the finished images. The differences between manufacturers in the production of the processed mammographic images means that image quality may vary from institution to institution. Also, the focus for mammography is on advancing the technology to better improve cancer detection, and not necessarily to improve density measurements. This means that density measurements made on mammographic equipment will be a dynamic and constantly changing endeavor.



Elsevier items and derived items © 2009 by Mosby, Inc., an affiliate of Elsevier Inc.

Figure 1-3 - X-ray characteristic curves showing differences in x-ray response of film and digital detectors⁷⁷. Film detectors have a sigmoidal response, while digital detectors show a linear response over many orders of magnitude.

Despite breast density being a known risk factor for developing breast cancer, women with high breast densities may not benefit as much from mammography due to a masking bias. As Egan and Mosteller hypothesized⁷⁴, a masking phenomenon exists that underestimates the number of cancers in dense breasts compared to fatty breasts. Because of this masking, tumors may in fact be present in a mammogram, but are obscured by the dense tissue in the breast. They will then manifest themselves as cancer in later years and lead to an increase in breast cancer incidence. Since early detection of breast cancer is key to successfully treating the disease, this masking of potential tumors

can have potentially harmful effects on the treatment. This masking bias of mammography was shown to exist in individual trials^{66, 78}, and in general population trials¹². The masking bias only affects the identification of tumors, not the underlying breast cancer risk. The relationship between breast density and breast cancer risk is calculated after correcting for the masking bias.

In addition to this masking bias, mammography may not be the ideal imaging modality to screen women with high densities due to the carcinogenic effects of the radiation used. Since asymptomatic women with an elevated cancer risk due to increased density may wish to be monitored more frequently, the increased radiation dose from the additional examination may in fact further harm these women. It is estimated that for every million screening mammograms performed, up to 8 women may develop cancer from the radiation⁷⁵. Although radiation dose is kept as low as reasonably achievable in mammography, its mere presence is a limiting factor in how frequently screening can occur for those most at risk.

Also, not all breast cancers can be detected by the use of mammography and some cancers that are detected still may have poor prognosis. Observations made in mammography can lead to follow up examinations, including biopsies, which are determined not to be cancer. This is referred to as a false-positive test result and can cause unnecessary pain, anxiety and inconveniences to the patient. It is estimated that after 10 years of annual mammographic screening, approximately 50% of women will receive at least one false-positive recall⁷⁶. Biennial screening reduces this probability to approximately 1 out of 3⁷⁹. Mammograms are based on the projected area of the breast tissue and not the volume, as thickness is not considered. No allowance for the technique

of the mammogram is made nor is any variation in film development of breast compression accounted for. Mammograms are performed by a trained observer and therefore have a degree of subjectivity. However, despite these limitations, mammography is the single most effective method of early detection in clinical practice since it can identify cancer several years before physical symptoms develop.

1.4 Volume Estimation Using Mammography

Breast density measurements using mammography are typically based on the 2-dimensional projected area of the breast instead of examining the entire 3-dimensional volume. For mammographic density measurements, each pixel is simply assumed to represent either completely dense or completely fatty tissue. In reality, each pixel represents the x-ray absorption and attenuation characteristics of both fibroglandular and fatty tissues combined. It is therefore possible that two women may show similar projected areas of dense tissue yet may have different volumes of dense tissue⁸⁰. Efforts have been made to estimate the volume of dense tissue based on these mammographic measurements. These efforts generally involve the use of algorithms or physics models that use the imaging acquisition parameters (tube voltage, film exposure time, anode-filter combination, breast thickness) to convert the mammographic pixel values into estimates of the thickness of the fibroglandular tissue^{81, 82}.

Highnam *et al*^{83, 84} have developed a fully automated physics model for screen-film mammography known as the standard mammographic form (SMF) to extract the thickness of fibroglandular tissue. This method can not only be applied prospectively, but also retrospectively to mammograms taken in the past. Van Engeland *et al*⁸⁵ described a simple physical model to calculate the volumetric density for full field digital

mammography (FFDM). Shepherd *et al*^{86, 87} and Maskarinec *et al*⁸⁸ have defined fibroglandular volume using similar fully automated technique called single x-ray absorptiometry (SXA) and dual energy x-ray absorptiometry (DXA) respectively. Pawluczyk *et al*⁸⁹ and Kaufhold *et al*⁹⁰ have developed methods relating the transmitted signal measured to breast equivalent calibration objects with known thicknesses and have applied this relationship to estimate the volume.

For any method that attempts to quantify the mammographic density from projection images, it is first necessary to test the accuracy of the method. All the methods described above produced volumetric measurements that correlated well with the standard area mammographic measurements. Of all the different volumetric measurements of density, volumetric percent density measurements showed the weakest, yet still relatively strong correlations with traditional mammographic area percent density measurements. These correlations ranged from $r^2 = 0.59$ for the SXA measurements⁸⁶, a Pearson coefficient of $r_p = 0.76$ for the FFDM measurement⁹¹ and Spearman coefficients of $r_s = 0.68$ for the SMF method⁹² and $r_s = 0.76$ for the DXA method⁸⁸. Correlations relating volume of dense tissue and area of dense tissue on the mammogram tended to be much stronger for all methods, with correlations greater than 0.9.

Despite these correlations to mammography, the attempts to measure the volumetric density in mammography have not improved risk prediction compared to the measurement of the projected area⁹¹⁻⁹³. The different volume and area measures had different distributions but did show similar associations with age and other risk factors for breast cancer. Yet, most volumetric data have yielded weaker gradients in breast cancer risk than the standard area measurements, although not all volumetric

measurements⁸⁶. This appears to be counterintuitive as the entire breast volume should logically contain more information than the projected area. The most likely explanation for why the area measurements appear to provide better risk prediction is due to the sensitivity of the volume measurements to errors in the measurements of breast thickness. Most of the algorithms require knowledge of the breast thickness and the calculated volumes are sensitive to small changes in the measured value. Compression paddles that are not parallel can cause small uncertainties in the measured thickness and even perfectly parallel paddles do not guarantee dependable thickness measurements. These small errors can lead to inaccurate estimations of volume of dense and non-dense tissue which can explain their poorer performance in risk prediction.

1.5 Alternatives to Mammography

In current practice, mammography is used for both breast cancer detection and breast density measurements. This is because it is less expensive and more efficient for one device to perform several different functions. Ideally, each of these individual tasks, cancer detection and density measurement, should be done with a device that is best suited for it. This is a common approach with measurements that are made in other medical fields. Since mammography is the only screening method that has been shown to reduce mortality from breast cancer⁶⁵, it is likely that it will remain as the principle method of breast cancer detection. Digital mammography is replacing film mammography as it improves the detection of breast cancer, yet it is not optimal for the measurement of breast density. Potential alternatives to mammography for breast imaging and breast density measurements include magnetic resonance (MR)⁹⁴⁻⁹⁸, double x-ray absorption (DEXA)^{81, 82, 88, 93, 99-103}, dedicated breast CT¹⁰⁴⁻¹⁰⁷, positron emission

mammography (PEM)¹⁰⁸⁻¹¹⁴ and ultrasound tomography (UST)¹¹⁵⁻¹²³. All these options are volumetric methods that do not obtain their volumetric information based on two dimensional projection mammograms.

Magnetic resonance imaging has been demonstrated to have superior sensitivity in assessing breast composition compared to mammography in younger, high-risk women⁹⁸. Correlations have been demonstrated between mammographic percent density and two MRI parameters: T_2 relaxation time and relative water content⁹⁴ and estimation of fat and parenchyma in breast tissue is feasible using T_1 times⁹⁶. The images produced from MR imaging are tomographic, with virtual slices showing the three dimensional anatomy. The benefit of these images is that the overlying and underlying tissue can be removed when viewing individual slices, which overcomes the superposition problems from projection mammography. Figure 1-4 shows a breast MRI image. However, while MR is useful as a research tool, its limited access and high expense make it impractical for widespread use. Furthermore, the image acquisition process for MR takes much longer than mammography. This means that a small fraction (~15%) of the general population will be unable to tolerate the process due to claustrophobia.

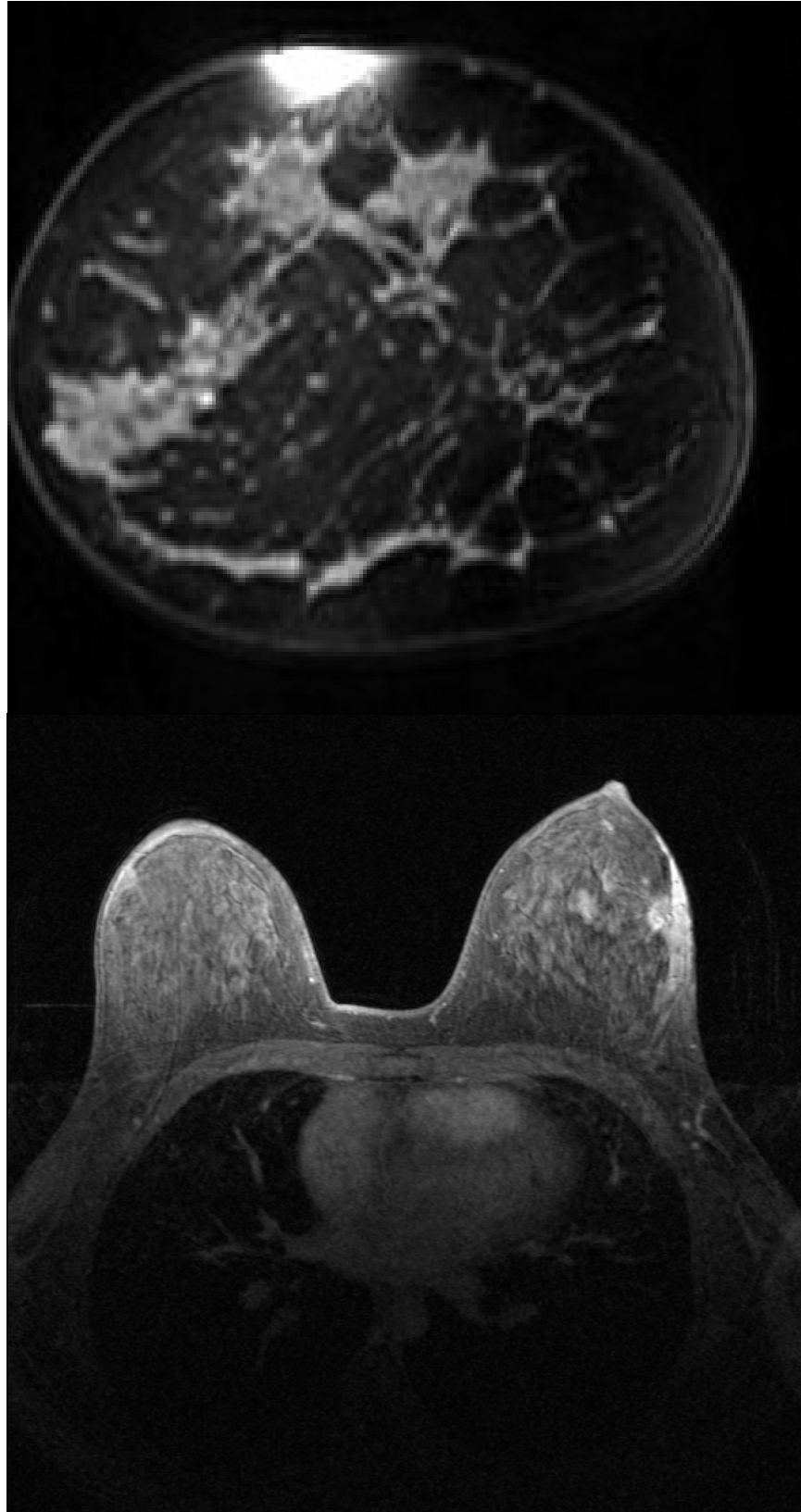


Figure 1-4 - Coronal (Top) and transverse (Bottom) breast MRI images.

Breast CT was initially investigated many years ago as a method of breast cancer screening¹²⁴ but was largely dismissed as impractical due to concerns about radiation dose and cost-effectiveness¹²⁵. Dose concerns arose because early studies used conventional CT units where images were acquired transversely. This caused the x-ray beam to penetrate the thoracic cavity which unnecessarily exposed a great deal of non-breast tissue to radiation. This geometry can also potentially reduce image quality due to cardiac and respiratory motion. More recent attempts to study breast CT have used a dedicated and specially designed scanner to obtain the three dimensional tomographic images¹⁰⁴⁻¹⁰⁶. The dose delivered using the system was found to be comparable to or even lower than the doses delivered at routine mammography¹⁰⁴. Compared to mammography, the image quality of breast CT varied depending on exactly what structures were being imaged. For imaging breast lesions, image quality was similar between the modalities, while CT provided superior image quality for the visualization of masses and mammography was better for visualization of microcalcifications¹⁰⁶. However, despite this, the limited and costly machinery limits the widespread implementation of breast CT. Still, further investigation is needed into clinical applications of breast CT. An example of the images obtained using a dedicated breast CT scanner are shown below in Figure 1-5.

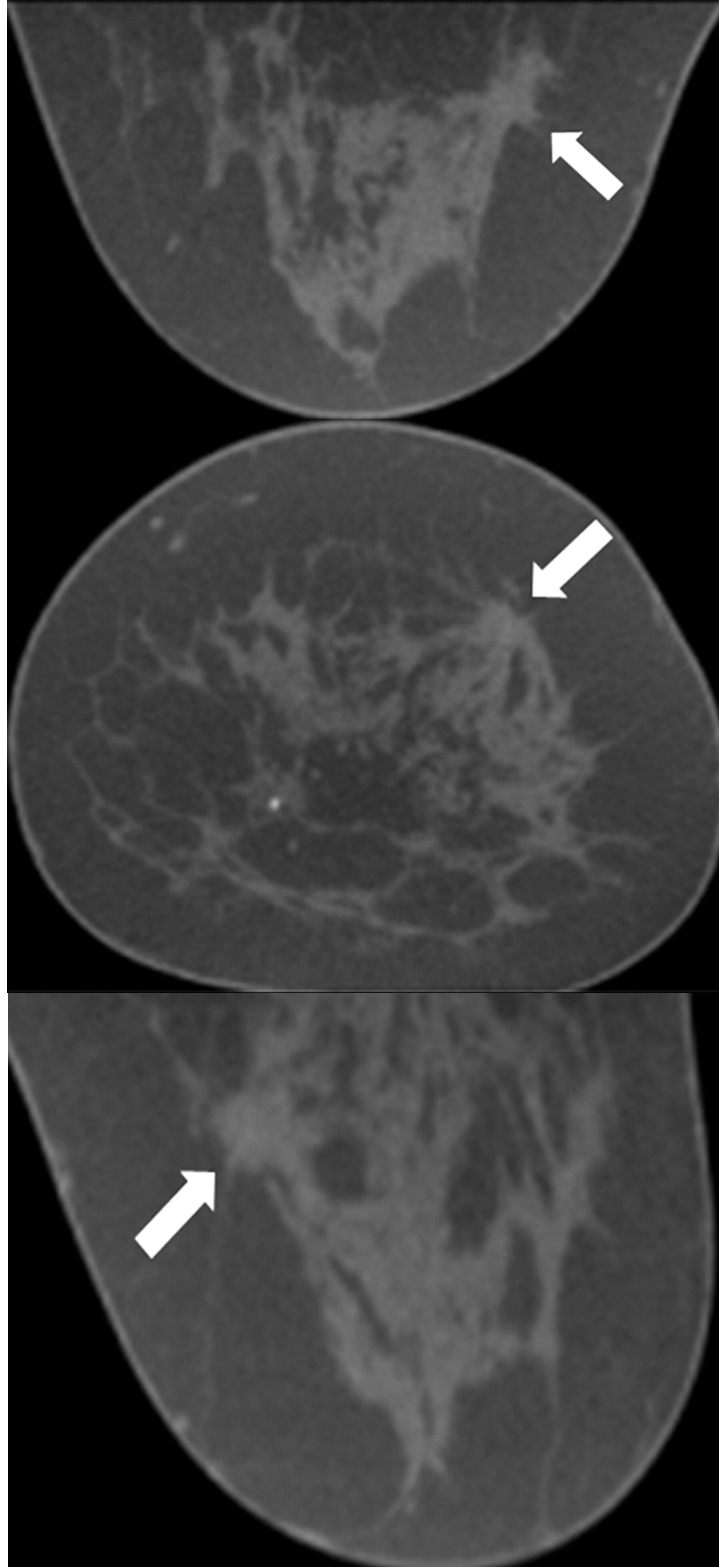
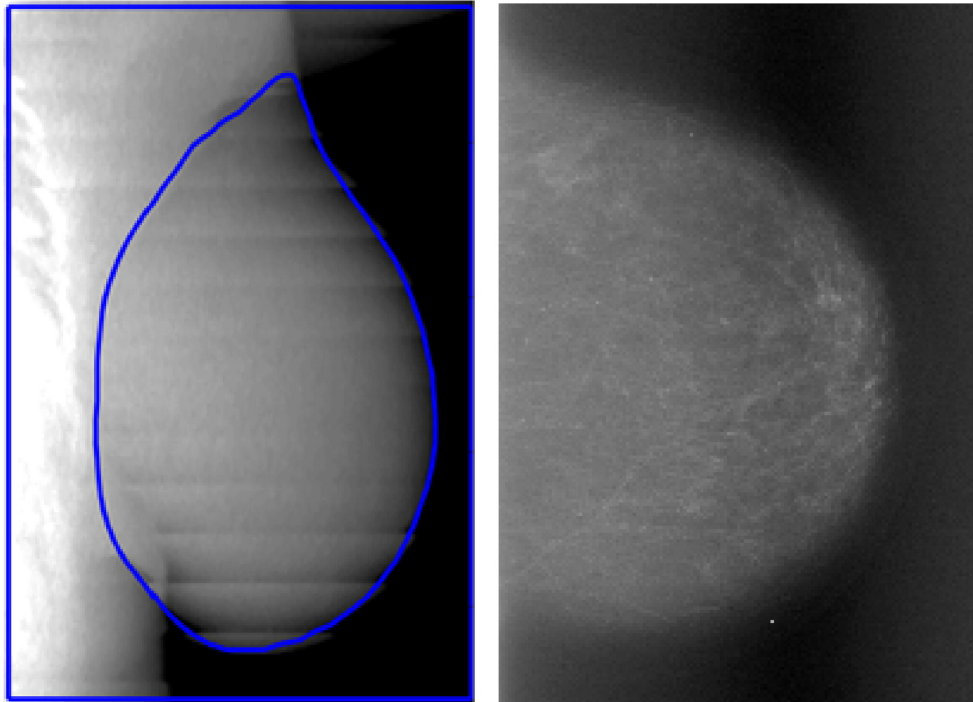


Figure 1-5 - (Top) Transverse, (Middle) coronal and (Bottom) sagittal breast CT scans of a breast that show a speculated mass¹⁰⁶.

Dual-energy x-ray absorptiometry (DXA) has been commonly used for many years to measure bone mass and density in the diagnosis of osteoporosis and whole body soft tissue composition expressed as percent fat mass^{99, 100}. It has recently been applied to the measurement of breast density^{81, 82, 101} due to its clinical success in the fields previously listed. By using two different x-ray beams with different effective energies, the volume of two different irradiated tissues can be calculated. In the breast, these two tissues are fibroglandular and fatty tissue. DXA is a low dose imaging system, with doses up to 10 times lower than that of mammography¹⁰⁰. Due to this low dose level, DXA has been used to measure breast density in adolescent girls^{102, 103} as well as adult women⁸⁸. Yet, methods not involving the use of ionizing radiation would still be preferable for these younger patients as well as for women at higher risk of developing breast cancer. This is because susceptibility to the carcinogenic effects of radiation are greatest at this time and repeated measurements might also be required. Also, most DXA measurements are made using devices designed for measuring bone density. Although these devices are common and do not require compression, a unit specially designed for imaging women's breasts would be preferred. Figure 1-6 shows the images obtained using a DXA device.

(A) Fatty breast



(B) Dense breast

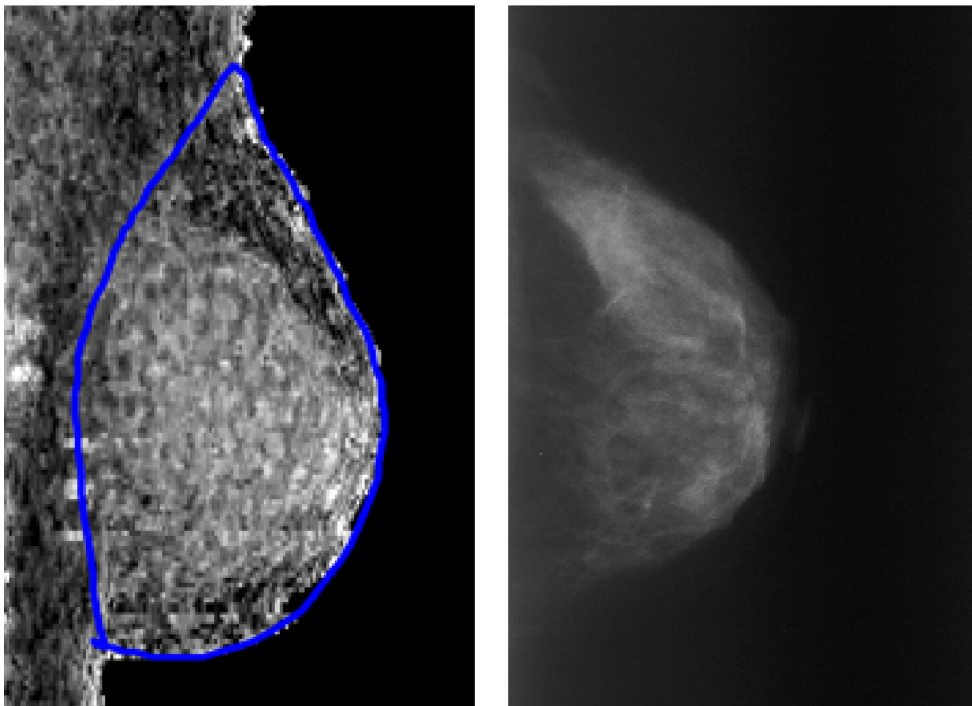


Figure 1-6 - Breast images by DXA (left) and conventional mammography (right)⁸⁸.

Positron emission mammography (PEM) is an imaging modality that can be used to screen for malignant tumors^{111, 113, 114}. It is a functional imaging method where physiologic changes, rather than structural changes, are observed. Figure 1-7 shows an example of several images obtained by using this modality. Through the use of FDG (¹⁸F-fluorodeoxyglucose), a positron-emitting glucose analog, metabolic activity in the breast can be monitored. Because localized increases in metabolic activity may indicate the presence of a neoplasm before mammography can indicate the morphological changes, PEM characterization of palpable breast masses is highly accurate^{108, 110, 112}. Few studies have examined the relationship between breast density and FDG uptake in the breast. Vranjesevic *et al*¹⁰⁹ found that average peak standardized uptake values (SUV) correlated with breast density ($P < 0.01$) while Berg *et al*¹¹² found that increasing FDG uptake correlated strongly with density, as measured using the BIRADS categories (Spearman coefficient $r_s = 0.76$). However, despite its ability to depict primary breast cancer, PEM is not a widespread imaging modality and there exist many hurdles to overcome to achieve implementation as a practical density assessment tool.

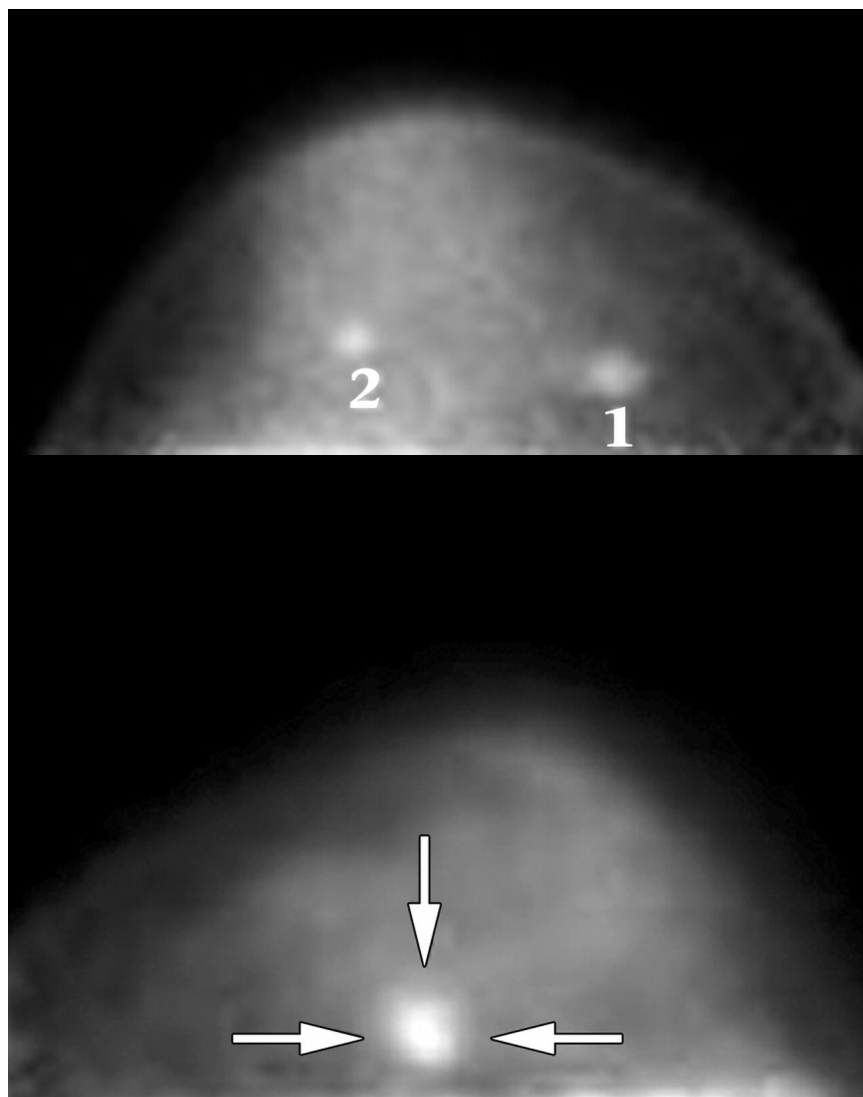


Figure 1-7 - (a) Transverse FDG PET image demonstrating two abnormalities. Lesion 1 represents invasive carcinoma that was depicted at conventional mammography while lesion 2 represents a noninvasive papillary carcinoma, which was not visible at conventional mammography. (b) Transverse PET image of the left breast depicts a single focus of increased FDG activity (arrows) at the site of the mass¹¹⁰.

Ultrasound (US) imaging has traditionally complemented mammographic imaging by helping to differentiate cysts from solid masses. It has also become the dominant mode for guiding needle biopsy. Standard ultrasound has demonstrated effectiveness in detecting breast cancers of smaller sizes and earlier stages for women with dense breasts¹²⁶. Efforts to improve the diagnostic accuracy of US have been carried out on two fronts. The first has been to improve current US devices and

techniques that rely on reflection, or B-mode, imaging¹²⁷⁻¹²⁹ while the other characterizes masses using transmission imaging.

In 1976, Greenleaf *et al* made the observation that acoustic measurements made with transmission US could characterize breast tissue¹³⁰. Using the transmission parameters of sound speed and attenuation they concluded that differentiation between benign masses and cancers was possible. *In vitro* samples of tissue were used to obtain plots of sound speed as a function of attenuation and it was observed that benign and malignant masses were well separated. This result led to the development of many different US transmission scanners in an attempt to measure the transmission parameters *in vivo*¹³¹⁻¹³⁵. Ultrasound tomography (UST) is one example of this type of ultrasound scanner. The breast UST scanner developed by Duric *et al* provides several advantages as a breast density assessment tool¹¹⁵⁻¹²³. UST does not use ionizing radiation or compression to create images. UST examinations take on the order of minutes to perform and the costs for the machine are expected to be low. Therefore, UST can be used for risk assessment in conjunction with mammographic screening for breast cancer and will add little in terms of cost and time.

Previous work done by Glide *et al.*^{119, 120} examined the preliminary relationship between UST density measurements and mammography density measurements. An anthropomorphic breast phantom was imaged using UST and CT. It was found that sound speed correlated strongly with the known mass densities (Pearson correlation coefficient $r_p = 0.87$) and CT numbers (Pearson correlation coefficient $r_p = 0.87$) of the different regions in the phantom. These phantom results lead to the investigation of UST *in vivo*. Comparing the measured sound speed in UST to film MPD measurements also

gave strong correlations (r_p ranged from 0.72-0.75). However, the correlations improved as the order of fit increased (r_p ranged from 0.81-0.88 for the higher order fits). Finally, a volumetric estimation of percent density (USPD) also showed strong correlations with MPD (r_p ranged from 0.75-0.84). These results all showed that ultrasound tomography is an imaging modality that could be used to accurately measure material density and that it has similar capabilities to mammography in determining breast density.

1.6 Dissertation Outline

The aim of this work is to evaluate ultrasound tomography (UST) of the breast as a novel method of measuring the breast tissue characteristic known as “breast density” (BD). There are many studies that have found that mammographic breast density is strongly associated with risk of breast cancer. This study of UST is a continuation of the work done by Duric *et al* and Glide *et al* on a clinical prototype located at the Karmanos Cancer Institute in Detroit, Michigan^{115, 116, 119}. Currently, mammography is the gold standard for the measurement of breast density. However, measurements of breast density by UST could be at least as strongly associated with breast cancer risk as the projected area of breast density measured by mammography.

An overview of the prototype itself and the algorithms used to create the images will be discussed. UST presents the density of the breast in terms of a new measurement known as the volume averaged sound speed (VASS). The method of extracting this information from the UST images will be explained.

Next, the results of a study involving approximately 250 patients who underwent both mammography and UST exams will be presented. These results will show the strong associations between densities as measured by the two different imaging

modalities which will allow us to pursue further investigation into finding a direct link between UST measurements and breast cancer risk. Relationships between the UST density measurements and other common breast cancer risk factors will also be shown.

Continuing, preliminary results are presented from a study that aims to track changes in breast density using UST measurement for patients undergoing treatment with tamoxifen. Tamoxifen is a SERM that is known to reduce the risk of breast cancer and reduce breast density. Changes in mammographic density associated with tamoxifen have been studied elsewhere and the preliminary data presented here shows promising early results that align with those outcomes.

The overall goal of this work is to show the ability of the UST imaging system to measure breast density. By showing its effectiveness at assessing density, UST may one day be a safe and cost-effective alternative in the field of breast density measurement and breast cancer risk prediction.

CHAPTER 2

ULTRASOUND TOMOGRAPHY

Ultrasound tomography (UST) has the potential to overcome many of the shortcomings present with mammography in the measurement of breast density. It uses non-ionizing ultrasonic waves to create images and poses no radiation risk to the patient allowing for essentially unlimited repeats of exams. It creates coronal slices of the whole breast anatomy and can therefore extract diagnostic information from the entire three-dimensional volume of the breast. It is also less expensive to implement than other three dimensional imaging modalities, such as MRI.

2.1 Measuring Breast Density Using UST

UST uses whole-breast acoustic velocity as an indicator of breast density. In breast tissue, the speed of sound (v) has the following relationship to the elastic constant (c) and material density (ρ):

$$v = \sqrt{\frac{c}{\rho}} \quad \text{Eq. 1}$$

Studies have shown that in human tissues, the elastic constant scales proportionally to the cube of density ($c \propto \rho^3$)¹³⁶⁻¹³⁸. Substitution into this equation reveals that in human breast tissue, the sound speed is directly proportional to the density. Therefore, the average density of the breast can be measured by calculating the volume averaged sound speed (VASS) of the breast. This measurement represents an absolute scale that can easily be replicated between current and future machines without the need for phantom calibrations.

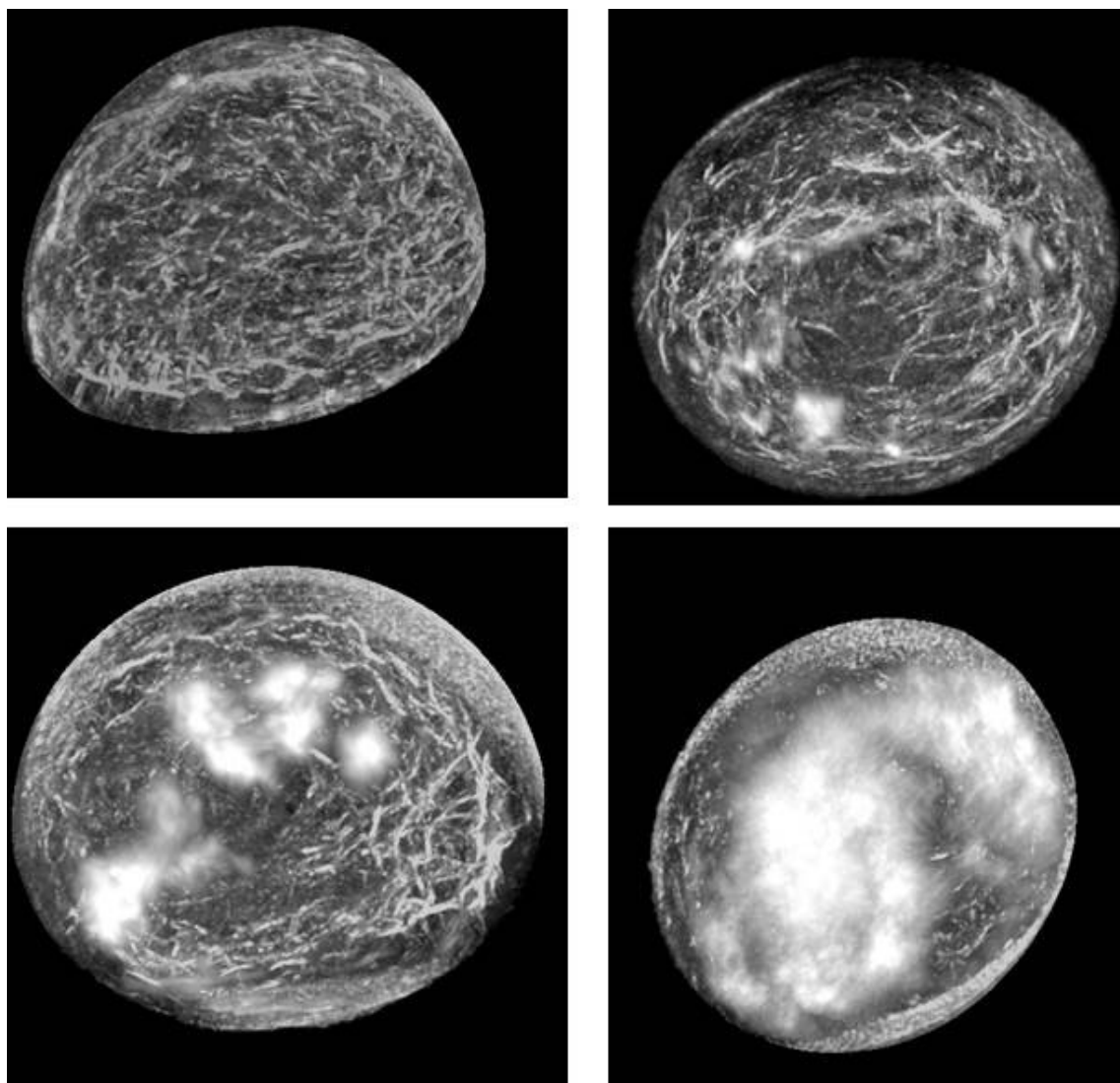


Figure 2-1 - UST sound speed images showing rough estimates of the BI-RADS density categories. Top Left – Category 1; Top Right – Category 2; Bottom Left – Category 3; Bottom Right – Category 4.

Breast sound speed images can be classified in many ways. Sound speed images are a quantitative way of determining density, as will be discussed later. Visualizing the sound speed images can also be used as a quick method of breast density estimation in much the same way it is performed in mammography. The same general BI-RADS categories can be applied to sound speed images to group breasts of similar densities (Figure 2-1). Since BI-RADS was designed for use with the two dimensional projection mammography images, applying the terminology to the three dimensional volumetric

images of UST is not necessarily expected to be compatible. The distribution of dense and fatty regions in mammography can appear very different to the distribution of dense and fatty regions in UST. However, the general principle holds, in that an image with more white regions is an image of a denser breast.

2.2 The UST Prototype

Figure 2-2 shows the system workstation and prototype patient bed for the UST scanner. It depicts a patient setup that is different than that for mammography and conventional ultrasound. The CURE, or Computerized Ultrasound Risk Evaluation, device was located at the Karmanos Cancer Institute (KCI) in Detroit, MI and has been used clinically for several clinical research studies. The patient climbs a few steps onto the bed and is positioned prone with the breast situated in a hole in the tensioned sailcloth bedding. The breast is suspended in the water tank located below. The water acts as a coupling medium and allows the breast to maintain its natural shape without deformation or tissue displacement.

Also inside the tank is the 20-cm diameter ring transducer. It operates at a central frequency of 2 MHz and is composed of 256 elements. The ultrasound signal is sequentially transmitted by each element and subsequently received by the rest of the elements. Data acquisition time for each slice is approximately 0.03 seconds which reduces intra-slice motion artifacts. A motorized gantry translates the ring away from the chest wall towards the nipple in 1 mm intervals. Depending on the size of the breast, this creates anywhere from 40 to 100 tomographic images of the breast and the entire exam takes about 1 minute to perform (Figure 2-3).



Figure 2-2 - (Top) Schematic diagram of the UST prototype showing patient positioning (Bottom) Actual UST prototype at the Karmanos Cancer Institute in Detroit, MI.

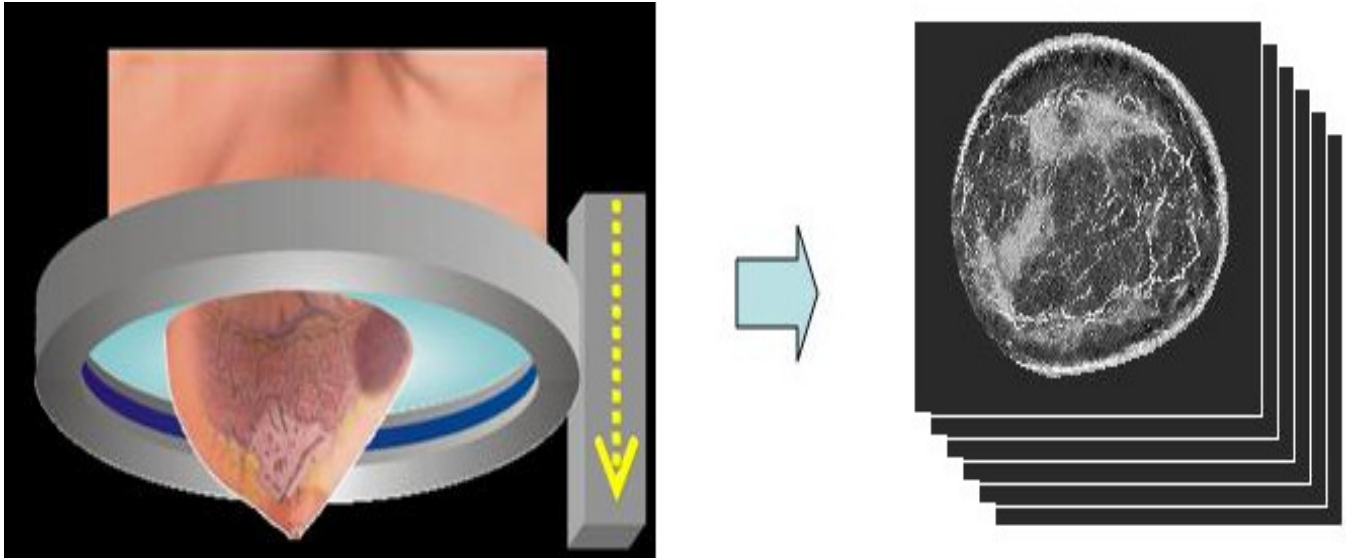


Figure 2-3 - Schematic showing the translation of the ring transducer to create UST image slices.

2.3 The Ultrasound Sound Speed Tomography Algorithm

There are several advantages for ultrasound transmission imaging (tomography) when compared to conventional B-mode imaging. Transmission images are quantitative and they provide sound-speed imaging of the whole breast. Transmission measurements are independent of echo images and encode different information about the whole anatomy of the breast. The measurements are also relatively easy to analyze mathematically. There are two basic types of UST methods, one based on ray theory and the second which applies inverse scattering principles. Using ray theory is fast and stable, while the inverse scattering principle method is more time consuming but gives higher resolutions^{133, 139-141}

The ray theory method used here uses the time-of-flight measurements of the transmission US signals to reproduce the sound-speed distribution in the breast. Based on Fermat's Principle and Snell's Law, the ultrasound ray path in an inhomogeneous medium (such as breast tissue) is not straight. This makes the inverse problem non-linear and it limited early applications of bent-ray algorithms to numerical simulations and

phantom studies¹⁴²⁻¹⁴⁴. Since most abnormal breast lesions have higher sound speed than normal breast tissue¹⁴⁵, a robust UST algorithm is critical to accurately and efficiently produce images of breast sound speed based on the ultrasound signals that are reflected by and transmitted through the breast tissue. Here, an iterative bent-ray UST method is used to extract sound speed information from *in vivo* ultrasound breast data. To solve the bent-ray ultrasound tomography problem, a rectangular grid model, whose boundaries enclose the transducer ring, was created on the image plane. During each iteration, both the forward and inverse problems were solved. The model was then updated for successive iterations. The details of the algorithm are described below.

2.3.1 Forward Modeling

Two-dimensional (2-D) ultrasound wave propagation is governed by the eikonal equation

$$(\nabla E)^2 = (\partial T / \partial x)^2 + (\partial T / \partial y)^2 = (1/v)^2 = (s_x^2 + s_y^2) \quad \text{Eq. 2}$$

where T is the travel time, v is the sound speed and (s_x, s_y) is the slowness vector of the wave, defined as the inverse of sound speed. The “wavefronts” are described by $E = \text{const.}$ and the orthogonal trajectories of these wavefronts are defined as the “rays”. This equation was solved with Klimes’s method¹⁴⁶ which has been proven to be both accurate and fast. The method calculates the slowness vector, (s_x, s_y) and travel time, T at the center point of each grid cell simultaneously with at least second order accuracy (relative to the grid size). The slowness vector and travel time, (s_x, s_y) and T , were interpolated by a 2-D fourth order Lagrange interpolation at an arbitrary point within the grid model.

By assuming the slowness is constant within each grid cell, the bent ray path can be traced back from the receiver to the transmitter fairly accurately. The method to do this is:

1. Starting from the receiver location (x_r, y_r) , trace the ray segment along the direction $\bar{G} = (-s_{x_r}, -s_{y_r})$ until it intercepts the breast boundary at point (x_i, y_i) ;
2. Set a new value for \bar{G} to be the negative slowness vector of the intercept point, $\bar{G} = (-s_{x_i}, -s_{y_i})$. Trace the ray segment along this vector to the next adjacent cell;
3. Repeat step 2 until the current ray arrives at the transmitter within a certain tolerance.

An illustration of the grid model and the backpropagation is shown below in Figure 2-4.

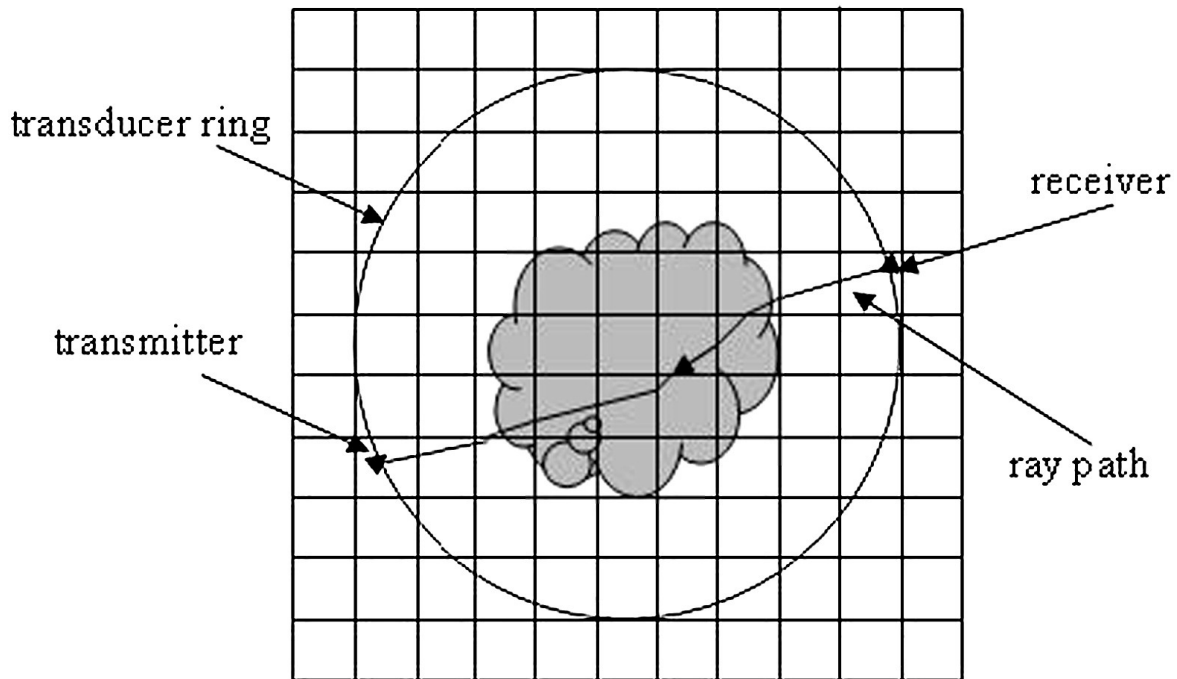


Figure 2-4 – An example of the grid model used for the forward modeling. Rays are traced from the receiver to the transmitter¹²¹.

2.3.2 The Inverse Problem

The inverse problem can be described as

$$\sum_j^M l_{ij} \Delta s_j = \Delta t_i \quad \text{Eq. 3}$$

where Δt_i is the difference between the i th picked time-of-flight (TOF) for the ultrasound data and the i th calculated TOF for the sound speed model, Δs_j is the slowness perturbation for the j th grid cell (which needs to be inverted), and l_{ij} is the ray length of the i th ray within the j th cell. This equation can be expressed in matrix form as

$$L\Delta S = \Delta T \quad \text{Eq. 4}$$

Due to ray bending, this is a nonlinear problem. The objective function for the inverse problem can be described as

$$f = \underset{\Delta S}{\operatorname{argmin}} \left(\|L\Delta S_\lambda - \Delta T\|^2 + \lambda TV(\Delta S_\lambda) \right) \quad \text{Eq. 5}$$

and

$$TV(\Delta S_\lambda) = \int \sqrt{|\nabla(\Delta S_\lambda)|^2} dx dy \quad \text{Eq. 6}$$

However, a small positive constant value is added to the equation because $TV(\Delta S_\lambda)$ is not differentiable at zero. Eq. 6 now becomes

$$TV(\Delta S_\lambda) = \int \sqrt{|\nabla(\Delta S_\lambda)|^2 + \beta^2} dx dy \quad \text{Eq. 7}$$

The quantity $\sqrt{|\nabla(\Delta S_\lambda)|^2 + \beta^2}$ is known as the gradient magnitude and this provides us with the information about the discontinuities in the image. The λ is the regularization parameter that balances the roughness of the inverted results and the fit to the data.

The quasi-Newton algorithm–L-BFGS method was applied to iteratively solve the nonlinear problem in Eq. 5 for ΔS . This method avoided the direct computation of Hessian matrices and was proven to be both time and memory efficient. After each iteration, the updated model was obtained by adding the solution ΔS to the initial homogeneous sound speed model. Rays were traced on the updated model using the same method as in the forward modeling section. The TOF data was updated at the same time as well. The iteration continued until the TOF misfit ΔT was not significantly improved from the previous iteration. This signified that the solution had converged. The regularization parameter, λ , was determined using the L-curve technique¹⁴⁷.

2.4 UST Image Reconstruction

Because of its circular shape, the CURE device captures most of the scattered and reflected fields (Figure 2-5). This additional information allows for the creation of both reflection and transmission images.

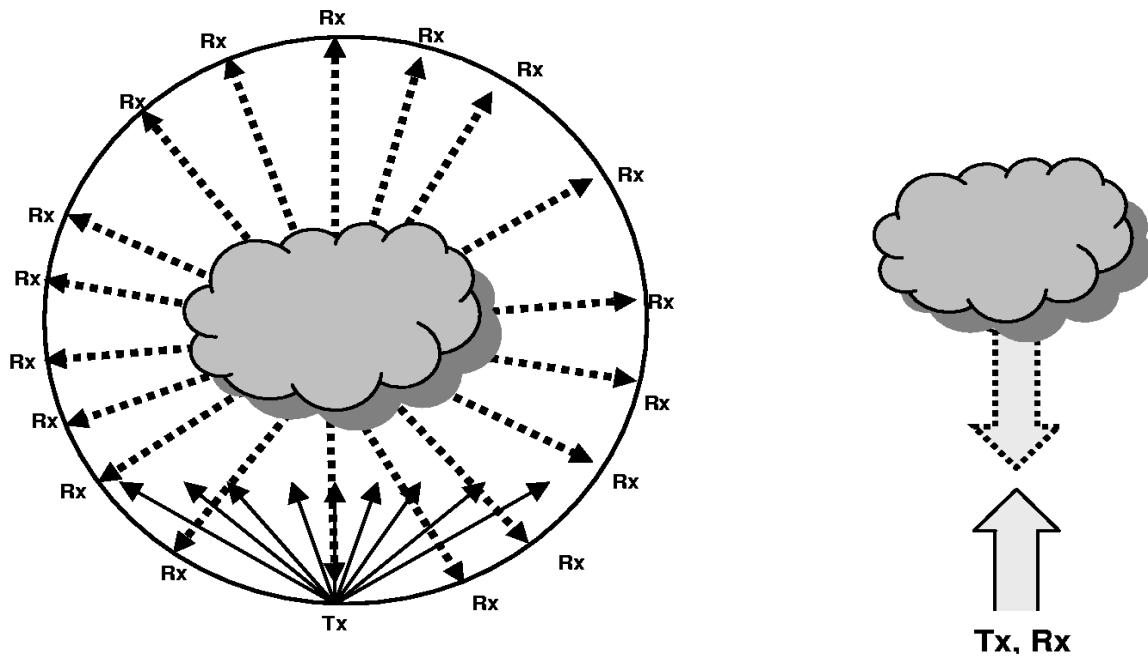


Figure 2-5 - The difference in how reflection (Rx) and transmission (Tx) ultrasound signals are collected between UST (left) and conventional ultrasound (right).

A signal generator is used to define a pulse shape, $\Psi_0(t)$, which in this case was a one-cycle sinusoid. The transmitting transducer elements are sequentially driven with that pulse to produce transmitting pulses, $A_i\Psi_0(t-t_i)$ for $\{i = 1, \dots, 256\}$. For each transmitted pulse, there is a set of received pulses, characterized by different shapes, amplitudes and arrival times and given by: $A_{ij}\Phi_{ij}(t-t_i-\tau_{ij})$ for $\{j = 1, \dots, 256\}$, where $\Phi_{ij}(t)$ is defined to be a normalized, time varying waveform so that the amplitude A_{ij} is the received amplitude and τ_{ij} is the propagation time delay for each transmit-receive pair (i,j) . Therefore, the known quantities are the transmitted amplitudes A_i and transmit times t_i . The measured values are the matrices of the received amplitudes A_{ij} and the propagation time delays τ_{ij} . Measurements of the amplitudes and time delays of the first signals to arrive at the receiving elements are used to construct the transmission images (attenuation and sound speed), while measurements of the amplitudes and time delays of the later signals to arrive are used to construct the reflection images. For N elements, there are $N(N+1)/2$ independent transmit-receive pairs, so for a ring with $N = 256$, there are nearly 33,000 such pairs.

2.4.1 Sound Speed Images

It is possible to perform a computed tomography-(CT-) like reconstruction of the sound speed based on the signals that are transmitted through the breast tissue to the other side of the ring array. When compared to a homogeneous medium, in an inhomogeneous medium such as the breast, the arrival times will deviate because the acoustic velocity varies spatially within the medium. The deviations in arrival can be inverted to obtain information about the sound speed changes in the isonified plane and then used to create maps of the sound-speed distribution. The propagation speed of a sound wave is

determined by the density of the medium that it is traveling through. So a map of the sound-speed distribution is also a map of the density distribution throughout the breast

2.5 Measuring Average Sound Speed

Analysis of the sound speed images was done primarily with the public domain software ImageJ, a package developed with support from the National Institutes of Health¹⁴⁸. The stack of sound speed images created by the CURE device was converted into ASCII images to preserve the measurements and units (km/s). The UST exams require that the subject's breast be placed in a body-temperature water bath, which has a sound speed of ~1.52 km/s. Unfortunately, this value falls within the range of breast tissue, being higher than fatty tissue and lower than dense glandular tissue. This means that the breast tissue cannot be segmented from the background image via simple thresholding. A more robust method that separates the breast from the water bath was used. A script was written for ImageJ that uses a semi-automated elliptical approximation of the breast to create a mask for each image slice.

The first step involved in using this script is to identify the slice where the nipple ends and the slice where the chest wall begins. Slices beyond the nipple contain only the water bath, so they must be discarded. In practice, determining the last slice with the nipple is complicated as a clear boundary around the breast is not always visible. Fortunately, selecting the nipple is not a critical step as the area on the slice is very small and will have a very small impact on the overall volume average. Figure 2-6 shows the selection of the last slice containing a nipple.

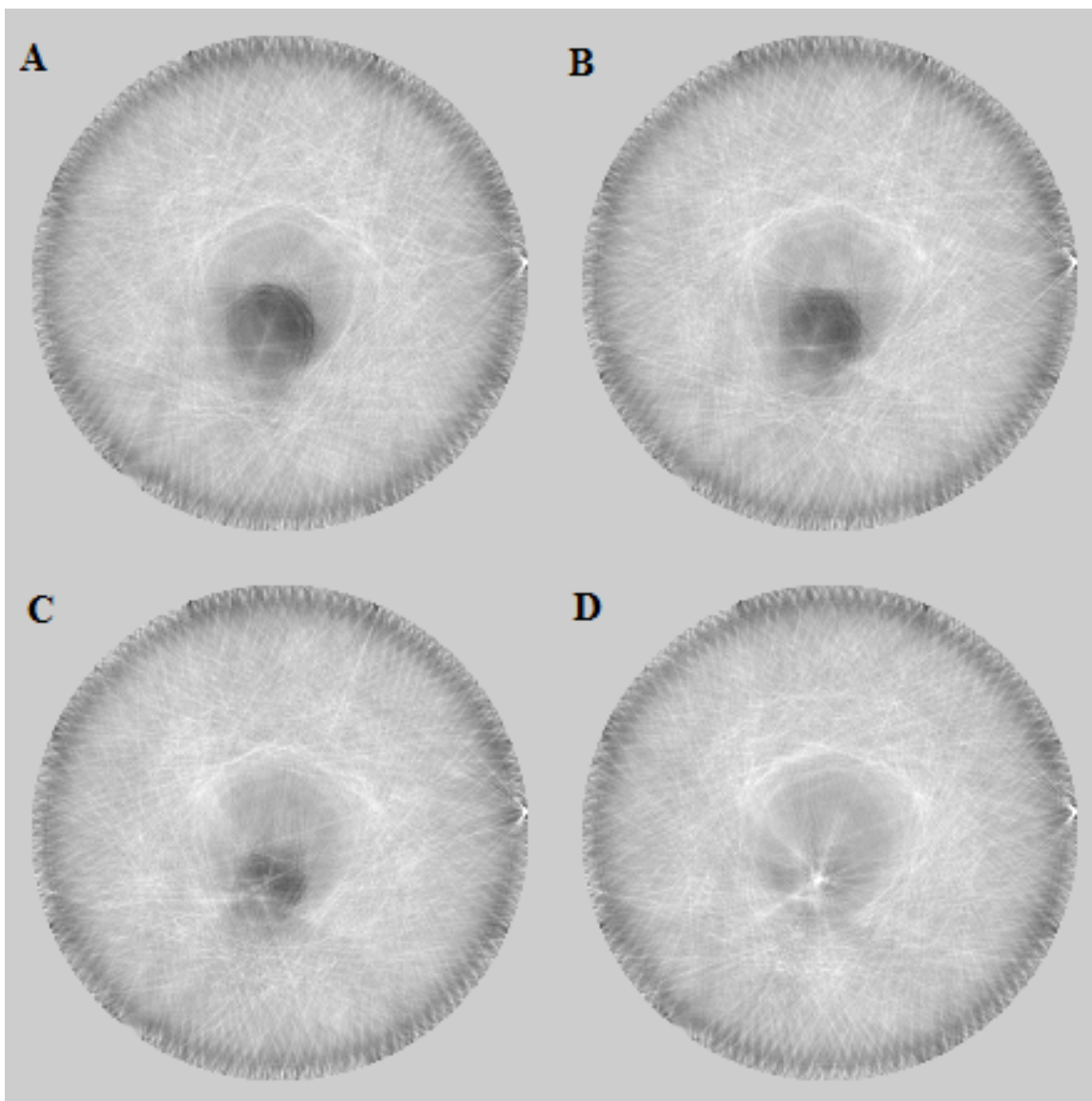


Figure 2-6 - An example of choosing the first slice that contains the nipple. Slice C was chosen to be the first slice with the nipple present. Slices A, B and C were therefore included in the final image stack.

Determining the slice where the chest wall appears is more critical. If the transducer is placed high enough up on the patient's chest wall at the beginning of the scan, the anatomy that is actually being imaged may include more than just the breast. It is important to exclude this anatomy from any measurements of VASS. As the images approach the chest wall, the clear borders surrounding the breast begin to blur. Sometimes, sections of the chest wall tissue were overhanging down below and next to

the breast. In both of these cases, the chest wall created very apparent artifacts on the image that signaled its presence. By removing any slice before these artifacts appeared, only the breast anatomy would be analyzed. Figure 2-7 shows the selection of the last slice without a chest wall. However, this is not a necessary step for every patient as some images will not include the chest wall.

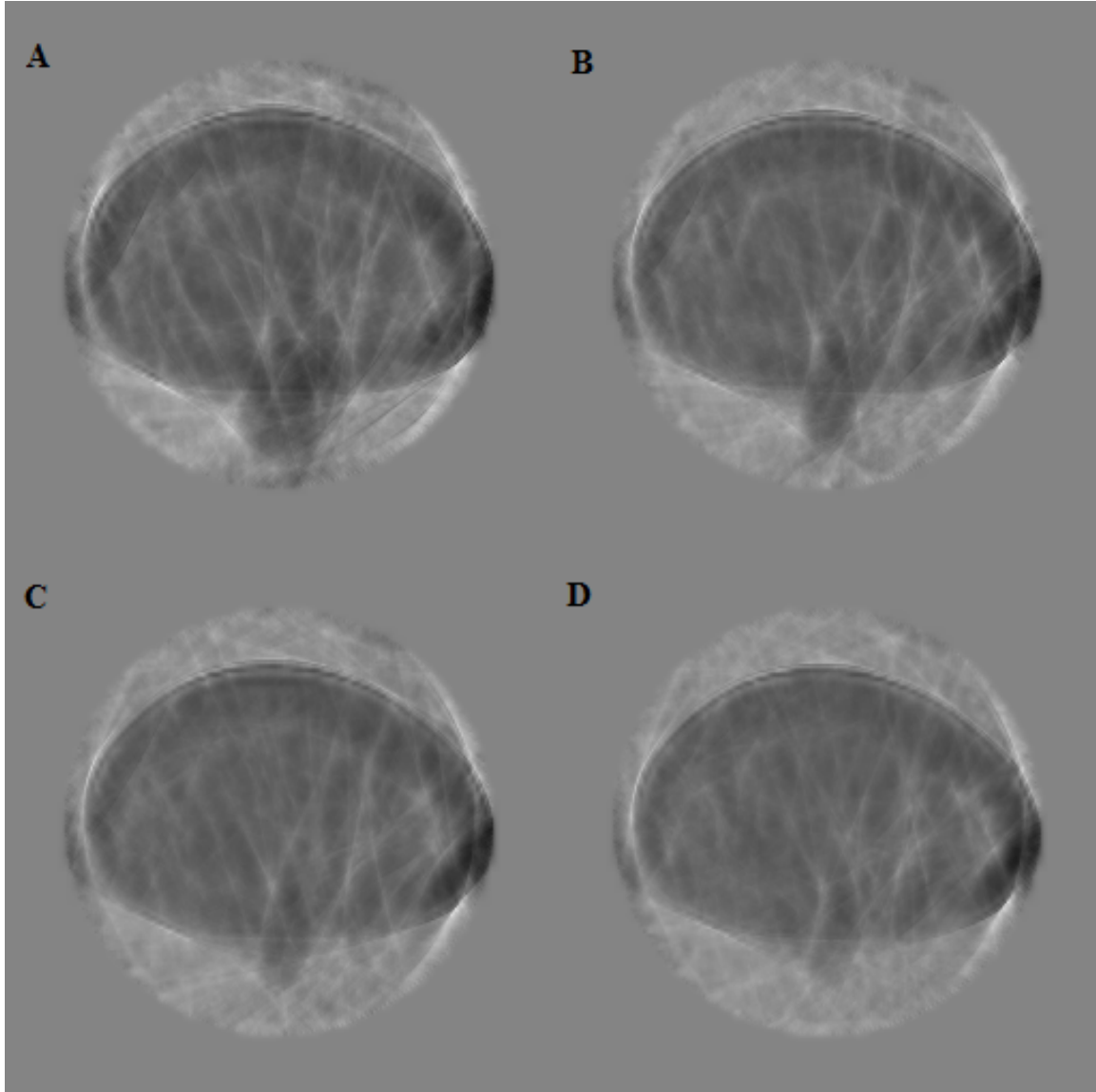


Figure 2-7 - An example of choosing the slice to remove the chest wall from the final sound speed image. Slice C was chosen to be the first slice without any chest wall present. Slices C and D will be included in the final sound speed image stack.

Once the slices containing the breast anatomy were chosen, segmentation of the breast from the background water bath could begin. For each slice, the script involved choosing 10 points to approximate the breast-water boundary. The points were chosen to equally surround the breast in all directions, as shown in Figure 2-8. The script would then use a built-in feature of ImageJ to approximate an ellipse based on the hand-picked points. The breast does not form a perfect ellipse in each slice, so in some instances the ellipse included a small volume of the surrounding water bath and in other slices the ellipse did not cover the entire volume of the breast. However, over the entire stack, these offsetting errors partially compensated for each other.

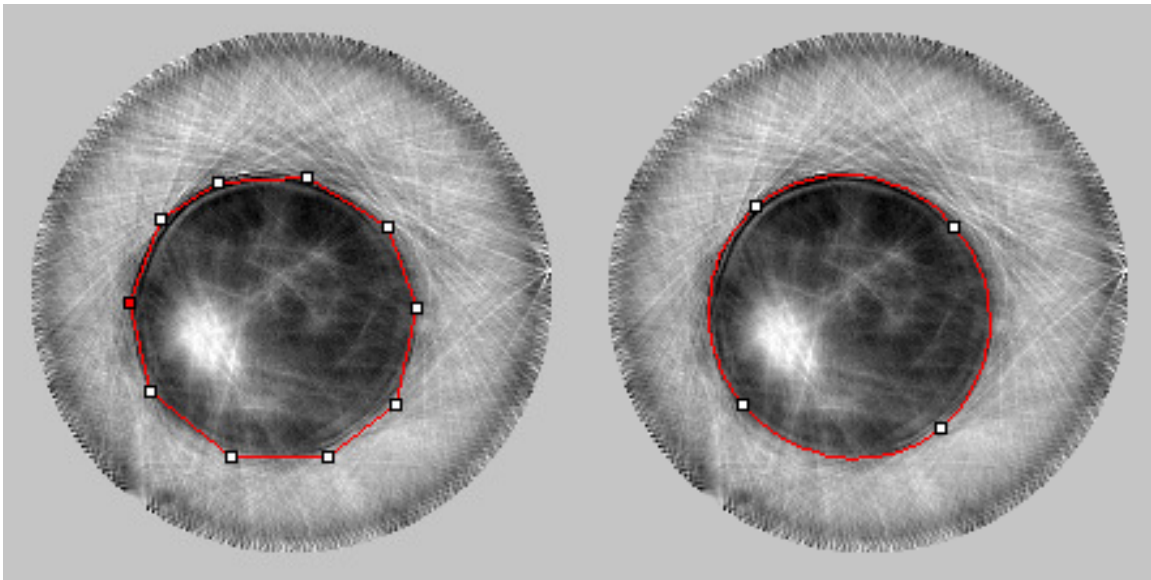


Figure 2-8 - The breast segmentation algorithm working on a sound speed image. Left: The breast/water bath interface is manually selected using 10 points Right: An ellipse is fit to the chosen points to approximate the shape of the breast in the current slice.

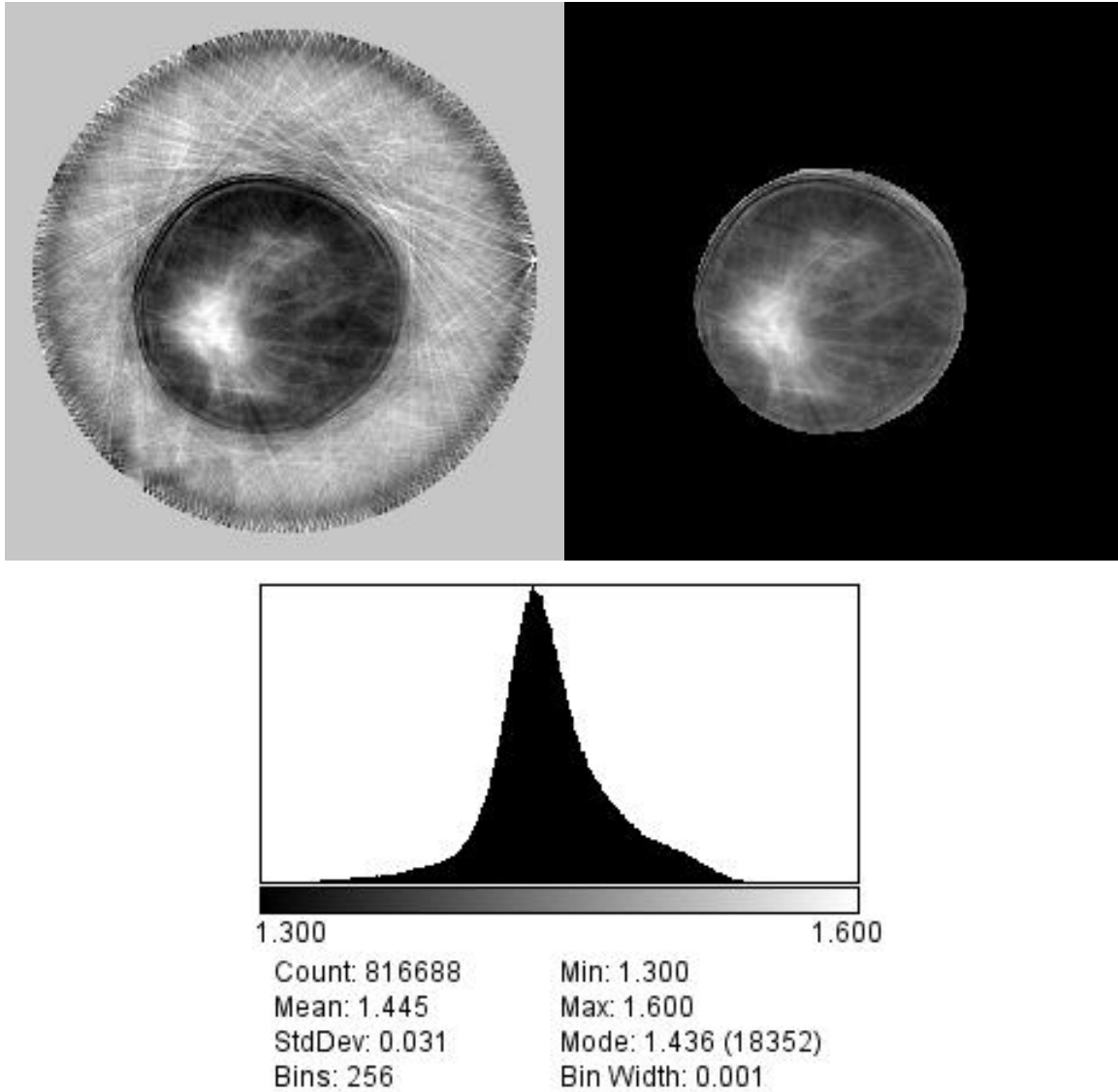


Figure 2-9 - Left: The original sound speed image before the masking algorithm was applied. Right: the masked sound speed image. Bottom: The histogram obtained from the masked images showing the distribution of sound speed within the entire image stack.

The best fitting ellipse was then used to create a mask of the breast. All pixels that lie inside the mask had a value of 1, while all pixels that lie outside the mask had a value of 0. In ImageJ, two images can be multiplied pixel by pixel. Taking the mask and the sound speed image and multiplying them resulted in an image where all pixels that correspond to the surrounding water bath now had a value of 0 and all pixels corresponding to the breast tissue had an unchanged pixel value. This image was known

as the masked sound speed image and it was also saved. Using the built in mathematical features of ImageJ, the mean, standard deviation, number of counts or volume and the standard error of the mean were calculated from the masked sound speed image. Histogram data was also collected. Figure 2-9 shows the final masked sound speed image in comparison with the original sound speed image and the calculated histogram from the entire volume.

Since an image stack corresponds to the entire breast volume, the histograms represent the statistical distribution of all sound speed voxels within the breast. The volume averaged sound speed (VASS) of the breast could be calculated very easily from the images in this form. The volume of the breast, V , can be calculated by a direct count of all voxels:

$$V = \sum_{x,y,z}^{N_x, N_y, N_z} \delta_{x,y,z} \Delta x \Delta y \Delta z \quad \text{Eq. 8}$$

where δ is a voxel located at position (x,y,z) , Δx , Δy and Δz are the dimensions of the voxels (typically 1 mm^3 for this device) and N_x , N_y and N_z are the dimensions of the sound speed image stack (typically $221 \times 221 \times 75$ pixels). For most images, the total number of voxels can range from 50,000 to more than 2 million which corresponds to breast volumes of 50 to 2000 cm^3 . The VASS can then be calculated by using the formula:

$$\text{VASS} = \frac{1}{V} \sum_{x,y,z} s(x, y, z) \quad \text{Eq. 9}$$

where $s(x,y,z)$ is the sound speed value of the voxel located at position (x,y,z) . The net result, the VASS, is a single-valued estimate of the average sound speed that is representative of the whole breast. It is this value that can be used as a quantitative

estimate of the average density of the breast. Additional counting statistics can also be obtained very easily from the distribution of sound speed within the breast.

2.6 K-means Clustering

The sound speed images were also analyzed through the use of a *k*-means clustering routine. This approach segments images via grouping gray-level pixels according to their proximity to randomly initialized centroid values. Here, the two clusters chosen correspond to volumes of dense and fatty tissue. This allows for the calculation of the total volume of dense and fatty tissues in the breast and, due to the quantitative nature of the sound speed images, the average sound speed of the dense and fatty volumes. The ultrasound percent density (USTPD) can then be calculated in a similar fashion to the mammographic percent density. The USTPD is simply the ratio of the volume of segmented dense tissue to the entire volume of the breast.

2.7 Statistical Analysis

A wide variety of statistical tests were used to analyze the results. The value of each voxel in the reconstructed UST image is assumed to represent a sound speed value that is normally distributed around the average sound speed, μ , with variance σ^2 . However, the volume averaged sound speed that is measured using the methods described above is actually the sample mean, \bar{x} . The distribution of the sound speed values of the voxels in the masked UST image is also assumed to be normally distributed. The standard deviation, σ , describes the distribution of the values of the voxels relative to the sample mean. The best measure of the uncertainty of the sample mean relative to the actual mean is through the use of the standard error ($SE_{\bar{x}}$), defined as:

$$SE_{\bar{x}} = \frac{\sigma}{\sqrt{N}} \quad \text{Eq. 10}$$

where N is the voxel count of the image. Using the standard error alongside the sample mean gives the best estimation of the volume averaged sound speed and its uncertainty.

Correlations between sound speed and patient characteristics were assessed using the Spearman's rank correlation coefficient (r_s). The Spearman correlation coefficient is a non-parametric measure of statistical dependence between two variables. It assesses how well the relationship between these two variables can be described using a monotonic function. A positive Spearman correlation corresponds to an increasing trend between the variables while a negative Spearman correlation corresponds to a decreasing trend. The Spearman coefficient was chosen instead of the Pearson correlation coefficient because the Spearman coefficient is less sensitive to strong outliers. Also, the Spearman coefficient is able to compare two variables related by any monotonic function, not just linear functions as with the Pearson coefficient. Figure 2-10 shows the differences between the two correlation coefficients on hypothetical sample data.

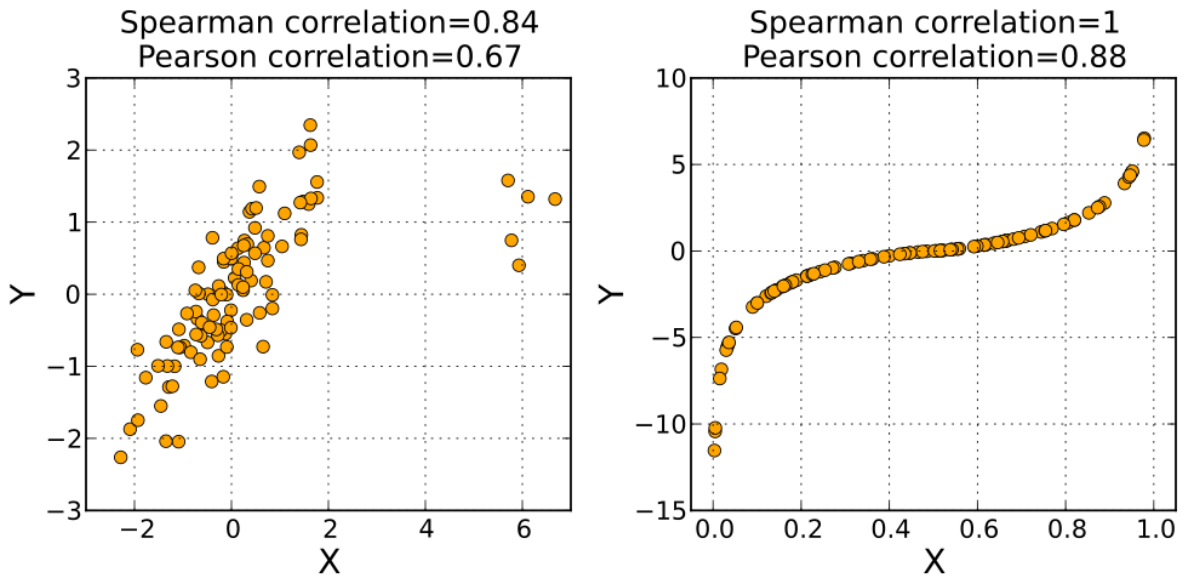


Figure 2-10 - Two examples using hypothetical data to highlight the difference between Spearman and Pearson coefficients¹⁴⁹. Left: The Spearman coefficient is less sensitive to outliers in the data. Right: Spearman coefficients are even useful on data that follows a non-linear but predictable pattern.

To test the repeatability of the sound speed measurements between different users, intra-class correlation coefficients (ICC) were calculated. The measurements on each scan by different raters were placed into groups and the ICC is a measure of how strongly these units resemble each other. Since the true mean sound speed is not known, the similarity of the sample means calculated by the different raters is measured. However, the ICC will not be able to differentiate between inter-observer and intra-observer variability. The ICC used here is usually attributed to Harris¹⁵⁰ and is described as:

$$ICC = \frac{K}{K-1} \cdot \frac{N^{-1} \sum_{n=1}^N (\bar{x}_n - \bar{x})^2}{s^2} - \frac{1}{K-1} \quad \text{Eq. 11}$$

where K is the number of raters, N is the number of scans being compared, \bar{x} is the sample mean of all measurements, \bar{x}_n is the sample mean of the n^{th} group and s^2 is the average variance of all measurements.

To test results between different groups, the Student's t-test was used. The independent sample t-test was used to compare two separate sets of independent and identically distributed samples. For example, when examining a cohort of patients, differences in the average breast density between pre- and post-menopausal women can be determined by using the independent sample t-test. A paired sample t-test was used to test samples of matched pairs and units that were tested twice in order to examine the effect of a specific treatment. For example, testing the effect of tamoxifen treatment on breast density was accomplished through the use of a paired sample t-test by comparing measurements made before treatment began with those made after treatment began. These t-tests are able to reject or fail to reject the null hypothesis of no change in breast density.

The asymmetry of the distribution of the patient data was also measured by respectively calculating the skewness. This is a descriptor commonly used to describe the shape of a probability distribution. The skewness of a random variable, X , is the third standardized moment denoted by γ_1 and defined by:

$$\gamma_1 = \frac{\mu_3}{\sigma^3} \quad \text{Eq. 12}$$

where μ_3 is the third moment about the mean and σ is the standard deviation. A distribution that is positively skewed is one with a longer right tail with relatively few high values. A negatively skewed distribution has a longer left tail with relatively few low values. Figure 2-11 shows examples of hypothetical sample data that is negatively and positively skewed.

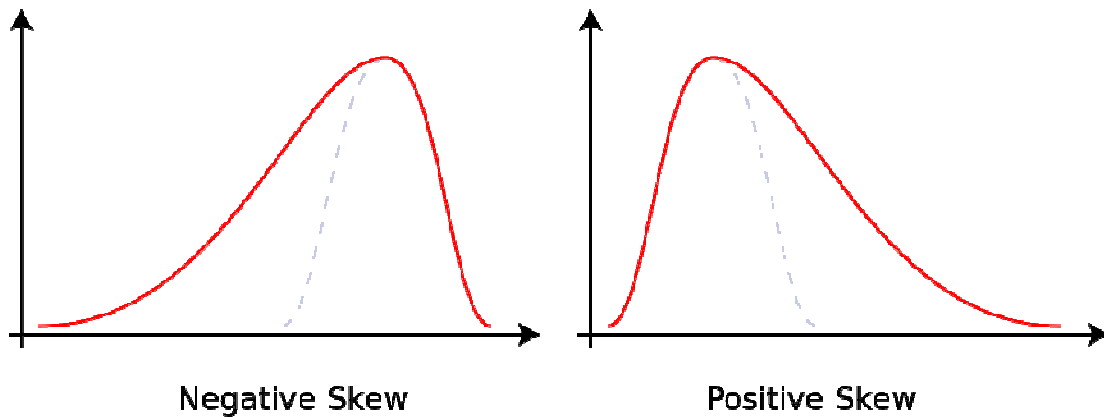


Figure 2-11 – Examples showing negatively skewed (Left) and positively skewed (Right) data using hypothetical data¹⁵¹.

The data was mostly organized and analyzed using Microsoft Excel. This spreadsheet software allowed for easy organization of the data, a wide variety of simple statistical calculations and the ability to easily create plots. Further analysis using the data was performed using the open-source statistical software program SOFA Statistics version 1.2.2. It allowed for the calculation of the Spearman correlation coefficient, the

calculation of both the independent and paired sample t-tests and the calculation of skewness.

CHAPTER 3

VASS VERSUS MPD STUDY

3.1 Patient Recruitment for VASS versus MPD Study

Patient data were acquired from patients recruited into ongoing studies in accord with a Karmanos Cancer Institute (KCI) and Wayne State University approved protocol. A population of 251 patients was examined with both the UST device to create sound speed images of the breast and with either digital or film mammography. The UST images were analyzed according to the methods described earlier to measure both the sound speed and cluster results. The mammograms were digitized and the mammographic percent density of each patient was analyzed by one reader (NFB) using the CUMULUS 4 Software. This software allowed for measurements of dense and total breast area which was then used to calculate the percent density and non-dense areas. The patient characteristics of the entire group were analyzed and the results are shown below in Table 3-1.

The patient data could also be sorted into specific groups in order to compare any potential differences or biases between the groups. These groups are either logical separation points or known breast cancer risk factors or factors that affect breast density. These groups are:

1. The type of mammogram received – Digital or Film
2. Menopausal status – Post-menopause or Pre-menopause
3. Race – African-American or White
4. Family history – A first degree relative with breast cancer or no
5. Parity – Nulliparous or Parous

Table 3-1 – Average Patient Characteristics

UST Related Characteristics	Average Value	Standard Error	# of Women
VASS (km/s)	1.4428	0.0016	251
USTPD	17.8	0.6	247
Volume of Dense Tissue (cm ³)	478	21	247
Volume of Non-Dense Tissue (cm ³)	2737	116	247
Total Volume of Breast Tissue (cm ³)	3214	124	247
Average SS of Dense Tissue (km/s)	1.4954	0.0015	247
Average SS of Non-Dense Tissue (km/s)	1.4358	0.0019	247
Mammography Related Characteristics	Average Value	Standard Error	# of Women
MPD	28.0	1.1	251
Dense Area on Mammogram (cm ²)	46.2	1.9	249
Fat Area on Mammogram (cm ²)	143.2	5.8	251
Total Area on Mammogram (cm ²)	189.0	5.8	251
Patient Related Characteristics	Average Value	Standard Error	# of Women
Age of Patient (years)	46.4	0.7	251
Weight of Patient (kg)	79.1	1.1	244
Height of Patient (cm)	163.1	0.4	235
Body Mass Index (kg/m ²)	29.7	0.4	233
Age at Menarche (years)	12.6	0.1	211
Age at Birth of First Child (years)	21.5	0.5	171
Age at Menopause (years)	43.9	0.9	52

3.1.1 Patient Characteristics – Type of Mammogram Received

Of the 251 patients that were examined, 85 received a digital mammogram while 166 received a film mammogram that was then digitized. The different mammogram types used are a result of a transition in mammography hardware at KCI that occurred during the patient enrollment period. Table 3-2 summarizes and compares the

characteristics of the data sets collected from patients that received digital and film mammography. It enumerates the number of patients in each specific group by category. It includes mammographic imaging characteristics such as MPD, the total area of dense tissue as measured on the mammogram, the non-dense area as measured on a mammogram and the total breast area as measured on the mammogram, UST imaging characteristics such as the VASS, USTPD and dense, non-dense and total breast volumes. It also includes patient information such as age, weight, height, age at menarche and menopausal status among others. Chi-squared and independent t-tests were performed on the data to test for any discrepancies between the categories. Any differences in the patient characteristics between these two groups should be coincidental not indicative of any causal relationship.

3.1.2 Patient Characteristics – Menopausal Status

When grouping by menopausal status, 154 women were pre-menopausal, 86 were post-menopausal and the menopausal status of the remaining 11 women was unknown. Menopause has a well-known influence on breast density and breast cancer risk, so mammography and UST-related characteristics could differ by menopausal status. Chi-squared and independent t-tests were performed on the data to test for differences by menopausal status. Table 3-3 summarizes the collected statistics between the pre- and post-menopausal women. Since the pre-menopausal women obviously have not begun menopause, their age at menopause could not be calculated and the comparison could not be completed for this category. The women whose menopausal status was unknown were also not included in this analysis.

Table 3-2 – Patient Characteristics – Type of Mammogram

	Count (%) or Mean (SEM)		
	Digital (n = 85)	Film (n = 166)	P ^a
Menopausal Status			
Post	26 (31 %)	60 (36 %)	0.302
Pre	57 (67 %)	97 (58 %)	
Unknown	2 (2 %)	9 (5 %)	
Race			
African-American	55 (65 %)	106 (64 %)	0.980
Unknown/Other	14 (17 %)	29 (18 %)	
White	16 (19 %)	31 (19 %)	
Family History of Cancer			
No	63 (74 %)	106 (64 %)	< 0.001
Unknown	1 (1 %)	29 (18 %)	
Yes	21 (25 %)	31 (19 %)	
Parity			
Nulliparous	23 (27 %)	22 (13 %)	< 0.001
Parous	59 (69 %)	113 (68 %)	
Unknown	3 (3 %)	31 (19 %)	
Mammography Related Characteristics			
MPD	25.0 (1.7)	29.5 (1.3)	0.043
Total Area (cm ²)	192.0 (12.5)	187.5 (6.0)	0.713
Dense Area (cm ²), n=84, 165	38.8 (2.5)	49.9 (2.5)	0.006
Non-Dense Area (cm ²)	153.7 (12.4)	137.9 (6.0)	0.197
UST Related Characteristics			
VASS (km/s)	1.448 (0.003)	1.440 (0.002)	0.210
Dense SS (km/s), n=84, 163	1.495 (0.003)	1.496 (0.002)	0.693
Non-Dense SS (km/s) , n=84, 163	1.438 (0.003)	1.435 (0.003)	0.417
USTPD, n=84, 163	18.0 (1.1)	17.7 (0.7)	0.778
Total Volume (cm ³), n=84, 163	3084 (219)	3281 (151)	0.453
Dense Volume (cm ³), n=84, 163	428 (32)	503 (27)	0.088
Non-Dense Volume (cm ³), n=84, 163	2656 (206)	2778 (139)	0.617
Patient Related Characteristics			
Age (years)	44.5 (1.2)	47.4 (0.8)	0.036
Height (m), n=82, 153	1.63 (0.01)	1.63 (0.01)	0.471
Weight (kg), n=84, 160	74.4 (1.8)	81.6 (1.3)	0.001
BMI, n=82, 152	28.3 (0.7)	30.3 (0.5)	0.024
Age at Menarche (years), n=79, 132	12.3 (0.2)	12.7 (0.2)	0.127
Age at First Birth (years), n=59, 112	21.6 (0.7)	21.4 (0.6)	0.885
Age at Menopause (years), n=17, 35	42.8 (1.7)	44.4 (1.1)	0.428

^aP is a p-value from the chi-squared test for menopausal status, race, family history and parity; two sample independent t-test for all Mammography, UST and Patient related characteristics.

Table 3-3 – Patient Characteristics – Menopausal Status

	Count (%) or Mean (SEM)		
	Post (n = 86)	Pre (n = 154)	P ^a
Mammogram			
Digital	26 (30 %)	57 (37 %)	0.290
Film	60 (70 %)	97 (63 %)	
Race			
African-American	54 (63 %)	102 (66 %)	0.832
Unknown/Other	15 (17 %)	26 (17 %)	
White	17 (20 %)	26 (17 %)	
Family History of Cancer			
No	64 (74%)	102 (66 %)	0.419
Unknown	7 (8 %)	16 (10 %)	
Yes	15 (17 %)	36 (23 %)	
Parity			
Nulliparous	10 (12 %)	34 (22 %)	0.125
Parous	66 (77 %)	102 (66 %)	
Unknown	10 (12 %)	18 (12 %)	
Mammography Related Characteristics			
MPD	23.8 (1.8)	30.1 (1.4)	0.005
Total Area (cm ²)	204.3 (10.8)	181.2 (6.9)	0.062
Dense Area (cm ²), n=84, 154	42.3 (3.2)	48.0 (2.5)	0.165
Non-Dense Area (cm ²)	163.0 (11.0)	133.2 (6.8)	0.016
UST Related Characteristics			
VASS (km/s)	1.435 (0.002)	1.447 (0.002)	< 0.001
Dense SS (km/s), n=85, 151	1.490 (0.003)	1.498 (0.002)	0.016
Non-Dense SS (km/s) , n=85, 151	1.429 (0.003)	1.439 (0.002)	0.012
USTPD, n=85, 151	15.7 (1.0)	18.6 (0.8)	0.025
Total Volume (cm ³), n=85, 151	3558 (229)	3065 (152)	0.064
Dense Volume (cm ³), n=85, 151	468 (38)	477 (24)	0.828
Non-Dense Volume (cm ³), n=85, 151	3091 (212)	2588 (141)	0.042
Patient Related Characteristics			
Age (years)	56.0 (1.0)	40.9 (0.6)	< 0.001
Height (m), n=82, 146	1.62 (0.01)	1.63 (0.01)	0.320
Weight (kg), n=85, 150	78.5 (1.8)	79.3 (1.4)	0.735
BMI, n=82, 145	29.8 (0.6)	29.5 (0.6)	0.794
Age at Menarche (years), n=78, 130	12.5 (0.2)	12.6 (0.2)	0.562
Age at First Birth (years), n=66, 101	20.6 (0.6)	21.8 (0.6)	0.196
Age at Menopause (years)	N/A	N/A	N/A

^aP is a p-value from the chi-squared test for mammogram, race, family history and parity; two sample independent t-test for all Mammography, UST and Patient related characteristics.

3.1.3 Patient Characteristics – Race

The race statistics of the cohort reflect those of the local general population. The metropolitan Detroit area in southeast Michigan is a predominantly African-American region and this is reflected in the enrollment. Of the 251 patients, there were 161 African-Americans, 47 White and 43 women who were another race or whose race was unknown. This last group of women was excluded in this section of the analysis. Table 3-4 shows the statistical breakdown by race and several important mammographic and UST-related statistics along with the results of chi-squared and independent t-tests. The use of UST could be useful in clarifying the uncertain relationship between race and breast density.

3.1.4 Patient Characteristics – Family History of Breast Cancer

Family history of breast cancer is another well-known breast cancer risk factor. Of the 251 patients, 169 had no family history of the disease while 52 patients had a first degree relative with breast cancer. A further 30 patients were unaware if they had a family member with cancer and they were excluded in this analysis. The mammography and UST results are shown below in Table 3-5. Since family history is a breast cancer risk factor, breast density should be greater for women with a family history of breast cancer. An increase in density could be a factor that causes an increased risk of breast cancer for those with a family history.

Table 3-4 – Patient Characteristics – Race

	Count (%) or Mean (SEM)		
	AA (n = 161)	White (n = 47)	P ^a
Mammogram			
Digital	55 (34 %)	16 (34 %)	0.988
Film	106 (66 %)	31 (66 %)	
Menopausal Status			
Post	54 (34 %)	17 (36 %)	0.233
Pre	102 (63 %)	26 (55 %)	
Unknown	5 (3 %)	4 (9 %)	
Family History of Cancer			
No	104 (65 %)	31 (66 %)	0.795
Unknown	23 (14 %)	5 (11 %)	
Yes	34 (21 %)	11 (23 %)	
Parity			
Nulliparous	27 (17 %)	10 (21 %)	0.304
Parous	106 (66 %)	33 (70 %)	
Unknown	28 (17 %)	4 (9 %)	
Mammography Related Characteristics			
MPD	29.2 (1.4)	25.1 (2.1)	0.154
Total Area (cm ²)	197.9 (7.6)	174.5 (12.4)	0.134
Dense Area (cm ²), n=160, 47	50.5 (2.6)	37.4 (2.9)	0.011
Non-Dense Area (cm ²)	147.7 (7.6)	137.1 (12.4)	0.497
UST Related Characteristics			
VASS (km/s)	1.444 (0.002)	1.438 (0.003)	0.187
Dense SS (km/s), n=157, 47	1.496 (0.002)	1.491 (0.003)	0.198
Non-Dense SS (km/s) , n=157, 47	1.437 (0.002)	1.432 (0.003)	0.274
USTPD, n=157, 47	18.3 (0.8)	16.1 (1.2)	0.188
Total Volume (cm ³), n=157, 47	3463 (163)	2587 (234)	0.008
Dense Volume (cm ³), n=157, 47	527 (29)	339 (25)	< 0.001
Non-Dense Volume (cm ³), n=157, 47	2936 (152)	2248 (223)	0.025
Patient Related Characteristics			
Age (years)	46.1 (0.8)	46.3 (1.7)	0.873
Height (m), n=151, 44	1.63 (0.01)	1.63 (0.01)	0.910
Weight (kg), n=159, 44	80.0 (1.3)	79.5 (2.9)	0.858
BMI, n=151, 43	30.0 (0.5)	29.7 (1.0)	0.790
Age at Menarche (years), n=131, 41	12.4 (0.2)	12.7 (0.3)	0.375
Age at First Birth (years), n=106, 33	20.6 (0.6)	24.0 (0.9)	0.003
Age at Menopause (years), n=32, 11	43.8 (1.1)	43.4 (2.4)	0.836

^aP is a p-value from the chi-squared test for mammogram, menopause status, family history and parity; two sample independent t-test for all Mammography, UST and Patient related characteristics.

Table 3-5 – Patient Characteristics – Family History of Breast Cancer

	Count (%) or Mean (SEM)		
	No History (n = 169)	Positive Family History (n = 52)	P ^a
Mammogram			
Digital	63 (37 %)	21 (40 %)	0.687
Film	106 (63 %)	31 (60 %)	
Menopausal Status			
Post	64 (38 %)	15 (29 %)	0.494
Pre	102 (60 %)	36 (69 %)	
Unknown	3 (2 %)	1 (2%)	
Race			
African-American	104 (62 %)	34 (65 %)	0.546
Unknown/Other	34 (20 %)	7 (14 %)	
White	31 (18 %)	11 (21 %)	
Parity			
Nulliparous	34 (20 %)	11 (21 %)	0.329
Parous	128 (76 %)	41 (79 %)	
Unknown	7 (4 %)	0 (0 %)	
Mammography Related Characteristics			
MPD	27.3 (1.3)	29.8 (2.4)	0.347
Total Area (cm ²)	188.5 (7.4)	179.8 (10.9)	0.554
Dense Area (cm ²), n=169, 50	43.0 (2.0)	49.1 (4.1)	0.152
Non-Dense Area (cm ²)	145.6 (7.5)	132.6 (11.1)	0.383
UST Related Characteristics			
VASS (km/s)	1.444 (0.002)	1.445 (0.004)	0.824
Dense SS (km/s), n=166, 51	1.496 (0.002)	1.500 (0.003)	0.279
Non-Dense SS (km/s), n=166, 51	1.438 (0.002)	1.438 (0.005)	0.962
USTPD, n=166, 51	17.2 (0.7)	19.8 (1.3)	0.101
Total Volume (cm ³), n=166, 51	3155 (152)	3070 (290)	0.789
Dense Volume (cm ³), n=166, 51	438 (23)	509 (44)	0.139
Non-Dense Volume (cm ³), n=166, 51	2718 (144)	2561 (265)	0.600
Patient Related Characteristics			
Age (years)	46.7 (0.8)	45.5 (1.4)	0.481
Height (m), n=165, 51	1.63 (0.01)	1.63 (0.01)	0.778
Weight (kg), n=166, 51	77.7 (1.3)	80.0 (2.6)	0.401
BMI, n=164, 50	29.4 (0.5)	30.1 (1.0)	0.471
Age at Menarche (years), n=158, 51	12.6 (0.2)	12.4 (0.3)	0.403
Age at First Birth (years), n=127, 41	21.4 (0.5)	21.6 (0.8)	0.811
Age at Menopause (years), n=38, 10	44.4 (1.1)	42.1 (2.1)	0.315

^aP is a p-value from the chi-squared test for mammogram, menopause status, race and parity; two sample independent t-test for all Mammography, UST and Patient related characteristics.

Table 3-6 – Patient Characteristics – Parity

	Count (%) or Mean (SEM)		
	Nulliparous (n = 45)	Parous (n = 172)	P ^a
Mammogram			
Digital	23 (51 %)	59 (34 %)	0.038
Film	22 (49 %)	113 (66 %)	
Menopausal Status			
Post	10 (22 %)	66 (38 %)	0.125
Pre	34 (76 %)	102 (59 %)	
Unknown	1 (2 %)	4 (2 %)	
Race			
African-American	27 (60 %)	106 (62 %)	0.896
Unknown/Other	8 (18 %)	33 (19 %)	
White	10 (22 %)	33 (19 %)	
Family History of Cancer			
No	34 (76 %)	128 (74 %)	0.671
Unknown	0 (0 %)	3 (2 %)	
Yes	11 (24 %)	41 (24 %)	
Mammography Related Characteristics			
MPD	29.9 (2.5)	27.3 (1.3)	0.345
Total Area (cm ²)	180.5 (17.5)	188.2 (6.6)	0.622
Dense Area (cm ²), n=45, 170	42.3 (3.6)	44.6 (2.1)	0.668
Non-Dense Area (cm ²)	137.8 (17.3)	144.1 (6.7)	0.691
UST Related Characteristics			
VASS (km/s)	1.449 (0.004)	1.443 (0.002)	0.138
Dense SS (km/s), n=45, 168	1.500 (0.004)	1.495 (0.002)	0.185
Non-Dense SS (km/s), n=45, 168	1.441 (0.005)	1.437 (0.002)	0.333
USTPD, n=45, 168	19.6 (1.5)	17.4 (0.7)	0.166
Total Volume (cm ³), n=45, 168	2778 (301)	3203 (150)	0.198
Dense Volume (cm ³), n=45, 168	413 (34)	463 (25)	0.328
Non-Dense Volume (cm ³), n=45, 168	2365 (285)	2739 (140)	0.226
Patient Related Characteristics			
Age (years)	42.4 (1.6)	47.1 (0.8)	0.008
Height (m), n=45, 168	1.62 (0.01)	1.63 (0.01)	0.273
Weight (kg), n=45, 168	77.0 (2.9)	79.3 (1.3)	0.438
BMI, n=45, 166	29.5 (1.1)	29.8 (0.5)	0.766
Age at Menarche (years), n=43, 166	11.7 (0.2)	12.8 (0.2)	0.002
Age at First Birth (years)	N/A	N/A	N/A
Age at Menopause (years), n=6, 42	46.0 (1.9)	43.7 (1.0)	0.417

^aP is a p-value from the chi-squared test for mammogram, menopause status, race and family history; two sample independent t-test for all Mammography, UST and Patient related characteristics.

3.1.5 Patient Characteristics – Parity

Parity is a factor in women that affects their hormonal levels and therefore could potentially have an effect on their breast densities. Of the 251 patients, 45 women were nulliparous (gave birth to no children) while 172 were parous (gave birth to at least one child). The parity of the final 34 women was not known and their results were not included in this analysis. Table 3-6 shows the mammographic and UST image analysis along with other patient characteristics. The nulliparous women have not given birth to a child, so calculating their age at first birth is obviously impossible. This category was therefore omitted from the analysis as well.

3.2 Distribution of Density Measurements

The frequency distributions for density measurements by both imaging modalities were also calculated and shown below in Figure 3-1. Each plot also includes a normal distribution overlaid on the measured data that uses the calculated mean and standard deviation. To examine the effect that the mammogram type had, they were separated accordingly. VASS and MPD are both positively skewed, but sound speed measurements are more strongly skewed than MPD measurements. The VASS is more sharply peaked around a value of 1.43-1.44 km/s while the MPD distribution is more uniformly spread out but still biased towards lower densities.

3.2.1 Distribution of Mammographic Imaging Characteristics

Figure 3-2 shows the frequency distributions for many other imaging characteristics related to mammography. It shows the distribution of dense area, non-dense area and total area separated by mammogram type. Once again, on each plot, a normal distribution is overlaid on top of the data that was created using the calculated

mean and standard deviation for each value. Like the overall MPD and VASS measurements, the mammography characteristics are positively skewed. All values appear to be peaked more towards the lower values. The digital data appears to be more skewed than the film data.

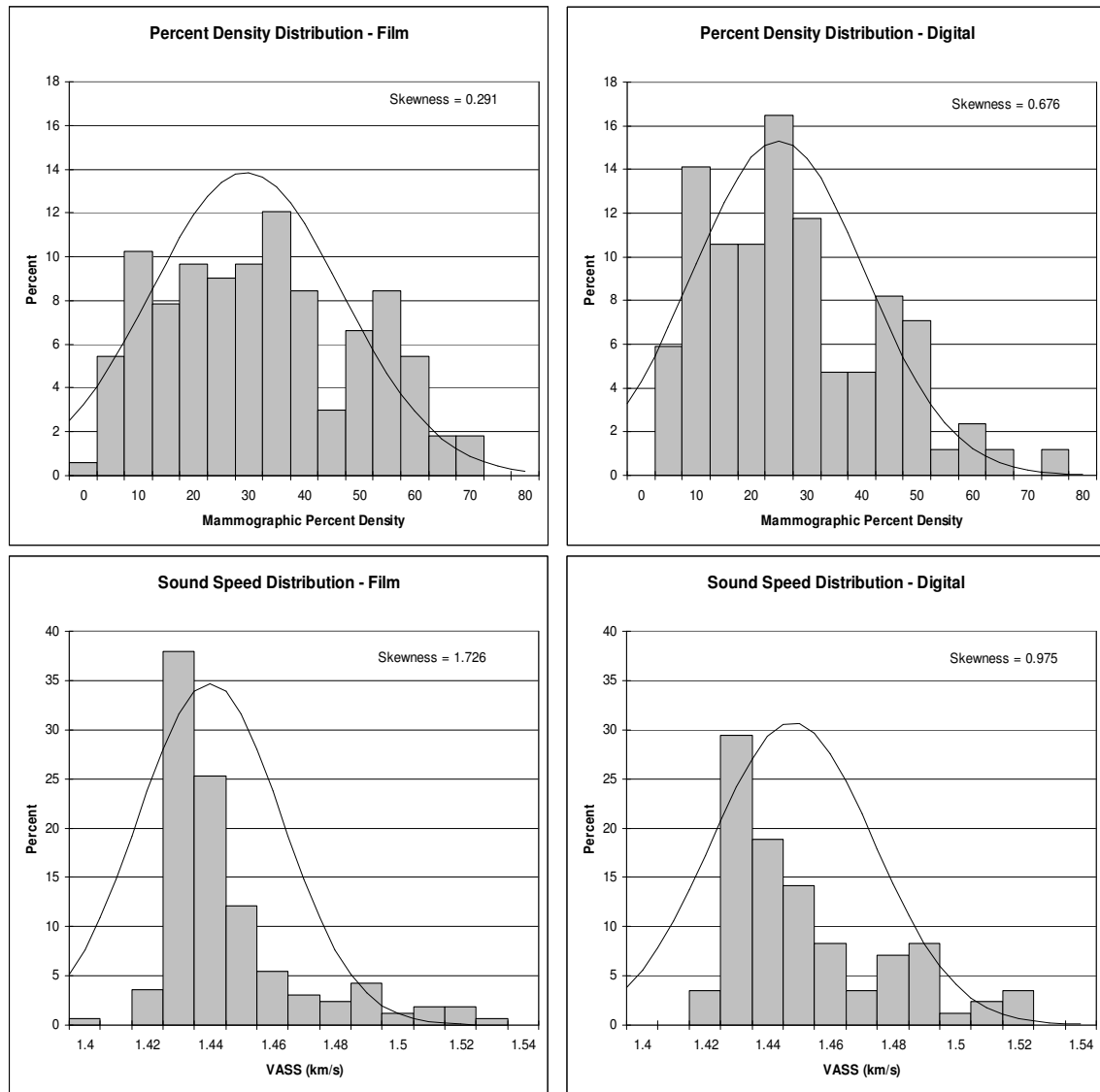


Figure 3-1 - Frequency distributions for the sound speed (VASS) and MPD measurements grouped by mammography type (bars). A normal distribution using the measured mean and standard deviation is overlaid on top of the data. For film distributions (Left), $n = 166$; for digital distributions (Right), $n = 85$.

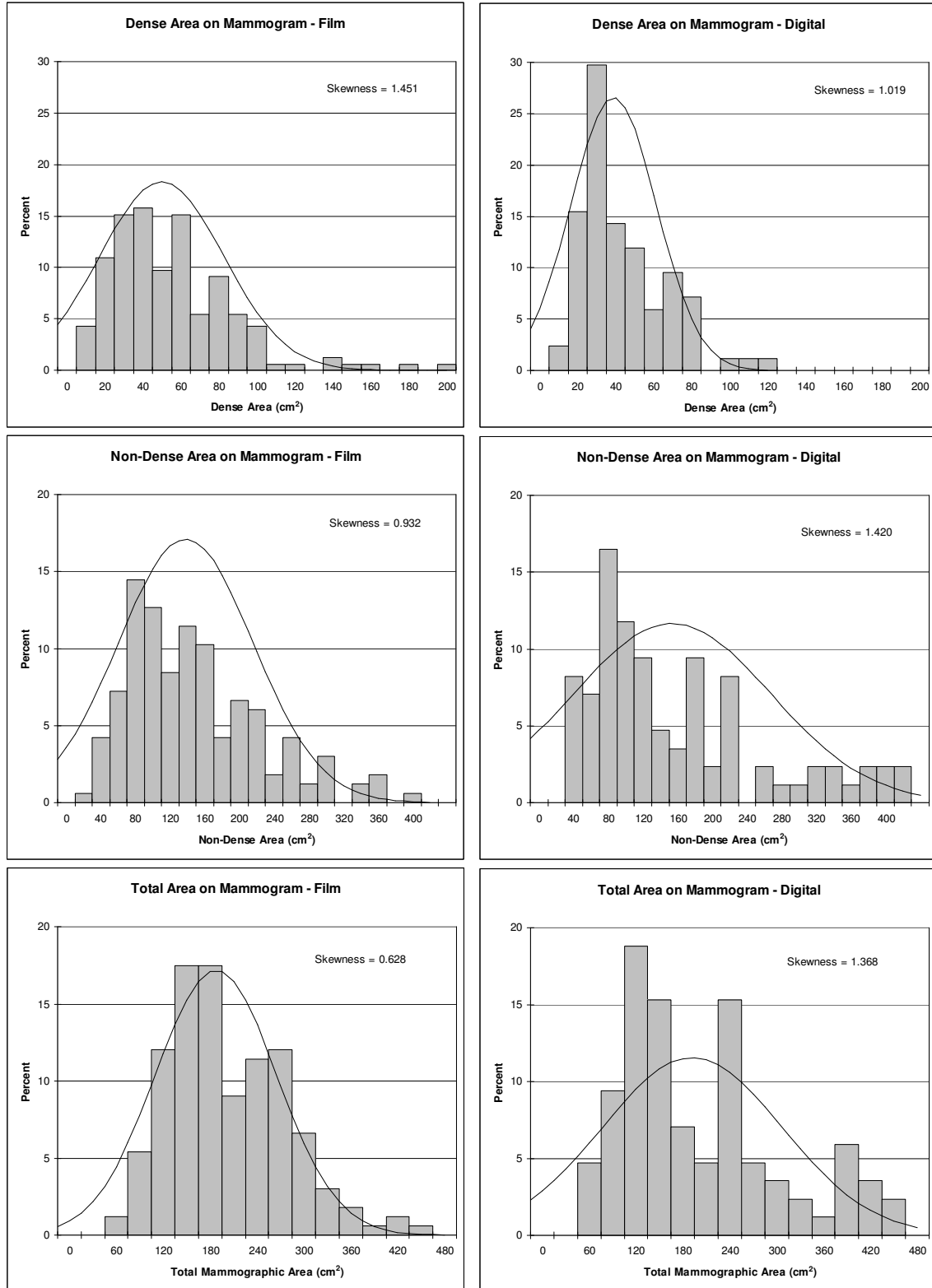


Figure 3-2 - Frequency distributions showing mammographic area measurements separated by mammogram type. A normal distribution is overlaid on each plot that was created by using the calculated mean and standard deviation. For film distributions (Left), $n = 166$; for digital distributions (Right), $n = 85$.

3.2.2 Distribution of UST Imaging Characteristics

Frequency distributions for the UST imaging characteristics were calculated and are plotted below in Figure 3-3. Since the UST characteristics were not dependent on the type of mammogram, the distributions were calculated for the entire population, $n = 247$. All distributions were positively skewed, with lower values being more common. The volume of dense tissue was the most heavily skewed, with the other volume measures and USTPD being skewed roughly the same amount. In all plots, a normal distribution was also fit using the measured mean and standard deviations.

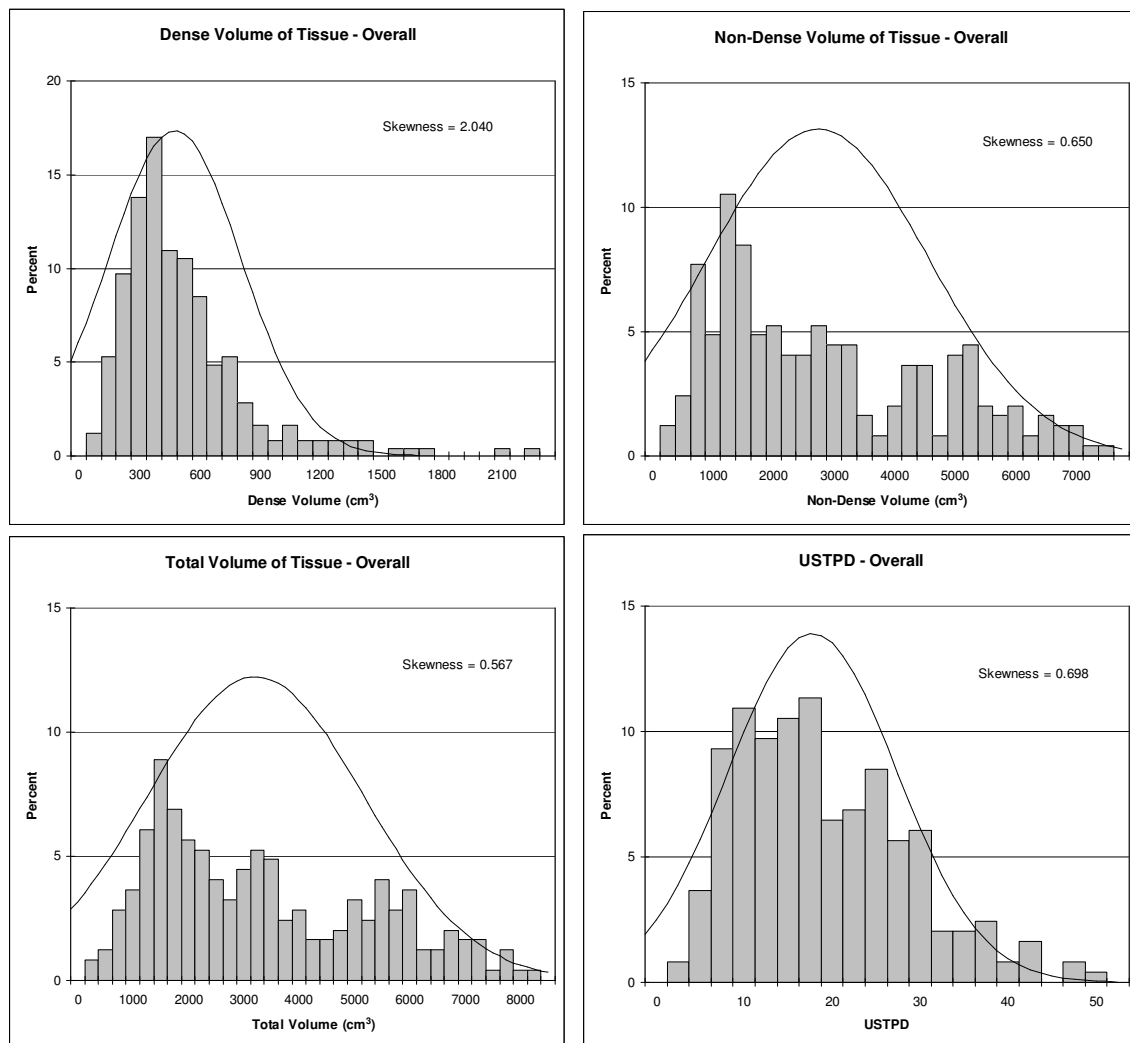


Figure 3-3 - Frequency distributions for the UST imaging characteristics for all patients with a normal distribution created by using the calculated mean and standard deviation. For all distributions, $n = 247$.

3.3 Correlations of VASS and MPD

Correlations involving the sound speed measurements and mammographic percent density were also completed using the Spearman correlation coefficient. The two different methods of calculating density, VASS and MPD, were related to many of the patient factors that were discussed above. Table 3-7 shows these correlations for the entire patient data grouped together. Grouping the data according to the groups listed before (mammogram type, menopausal status, race, family history of breast cancer and parity) was also done to see if the sub-groups showed stronger or weaker trends than the overall groups. Although there are a total of 251 patients, not all categories have data for all patients.

The strongest correlations exist between both the density measurements and many of the imaging characteristics. Strong and positive correlations are found for both VASS and MPD with USTPD, average speed of both dense and non-dense tissue and the mammographic area of dense tissue. Strong and negative correlations are found for both VASS and MPD with non-dense and total breast volume and mammographic area. There was no strong correlation found between the density measurements and total dense tissue volume however. All other patient characteristics showed weaker correlations. Age, weight and BMI were found to be moderately and negatively correlated with both density measurements, although the correlation between age and MPD was the weakest. All other characteristics were found to have no strong correlation or were not statistically significant.

Table 3-7 – VASS and MPD Correlations for All Patients

	Spearman Coefficient (p-value)	
	VASS Correlated With:	MPD Correlated With:
MPD, n=251	0.726 (<0.001)	N/A
USTPD, n=247	0.647 (<0.001)	0.648 (<0.001)
Volume of Dense Tissue (cm ³), n=247	0.070 (0.273)	0.085 (0.185)
Volume of Non-Dense Tissue (cm ³), n=247	-0.553 (<0.001)	-0.568 (<0.001)
Total Volume of Breast Tissue (cm ³), n=247	-0.497 (<0.001)	-0.509 (<0.001)
Average SS of Dense Tissue (km/s), n=247	0.765 (<0.001)	0.651 (<0.001)
Average SS of Non-Dense Tissue (km/s), n=247	0.837 (<0.001)	0.642 (<0.001)
Dense Area on Mammogram (cm ²), n=249	0.431 (<0.001)	0.731 (<0.001)
Fat Area on Mammogram (cm ²), n=251	-0.649 (<0.001)	-0.757 (<0.001)
Total Area on Mammogram (cm ²), n=251	-0.472 (<0.001)	-0.477 (<0.001)
Age of Patient (years), n=251	-0.314 (<0.001)	-0.167 (0.008)
Weight of Patient (kg), n=244	-0.440 (<0.001)	-0.402 (<0.001)
Height of Patient (cm), n=235	-0.052 (0.425)	-0.066 (0.311)
Body Mass Index (BMI), n=233	-0.441 (<0.001)	-0.382 (<0.001)
Age at Menarche (years), n=211	0.111 (0.106)	0.161 (0.020)
Age at Birth of First Child (years), n=171	0.013 (0.863)	0.104 (0.176)
Age at Menopause (years), n=52	0.056 (0.691)	0.118 (0.405)

A direct comparison between the two different imaging modalities is the comparison of the VASS and MPD. Both these values are representations of the same quantity, breast density, but expressed in two different methods. VASS is a volumetric and quantitative analysis of the density, while MPD is the standard method, but a two-dimensional assessment. The plot of VASS versus MPD for all the patients is shown below in Figure 3-4. The Spearman correlation coefficient between these two values was found to be $r_s = 0.726$ (p-value < 0.001). This is a strong correlation and it suggests that

measurement of breast density using the VASS and UST is comparable to the measurement of density using mammography and MPD.

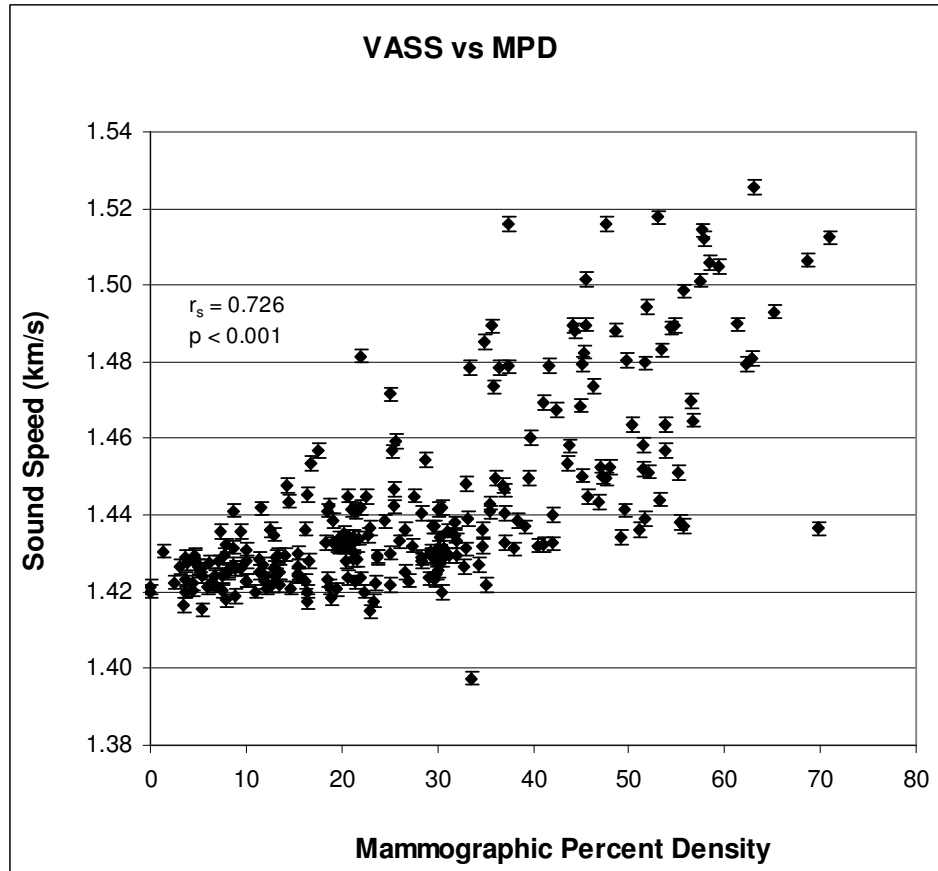


Figure 3-4 - Plot of volume averaged sound speed (VASS) as measured by UST compared to the mammographic percent density (MPD) as measured by mammography for all patients, $n = 251$.

3.3.1 Correlations of VASS and MPD – Type of Mammogram

The data were once again separated into groups and the correlations between both VASS and MPD were recalculated. Table 3-8 shows these correlations for patients grouped by the type of mammogram that was received. These correlations could show whether or not there is any systematic difference between digital and film mammography. Any differences between the types of mammogram are likely to only be evident when comparing the correlations involving the MPD. The type of image receptor used may affect the measurement of the percent density, so only the correlations

involving MPD are considered. Of the 251 patients enrolled, 166 received a film mammogram and 85 received a digital mammogram.

Table 3-8 – MPD Correlations – Type of Mammogram

MPD Correlated With:	Spearman Correlation Coefficient (p-value)	
	Film	Digital
VASS, n=166, 85	0.794 (< 0.001)	0.706 (< 0.001)
USTPD, n=163, 84	0.608 (< 0.001)	0.747 (< 0.001)
Volume of Dense Tissue (cm ³), n=163, 84	0.064 (0.416)	0.104 (0.346)
Volume of Non-Dense Tissue (cm ³), n=163, 84	-0.549 (< 0.001)	-0.642 (< 0.001)
Total Breast Volume (cm ³), n=163, 84	-0.485 (< 0.001)	-0.585 (< 0.001)
SS of Dense Tissue (km/s), n=163, 84	0.662 (< 0.001)	0.624 (< 0.001)
SS of Non-Dense Tissue (km/s), n=163,84	0.687 (< 0.001)	0.607 (< 0.001)
Area of Dense Tissue (cm ²), n=165, 84	0.755 (< 0.001)	0.612 (< 0.001)
Area of Non-Dense Tissue (cm ²), n=166, 85	-0.774 (< 0.001)	-0.764 (< 0.001)
Total Breast Area (cm ²), n=166, 85	-0.436 (< 0.001)	-0.576 (< 0.001)
Age (years), n=166, 85	-0.253 (< 0.001)	-0.057 (0.605)
Weight (kg), n=160, 84	-0.393 (< 0.001)	-0.529 (< 0.001)
Height (cm), n=153, 82	-0.134 (0.099)	0.055 (0.624)
Body Mass Index (BMI), n=151, 82	-0.344 (< 0.001)	-0.567 (< 0.001)
Age at Start of Menarche (years), n=132, 79	0.116 (0.186)	0.191 (0.091)
Age at Birth of First Child (years), n=112, 59	0.136 (0.154)	0.033 (0.807)
Age at Start of Menopause (years), n=35, 17	0.104 (0.554)	0.178 (0.495)

When separating by mammogram group, the same general trends hold overall. The strongest correlations once again are between the density measurements and the different imaging characteristics with the exception of the volume of dense tissue. Most of the correlations are of similar strength between the two different types of mammography, with a few small exceptions. Digital MPD had a stronger correlation

with USTPD when compared to the film measurements (r_s of 0.747 compared to r_s of 0.608). Dense area correlated to MPD more strongly on film than on digital images (r_s of 0.755 compared to r_s of 0.612). Most of the non-imaging characteristics showed weak or statistically insignificant results. Age, weight and BMI all showed negative and moderate correlations with density measurements made by both types of mammography once again.

The plot of VASS versus MPD for patients receiving film and digital mammograms is shown in Figure 3-5. The Spearman correlation coefficients for the plots are 0.794 for patients that received a film mammogram and 0.706 for patients that received a digital mammogram. This indicates that a strong and positive correlation between VASS and MPD exists. The correlation is slightly stronger for film mammography than it is for digital mammography. The relationship between VASS and MPD appears to be more curvilinear for the film mammograms than it is for the digital mammograms. This may be due to the x-ray response of the detector being used. Film detectors show a sigmoidal response to x-rays while digital detectors have a linear response.

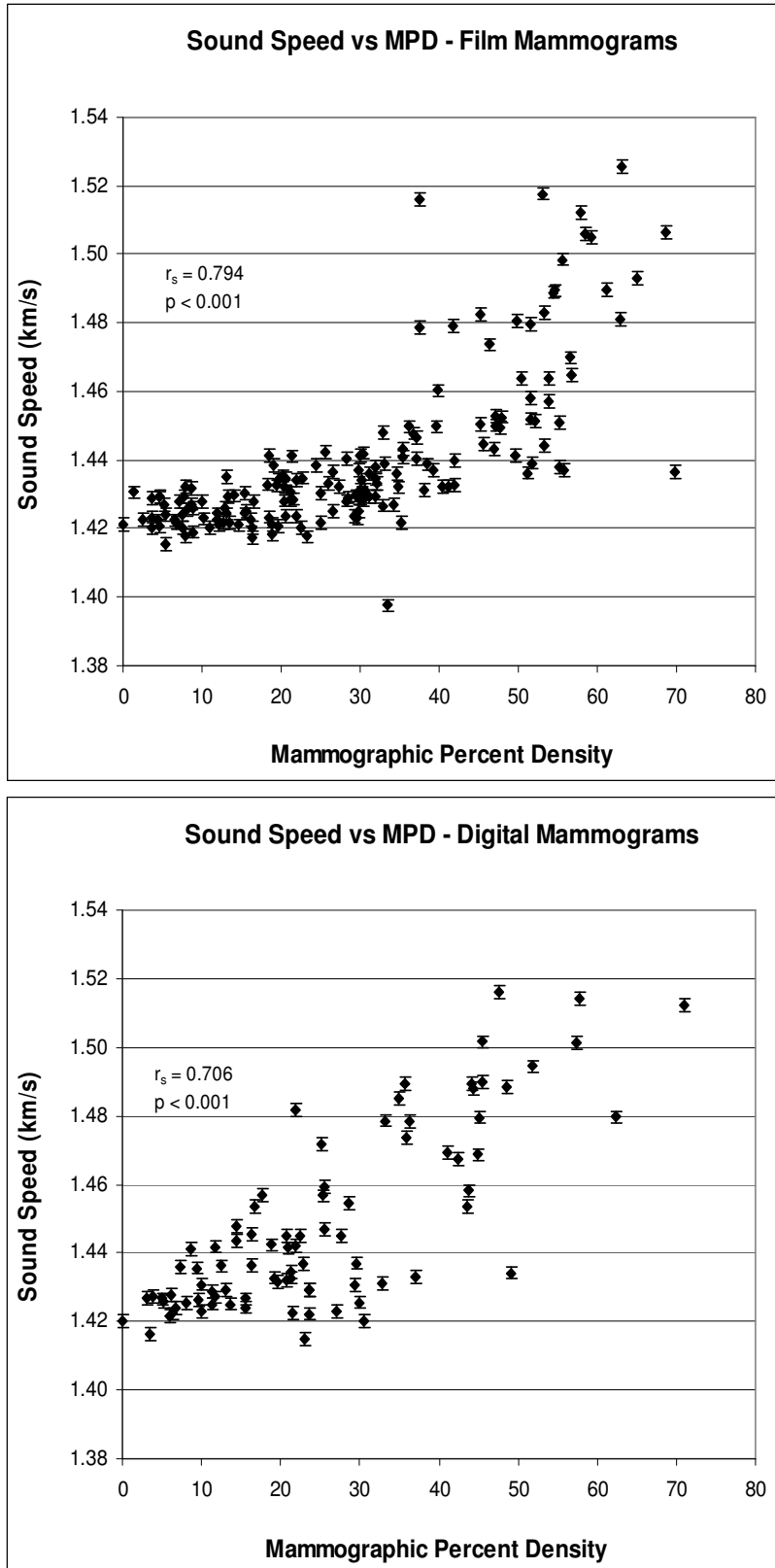


Figure 3-5 - Plots of the UST measured sound speed versus the mammographic percent density grouped according to the type of mammogram received. Top: Film, $n = 166$; Bottom: Digital, $n = 85$

Some studies¹⁵² have also suggested that the relationship between a volumetric- (VASS) and area-based (MPD) density measurement may in fact be curvilinear. This was tested here by performing both linear and non-linear regression on the data. A slightly stronger fit was observed when using a 2nd degree polynomial compared to a linear fit. For patients receiving digital mammograms, the R^2 value increased to 0.640 from 0.630 when moving to a 2nd degree polynomial from a linear fit, while the R^2 value increased to 0.606 from 0.542 for patients that received a film mammogram. The effect was stronger for patients that received a film mammogram, which suggests that the x-ray response of film may be the reason. For film mammograms, the sound speed shows a narrow range for patients with low MPD's. For patients with an MPD of less than ~35%, the sound speed has a range of about 1.42 to 1.44 km/s. The range is much wider for MPD's greater than 35%, ranging from 1.44 km/s to 1.52 km/s. The digital response is much more linear, so this further suggests the detector x-ray response is responsible for the shape of the curve.

3.3.2 Correlations of VASS and MPD – Menopausal Status

The data were grouped according to menopausal status and correlations were then performed. Since menopausal status is known to affect breast density and breast cancer risk, it may also affect the strength of the correlations. Of the 251 patients enrolled, 86 were post-menopausal and 154 were pre-menopausal. The menopausal status of the remaining women was not known and was not included in this analysis. Table 3-9 shows the correlations between the patient characteristics and both density measurements grouped by menopausal status. Since pre-menopausal women have obviously not reached menopause, the correlation with age at menopause could not be calculated.

Table 3-9 – VASS and MPD Correlations – Menopausal Status

VASS Correlated With:	Spearman Correlation Coefficient (p-value)	
	Post	Pre
MPD, n=86, 154	0.669 (< 0.001)	0.727 (< 0.001)
USTPD, n=85, 151	0.612 (< 0.001)	0.682 (< 0.001)
Volume of Dense Tissue (cm ³), n=85, 151	0.142 (0.196)	-0.036 (0.661)
Volume of Non-Dense Tissue (cm ³), n=85, 151	-0.499 (< 0.001)	-0.629 (< 0.001)
Total Breast Volume (cm ³), n=85, 151	-0.430 (< 0.001)	-0.581 (< 0.001)
SS of Dense Tissue (km/s), n=85, 151	0.665 (< 0.001)	0.779 (< 0.001)
SS of Non-Dense Tissue (km/s), n=85, 151	0.689 (< 0.001)	0.898 (< 0.001)
Area of Dense Tissue (cm ²), n=84, 154	0.464 (< 0.001)	0.387 (< 0.001)
Area of Non-Dense Tissue (cm ²), n=86, 154	-0.585 (< 0.001)	-0.686 (< 0.001)
Total Breast Area (cm ²), n=86, 154	-0.410 (< 0.001)	-0.514 (< 0.001)
Age (years), n=86, 154	-0.140 (0.198)	-0.110 (0.174)
Weight (kg), n=85, 150	-0.295 (0.006)	-0.562 (< 0.001)
Height (cm), n=82, 146	-0.007 (0.951)	-0.118 (0.156)
Body Mass Index (BMI), n=82, 144	-0.303 (0.006)	-0.536 (< 0.001)
Age at Menarche (years), n=78, 130	0.134 (0.242)	0.106 (0.230)
Age at Birth of First Child (years), n=66, 101	-0.070 (0.578)	0.045 (0.653)
Age at Menopause (years), n=52	0.056 (0.691)	N/A
MPD Correlated With:		
USTPD, n=85, 151	0.638 (< 0.001)	0.616 (< 0.001)
Volume of Dense Tissue (cm ³), n=85, 151	0.076 (0.490)	0.029 (0.724)
Volume of Non-Dense Tissue (cm ³), n=85, 151	-0.571 (< 0.001)	-0.571 (< 0.001)
Total Breast Volume (cm ³), n=85, 151	-0.508 (< 0.001)	-0.522 (< 0.001)
SS of Dense Tissue (km/s), n=85, 151	0.576 (< 0.001)	0.670 (< 0.001)
SS of Non-Dense Tissue (km/s), n=85, 151	0.560 (< 0.001)	0.673 (< 0.001)
Area of Dense Tissue (cm ²), n=84, 154	0.800 (< 0.001)	0.688 (< 0.001)
Area of Non-Dense Tissue (cm ²), n=86, 154	-0.758 (< 0.001)	-0.755 (< 0.001)
Total Breast Area (cm ²), n=86, 154	-0.495 (< 0.001)	-0.466 (< 0.001)
Age (years), n=86, 154	-0.178 (0.101)	0.020 (0.801)
Weight (kg), n=85, 150	-0.315 (0.003)	-0.459 (< 0.001)
Height (cm), n=82, 146	-0.008 (0.946)	-0.125 (0.134)
Body Mass Index (BMI), n=82, 144	-0.323 (0.003)	-0.404 (< 0.001)
Age at Menarche (years), n=78, 130	0.226 (0.047)	0.123 (0.163)
Age at Birth of First Child (years), n=66, 101	0.135 (0.279)	0.046 (0.646)
Age at Menopause (years), n=52	0.118 (0.405)	N/A

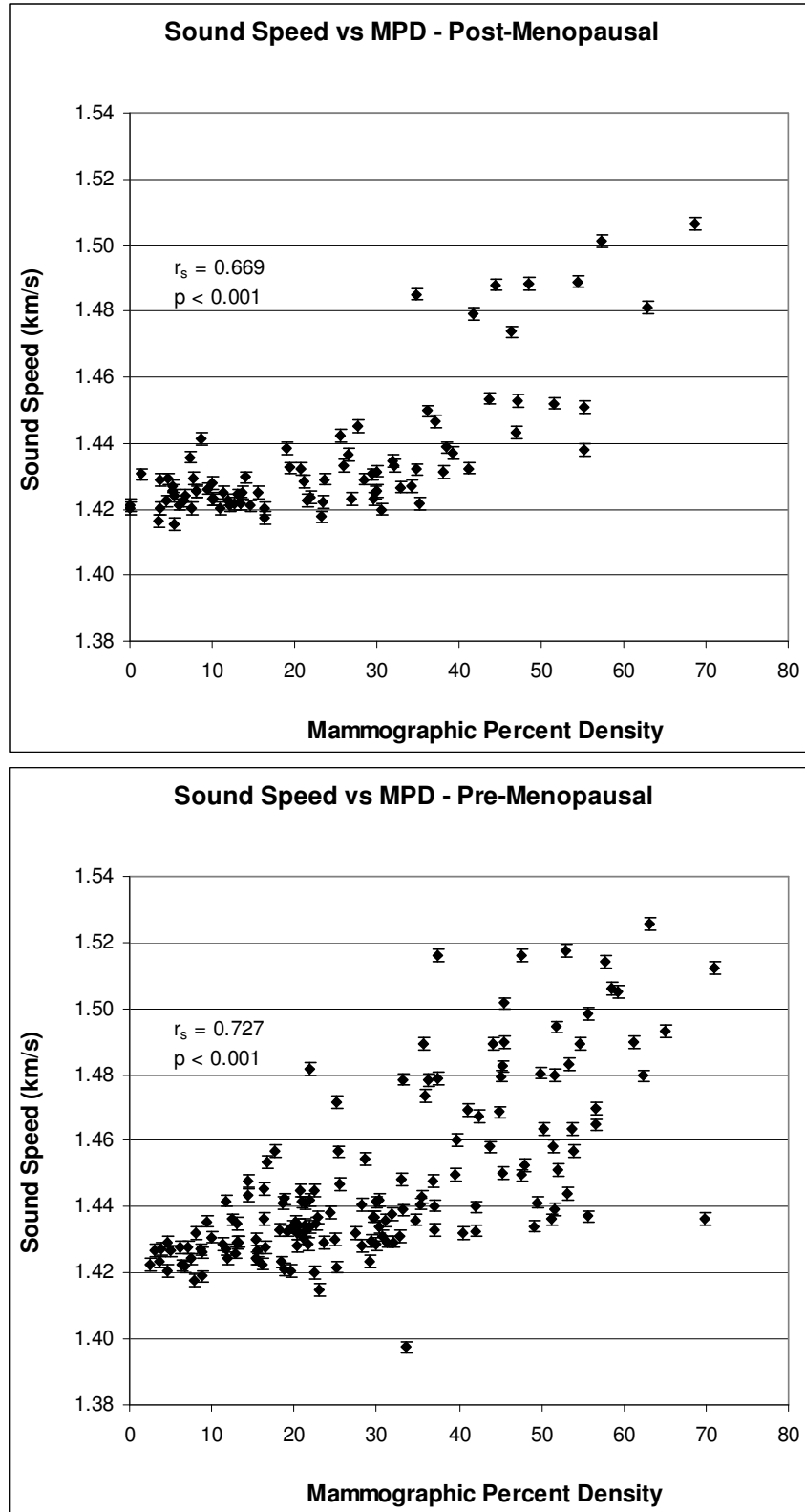


Figure 3-6 - Plot of sound speed versus mammographic density grouped by menopause status. Top: Post-menopausal women, $n = 86$; Bottom: Pre-menopausal women, $n = 154$.

The same general trends remain the same for these groups. The strongest correlations exist between both density measurements and the imaging characteristics with the exception of the volume of dense tissue, which shows a statistically irrelevant correlation. Of the patient-specific characteristics, age, weight and BMI show moderate correlations with all other factors either showing no relation or are statistically uncertain. When comparing the two groups, most of the correlations involving the VASS are stronger for the pre-menopausal women. For the correlations involving MPD, both groups tend to show correlations of similar strength. The plot of the VASS versus the MPD is shown below in Figure 3-6 for both groups. Both groups are mixed with patients who received film and digital mammograms; the plot relating the two density measurements is not linear.

3.3.3 Correlations of VASS and MPD – Race

The data were then grouped according to race and the correlations were performed once again on both density measurements. Table 3-10 shows the results of these correlations for African-American and white patients. The same trends that existed for all the data show themselves when grouped by race. Strong correlations between the density measurements and imaging characteristics exist while moderate correlations exist with the same patient related characteristics. There is little to no difference in the strength of the correlations between races. Figure 3-7 shows the correlation between VASS and MPD grouped by race.

Table 3-10 – VASS and MPD Correlations – Race

VASS Correlated With:	Spearman Correlation Coefficient (p-value)	
	African-American	White
MPD, n=161, 47	0.720 (< 0.001)	0.706 (< 0.001)
USTPD, n=157, 47	0.673 (< 0.001)	0.517 (< 0.001)
Volume of Dense Tissue (cm ³), n=157, 47	0.057 (0.481)	0.131 (0.379)
Volume of Non-Dense Tissue (cm ³), n=157, 47	-0.578 (< 0.001)	-0.435 (0.002)
Total Breast Volume (cm ³), n=157, 47	-0.521 (< 0.001)	-0.411 (0.004)
SS of Dense Tissue (km/s), n=157, 47	0.759 (< 0.001)	0.782 (< 0.001)
SS of Non-Dense Tissue (km/s), n=157, 47	0.842 (< 0.001)	0.814 (< 0.001)
Area of Dense Tissue (cm ²), n=160, 47	0.400 (< 0.001)	0.460 (0.001)
Area of Non-Dense Tissue (cm ²), n=161, 47	-0.678 (< 0.001)	-0.567 (< 0.001)
Total Breast Area (cm ²), n=161, 47	-0.500 (< 0.001)	-0.391 (0.007)
Age (years), n=161, 47	-0.296 (< 0.001)	-0.236 (0.110)
Weight (kg), n=159, 44	-0.453 (< 0.001)	-0.445 (0.002)
Height (cm), n=151, 44	-0.018 (0.823)	-0.128 (0.406)
Body Mass Index (BMI), n=151, 43	-0.447 (< 0.001)	-0.453 (0.002)
Age at Menarche (years), n=131, 41	0.087 (0.323)	0.291 (0.065)
Age at Birth of First Child (years), n=106, 33	-0.085 (0.386)	0.376 (0.031)
Age at Menopause (years), n=32, 11	0.035 (0.849)	-0.350 (0.291)
MPD Correlated With:		
USTPD, n=157, 47	0.665 (< 0.001)	0.535 (< 0.001)
Volume of Dense Tissue (cm ³), n=157, 47	0.097 (0.228)	0.098 (0.513)
Volume of Non-Dense Tissue (cm ³), n=157, 47	-0.566 (< 0.001)	-0.494 (< 0.001)
Total Breast Volume (cm ³), n=157, 47	-0.503 (< 0.001)	-0.476 (< 0.001)
SS of Dense Tissue (km/s), n=157, 47	0.647 (< 0.001)	0.569 (< 0.001)
SS of Non-Dense Tissue (km/s), n=157, 47	0.644 (< 0.001)	0.603 (< 0.001)
Area of Dense Tissue (cm ²), n=160, 47	0.734 (< 0.001)	0.706 (< 0.001)
Area of Non-Dense Tissue (cm ²), n=161, 47	-0.749 (< 0.001)	-0.770 (< 0.001)
Total Breast Area (cm ²), n=161, 47	-0.441 (< 0.001)	-0.559 (< 0.001)
Age (years), n=161, 47	-0.157 (0.046)	0.047 (0.752)
Weight (kg), n=159, 44	-0.409 (< 0.001)	-0.480 (< 0.001)
Height (cm), n=151, 44	-0.015 (0.856)	-0.088 (0.572)
Body Mass Index (BMI), n=151, 43	-0.387 (< 0.001)	-0.511 (< 0.001)
Age at Menarche (years), n=131, 41	0.158 (0.071)	0.214 (0.179)
Age at Birth of First Child (years), n=106, 33	0.028 (0.774)	0.454 (0.008)
Age at Menopause (years), n=32, 11	0.118 (0.521)	-0.198 (0.560)

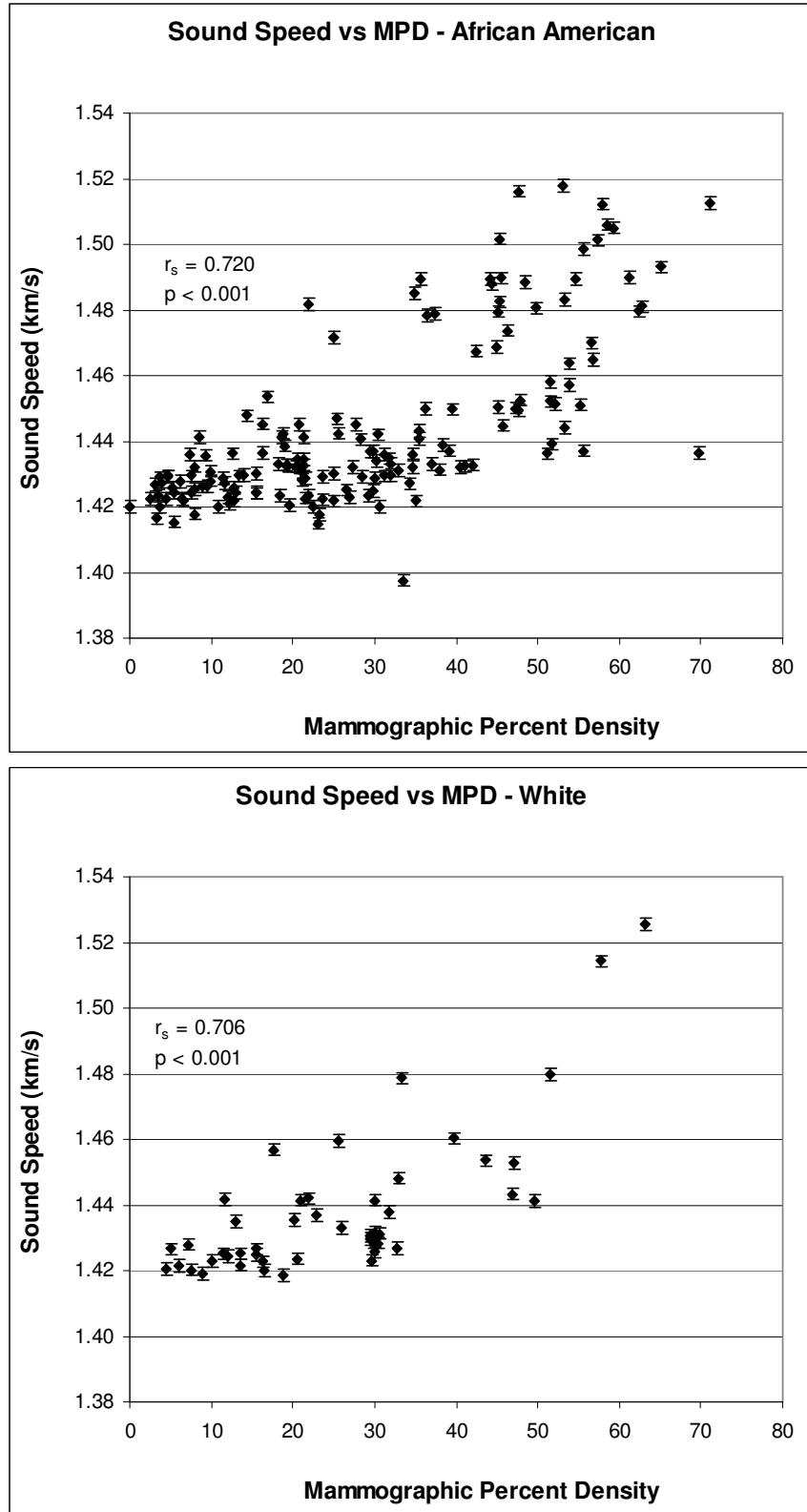


Figure 3-7 - Sound speed versus mammographic density as grouped by race. Top: African-American, $n = 161$; Bottom: White, $n = 47$

3.3.4 Correlations of VASS and MPD – Family History of Breast Cancer

Family history of breast cancer is a known risk factor for breast cancer and it is included in the Gail model. Examining the effect of family history was accomplished by calculating the correlations between the density measurements and the various imaging and patient characteristics while grouping patients with a family history and those without. Table 3-11 shows these results. The same overall trends exist once again. The strongest correlations involve the density measurements with the imaging characteristics while the select patient characteristics show moderate correlations. However, patients with a family history of breast cancer tend to show weaker correlations than those without a family history, especially for measurements made with UST. Figure 3-8 shows the plot of the VASS versus MPD grouped by family history.

3.3.5 Correlations of VASS and MPD – Parity

When a woman carries a pregnancy to full term, the hormones associated with this event can affect breast density and breast cancer risk. To see if this change is evident when measuring density, the correlations were performed but grouped according to the parity. Table 3-12 shows these results. The trends involving the imaging and patient characteristics generally behave as before. However, correlations between VASS and the various UST imaging characteristics tended to be stronger for the women who have not given birth (nulliparous). Figure 3-9 shows the plots of the VASS versus the MPD grouped by parity.

Table 3-11 – VASS and MPD Correlations – Family History of Breast Cancer

VASS Correlated With:	Spearman Correlation Coefficient (p-value)	
	Family History	No History
MPD, n=52, 169	0.603 (< 0.001)	0.769 (< 0.001)
USTPD, n=51, 166	0.567 (< 0.001)	0.707 (< 0.001)
Volume of Dense Tissue (cm ³), n=51, 166	0.021 (0.884)	0.104 (0.183)
Volume of Non-Dense Tissue (cm ³), n=51, 166	-0.530 (< 0.001)	-0.602 (< 0.001)
Total Breast Volume (cm ³), n=51, 166	-0.474 (< 0.001)	-0.543 (< 0.001)
SS of Dense Tissue (km/s), n=51, 166	0.656 (< 0.001)	0.792 (< 0.001)
SS of Non-Dense Tissue (km/s), n=51, 166	0.712 (< 0.001)	0.900 (< 0.001)
Area of Dense Tissue (cm ²), n=50, 169	0.256 (0.073)	0.484 (< 0.001)
Area of Non-Dense Tissue (cm ²), n=52, 169	-0.652 (< 0.001)	-0.671 (< 0.001)
Total Breast Area (cm ²), n=52, 169	-0.509 (< 0.001)	-0.507 (< 0.001)
Age (years), n=52, 169	-0.246 (0.079)	-0.339 (< 0.001)
Weight (kg), n=51, 166	-0.388 (0.005)	-0.463 (< 0.001)
Height (cm), n=51, 165	-0.198 (0.163)	0.019 (0.813)
Body Mass Index (BMI), n=50, 164	-0.329 (0.020)	-0.492 (< 0.001)
Age at Menarche (years), n=51, 158	0.122 (0.395)	0.129 (0.106)
Age at Birth of First Child (years), n=41, 127	0.048 (0.765)	0.009 (0.919)
Age at Menopause (years), n=10, 38	0.218 (0.545)	0.053 (0.751)
MPD Correlated With:		
USTPD, n=51, 166	0.612 (< 0.001)	0.680 (< 0.001)
Volume of Dense Tissue (cm ³), n=51, 166	0.186 (0.191)	0.038 (0.623)
Volume of Non-Dense Tissue (cm ³), n=51, 166	-0.460 (< 0.001)	-0.646 (< 0.001)
Total Breast Volume (cm ³), n=51, 166	-0.386 (0.005)	-0.594 (< 0.001)
SS of Dense Tissue (km/s), n=51, 166	0.703 (< 0.001)	0.660 (< 0.001)
SS of Non-Dense Tissue (km/s), n=51, 166	0.504 (< 0.001)	0.731 (< 0.001)
Area of Dense Tissue (cm ²), n=50, 169	0.724 (< 0.001)	0.730 (< 0.001)
Area of Non-Dense Tissue (cm ²), n=52, 169	-0.763 (< 0.001)	-0.785 (< 0.001)
Total Breast Area (cm ²), n=52, 169	-0.448 (< 0.001)	-0.552 (< 0.001)
Age (years), n=52, 169	-0.099 (0.486)	-0.177 (0.022)
Weight (kg), n=51, 166	-0.322 (0.021)	-0.475 (< 0.001)
Height (cm), n=51, 165	-0.190 (0.182)	-0.004 (0.962)
Body Mass Index (BMI), n=50, 164	-0.271 (0.057)	-0.484 (< 0.001)
Age at Menarche (years), n=51, 158	0.239 (0.091)	0.156 (0.050)
Age at Birth of First Child (years), n=41, 127	0.105 (0.514)	0.098 (0.271)
Age at Menopause (years), n=10, 38	0.321 (0.365)	0.133 (0.425)

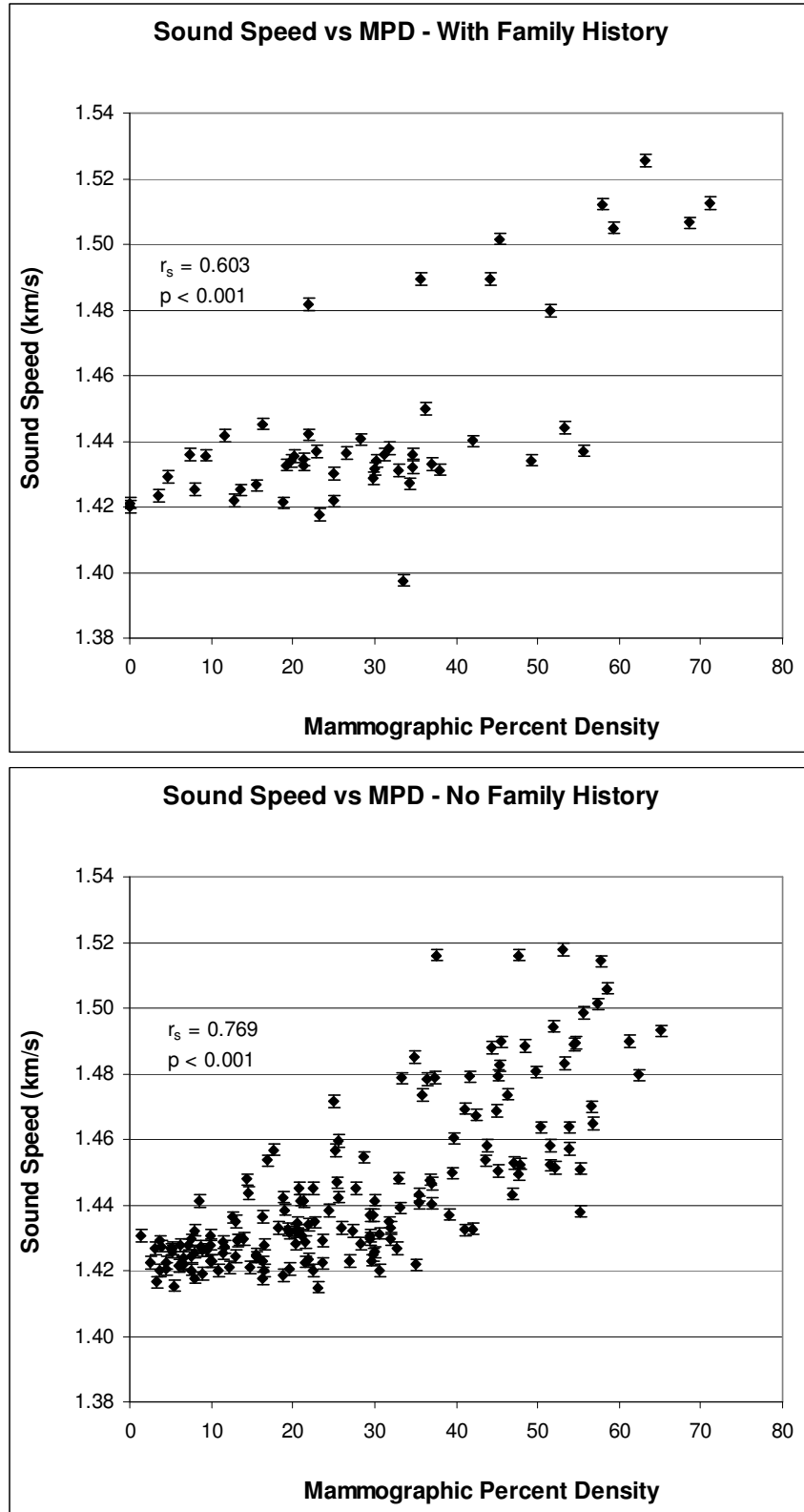


Figure 3-8 - Sound speed versus mammographic percent density for women grouped by family history of breast cancer. Top: Women with a family history of the disease, $n = 52$; Bottom: Women with no family history of the disease, $n = 169$

Table 3-12 – VASS and MPD Correlations – Parity

VASS Correlated With	Spearman Correlation Coefficient (p-value)	
	Parous	Nulliparous
MPD, n=172, 45	0.711 (< 0.001)	0.792 (< 0.001)
USTPD, n=168, 45	0.644 (< 0.001)	0.779 (< 0.001)
Volume of Dense Tissue (cm ³), n=168, 45	0.127 (0.101)	-0.076 (0.619)
Volume of Non-Dense Tissue (cm ³), n=168, 45	-0.524 (< 0.001)	-0.738 (< 0.001)
Total Breast Volume (cm ³), n=168, 45	-0.463 (< 0.001)	-0.683 (< 0.001)
SS of Dense Tissue (km/s), n=168, 45	0.751 (< 0.001)	0.871 (< 0.001)
SS of Non-Dense Tissue (km/s), n=168, 45	0.873 (< 0.001)	0.833 (< 0.001)
Area of Dense Tissue (cm ²), n=170, 45	0.427 (< 0.001)	0.450 (0.002)
Area of Non-Dense Tissue (cm ²), n=172, 45	-0.658 (< 0.001)	-0.670 (< 0.001)
Total Breast Area (cm ²), n=172, 45	-0.501 (< 0.001)	-0.504 (< 0.001)
Age (years), n=172, 45	-0.314 (< 0.001)	-0.345 (0.020)
Weight (kg), n=168, 45	-0.427 (< 0.001)	-0.464 (< 0.001)
Height (cm), n=168, 45	-0.071 (0.363)	0.138 (0.366)
Body Mass Index (BMI), n=166, 45	-0.421 (< 0.001)	-0.504 (< 0.001)
Age at Menarche (years), n=166, 43	0.130 (0.095)	0.181 (0.245)
Age at Birth of First Child (years), n=171	0.013 (0.863)	N/A
Age at Menopause (years), n=42, 6	0.118 (0.457)	-0.143 (0.787)
MPD Correlated With		
USTPD, n=168, 45	0.643 (< 0.001)	0.710 (< 0.001)
Volume of Dense Tissue (cm ³), n=168, 45	0.119 (0.125)	-0.106 (0.488)
Volume of Non-Dense Tissue (cm ³), n=168, 45	-0.555 (< 0.001)	-0.696 (< 0.001)
Total Breast Volume (cm ³), n=168, 45	-0.497 (< 0.001)	-0.671 (< 0.001)
SS of Dense Tissue (km/s), n=168, 45	0.649 (< 0.001)	0.802 (< 0.001)
SS of Non-Dense Tissue (km/s), n=168, 45	0.675 (< 0.001)	0.639 (< 0.001)
Area of Dense Tissue (cm ²), n=170, 45	0.754 (< 0.001)	0.627 (< 0.001)
Area of Non-Dense Tissue (cm ²), n=172, 45	-0.775 (< 0.001)	-0.763 (< 0.001)
Total Breast Area (cm ²), n=172, 45	-0.518 (< 0.001)	-0.542 (< 0.001)
Age (years), n=172, 45	-0.159 (0.037)	-0.238 (0.115)
Weight (kg), n=168, 45	-0.430 (< 0.001)	-0.332 (0.026)
Height (cm), n=168, 45	-0.056 (0.473)	-0.043 (0.778)
Body Mass Index (BMI), n=166, 45	-0.429 (< 0.001)	-0.304 (0.042)
Age at Menarche (years), n=166, 43	0.184 (0.018)	0.141 (0.368)
Age at Birth of First Child (years), n=171	0.104 (0.176)	N/A
Age at Menopause (years), n=42, 6	0.220 (0.161)	-0.029 (0.957)

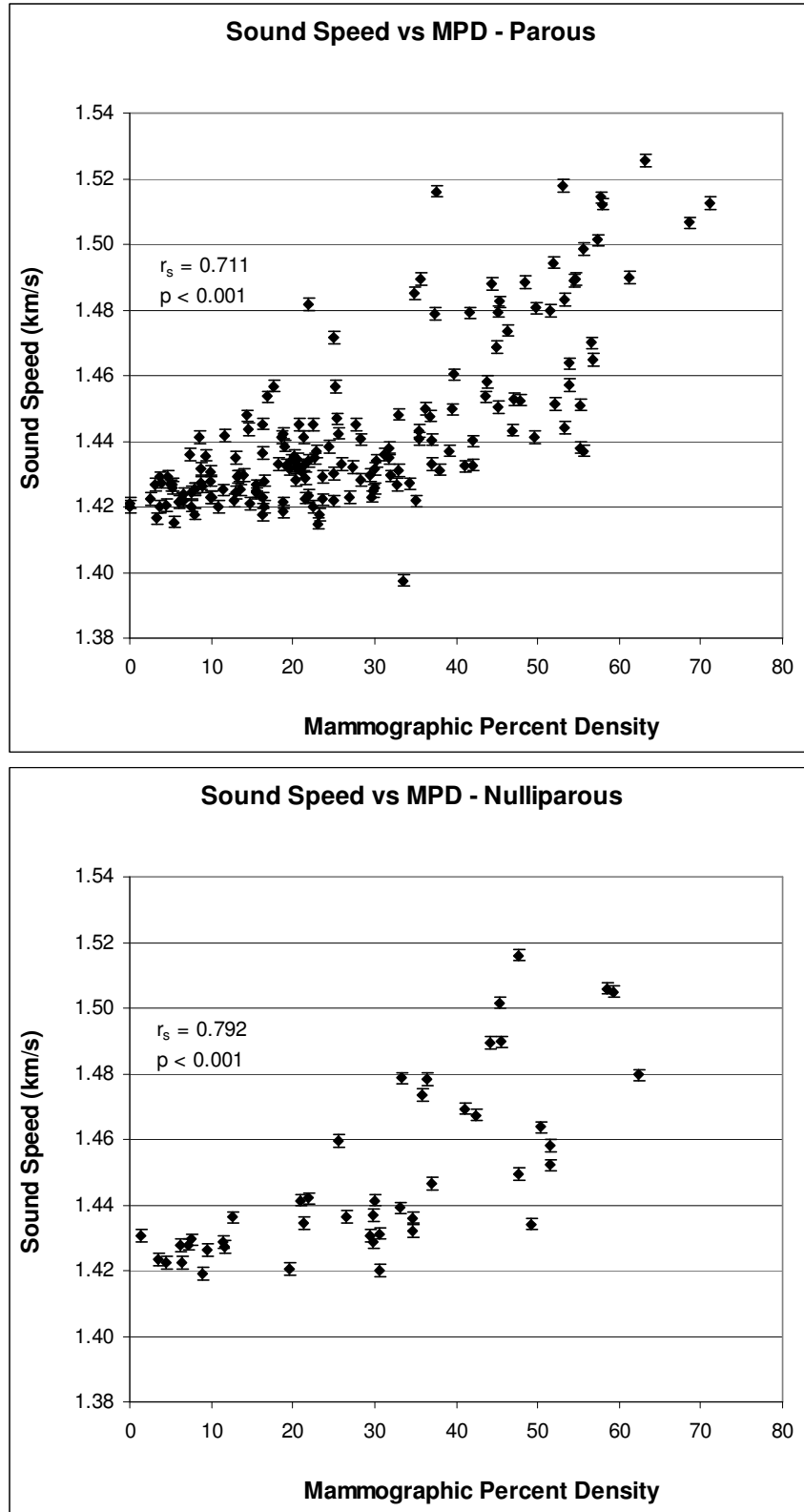


Figure 3-9 - Sound speed versus mammographic density comparisons grouped by parity. Top: Parous women (have given birth at least once), $n = 172$; Bottom: Nulliparous women (never given birth), $n = 45$

3.4 UST Measurements Made with Different Ring Transducers

The sound speed is a measure that is obtained by determining the arrival times of signals that are emitted from one portion of the transducer ring and received on another. Since the physical parameters of the ring are determined precisely at the time of manufacture, the sound speed can be calculated precisely. However, during the course of collecting patient data, the UST prototype underwent several hardware revisions. This included the use of several separate ring transducers for patients that received a film mammogram. Since the measure of sound speed depends on the exact physical parameters of the device, small differences in the construction of the different rings could manifest themselves as differences in sound speed in the finished image. The physical differences also cause electronic delays that, if not properly calibrated for, can lead to more uncertainties in the final sound speed.

Of the patients that received a film mammogram, 17 were imaged with the first ring (Ring 2), 74 with the second (Ring 3) and 76 with the third transducer (Ring 4). Figure 3-10 below shows the same VASS versus MPD results for film mammography plotted earlier, but separated by which ring transducer was used to make the sound speed image. Of the patients that received digital mammograms, all but 7 were imaged using the same ring (Ring 4). The results are not replotted in a similar fashion due to the small number of patients imaged with Ring 5.

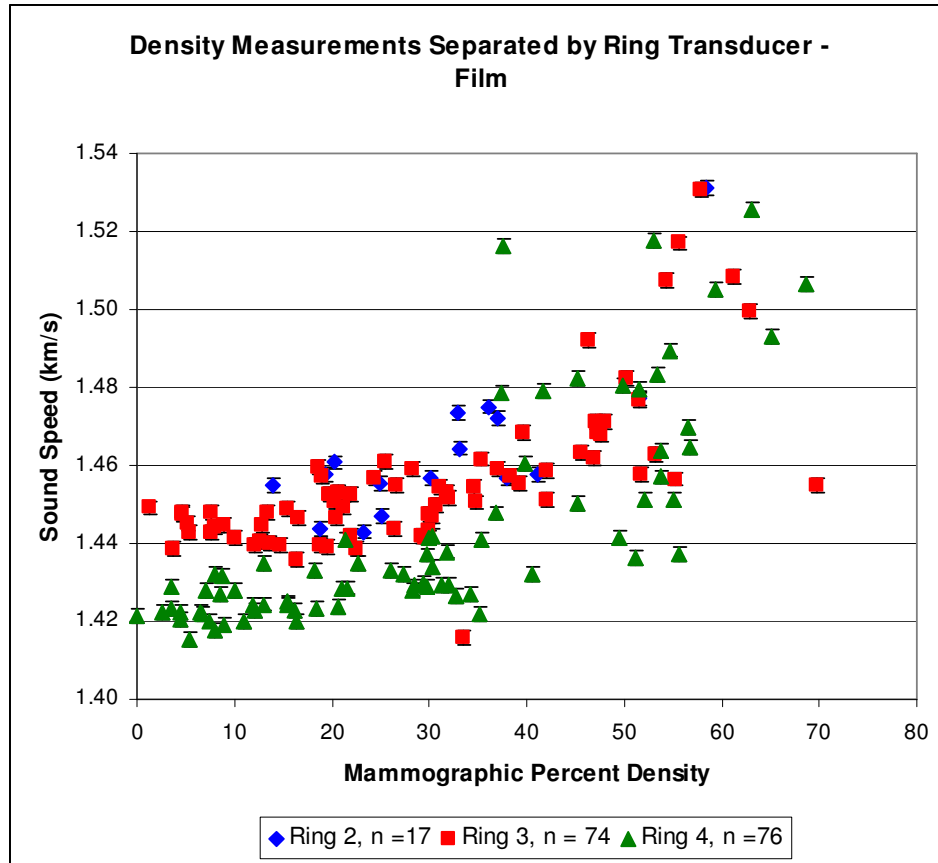


Figure 3-10 - The plot of sound speed versus mammographic percent density for patients that received a film mammogram separated by the ring transducer hardware that was used to create the UST image.

Since all patients have been pulled from the same general population, we expect no fundamental difference in overall average sound speed between different rings. However, from Figure 3-10, we can see that there is a systematic difference in sound speed between patients imaged with different ring transducers. The differences are most apparent at low densities where the data appears linear and become less apparent at high densities where the data becomes scattered. In order to remove this systematic error in the results, a simple shift was used. The data from ring 4 was created using the most up to date reconstruction algorithm which included properly calibrated ring geometries and electronic delays. So this meant that the data from ring 2 and ring 3 were shifted to align with the data from ring 4. Breasts with mammographic densities lower than

approximately 35% have a narrow range of possible sound speed values. Breasts with higher densities show a larger range of potential sound speeds. The shift was therefore only calculated using sound speed values for breasts with mammographic densities lower than 35%, but it was then applied to all points, regardless of density. Doing this ensured that there would be good agreement between all three rings for the patients with low mammographic density where sound speed appears to be more uniform.

The data for each ring was plotted individually for patients with mammographic densities lower than 35%. Linear trendlines were fitted to each ring and the equations of these lines were calculated. Using these lines of best fit, the average sound speed value was calculated for each ring. The difference in average sound speed between each ring and ring 4 was then calculated. These results are shown below in Table 3-13. This difference was then applied as a simple shift to all data collected from the specific ring, including patients with higher densities. This new shifted patient data was plotted and is shown below in Figure 3-11. By applying the shift, the systematic errors between each ring disappeared.

Table 3-13 – Calculating the Shift for Different Ring Transducers

	Linear Fit	Average Sound Speed (m/s)	Shift in Sound Speed (m/s)
Ring 2	SS = 0.3847x + 1446	1453.1	-25.3
Ring 3	SS = 0.1195x + 1444	1446.3	-18.5
Ring 4	SS = 0.3656x + 1421	1427.8	0.0

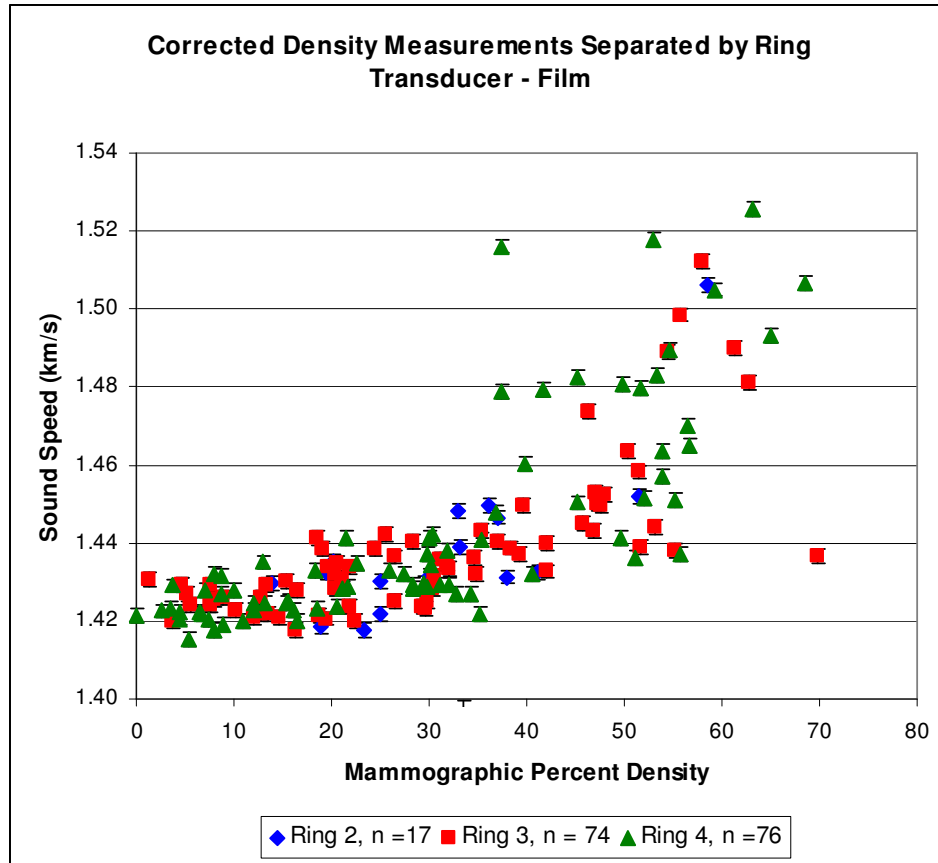


Figure 3-11 - The VASS versus mammographic percent density for the film patients after the corrections were applied to the data from the different ring transducers.

Correlations were measured and trendlines were fit to all the data both before and after the shift occurred. In all situations, applying the shift improved the relationship between sound speed and mammographic density. The results are summarized in Table 3-14. For the unshifted VASS vs MPD data, the Spearman correlation coefficient was found to be $r_s = 0.701$ ($p < 0.001$). A linear and 2nd order polynomial fit was also applied to the unshifted data. The linear fit showed an R^2 of 0.5104 while the 2nd order fit gave an R^2 of 0.5385. This suggests that there was a moderately strong correlation between sound speed and MPD. However, after the shift was applied, the correlations grew stronger. For the shifted data, the Spearman correlation coefficient was measured to be $r_s = 0.794$. The linear fit gave an R^2 of 0.5422 and the 2nd order polynomial fit showed an

R^2 of 0.6055. Since the corrections improve the strength of the correlations, all plots and correlations that involve sound speed data use this shifted sound speed.

Table 3-14 – Correlations for Raw and Shifted Transducer Rings

	Spearman Coefficient	Linear Fit	Polynomial Fit
Raw	0.701	SS = 1.0092x + 1421 $R^2 = 0.5104$	SS = 0.0136x ² + 0.1387x + 1431 $R^2 = 0.5385$
Shifted	0.794	SS = 0.9968x + 1411 $R^2 = 0.5422$	SS = 0.0195x ² - 0.2539x + 1425 $R^2 = 0.6055$

3.5 Association of VASS and MPD with USTPD

With the use of the k-means clustering algorithm, the three dimensional volume of a UST scan can be segmented into dense and fatty subregions. This allows for the calculation of a volumetric percent density (USTPD), which is shown in Figure 3-12 plotted against the VASS of the entire breast. The measurement of this volumetric density does not depend on the type of mammogram received, so the figure plots all 247 patients on the same plot. The Spearman correlation coefficient is 0.647, which suggests that there is a correlation between VASS and USTPD, but that it is not as strong as the relationship between VASS and MPD. This is most likely because the algorithm that segments the volumetric images chooses the regions differently and perhaps less effectively than the Cumulus software.

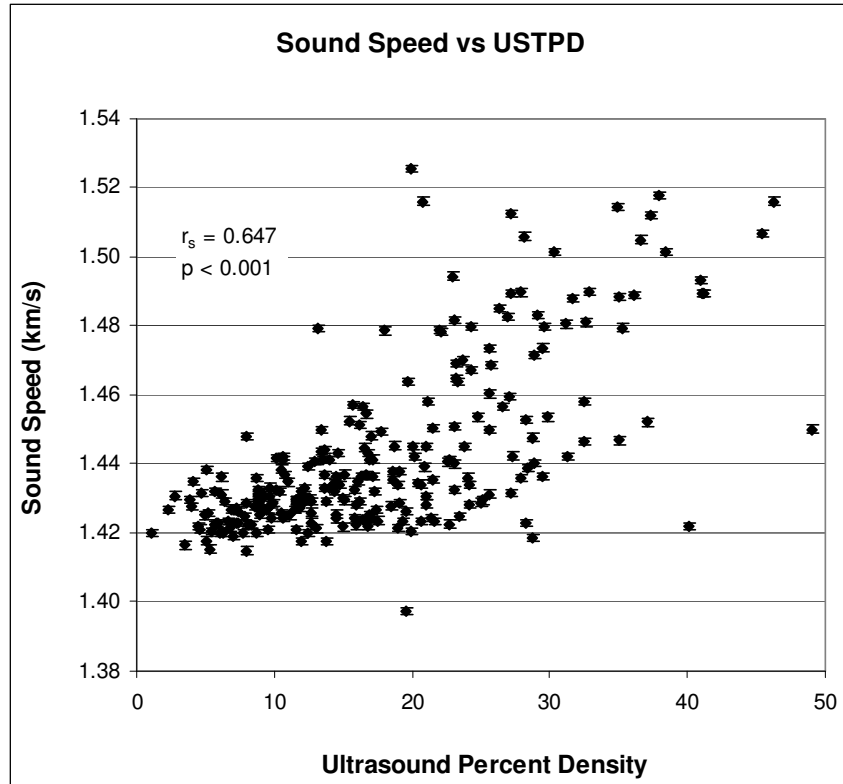


Figure 3-12 - Plot of average sound speed versus ultrasound percent density for the entire population of patients, $n = 247$.

A more direct comparison between the two imaging modalities (UST and mammography) can be made by comparing the percent density measurements. Figure 3-13 shows the relationship between the USTPD and the MPD. The Spearman coefficients for these plots are $r_s = 0.608$ and $r_s = 0.747$ for patients receiving film and digital mammograms. The correlations are similar to those found between VASS and MPD ($r_s = 0.794$ and $r_s = 0.706$ for film and digital mammograms). However, this is a more direct comparison of the two imaging modalities as both USTPD and MPD are a measure of the same characteristic (density), but measured in different ways. This shows the relationship directly between a three dimensional density measurement (USTPD) and a two dimensional density measurement (MPD). The curvilinear nature of the film mammograms is less apparent when compared to the VASS plot (Figure 3-5).

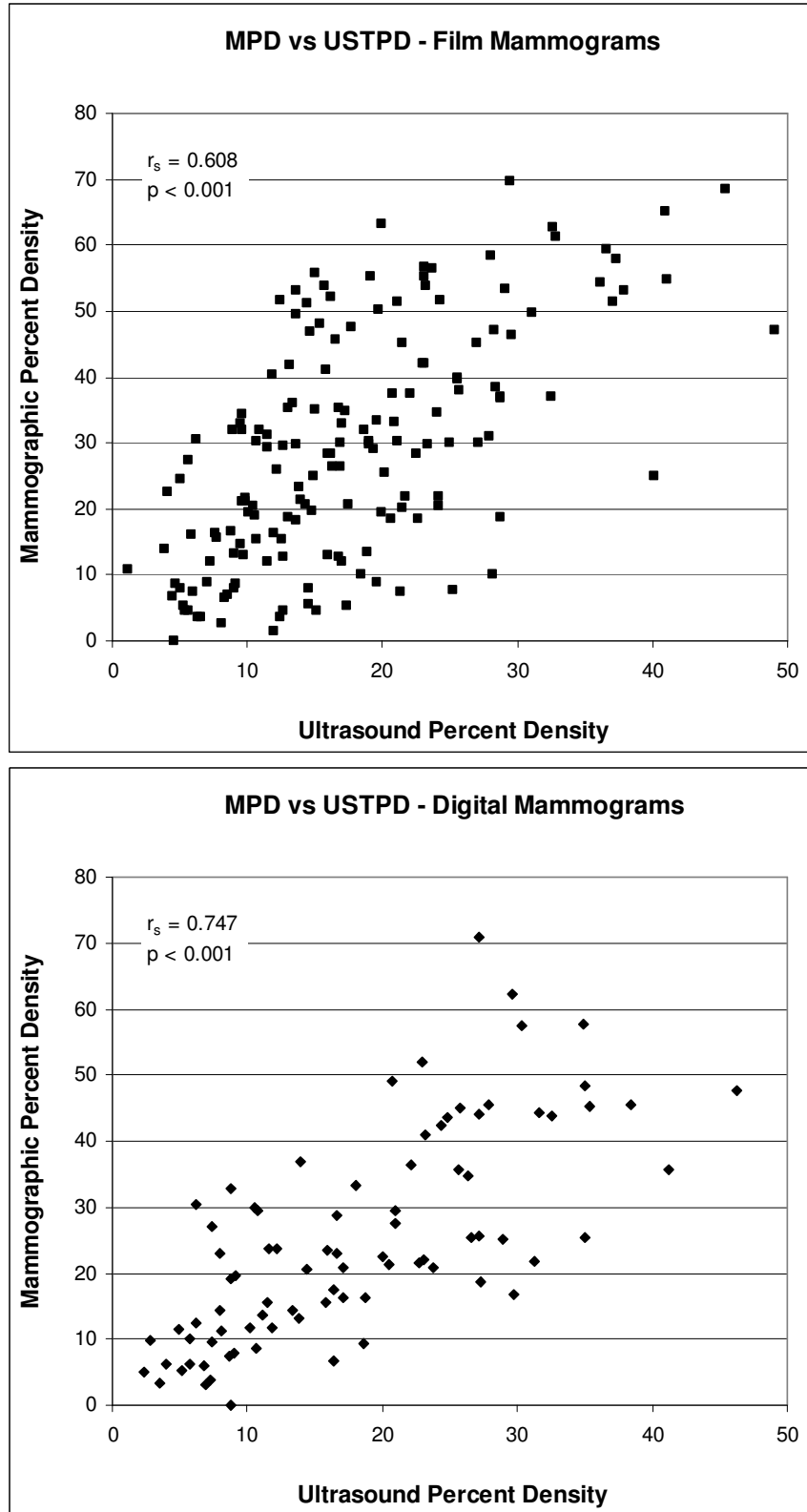


Figure 3-13 - Plots of the mammographic percent density versus the ultrasound percent density, grouped by patients receiving a film mammogram (Top, $n = 163$) and a digital mammogram (Bottom, $n = 84$).

3.6 Subregion Analysis

The regions of dense and fatty tissues in the breast can also be used to determine more than percent density. By separating these regions, further associations with these subregions can be analyzed for both mammography and UST sound speed images. These associations may provide more information about the nature of breast density.

3.6.1 Two-Dimensional Subregion Analysis

The Cumulus software can take the projected anatomy onto an x-ray and segment dense and fatty regions of the breast. Associations of VASS with the dense, non-dense and total areas of the breast were calculated. VASS was positively correlated with dense areas as measured on a mammogram for both digital and film mammograms. The Spearman correlation coefficient was $r_s=0.509$ for film mammography, $r_s=0.404$ for digital mammography and $r_s=0.431$ for all patients. VASS was negatively correlated with fatty areas with a Spearman coefficient of $r_s=-0.687$ for film mammograms, $r_s=-0.589$ for digital mammograms and $r_s=-0.649$ for all patients. Also, the VASS was negatively correlated with the total area on a mammogram. The Spearman coefficient was $r_s=-0.446$ for film mammography and $r_s=-0.461$ for digital mammography and $r_s=-0.472$ for all patients. These plots are shown below in Figure 3-14 and the results which were listed before in Table 3-7 are now summarized below in Table 3-15.

Table 3-15 – VASS and Mammography Correlations

	Spearman Coefficient (p value)		
	Film Mammograms (n = 165)	Digital Mammograms (n = 84)	All Mammograms (n = 249)
Dense Area	0.509 (< 0.001)	0.404 (< 0.001)	0.431 (< 0.001)
Non-Dense Area	-0.687 (< 0.001)	-0.589 (< 0.001)	-0.649 (< 0.001)
Total Area	-0.446 (< 0.001)	-0.461 (< 0.001)	-0.472 (< 0.001)

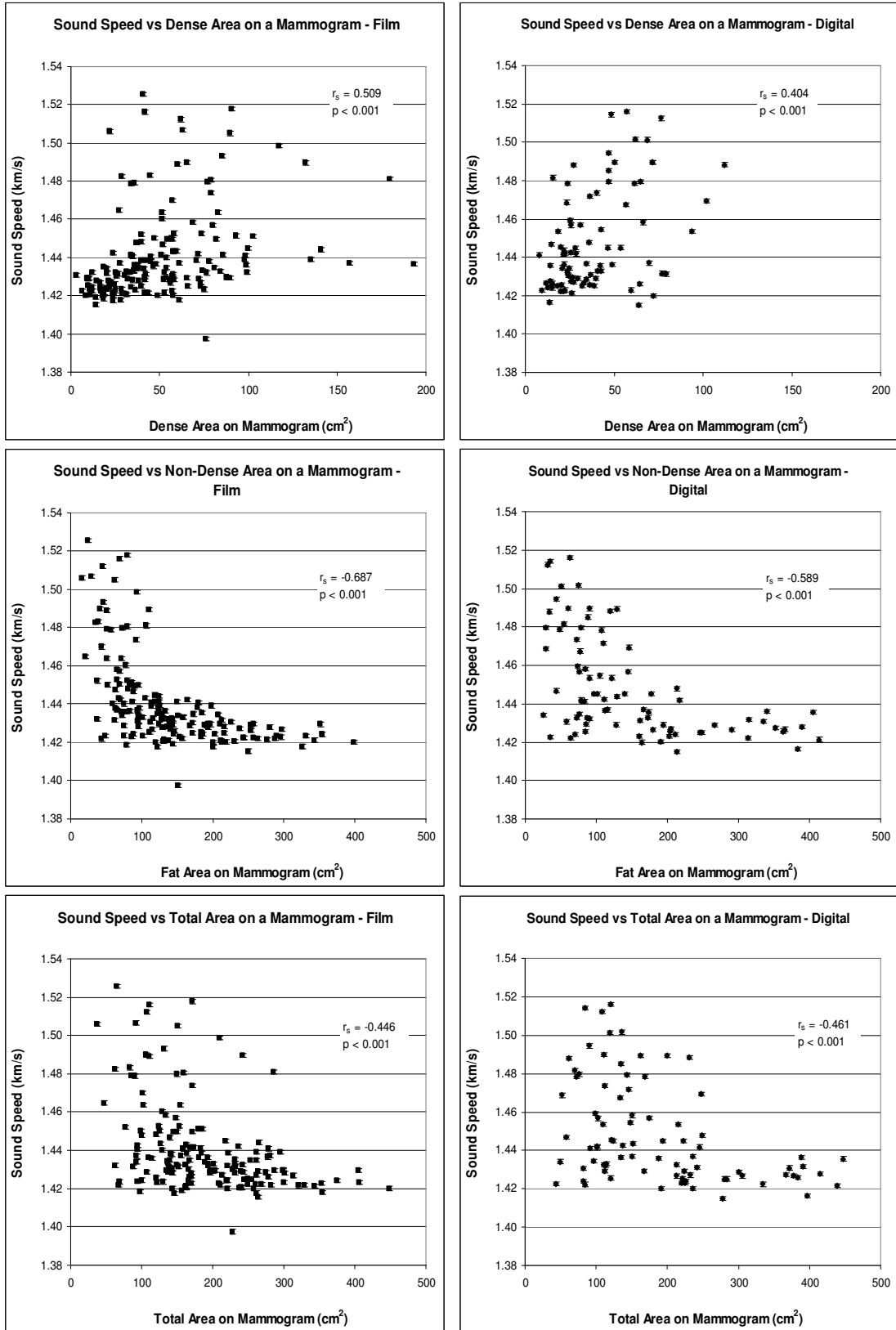


Figure 3-14 - Plots of the sound speed associated with several different mammographic characteristics grouped by mammogram type. Left: Film, n = 165; Right: Digital, n = 84.

The same correlations were made between the dense, fat and total areas on a mammogram and the mammographic percent density. Figure 3-15 shows the plots of the data and Table 3-16 summarizes the correlations that were listed previously in Table 3-7. The Spearman coefficients between MPD and dense area are $r_s = 0.755$, $r_s = 0.612$ and $r_s = 0.731$ for the film group, digital group and all patients. This indicates a strong and positive correlation with dense area. For MPD and non-dense area, the Spearman coefficients are $r_s = -0.774$, $r_s = -0.764$ and $r_s = -0.757$ for film, digital and all patients. There is a strong and negative correlation between MPD and non-dense area. There is also a moderate and negative correlation with the total area as well. The Spearman correlation coefficients are $r_s = -0.436$, $r_s = -0.576$ and $r_s = -0.477$ for film, digital and all patients. The correlations are stronger for MPD than they are for the VASS. This is expected since the mammographic density and areas were both measured on the same mammogram.

Table 3-16 – MPD and Mammography Correlations

	Spearman Coefficient (p value)		
	Film Mammograms (n = 165)	Digital Mammograms (n = 84)	All Mammograms (n = 249)
Dense Area	0.755 (< 0.001)	0.612 (< 0.001)	0.731 (< 0.001)
Non-Dense Area	-0.774 (< 0.001)	-0.764 (< 0.001)	-0.757 (< 0.001)
Total Area	-0.436 (< 0.001)	-0.576 (< 0.001)	-0.477 (< 0.001)

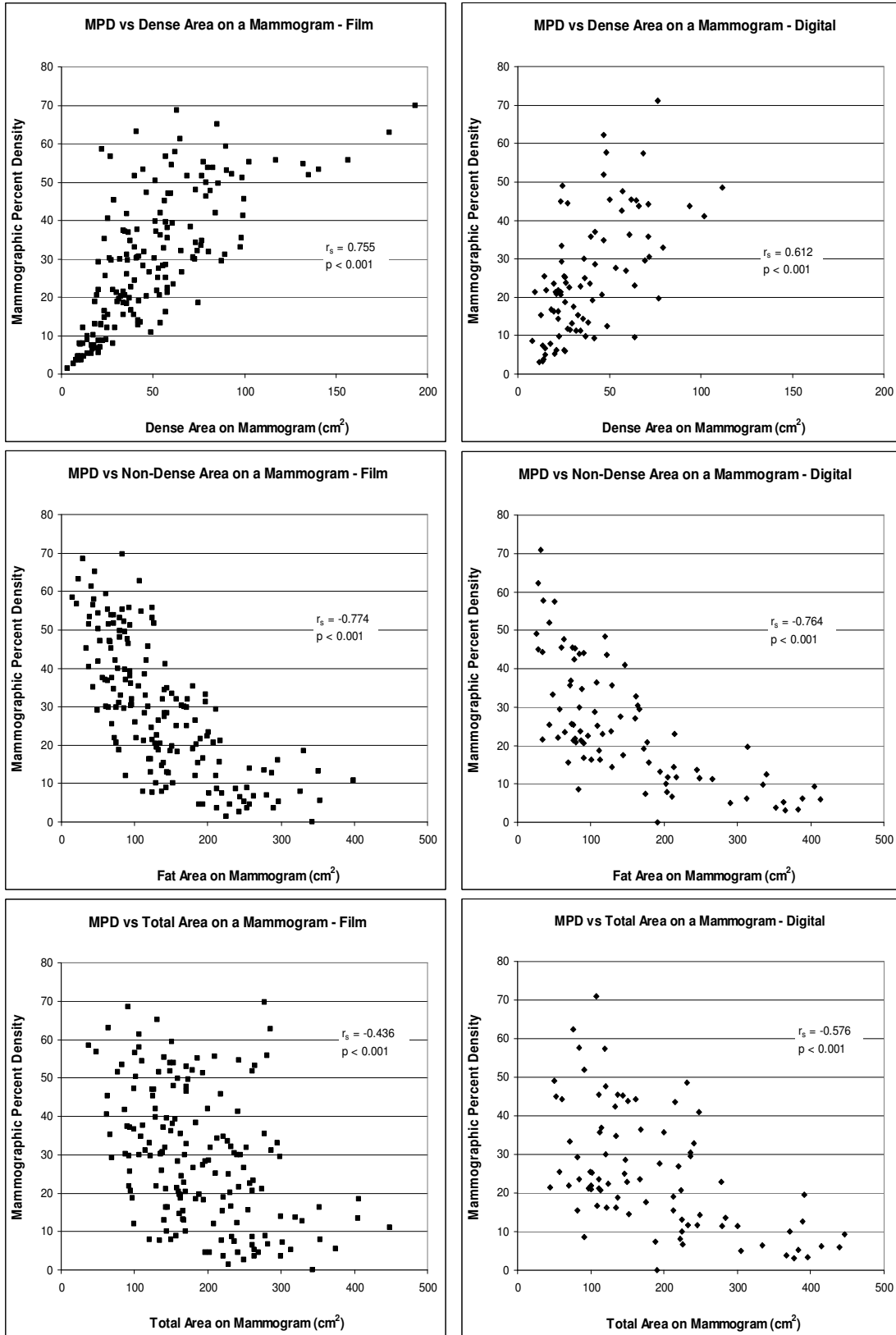


Figure 3-15 - Plots of the mammographic percent density associated with several different mammographic characteristics grouped by mammogram type. Left: Film, n = 165; Right: Digital, n = 84.

3.6.2 Three-Dimensional Subregion Analysis

The subregions that were calculated using the k-means clustering algorithm were also plotted against the overall measurements of density to determine if any correlations existed. Since UST is a volumetric analysis, instead of calculating mammographic areas, dense, non-dense and total breast volumes could be calculated. Figure 3-16 shows the plots of the VASS versus the measured dense, non-dense and total breast volumes. Since both values were measured using the UST device, they are not dependent on mammography type and the data are therefore not separated. The Spearman correlation coefficients were found to be $r_s = 0.070$ for the dense volume, $r_s = -0.553$ for the non-dense volume and $r_s = -0.497$ for the total breast volume. Table 3-17 summarizes these results although they were already listed before in Table 3-7. The correlations involving the non-dense and total volumes are both moderate and negative which mirrors the relationship with the mammographic areas. However, the correlation involving the dense volume was near zero and statistically insignificant. This indicates that either the algorithm that was used to segment the volumes was unable to accurately separate the dense volume or that dense volume manifests itself in a different manner in UST imaging.

Table 3-17 – VASS and UST Volume Correlations

	Spearman Coefficient (p-value)
Dense Breast Volume, n = 247	0.070 (0.273)
Non-Dense Breast Volume, n = 247	-0.553 (< 0.001)
Total Breast Volume, n = 247	-0.497 (<0.001)

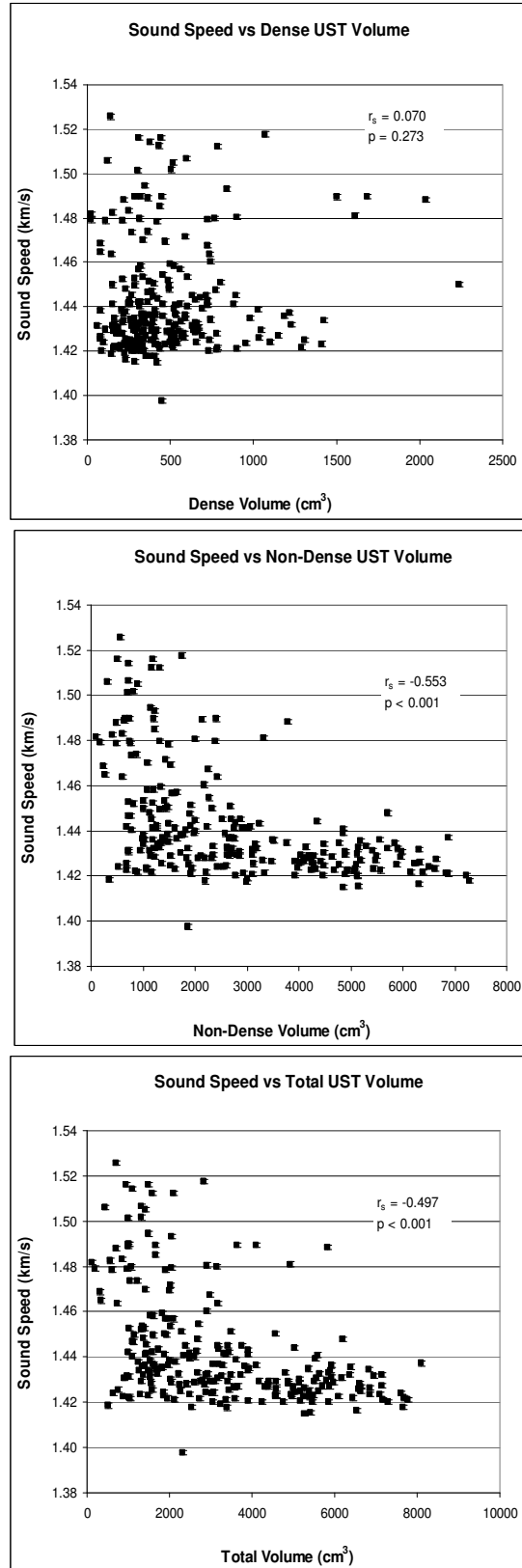


Figure 3-16 - Plots of sound speed versus UST imaging characteristics for all patients, n = 247.

The same volume measurements were then plotted against the mammography data to compare their relationships with VASS. Since the mammography data was being used, it was split according to the type of mammogram received to observe whether or not there were any differences. The Spearman coefficients for the dense volume were found to be $r_s = 0.064$, $r_s = 0.104$ and $r_s = 0.085$ for the film patients, digital patients and all patients respectively. For the non-dense volume, correlations of $r_s = -0.549$, $r_s = -0.642$ and $r_s = -0.568$ were found for film, digital and all patients, while for the total volume the correlations were $r_s = -0.485$, $r_s = -0.585$ and $r_s = -0.509$. These correlations align with the results that were measured for the VASS and the non-dense and total volume measurements align with the correlations found when examining the corresponding mammographic areas. Table 3-18 summarizes these correlations that were originally listed previously and Figure 3-17 shows the plots that for the film and digital groups.

Table 3-18 – MPD and UST Volume Correlations

	Spearman Coefficient (p value)		
	Film Mammograms (n = 163)	Digital Mammograms (n = 84)	All Mammograms (n = 247)
Dense Volume	0.064 (0.416)	0.104 (0.346)	0.085 (0.185)
Non-Dense Volume	-0.549 (< 0.001)	-0.642 (< 0.001)	-0.568 (<0.001)
Total Volume	-0.485 (< 0.001)	-0.585 (< 0.001)	-0.509 (<0.001)

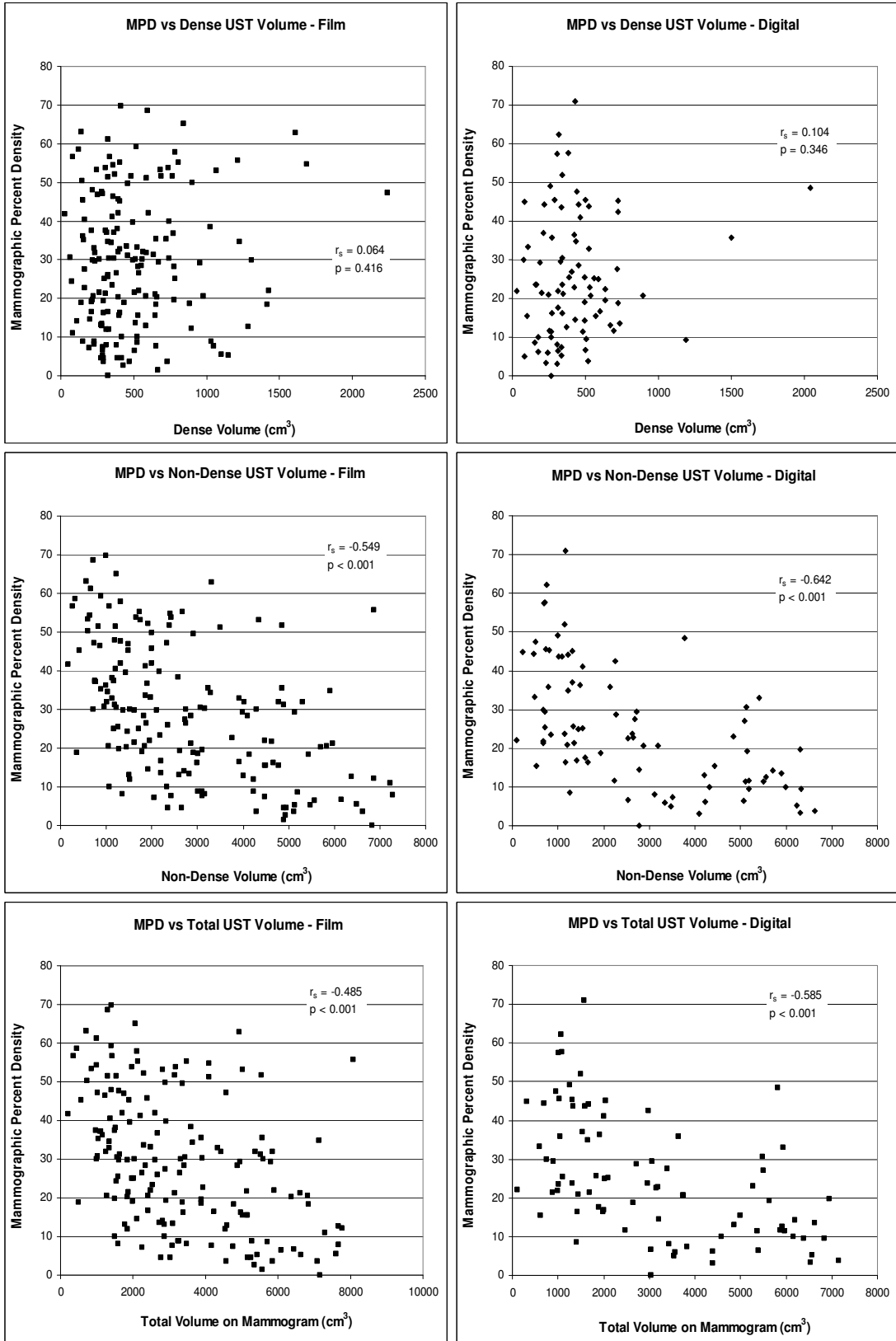


Figure 3-17 - Plots of mammographic percent density associated with UST imaging characteristics separated by mammogram type. Left: Film, n = 163; Right: Digital, n = 84.

Due to the quantitative nature of the UST device, it is possible to extract more information about these subregions by analyzing their sound speeds. Since each pixel holds sound speed information about the voxel, by segmenting the breast into dense and non-dense volumes, sound speed information, and subsequently density information can be measured by performing calculations to the subregion volume. Figure 3-18 shows the average sound speed of the non-dense volume as a function of the average sound speed of the dense volume. The Spearman correlation coefficient is $r_s=0.674$, but the plot appears curvilinear.

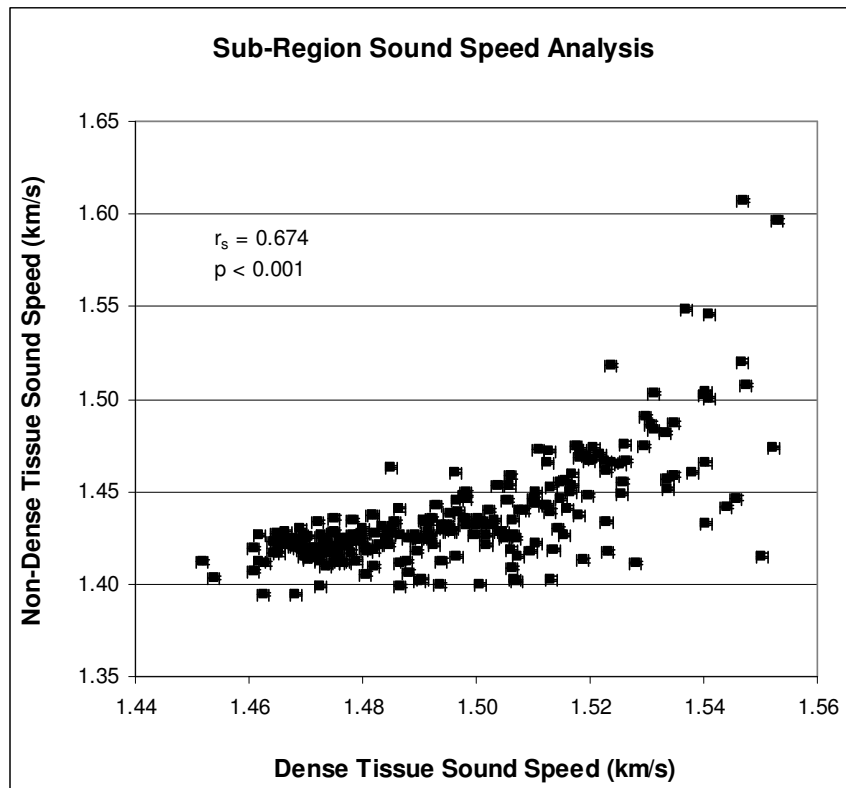


Figure 3-18 - Plot of the average sound speed for the dense and non-dense sub-regions of the breast measured using UST, $n = 247$.

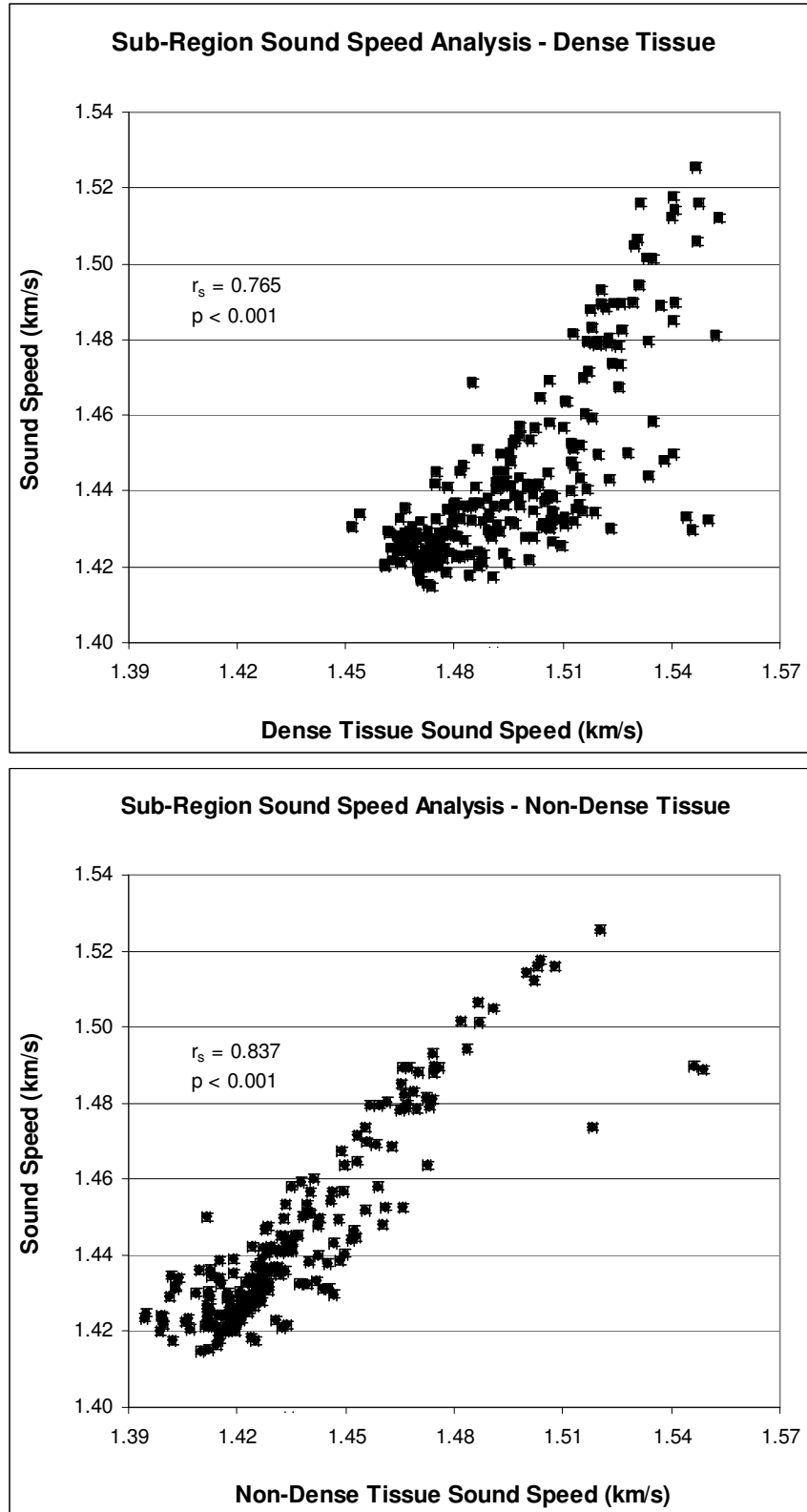


Figure 3-19 - Plot of the overall average sound speed associated with the average sound speed of the dense sub-region (Top) and the non-dense sub-region (Bottom) as measured by UST, $n = 247$.

The association of VASS with both the dense and non-dense average sound speeds is shown in Figure 3-19. The Spearman coefficients of $r_s=0.765$ for the dense volume and $r_s=0.837$ for the non-dense volume indicate that the density of the sub regions themselves can be a good indicator of overall breast density. The correlations are much stronger when using subregion volumes than area on a mammogram. This is likely due to the fact that areas on a mammogram are dependent on the volume of the patient's breast, whereas the average sound speed of the subregion is a normalized value that is not as easily influenced by the relative volume of the breast between patients. This quantitative information that was obtained through UST is something that is unavailable from mammography.

3.6.3 Comparison of Two and Three Dimensional Segmentation

To compare the effectiveness of measuring the sub-regions within the breast, the dense, non-dense and total volumes measured by UST and dense, non-dense and total mammographic areas were plotted against each other. Spearman correlations of $r_s = 0.326$ for the dense tissue, $r_s = 0.808$ for the non-dense tissue and $r_s = 0.769$ for the entire breast were calculated. The correlation between the dense volume and dense mammographic area is the weakest of the three, but still statistically significant. Density has traditionally been determined by separating dense tissue from non-dense tissue. However, this suggests that dense tissue is represented in different ways in UST imaging compared to mammography. When grouped by mammogram type, as shown in Table 3-19 and Figure 3-20, all correlations were stronger between UST and digital mammography, compared to film. This is more evidence to suggest that the difference in x-ray response between film and digital detectors affects their ability to measure density.

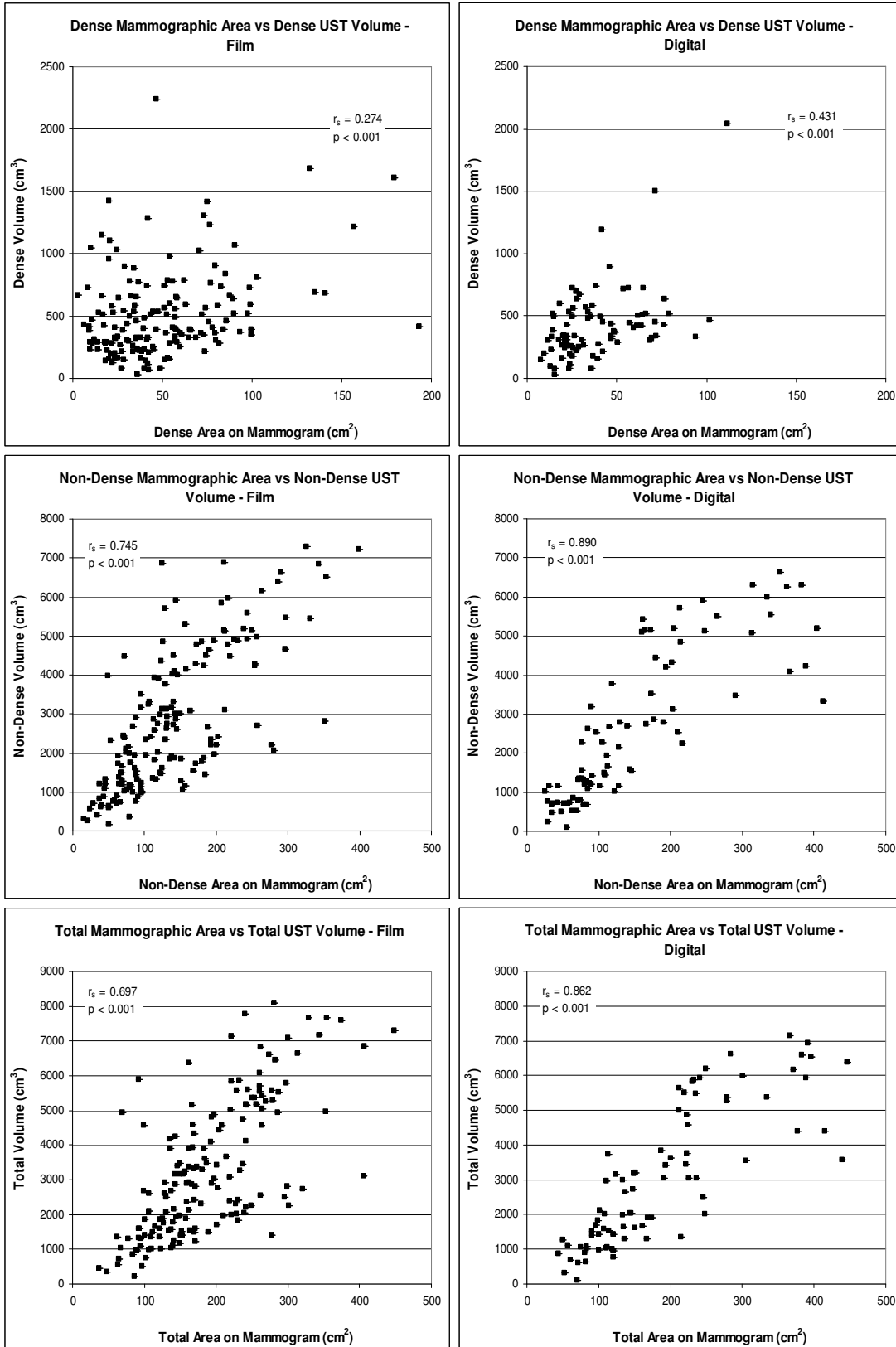


Figure 3-20 - Correlations involving the measured sub-region volumes and areas separated by mammography type. Left: Film, n = 163; Right: Digital, n = 84.

Table 3-19 – Area and Volume Correlations

	Spearman Coefficient (p value)		
	Film Mammograms (n = 163)	Digital Mammograms (n = 84)	All Mammograms (n = 247)
Dense Area/Volume	0.274 (< 0.001)	0.431 (< 0.001)	0.326 (< 0.001)
Non-Dense Area/Volume	0.745 (< 0.001)	0.890 (< 0.001)	0.808 (< 0.001)
Total Area/Volume	0.697 (< 0.001)	0.862 (< 0.001)	0.769 (< 0.001)

3.7 Distribution of Density within the Breast

The use of the k-means clustering algorithm was an attempt to characterize the distribution of sound speed within the breast. To further test the sub-region results obtained using the algorithm, visual inspection was done on several images and their corresponding sound speed distributions.

3.7.1 Sound Speed Distributions across Different Average Densities

To further examine the nature of breast density in the sub-regions, histograms of the voxel sound speed distributions were analyzed for several different patients. A total of 12 patients were analyzed. They were chosen to ensure the average sound speed of each patient was roughly spread out evenly along the entire range. The data were grouped into three groups that represented breasts with low average sound speed, breasts with moderate average sound speed and breasts with high average sound speed. Table 3-20 lists the patients selected for this examination, which group they were placed in and their average sound speed. The histogram of the distribution of sound speed voxels within each patient was plotted by group in Figure 3-21, Figure 3-22 and Figure 3-23 for the low, moderate and high sound speed groups respectively. The histograms were normalized relative to the volume of each breast in order to be plotted on similar scales. The area under each curve is therefore normalized to a value of 100%. In an attempt to

estimate the average effect seen on each group, the histogram data was averaged. Figure 3-24 shows the average distribution of sound speed voxels in each group. This can potentially show how dense and non-dense tissues are distributed across “average” breasts of specific density.

Table 3-20 – Patients Selected and Their Average Sound Speed

Low Sound Speed		Moderate Sound Speed		High Sound Speed	
Patient	Average SS (km/s)	Patient	Average SS (km/s)	Patient	Average SS (km/s)
CURE 340	1.4222	CURE 317	1.4362	CURE 301	1.4894
CURE 319	1.4223	CURE 309	1.4451	CURE 299	1.5043
CURE 302	1.4257	CURE 294	1.4453	CURE 300	1.5148
CURE 315	1.4308	CURE 298	1.4535	CURE 301	1.5196

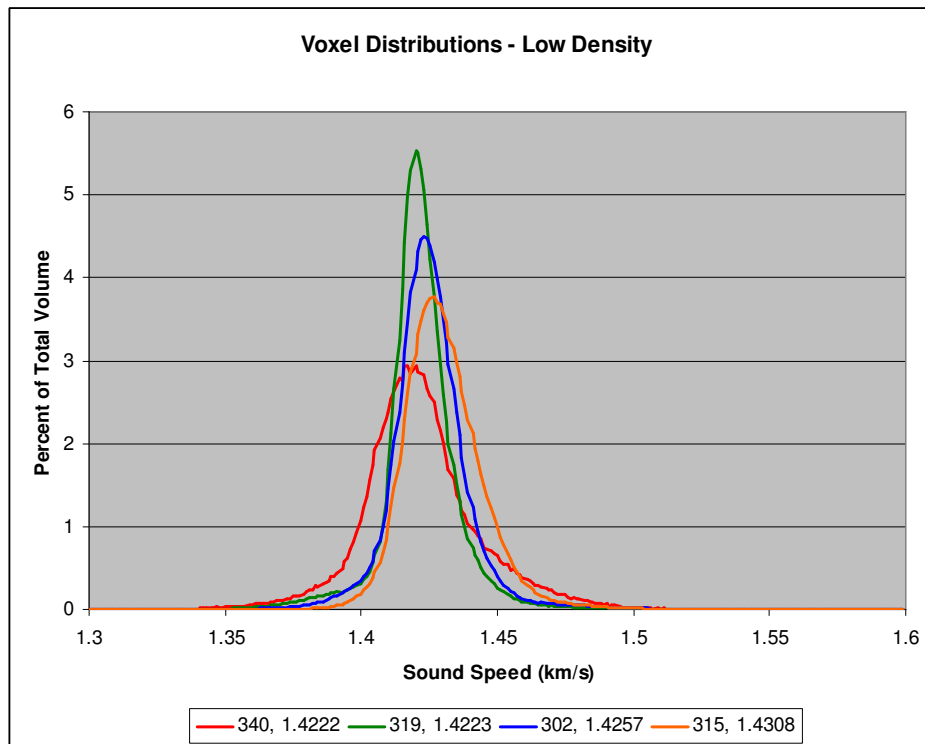


Figure 3-21 – The histogram of the distribution of the sound speed voxels for the low average sound speed group. The histograms are each normalized relative to the total volume in each scan.

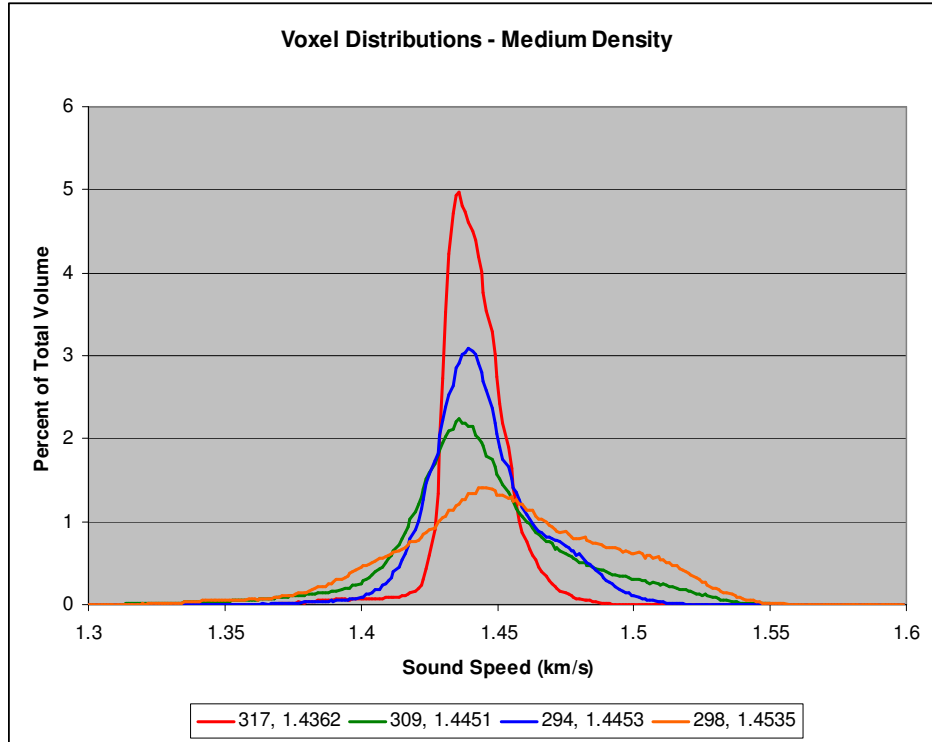


Figure 3-22 – The histogram of the distribution of the sound speed voxels for the moderate average sound speed group. The histograms are each normalized relative to the total volume in each scan.

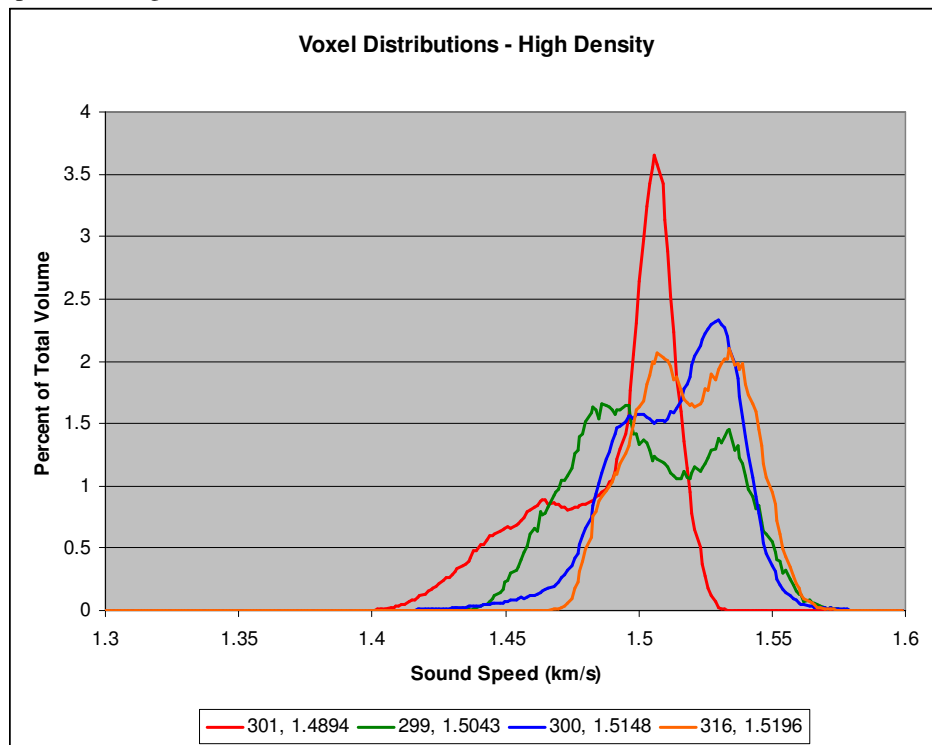


Figure 3-23 – The histogram of the distribution of the sound speed voxels for the moderate average sound speed group. The histograms are each normalized relative to the total volume in each scan.

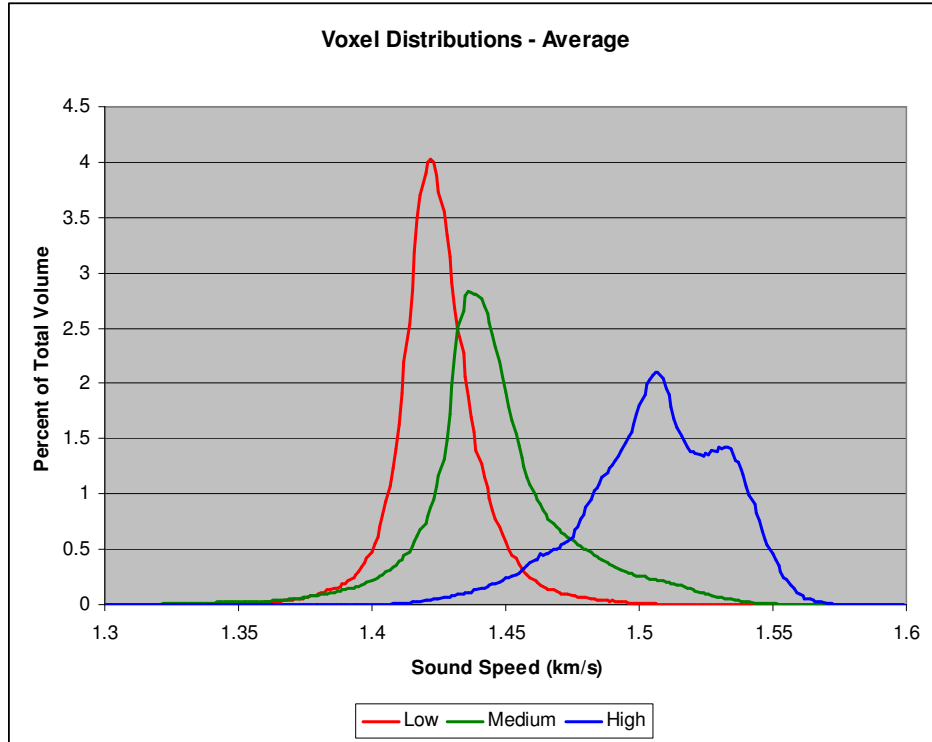


Figure 3-24 – The average distribution of sound speed for each group.

3.7.2 Image ROI Analysis

By averaging over the entire breast volume, differences in dense and non-dense tissues among the different categories may be masked. An attempt to analyze the individual tissue types on a more independent level was made by analyzing a small region-of-interest (ROI) that was drawn over non-dense tissue on breasts with different average densities. Two different images were analyzed that corresponded to a fatty breast and a heterogeneously dense breast. By ensuring that only one tissue type was being examined in the ROI, this would allow for observations on how density affected the non-dense tissue that composes most of the breast volume. These non-dense regions were selected by visual inspection of the sound speed images and not with an automated segmentation algorithm. The small ROI used allowed for only a specific small volume of the breast to be analyzed instead of volume averaging the entire breast which could

potentially cause small variations in density to go unnoticed. The ROI was measured in four consecutive slices that contained visible non-dense tissue to minimize any partial volume effects. Table 2 shows the different imaging characteristics of the two different breasts that were analyzed. The average sound speed, mode, median, minimum and maximum values of the ROI were calculated along with many other values. These results are summarized in Table 3.

Table 3-21 – Overall Imaging Characteristics of Images Analyzed

Patient	Sound Speed (km/s)	Standard Deviation (km/s)	MPD	USTPD	Dense Mean SS (km/s)	Non-Dense Mean SS (km/s)
CURE275	1.4795	0.0334	45.2	35.3	1.5168	1.4591
CURE315	1.4308	0.0143	9.9	2.8	1.5041	1.4287

Table 3-22 – ROI Tissue Analysis

Patient	ROI Area (voxels)	Mean (km/s)	Standard Deviation (km/s)	Mode (km/s)	Min (km/s)	Max (km/s)	Median (km/s)	Skew
CURE275 Heterogeneously Dense	2163	1.4319	0.0129	1.4322	1.3950	1.4828	1.4312	0.352
	2163	1.4311	0.0151	1.4275	1.3890	1.4774	1.4299	0.302
	2163	1.4316	0.0173	1.4290	1.3828	1.4909	1.4298	0.331
	2163	1.4337	0.0212	1.4216	1.3855	1.5096	1.4332	0.272
CURE315 Fatty	2040	1.4170	0.0066	1.4154	1.3988	1.4480	1.4169	0.216
	2040	1.4174	0.0064	1.4181	1.3974	1.4406	1.4174	0.062
	2040	1.4178	0.0060	1.4155	1.3970	1.4398	1.4177	0.146
	2040	1.4186	0.0059	1.4161	1.3996	1.4367	1.4184	0.146

3.8 Sound Speed Inter-rater Analysis

Inter-rater reliability is the degree of agreement among different raters who measure or analyze the same data. It is used in statistical analysis to determine how much consistency or consensus there is in the ratings given by different raters. If various

raters get the same results using the same scale, the reading can be characterized as highly reliable. Here, the VASS was measured for 64 images by two independent raters, as reported by Faiz¹⁵³. Each rater independently determined the number of slices that corresponded to the majority of the breast tissue by selecting the nipple and chest wall cutoffs. Masks were then created for the chosen slices. Figure 3-25 plots the VASS for each image as measured by the two independent raters. The Pearson correlation coefficient for the relationship was $r_p=0.99995$, which is very strong. The percent error between each measurement was also measured with the largest error being 0.65%. Linear regression was also performed and the best-fit straight line had an equation of $y = 1.0167x - 0.0241$ with an $R^2 = 0.9913$. These results suggest that there is a very high degree of agreement between these two independent raters. The VASS measurements obtained using the UST device are highly reliable and consistent.

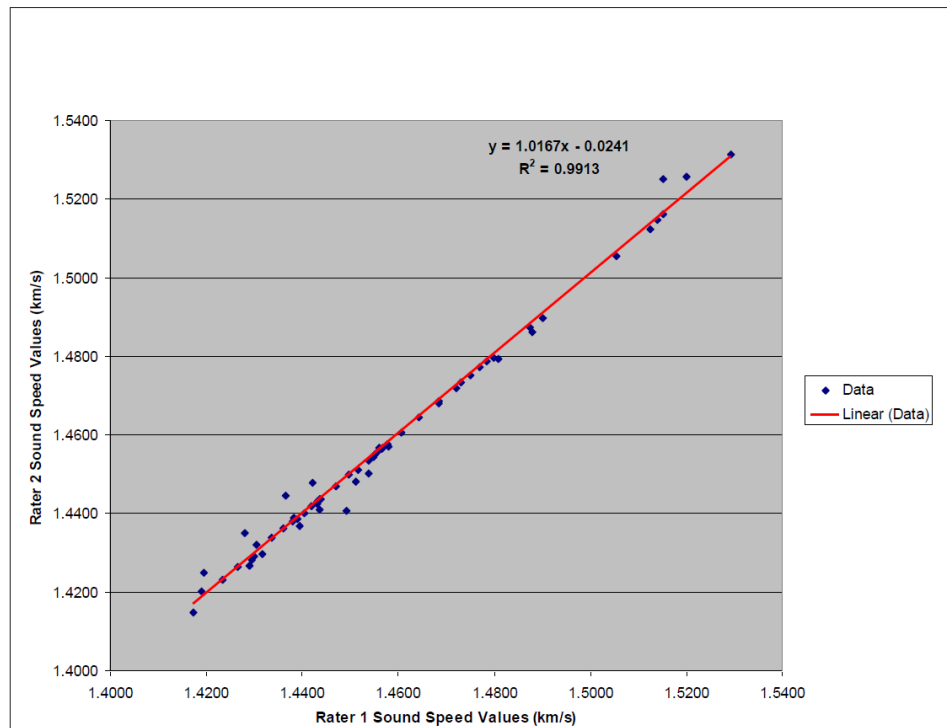


Figure 3-25 - Sound speed measurements of the same data as measured by two separate readers showing a strong intra-rater correlation¹⁵³.

3.9 Future Studies

Currently, multiple studies have linked mammographic percent density to the risk of developing breast cancer. There are no studies that link VASS with breast cancer risk. The work presented above has only correlated UST breast density measurements with the current gold standard of breast imaging, mammography. It has shown that breast density, as measured by VASS, is at least comparable to density as measured by mammography. Future work would involve a study to investigate the relationships between density measured using VASS in UST imaging and the risk of developing breast cancer.

CHAPTER 4

THE ULTRASOUND STUDY OF TAMOXIFEN

4.1 Tamoxifen Use in the Prevention of and Treatment of Breast Cancer

Tamoxifen has been shown to reduce the incidence of breast cancer in women who have had breast cancer by up to 50%^{154, 155}. Therefore, it is commonly used as a breast cancer preventative agent. This indicates that tamoxifen causes a reduction in the incidence, or risk, of invasive breast cancer. Although tamoxifen has been shown to reduce the number of breast cancers during many studies, the term “prevention” does not necessarily imply that all these cancers have been eliminated. Tamoxifen has been used to treat advanced breast cancers alone and in combination with chemotherapy¹⁵⁶⁻¹⁵⁹. It also has a proven efficacy in reducing tumor recurrence and prolonging survival when administered as postoperative adjuvant therapy in early stage disease^{62, 160-162}. Patients who use tamoxifen have also shown lower incidences of contralateral breast cancer^{62, 162, 163}. It has also shown an ability to reduce invasive and non-invasive breast cancers in other women who have an increased risk of the disease, including younger and premenopausal women^{62, 164-166}. Tamoxifen is usually administered for between 2 to 5 years, although 5 years of therapy is the recommended duration. The preventative effects of tamoxifen are seen in patients with up to an additional 10 years of follow-up¹⁶⁴. The use of tamoxifen for prevention may be limited due to its side effect profile¹⁶⁵, although the effects are minimal. Still, tamoxifen remains a cheap and highly effective treatment.

4.1.1 Biological Effects of Tamoxifen

Tamoxifen is a selective estrogen receptor modulator (SERM) that prevents estrogen from binding to estrogen receptors. It was approved by the Food and Drug

Administration in 1977 for the treatment of advanced breast cancer and several years later for adjuvant treatment of primary breast cancer¹⁶⁷ and also as a chemopreventive agent among high risk women⁶². Tamoxifen is absorbed readily after oral administration with a usual dosage of 20 mg per day¹⁶⁷⁻¹⁷⁰. The half-life of tamoxifen in serum ranges from 7 to 14 days, permitting once-daily administration^{167, 171-173}. For long-term treatments, the steady state concentrations of tamoxifen in serum can remain constant for 10 years. After treatment is discontinued, tamoxifen can still be detected in serum for several weeks and in tumor tissue for several months¹⁷³. Tamoxifen is one of the most commonly used adjuvant hormonal therapy for hormone receptor-positive breast cancers, along with aromatase inhibitors. The antitumor effects of tamoxifen are thought to be due to its estrogen receptor antagonism. It inhibits the expression of estrogen-related genes that include growth factors secreted by the tumor which causes a slowing of tumor cell proliferation¹⁷⁴. Therefore, tamoxifen prevents only estrogen receptor (ER)-positive breast cancer and has little to no effect on ER-negative cancers^{175, 176}. For prevention to be successful, it is important to define and identify women at high risk of developing ER-positive breast cancer.

4.1.2 Effect of Tamoxifen on Breast Density

Most attempts at defining a high risk for breast cancer have focused on family history, which has an attributable risk of 7%. However, women with higher mammographic densities (MPD > 50%) have an attributable risk of approximately 30%^{22, 177, 178}. Density can also be increased by menopausal hormone therapy and can be affected by other hormonal stimuli¹⁷⁹⁻¹⁸³. Not only does tamoxifen reduce the risk of breast cancer, it also decreases breast density particularly in premenopausal women^{19, 154,}

^{168-170, 176, 184-186}. Should these two effects be due to the same mechanism, the reduction in breast cancer risk may be partially explained by tamoxifen's effect on breast density¹⁸⁵. Therefore, monitoring breast density in an individual woman during an antiestrogenic intervention such as tamoxifen may indicate whether or not the treatment will be effective.

Many groups have performed observations on the effects of tamoxifen on breast density as measured qualitatively or quantitatively on mammography and even breast MRI. Son and Oh¹⁸⁴ observed decreased breast parenchyma on mammograms in 60% of women treated with tamoxifen for an average of 22 months, compared to 36% of nontamoxifen patients. Brisson *et al*¹⁵⁴ observed treatment with tamoxifen for almost 3.5 years. There, 44.4% of those treated showed a decrease in density as measured by Wolfe's patterns compared to 15.2% of women on placebo. Atkinson *et al*¹⁶⁸ also measured a change to a less dense Wolfe pattern in 31% of women on tamoxifen. The use of a quantitative or semi-automated criteria for measuring density changes was proposed by Chow *et al*¹⁷⁰. There, 56% of patients showed a relative decrease in mammographic percent density of >10% relative to their pre-tamoxifen scans. They also measured an average decrease in mammographic percent density of 4.3% per year. Decensi *et al* tracked the effects of tamoxifen in combination with fenretinide¹⁸⁶, another drug that reduces premenopausal breast cancer risk. It was observed that the combination of the two drugs reduced density more than either drug on its own. Density changes as measured by MRI were observed by Chen *et al*¹⁶⁹ for a small cohort of sixteen patients. A 5.8% reduction in percent density was measured for patients that had only been taking tamoxifen for only 2 years.

Cuzick *et al* have released several studies from the International Breast Cancer Intervention Study I (IBIS-I) that monitored almost 1000 women undergoing either tamoxifen or placebo treatment for prevention. When observing more than 800 breast cancer free women¹⁷⁶, after 18 months of treatment, statistically significant differences in the decrease in density were observed between women taking tamoxifen and those receiving placebo. After 54 months, the average decrease in percent density for the tamoxifen group was 13.7% compared to only a 7.3% decrease in the placebo group. When Cuzick later also included women who later developed breast cancer¹⁸⁵, 46% of women in the tamoxifen arm showed a reduction in breast density of >10% at their 12-18 month scan. They found that changes in mammographic breast density at 12- to 18-months were an excellent predictor of response to tamoxifen in the preventive setting. Although the measured changes in breast density are small with tamoxifen, on the order of a few percent, the effect on breast cancer risk is much larger. This suggests that changes in breast density may only be a marker of tamoxifen activation and only be causally related to decreases in breast cancer risk.

4.2 The Ultrasound Study of Tamoxifen Protocol

In collaboration with researchers at the Karmanos Cancer Institute, Henry Ford Hospital, the University of Toronto and the National Cancer Institute, the Ultrasound Study of Tamoxifen was launched in 2011. The protocol calls for an enrollment of 150 patients into the study. UST will be used to assess volumetric breast density within the first year of tamoxifen for patients referred to take tamoxifen for clinical indications, including a diagnosis of incident atypical lobular or ductal hyperplasia (ALH/ADH), ductal carcinoma *in situ* (DCIS), lobular carcinoma *in situ* (LCIS), or invasive breast

cancer. Breast density will be assessed in the breast that is contralateral to the diagnosis. To assess whether tamoxifen-related declines in mammographic density found at 12 months can be identified earlier with UST, multiple repeat exams will be performed on the patients. An additional 150 women with negative mammographic screens will be examined to ensure that the changes in UST density associated with tamoxifen use are greater than changes in density we might expect over time. This control group will be frequency matched to the cases on age, race and menopausal status. In order to assess whether early changes in density from tamoxifen are predictive of the changes at one year, the patients receiving tamoxifen will also undergo additional UST exams which will occur approximately 1-3 months and 3-6 months post-tamoxifen initiation.

To be eligible for the study, all subjects must be aged 30 to 70 at the baseline visit and they must weigh less than 250 lbs. They may not be currently pregnant or breastfeeding and have no breast implants. There should be no active skin infections or wounds overlying the breast and the breast must be able to fit through the ultrasound tomography ring. Finally, they must have no serious medical or psychiatric illness that would prevent them from giving voluntary informed consent. The patients eligible for the case study must also be planning to take tamoxifen for clinical indications such as a referral from a health care professional based on a woman's personal risk of breast cancer or a diagnosis with invasive, estrogen receptor positive breast cancer, DCIS, LCIS or atypical lobular or ductal hyperplasia that affects only one breast. Also, the patient must have never been diagnosed with breast cancer in the breast contralateral to the current diagnosis and is not receiving or planning to take chemotherapy. The patients eligible for the screen-negative comparison group must also have a recent mammogram that resulted

in recommendations for continued routine screening. They must not be taking oral contraceptives, menopausal hormone therapy or medicines (such as tamoxifen or raloxifene) to lower their breast cancer risk. They must also not have been previously diagnosed with breast cancer or received medications or radiation for any type of cancer.

4.3 Measuring Breast Density

The methods described earlier (Section 2.5) to calculate the average breast sound speed for the MPD patients were applied once again to calculate the VASS for the Tamoxifen study. For this study, this density measurement was defined as the whole volume sound speed (WVSS). Different methods of measuring the density were also developed to deal with issues that presented themselves in regards to imaging the same patient's breast volume multiple times and with image artifacts that were encountered while the images were being analyzed.

4.3.1 Measuring the Sound Speed over Time

Since this study is looking at the changes in breast density over time, different methods of calculating the density were also investigated. Because patient positioning between scans is not uniform, to accurately track changes in sound speed, roughly the same volume of the breast was also analyzed for each scan. This was done by first determining a common volume between scans. The process for this is described below. For each UST scan, most of the breast anatomy is imaged on average. Each image captures the patient's breast starting with the nipple and extending as far towards the chest wall as possible. However, due to patient positioning and breast size, the chest wall may not be visible in the image. This means that some of the breast anatomy also may not have been imaged, which potentially omits information about the breast's density.

Even as the same patient comes in and receives multiple scans, there is no guarantee that the same patient will have the same breast volume imaged each time. By using a common volume, changes to the same breast anatomy can be examined during the course of Tamoxifen treatment.

4.3.2 Determining the Common Volume

In order to properly measure changes in breast density in patients between scans, a common volume was determined. In cases where the volume of the breast from nipple to chest wall was similar in multiple scans, no additional steps were required to obtain a common volume. However, this situation is rare due to differences in patient positioning between scans. When the overall volume of the breasts varied between scans, the scan with the smaller volume was used as the cutoff. Landmarks on the first non-chest wall slice were found on the reflection image and were matched up with similar landmarks from the other scan (Figure 4-1). The reflection images provided more detail than either the sound speed or attenuation images and allowed for multiple landmarks to be visualized between scans. Multiple landmarks were used in the different images in case changes in the parenchymal patterns occurred due to tamoxifen's effect on breast density. Since the landmarks were usually visible in multiple images, similar volumes between the scans were obtained with a careful slice choice. The sections of the breasts that were chosen using this method was known as the common volume. As patients received a third or fourth scan, the common volume may have been recalculated for previous scans to account for the new imaged volume. Otherwise, the common volume would just be calculated for the new image. The new sound speed for each scan was calculated using

only the masked slices that were chosen to be in this common volume using this method.

This measurement is known as the common volume sound speed (CVSS).

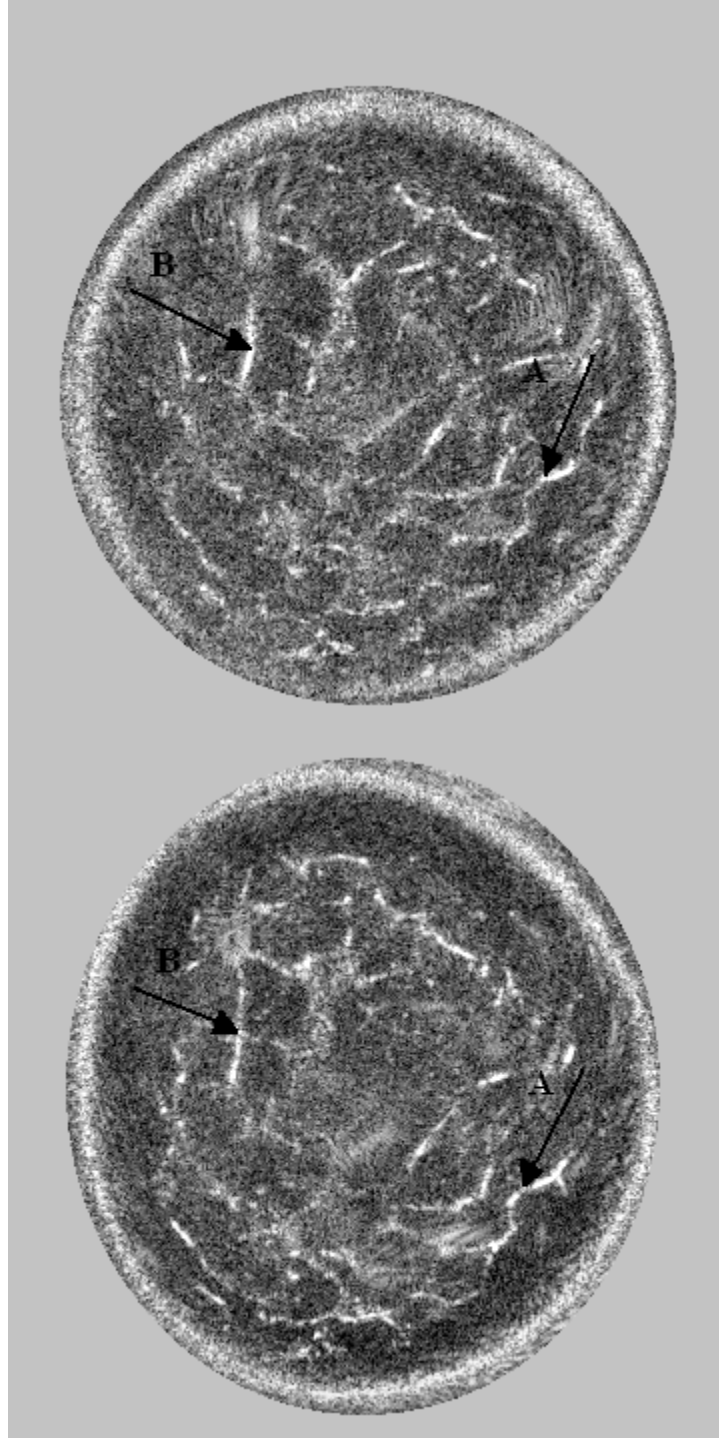


Figure 4-1 - Observing similar landmarks in the same patient scanned at two different times. In both images, the same parenchymal patterns are apparent, indicating the slices represent the same volume is being imaged.

The UST images show the breast anatomy from the chest wall to the nipple. The anatomy is presented with the slice closest to the chest wall as the first slice. Higher numbered slices represent anatomy that is further from the chest wall, towards the nipple. This continues even past the nipple, where most of the highest numbered slices in the image contain only the water bath. However, the volume measured by the common volume essentially counts the voxels starting from the nipple and moving towards the chest wall. The effect of the common volume is to remove slices from the entire volume that correspond to breast anatomy that is closer to the chest wall. This ensured that roughly the same volume of tissue, measured from the nipple towards the chest wall, was analyzed between scans. Figure 4-2 shows an exaggerated example of the differences between the whole volume (WV) and the common volume (CV) for the same patient as they undergo three scans. For the scan with the smallest volume imaged, the common volume is identical to the whole volume.

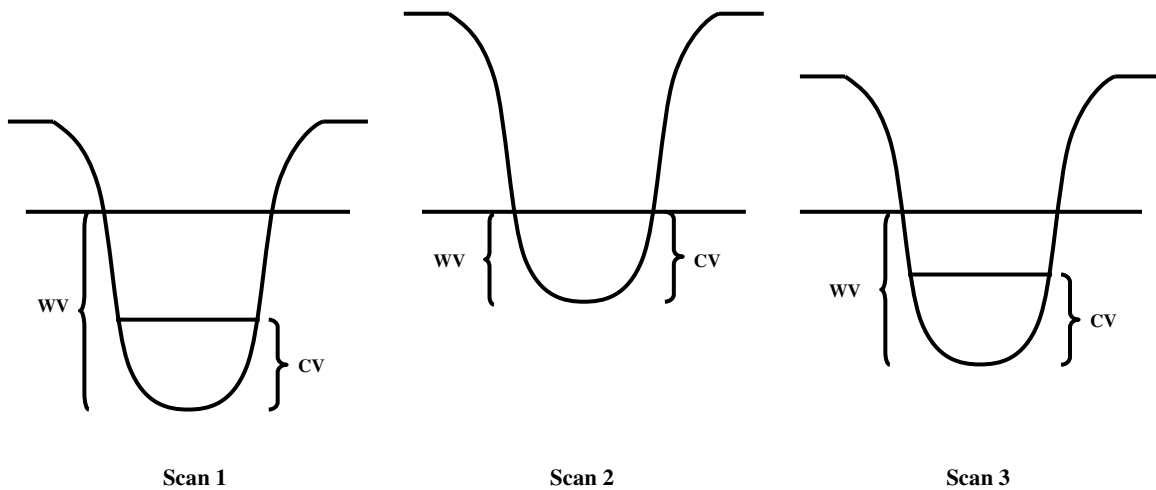


Figure 4-2 - An exaggerated example of a patient receiving three separate scans and the differences in calculating the whole volume (WV) and common volume (CV) between them.

4.3.3 Dark Ring Artifacts

Further complicating the measurement of the sound speed was an artifact that appeared in some sound speed images. This artifact presented itself as a dark ring or

donut near the surface of the breast (Figure 4-3). This artifact did not appear in every image. When it did appear, it was much more visible in slices that are nearest to the chest wall. It disappeared completely in the slices closer towards the nipple. This dark region on the image is of low sound speed and will cause the true sound speed of the breast to be underestimated. This may affect the measured results, especially when a patient receives an image with the artifact and another image without the artifact. The source of the artifact was the transducers measuring a slow moving surface wave as it traveled across the breast. Removal of the artifact cannot be done with a new reconstruction algorithm, but there is a parameter in the algorithm that can be adjusted to decrease the presence of the artifact. However, it comes at a cost of being able to identify the breast/water bath boundary. The dark regions were therefore removed manually from the images themselves using ImageJ. This allowed for only the breast anatomy itself to be measured, not any artifacts that did not physically correspond to any anatomy.

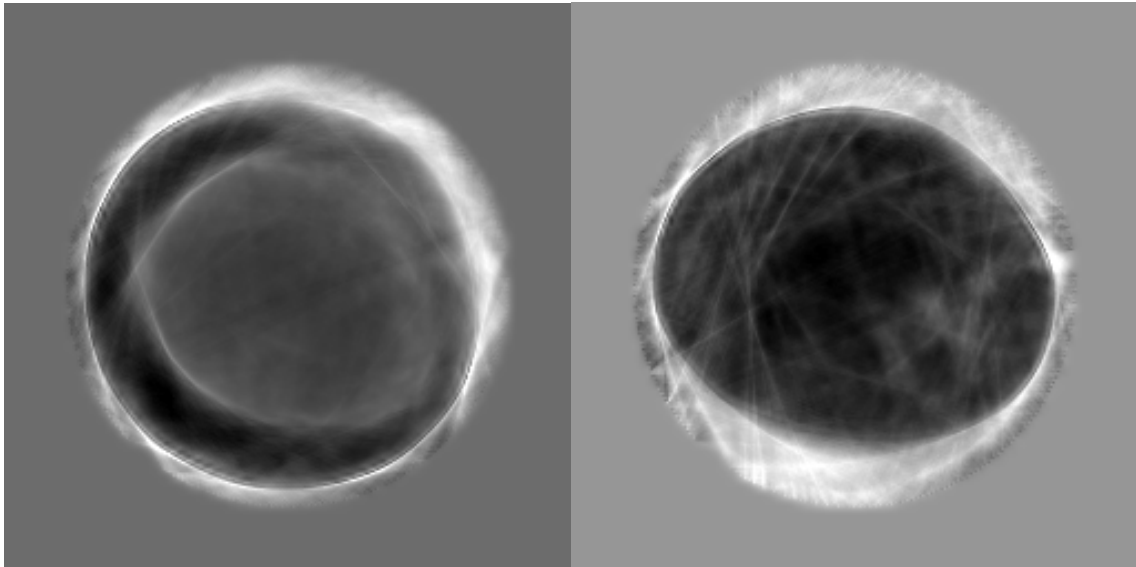


Figure 4-3 - Left: Sound speed image showing the presence of the dark ring artifact near the surface of the breast. Right: Sound speed image without dark ring artifact.

Removal of the dark ring occurred after the whole breast volume was masked as described before. On images where the artifact appeared, another mask was fitted that covered the affected regions. The dark regions were oddly shaped, but appeared towards the surface of the breast, away from the center. Using ImageJ, a large ellipse was fit to the boundary between the artifact and the normal breast tissue. By selecting a large enough ellipse, part of the dark region would lie outside this ellipse, while the rest of the breast would lie inside the ellipse. ImageJ allowed for the pixels on the outside of this ellipse to be cleared, or set to a value of zero. Clearing the outside of the ellipse in this fashion eliminated the dark region, while keeping the breast anatomy untouched. This process of carefully placing the ellipse to eliminate the dark region was repeated until the entire artifact was removed. Figure 4-4 shows the steps in this process. This could then be repeated for any other slice where the artifact was present. Once all slices were cleared of the artifact, the sound speed could then be calculated from the remaining voxels. This new mask was then saved.

The slices that were used to make this measurement were the same slices used for the whole volume sound speed measurement. Therefore this measurement was known as the donut removed whole volume (DRWV) sound speed. Applying these newly created masks to the slices of the common volume allowed for the measurement of the donut removed common volume (DRCV) sound speed. In images where there is no artifact, the DRWV sound speed is equal to the WV sound speed and the DRCV sound speed is equal to the CV sound speed. Since the artifact appears primarily in the slices close the chest wall and the common volume may eliminate many of the same slices near the chest wall, the DRCV may be very close or even equal to the CV for images with the artifact.

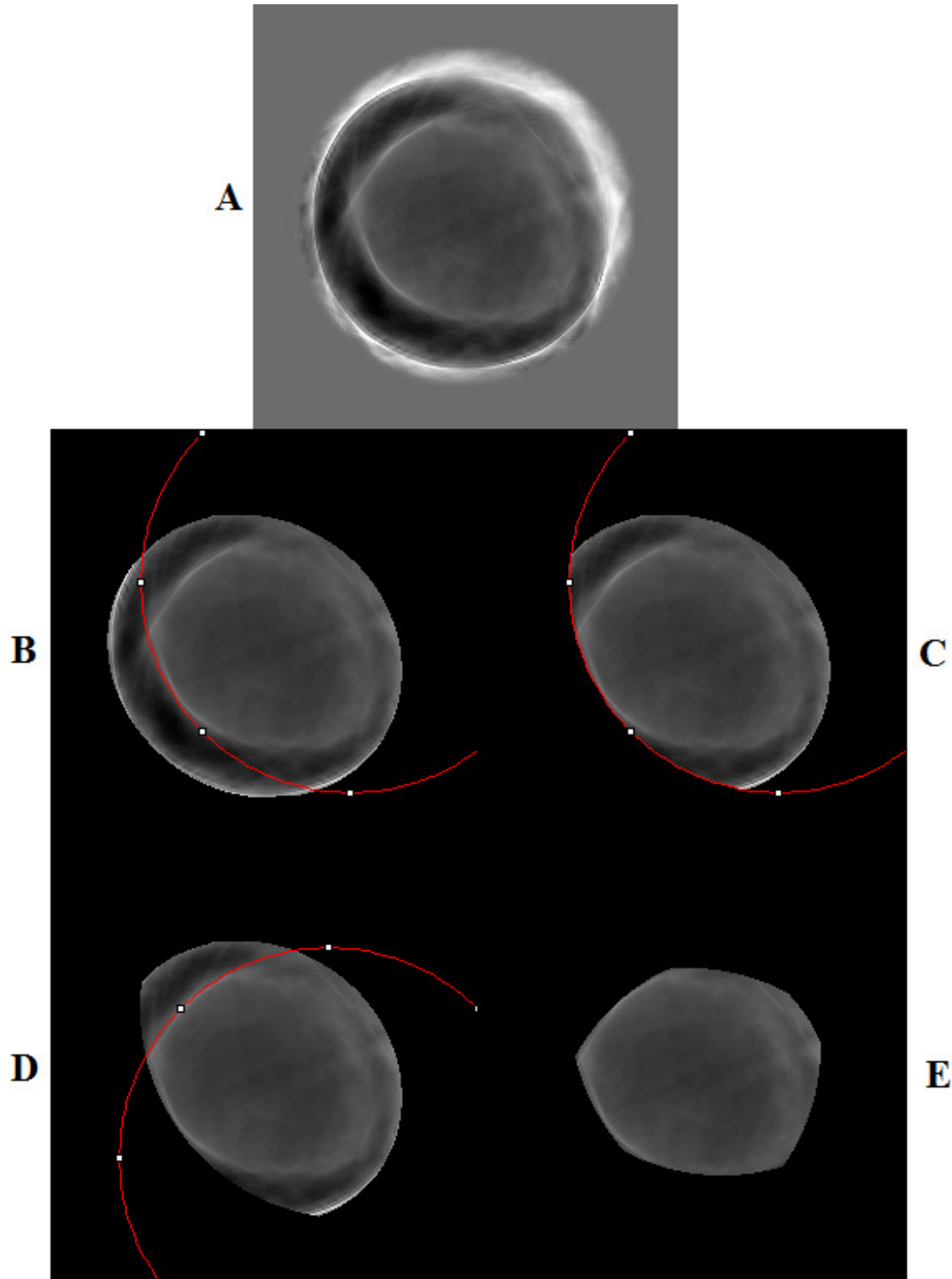


Figure 4-4 - The steps involved in removing the dark ring artifact from a single slice. A The original image with artifact. B An ellipse is fit tangent to part of the artifact. C The pixels outside the ellipse are cleared, removing a portion of the artifact, but leaving the remaining breast volume. D The ellipse is fit tangent to another part of the artifact where step C is repeated. E The final image with the artifact completely removed.

Since the artifact was a result of a surface wave moving across the breast surface, it did not represent true breast anatomy in the final reconstruction. On the sound speed image, the artifact appeared as a region of lower sound speed than the surrounding tissue. Including the artifact in the analysis of the breast density could introduce a systematic error causing the density to appear to be lower than it actually is. Removing the pixels that are known to not correspond to the physical tissue is important to accurately measuring the true breast density. This exclusion of pixels does introduce some additional uncertainty into the final measurement of the average sound speed of the breast, but the effect is small as the volume of the artifact is small compared to the volume of the breast. Therefore, the best estimate of the true breast density was accomplished by using the donut removed whole volume sound speed (DRWV). Unless otherwise noted, this sound speed value was used for all measurements made.

4.4 Preliminary Results

A total of 52 patients have been admitted into the study so far. Of these 52 patients, 26 are case studies who will receive tamoxifen and 26 are untreated comparison cases with negative screening mammograms. All 26 case patients have received their baseline scan. Of these 26 case patients, 20 of them have also received a second scan (1-3 month follow up) and 15 of these patients have also received a third scan (3-6 month follow up). The second scan was obtained an average of 51 days after treatment with tamoxifen started and the third scan was obtained an average of 143 days after starting treatment. After enrollment, one of the case patients decided to not begin taking tamoxifen after completing her baseline scan. All 26 comparison patients have only

received their baseline scan. No patient has yet to receive their 12 month scan. These results are summarized below in Table 4-1.

Table 4-1 – Summary of Patient Scans

Scan	# of Patients that Received the Scan			Average Scan Time in Days (SD)	Earliest/Latest Time
	Case	Comparison	Total		
Baseline Scan	26	26	52	N/A	N/A
1-3 Month Scan	20	N/A	20	51 (16)	(33 – 97)
3-6 Month Scan	15	N/A	15	143 (34)	(85 – 193)
12 Month Scan	0	0	0	N/A	N/A

The overall patient characteristics can be grouped and analyzed in several different ways:

1. By status in the study (Case/Comparison group)
2. By menopausal status (Pre/Post Menopause)
3. By Race (African American/White/Other)

4.4.1 Patient Characteristics – Status in the Study

Of the 52 patients enrolled so far, 26 are case studies who will undergo treatment with tamoxifen and 26 are controls who will not undergo treatment. The average baseline volume averaged sound speed for the case study patients is 1.457 km/s and 1.453 km/s for the control group. In the case group, 14 patients are pre-menopausal and 12 are post-menopausal while in the control group, 12 patients are pre-menopausal and 14 are post-menopausal. Sorting by race gives 16 African Americans, 8 White and 2 Others in the case group and 15 African Americans, 10 White and 1 Other in the control group. These results along with measured averages for age, weight, height and BMI are shown below in Table 4-2 for the case and control groups.

Table 4-2 – Descriptive Statistics for Case and Control Groups

	Count (%) or Mean (EOM)		
Menopausal Status	Case (n = 26)	Control (n = 26)	P^a
Pre-Menopausal	14 (54 %)	12 (46 %)	0.579
Post-Menopausal	12 (46 %)	14 (54 %)	
Race			
African-American	16 (62 %)	15 (58 %)	0.740
White	8 (31 %)	10 (38 %)	
Other	2 (8%)	1 (4 %)	
Other Statistics			
VASS (km/s)	1.457 (0.003)	1.453 (0.002)	0.157
Age (years)	51.0 (1.7)	52.3 (1.5)	0.571
Weight (lbs)	168.4 (5.7)	167.0 (6.3)	0.863
Height (inches)	63.9 (0.5)	64.3 (0.5)	0.567
BMI (kg/m ²)	29.0 (0.9)	28.5 (1.1)	0.762

^aP is a p-value from the chi-squared test for menopause status and race and from the two sample independent t-test for VASS, age, weight, height and BMI

4.4.2 Patient Characteristics – Menopausal Status

Out of the 52 patients, 26 are pre-menopausal and 26 are post-menopausal. The average baseline sound speed is 1.459 km/s for the pre-menopausal women and 1.451 km/s for the post-menopausal women. For the pre-menopausal women, 14 are case studies and 12 are in the comparison group, while for post-menopausal women, 12 are case studies and 14 are in the comparison group. In the pre-menopausal group, 15 women are African-American, 9 are white and 2 others while in the post-menopausal group, there are 16 African-Americans women, 9 white women and 1 other. These results along with the averaged age, weight, height and BMI are shown below in Table 4-3 for the different menopausal status.

Table 4-3 – Descriptive Statistics for Menopausal Status

	Count (%) or Mean (EOM)		
Status in Study	Pre (n = 26)	Post (n = 26)	P ^a
Case Group	14 (54 %)	12 (46 %)	0.579
Comparison Group	12 (46 %)	14 (54 %)	
Race			
African-American	15 (58 %)	16 (62 %)	0.387
White	9 (35 %)	9 (35 %)	
Other	2 (8%)	1 (4 %)	
Other Statistics			
VASS (km/s)	1.459 (0.003)	1.451 (0.002)	0.010
Age (years)	45.3 (1.0)	57.9 (1.1)	< 0.001
Weight (lbs)	172.9 (6.8)	162.5 (4.9)	0.220
Height (inches)	64.6 (0.4)	63.5 (0.5)	0.095
BMI (kg/m ²)	29.1 (1.1)	28.4 (0.9)	0.612

^aP is a p-value from the chi-squared test for status in study and race and from the two sample independent t-test for VASS, age, weight, height and BMI

4.4.3 Patient Characteristics – Race

Of the 52 patients enrolled in the study, 31 are African American, 18 are white, 2 are Asian and 1 is Native Indian. The average sound speed of the African-American women is 1.454 km/s and the average sound speed of the white women is 1.455 km/s. 16 African-American women are case studies and 15 are in the comparison group while 8 white women are case studies and 10 are in the comparison group. There are 15 pre-menopausal and 16 post-menopausal African-American women and 9 pre- and post-menopausal white women. These results along with the averaged age, weight, height and BMI are shown below in Table 4-4 for the different races.

Table 4-4 – Descriptive Statistics for Racial Status

	Count (%) or Mean (EOM)		
Status in Study	African-American (n = 31)	White (n = 18)	P ^a
Case Group	16 (52 %)	8 (44 %)	0.628
Comparison Group	15 (48 %)	10 (56 %)	
Menopausal Status			
Pre-Menopause	15 (48 %)	9 (50 %)	0.913
Post-Menopause	16 (52 %)	9 (50 %)	
Other Statistics			
VASS (km/s)	1.454 (0.002)	1.455 (0.003)	0.597
Age (years)	51.2 (1.7)	51.7 (1.6)	0.850
Weight (lbs)	177.5 (5.1)	153.9 (7.1)	0.008
Height (inches)	64.0 (0.4)	64.4 (0.6)	0.526
BMI (kg/m ²)	30.5 (0.8)	26.1 (1.2)	0.004

^aP is a p-value from the chi-squared test for status in the study and menopause status and from the two sample independent t-test for VASS, age, weight, height and BMI

4.4.4 Overall Patient Characteristic Trends

Trends between the baseline volume averaged sound speed and age, weight, height and BMI were measured. Trends were all negative and weak to moderate in strength. The trends were calculated using all patient data, regardless of study status, menopausal status or race. The results are summarized in Table 4-5 and plotted in Figure 4-5.

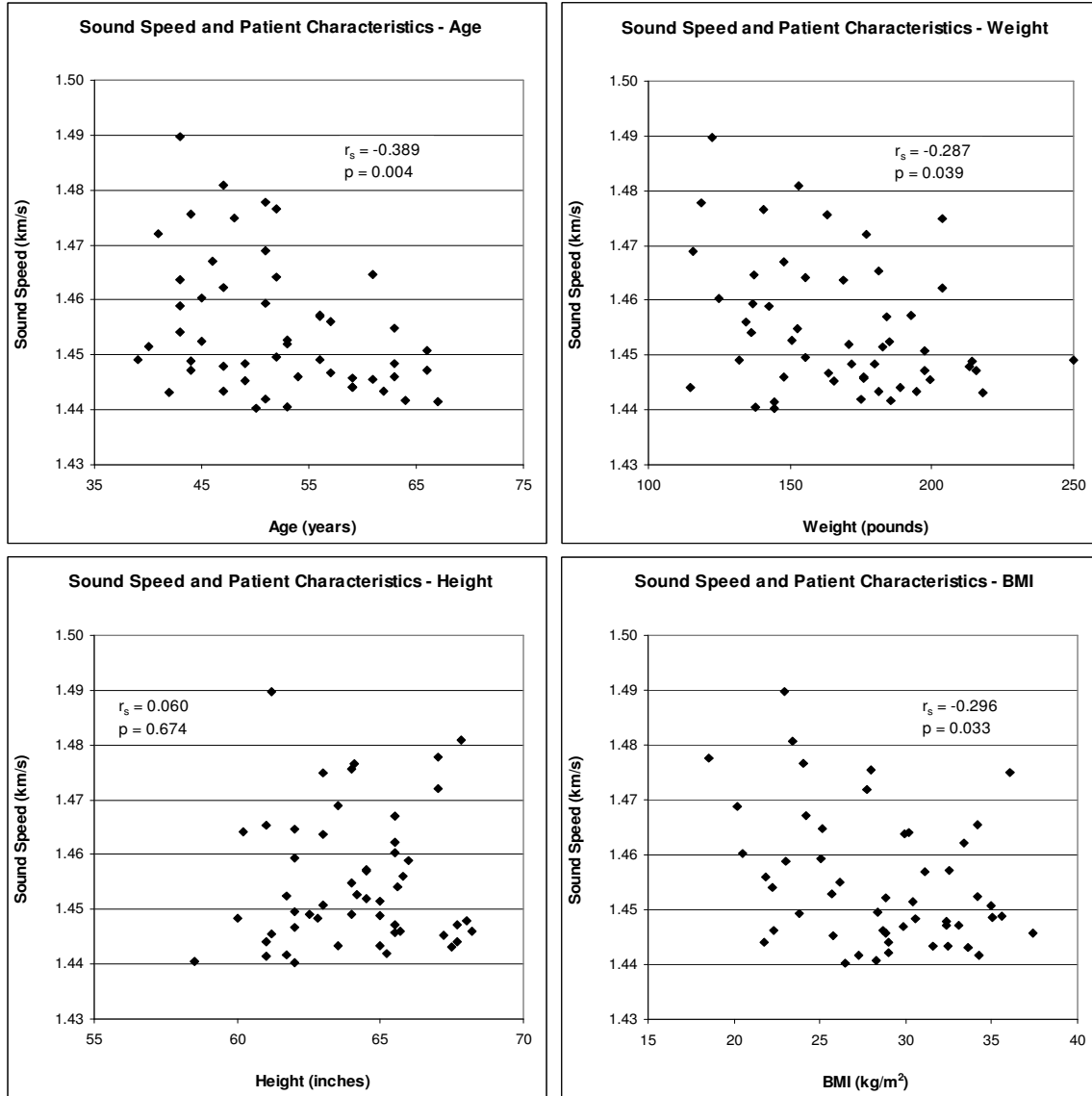


Figure 4-5 - Correlations between volume averaged sound speed and age, weight, height and BMI for all patients with a baseline scan (n = 52).

Table 4-5 – Sound Speed Correlations (n = 52)

Patient Characteristic	Spearman Correlation Coefficient	p-value
Age (years)	-0.389	0.004
Weight (lbs)	-0.287	0.039
Height (inches)	0.060	0.674
BMI (kg/m ²)	-0.296	0.033

4.5 Mammographic Measurements

Digital mammograms were also obtained for each patient in the study to be used for further analysis. All 52 patients enrolled in the study received a mammogram, but 46 had their mammographic density analyzed with Cumulus for comparative studies. To test for reliability of the density measurements, the mammograms were randomized and five patients had their mammograms read twice. There was one additional mammogram that could not be analyzed due to file corruption.

4.5.1 Mammographic Percent Density and Patient Characteristic Trends

The mammographic percent density along with other mammographic imaging characteristics were calculated using the obtained mammograms. The average MPD stratified by the different groupings is shown below in Table 4-6.

Table 4-6 – Average MPD by Different Groupings

Grouping	First Group Average (EOM)	Second Group Average (EOM)	p-value
Case/Comparison	34.6 (5.0)	22.2 (4.2)	0.062
Pre/Post Menopausal	31.7 (4.7)	23.6 (4.6)	0.230
African-American/White	28.1 (4.9)	27.1 (5.0)	0.888

Correlations involving the MPD and many of the other mammographic characteristics were also plotted. The correlations involving age, weight, BMI and height were similar to those involving the VASS with age, weight and BMI showing modest but negative correlations. These patient characteristics are shown below in Figure 4-6 and the results are summarized in Table 4-7.

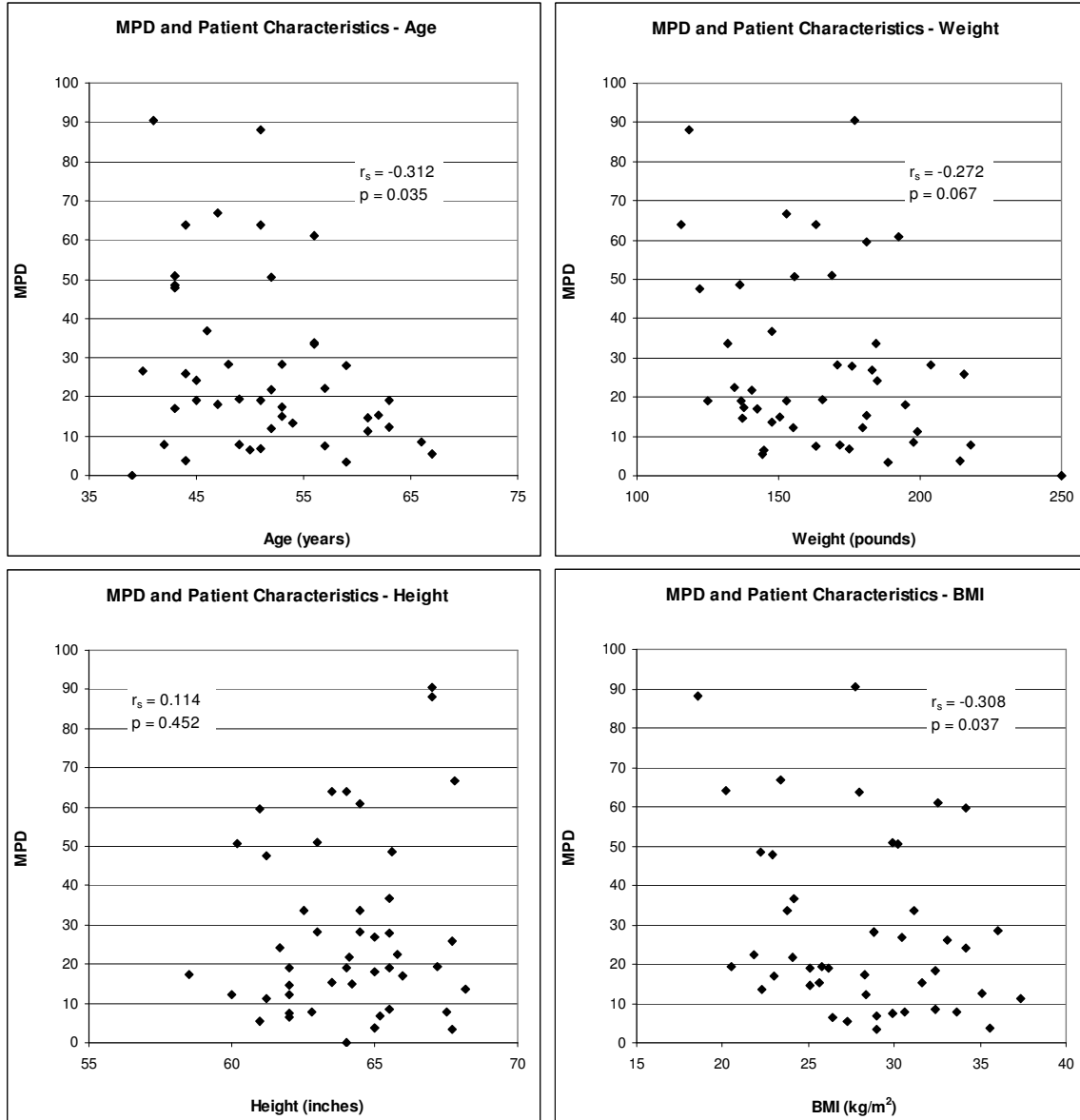


Figure 4-6 - Correlations between mammographic percent density and age, weight, height and BMI for all patients with a baseline scan ($n = 46$).

Table 4-7 – MPD and Patient Characteristic Correlations ($n = 46$)

Patient Characteristic	Spearman Correlation Coefficient	p-value
Age (years)	-0.312	0.035
Weight (lbs)	-0.272	0.067
Height (inches)	0.114	0.452
BMI (kg/m^2)	-0.308	0.037

4.5.2 Mammographic Imaging Characteristic Trends

Along with the calculation of mammographic percent density, measurements of the total amounts of dense, non-dense and total breast areas were also made. Correlations involving the MPD and VASS with these imaging characteristics were made and are shown below. Even with the smaller number of patients involved in this study, the results that are seen are consistent with those observed with the larger population of patients earlier (Table 3-7). The correlation between UST and mammographic density measures showed a Spearman correlation of $r_s = 0.736$ (Figure 4-7), which is similar in strength to the previous study. The relationship between VASS and MPD also appears to be linear, which is what was observed before for digital mammograms. The linear relationship is likely due to the linear x-ray response of digital detectors.

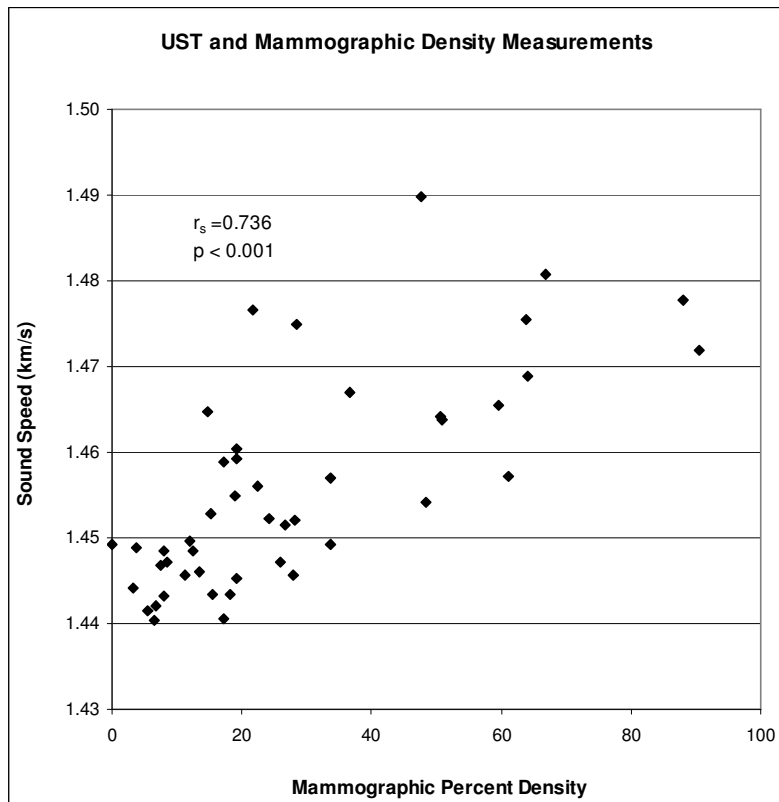


Figure 4-7 - Plot of volume averaged sound speed versus mammographic percent density for the patients in the UST study, $n = 46$.

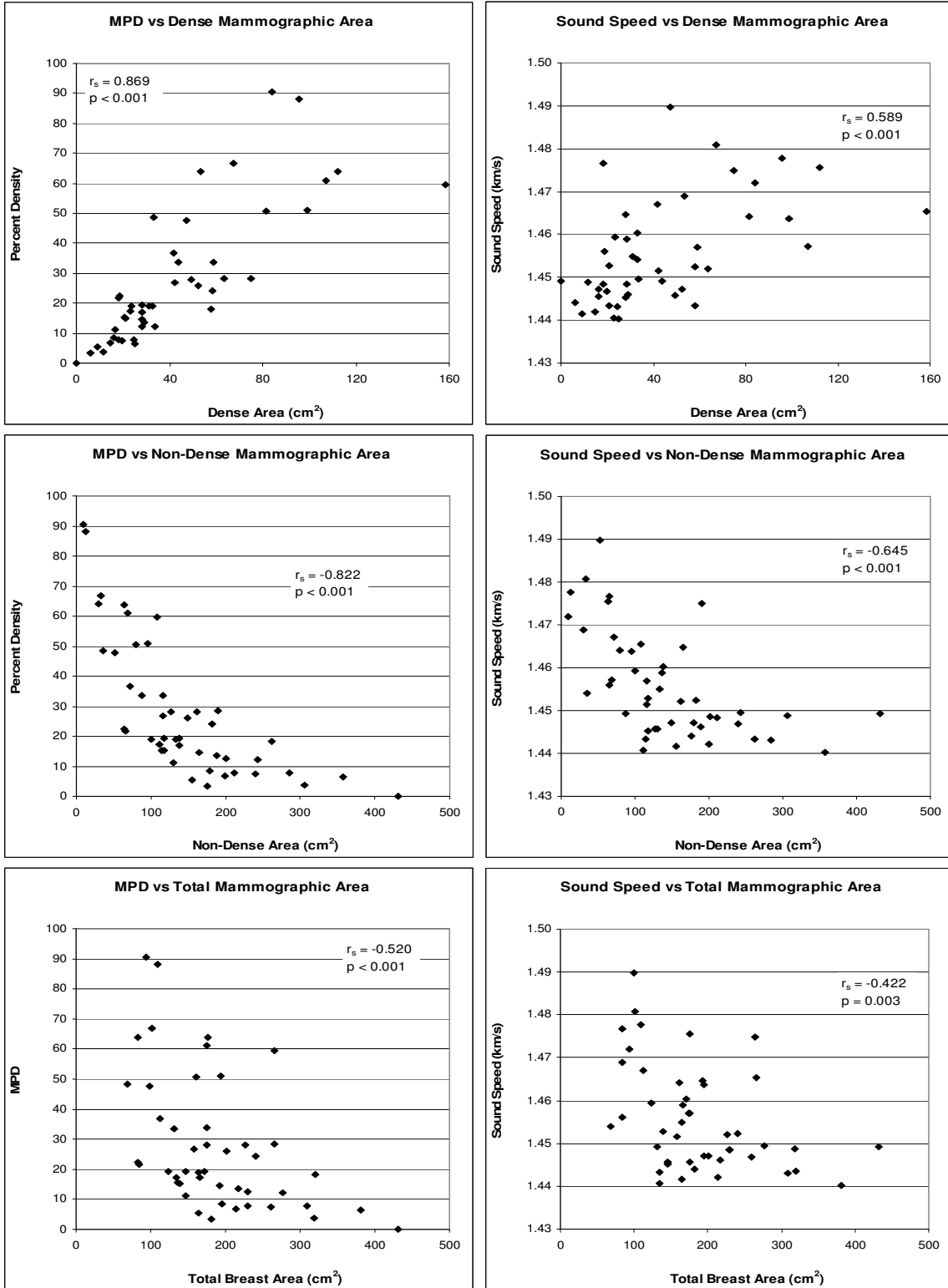


Figure 4-8 - Correlations involving the mammographic imaging characteristics and the mammographic percent density (Left) and the volume averaged sound speed (Right), n = 46.

The correlations between the sound speed and MPD with the mammographic imaging characteristics are strong and are shown in Figure 4-8. Stronger correlations are observed for the MPD measurements than for the VASS measurements. This is expected as the measurement of MPD is made directly from the measurements of the dense area on the mammogram. The results for these correlations are summarized below in Table 4-8. Once again, these results are similar to those observed previously with more data.

Table 4-8 – Sound Speed and MPD Correlations with Mammographic Characteristics

Mammographic Factor	Spearman Correlation Coefficient (p-value)	
	Correlation with MPD (n = 46)	Correlation with VASS (n = 46)
Dense Area	0.869 (< 0.001)	0.589 (< 0.001)
Non-Dense Area	-0.822 (< 0.001)	-0.645 (< 0.001)
Total Area	-0.520 (< 0.001)	-0.422 (0.003)

4.6 Measuring the Effects of Tamoxifen over Time

To compare their performance, all methods of sound speed measurement (WVSS, CVSS, DRWVSS and DRCVSS) were calculated. This was done to see if differences in the methods used in measuring sound speed produced differences in the relative changes within them. If the uncertainties produced by not removing the artifact or by measuring different volumes of breast tissue are uniform between scans, the extra effort required to compensate for them may not be required if the interest is only to track relative changes in density over time.

4.6.1 Overall Average Response

Averaging the sound speed of all the patients can give us an estimate of how much of an effect tamoxifen has on breast density. For the 20 patients with two scans, the baseline average sound speed was 1.4530 km/s and the second scan average was

1.4518 km/s as measured using the donut removed whole volume sound speed (DRWVSS). The results for the remaining methods of sound speed calculation are shown below in Table 4-9 and plotted in Figure 4-9. A different method of viewing the change over time is to average the difference from the baseline scan for each patient. This essentially normalizes the changes such that the baseline scan for each different method of calculation gives a change of zero. This plot is also shown in Figure 4-9.

Table 4-9 – Results for Tamoxifen Cases with Two Scans (n = 20)

Measurement	Baseline Average (km/s)	Second Scan Average (km/s)	Change from Baseline (m/s)	p-value
WVSS	1.4514	1.4507	-0.7	0.661
CVSS	1.4518	1.4509	-0.9	0.628
DRWVSS	1.4530	1.4518	-1.2	0.366
DRCVSS	1.4523	1.4513	-1.0	0.605

WVSS – whole volume sound speed; CVSS – common volume sound speed; DRWVSS – donut removed whole volume sound speed; DRCVSS – donut removed common volume sound speed. The p-value was from the paired t-test between the baseline and final scan.

Of the 15 patients with three scans, when using the donut removed whole volume sound speed, the baseline average sound speed was 1.4524 km/s, the second scan average was 1.4518 km/s and the third scan average was 1.4516 km/s. Once again, this overall change was negligible and too small, compared to the uncertainty, to indicate any overall trend as a result of tamoxifen treatment. These results, along with the results for the other methods of measurement are shown below in Table 4-10 and plotted in Figure 4-10. The difference from the baseline scan for each method was also plotted in Figure 4-10.

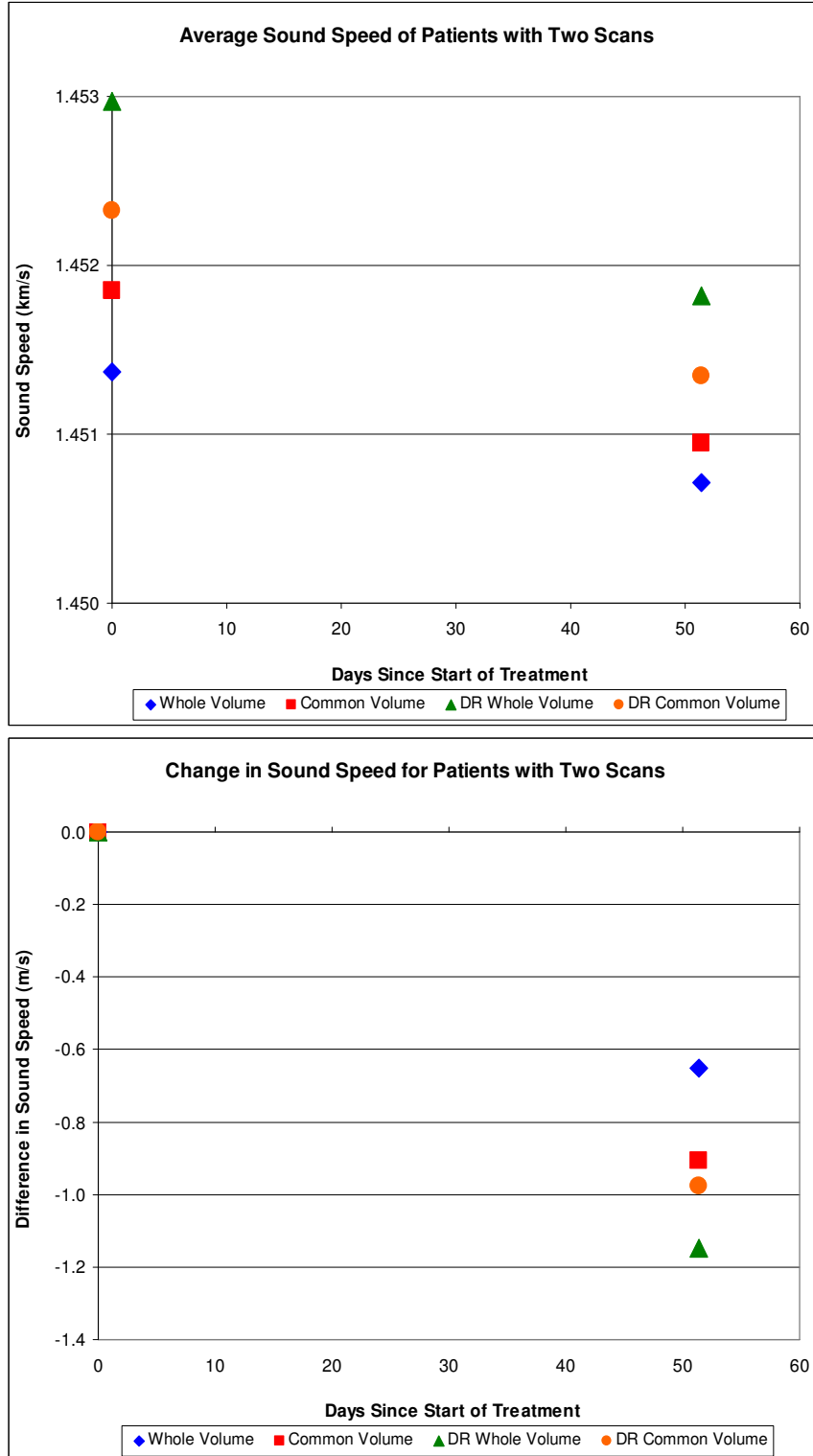


Figure 4-9 - The average sound speed (Top) and the average change in sound speed from baseline (Bottom) for patients with 2 scans (n = 20) using the different methods of measuring sound speed.

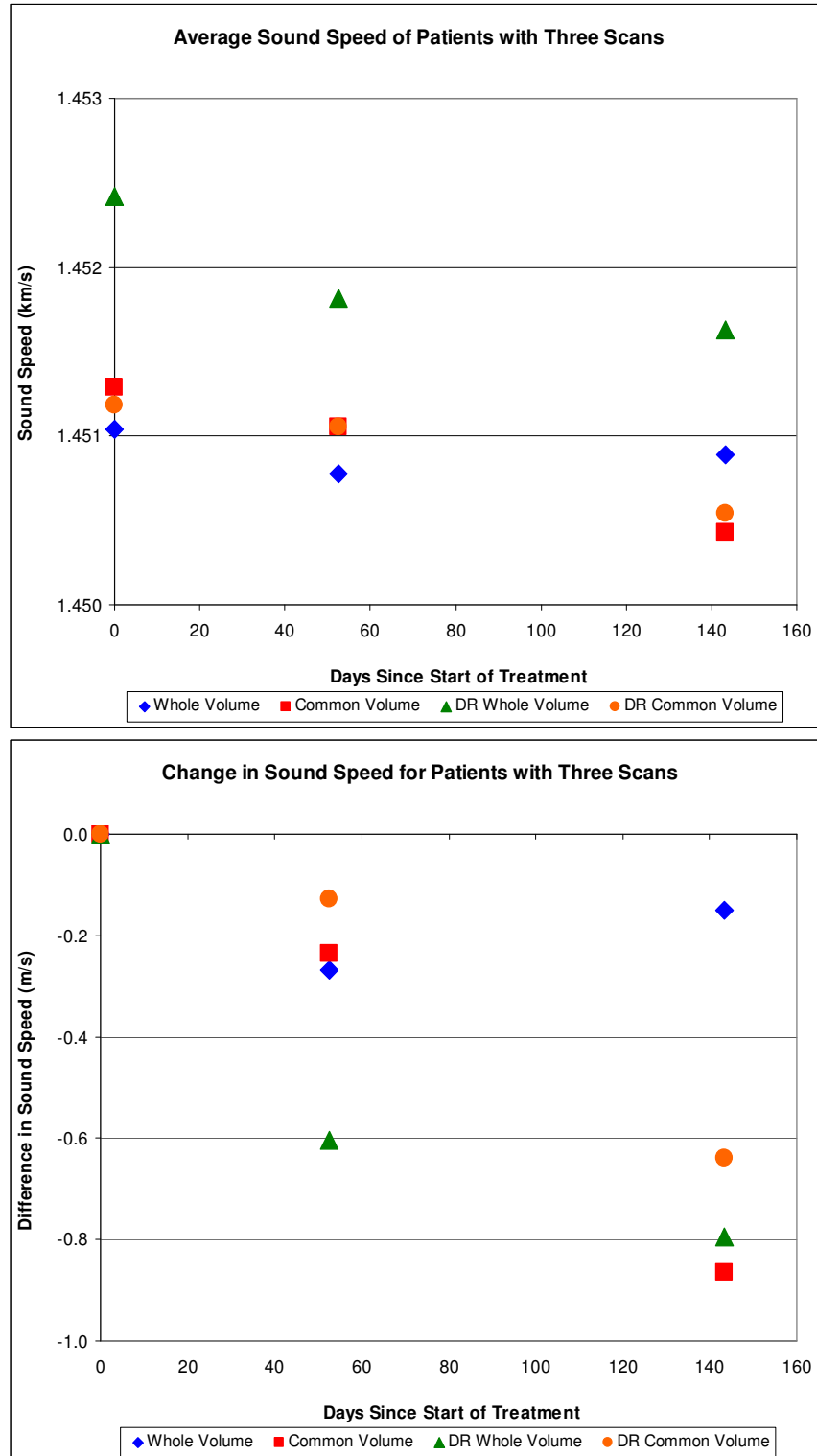


Figure 4-10 - The average sound speed (Top) and the average change in sound speed from baseline (Bottom) for patients with 3 scans ($n = 15$) using the different methods of measuring sound speed.

Table 4-10 – Results for Patients with Three Scans

Measurement	Baseline Average (km/s)	Second Scan Average (km/s)	Third Scan Average (km/s)	Change from Baseline (m/s)	p-value
WVSS	1.4510	1.4508	1.4509	-0.1	0.919
CVSS	1.4513	1.4511	1.4504	-0.9	0.638
DRWVSS	1.4524	1.4518	1.4516	-0.8	0.503
DRCVSS	1.4512	1.4511	1.4505	-0.6	0.729

WVSS – whole volume sound speed; CVSS – common volume sound speed; DRWVSS – donut removed whole volume sound speed; DRCVSS – donut removed common volume sound speed. The p-value was from the paired t-test between the baseline and final scan.

The changes in sound speed over this time frame are too small to draw firm conclusions, especially when compared to the uncertainty in the measurement of the average values. For the small number of patients used, the standard error of the average values calculated is on the scale of 3-4 m/s, so changes on the order of the 1 m/s that were obtained here may be lost in the noise. The uncertainty will decrease as more data are collected. Currently there is not any statistically significant trend that can be inferred from the overall average measurements of all the patients. However, among tamoxifen treated patients, approximately half appear to be density responders by showing a decrease in breast density. So analysis of changes in density per patient may be more appropriate and may provide the basis for further study.

4.6.2 Patients Responding to Treatment

The data plotted above show the average change in sound speed of all patients undergoing treatment with tamoxifen. The small overall change in sound speed across all patients may mask heterogeneity in responses because change in sound speed was averaged across patients whose density declined, remained unchanged or increased. To

further examine the effects of tamoxifen on UST-measured breast density, the response of the patients was grouped into two categories:

1. Those that showed a decrease in sound speed
2. Those that showed an increase in sound speed

Of the 20 patients that received two scans, 11 showed a decrease and 9 showed an increase in sound speed, while of the 15 that received three scans, 8 showed a decrease and 7 showed an increase in sound speed. Table 4-11 gives the results for the average sound speed of the patients that showed a decrease while Figure 4-11 plots the differences for the different methods used to calculate sound speed. When observing these patients, the changes in sound speed are much more apparent than when changes are averaged across the entire group. Also, the changes measured here are similar in size or greater than the uncertainties in the measurements. This suggests that the trends visible in the plots may be more statistically relevant.

Table 4-11 – Average Sound Speed of Patients Showing A Decrease

	Measurement	Baseline Average (km/s)	Second Scan Average (km/s)	Third Scan Average (km/s)	Change (m/s)	p-value
Patients With Two Scans (n = 11)	WVSS	1.4540	1.4498	N/A	-4.2	0.016
	CVSS	1.4546	1.4494	N/A	-5.2	0.037
	DRWVSS	1.4560	1.4513	N/A	-4.7	0.005
	DRCVSS	1.4556	1.4501	N/A	-5.4	0.045
Patients With Three Scans (n = 8)	WVSS	1.4523	1.4476	1.4482	-4.1	0.007
	CVSS	1.4520	1.4471	1.4468	-5.2	0.004
	DRWVSS	1.4531	1.4494	1.4489	-4.2	0.001
	DRCVSS	1.4519	1.4470	1.4470	-4.9	0.001

WVSS – whole volume sound speed; CVSS – common volume sound speed; DRWVSS – donut removed whole volume sound speed; DRCVSS – donut removed common volume sound speed. The p-value was from the paired t-test between the baseline and final scan.

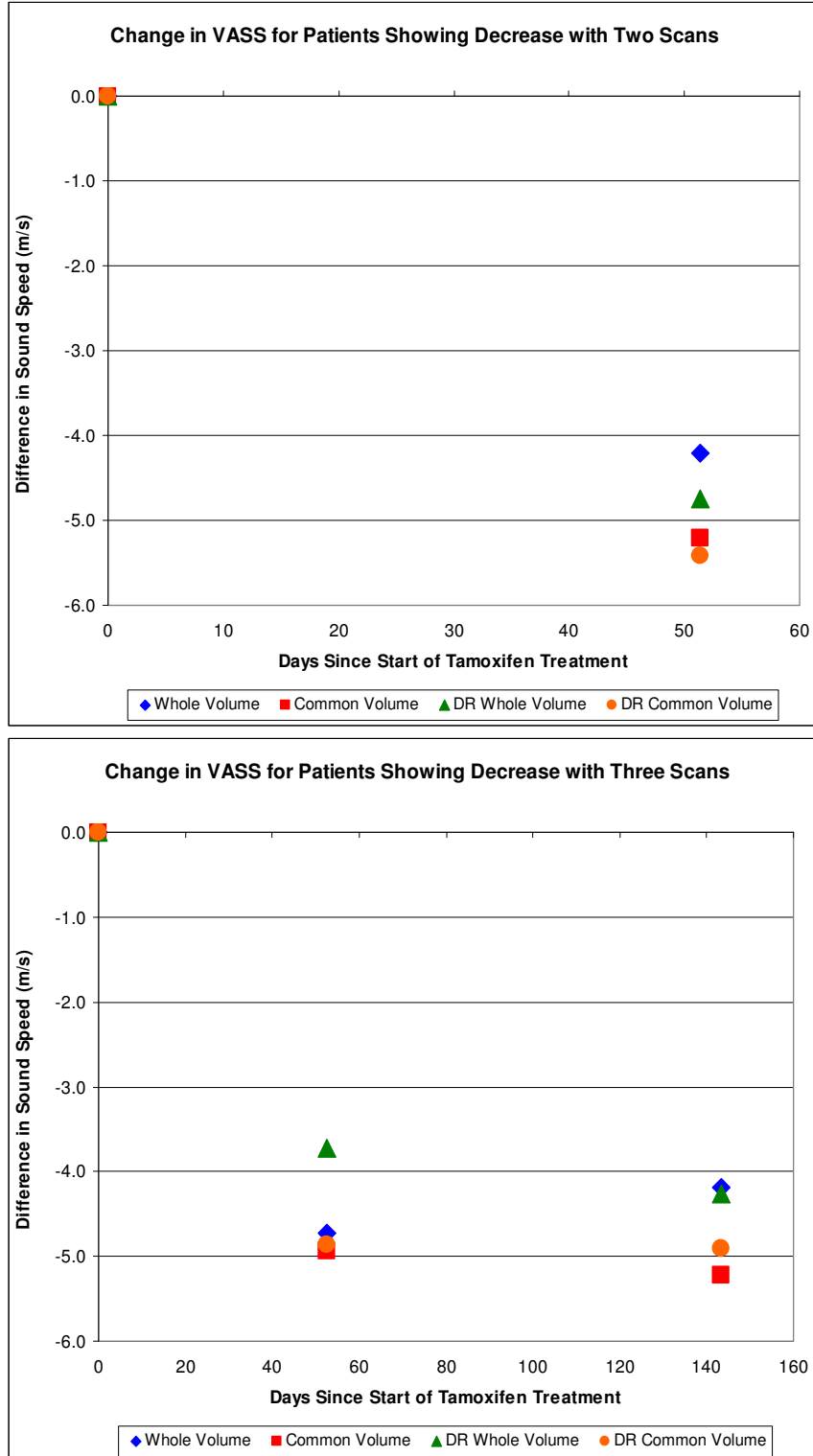


Figure 4-11 - Plots of the average change in sound speed measured using all separate measures of sound speed for patients that showed a decrease for patients with two scans (Top) and patients with three scans (Bottom).

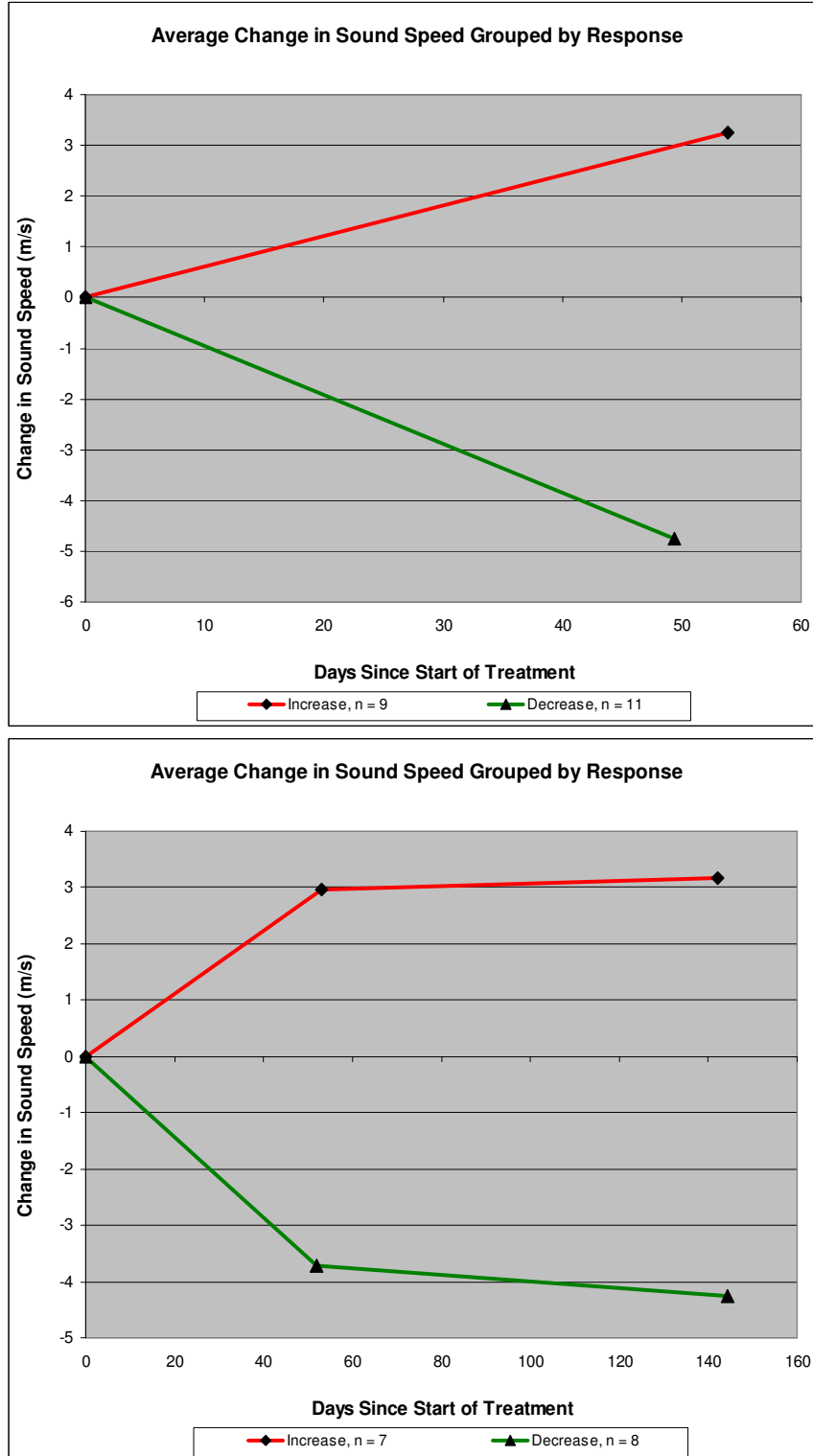


Figure 4-12 - The average change in sound speed grouped by response type for patients that received two scans (Top) and three scans (Bottom).

To make the effects of the patients whose breast density decreased with tamoxifen treatment more evident, the average sound speed of each response group (i.e. those showing an increase or decrease in sound speed) was plotted as a function of time. This plot is shown above in Figure 4-12 for patients with two and three scans. From the preliminary data shown here, the change in sound speed that occurs after the second scan, approximately 50 days after treatment begins, resulted in the largest visible change. This change was maintained after the third scan. These preliminary data do not permit definitive conclusions regarding whether serial UST examinations may enable rapid identification of women who will show discernible declines in mammographic density at 12 months and beyond. However, it appears that it may be possible to use UST to detect changes in breast density associated with tamoxifen treatment after only approximately 50 days of treatment, at least in some women.

4.6.3 Changes in Patient Weight

Since a patient's weight is a factor that is known to affect breast density and can fluctuate in a short period of time, it is important to track to ensure that any measured changes in breast density are likely due to tamoxifen and not to a patient's weight loss or gain. The patient's weight was recorded at each scan and the average values for patients with two and three scans are shown in Table 4-12 grouped for the entire group as well as for those patients that showed an increase and decrease in sound speed. The results show that there was a small decrease in sound speed of no greater than a few pounds, but the difference was not statistically significant.

Table 4-12 – Average Changes in Patient Weight between Scans

	Group	Weight at First Scan (lbs)	Weight at Second Scan (lbs)	Weight at Third Scan (lbs)	Difference (lbs)	p-value
Patients With Two Scans	Overall, n = 20	170.9	170.1	N/A	-0.8	0.382
	Decreasing, n = 11	159.3	159.5	N/A	+0.2	0.890
	Increasing, n = 9	185.0	183.1	N/A	-1.9	0.138
Patients with Three Scans	Overall, n = 15	164.9	164.2	162.7	-2.2	0.084
	Decreasing, n = 8	160.4	159.8	158.8	-1.5	0.462
	Increasing, n = 7	170.2	169.3	167.2	-3.0	0.059

The difference was calculated between the first and final scan. The p-value was from the paired t-test between the first and final scan.

4.7 Response Grouped by Baseline Sound Speed

Since one of the presumed effects of tamoxifen is to reduce breast density, women with higher starting densities may be more inclined to show greater decreases in sound speed. Women with low baseline breast densities should be less likely to further reduce their density, so tamoxifen may not produce the same changes in these patients. To test this, the data was grouped into thirds (or tertiles) according to the baseline sound speed and the changes in sound speed were calculated. The results for patients with two and three scans are shown below in Table 4-13 and plotted in Figure 4-13. The average baseline sound speed of the highest tertile was approximately 15 m/s higher than the middle tertile, which is a large difference. The change in sound speed for the highest tertile was almost 4 m/s while the middle and lowest tertile showed little change to a small increase in sound speed. For the small number of patients in each group, about 5 to 7, the standard error of the average sound speed is on the order of 3-4 m/s. So the 3-4 m/s decrease in sound speed for the highest tertile may indicate a statistically significant trend.

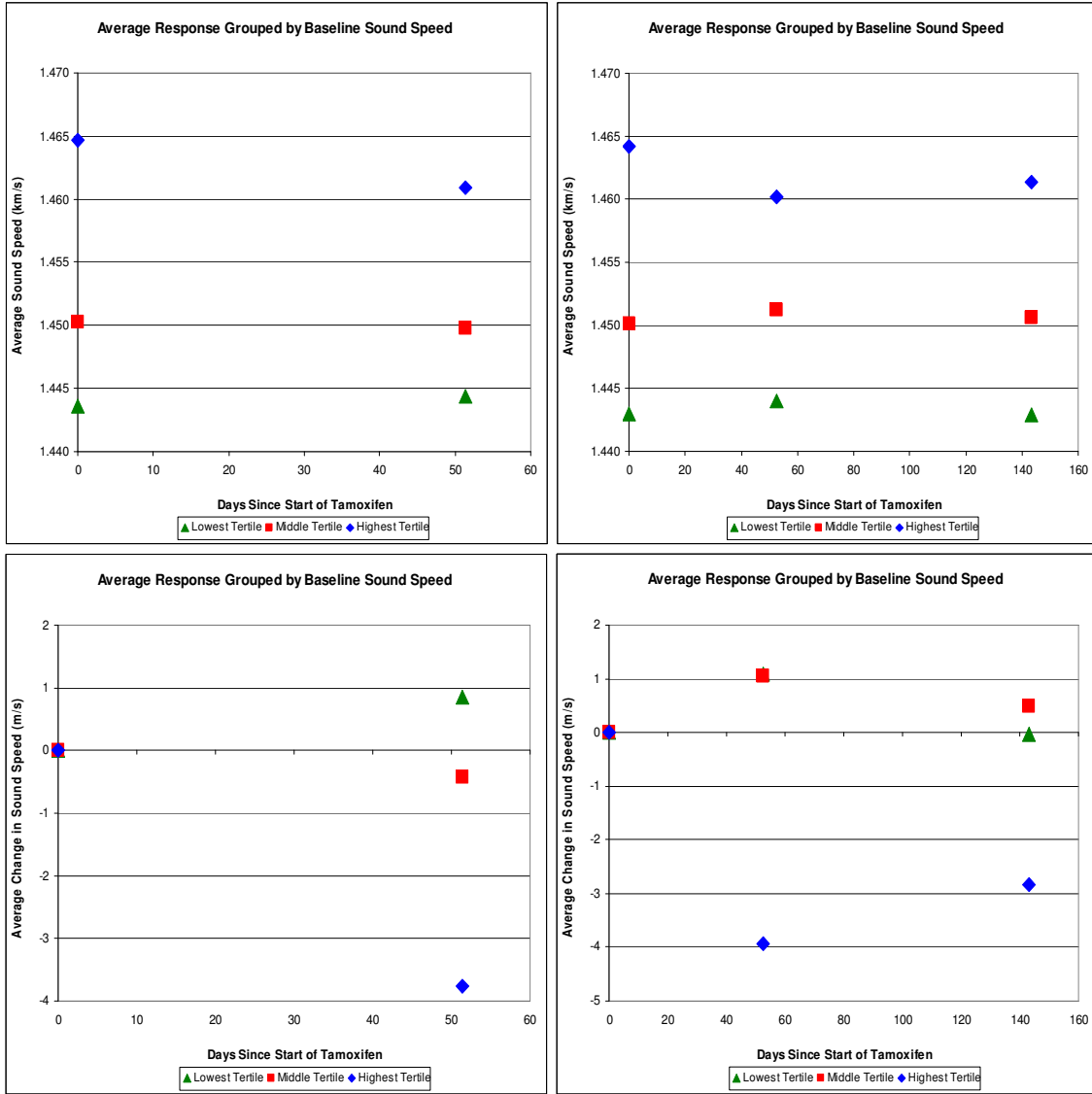


Figure 4-13 - The average sound speed (Top) and average change in sound speed (Bottom) grouped by baseline sound speed for patients that received two scans (Left) and three scans (Right).

Table 4-13 – Change in Sound Speed Grouped by Baseline Sound Speed

	Tertile	Baseline Average (km/s)	Second Scan Average (km/s)	Third Scan Average (km/s)	Change From Baseline (m/s)	p-value
Patients With Two Scans (n = 20)	Lowest	1.4436	1.4444	N/A	+0.8	0.258
	Middle	1.4503	1.4498	N/A	-0.4	0.889
	Highest	1.4647	1.4609	N/A	-3.8	0.163
Patients With Three Scans (n = 15)	Lowest	1.4430	1.4440	1.4429	-0.1	0.980
	Middle	1.4501	1.4512	1.4506	+0.5	0.859
	Highest	1.4642	1.4602	1.4613	-2.8	0.225

The p-value was from the paired t-test between the baseline and final scan.

4.8 Sound Speed Inter Rater Correlations

Since measuring the average sound speed from a UST image was semi-automated, the obtained values may be dependent on the subjectivity of the current reader. Each reader is responsible for deciding which slices are to be included in the final calculations, along with estimating the shape of the breast in each slice. The selection of the common volume as well as the removal of the artifact, if present, from the images is also dependent on the user. Therefore, the inter rater correlations were tested for the different sound speed measurements made by several different users.

4.8.1 Whole Volume Sound Speed Inter Rater Correlation

The intra rater correlation was calculated for WVSS measurements between five different raters (MS, SJ, BH, BR and ZM). To calculate the WVSS, each rater was responsible for determining the first slice that contains the nipple region, the last slice that does not contain any of the chest wall and for selecting the boundary of the breast that is to be masked. Since the WVSS is the first measurement made for each scan regardless of the patient's status in the study, a total of 64 scans over 43 patients were

analyzed and correlations between different pairs of raters were calculated. For five raters, a total of 10 Spearman's correlation coefficients were measured. The results are shown below in Table 4-14. The average correlation coefficient was found to be $r_s = 0.960$. This strong correlation between raters shows that the selection of start and end slices is not that critical. This is most likely due to the large volumes measured for each scan which reduce the effects of the small differences in pixels that the choice of slices and mask creation produces. The Intraclass correlation coefficient is $ICC = 0.966$, which indicates a very strong correlation between raters.

Table 4-14 – Spearman Correlation Coefficients for Inter-Rater WVSS Measurements

Raters	MS	SJ	BH	BR
SJ	0.951	N/A	N/A	N/A
BH	0.983	0.949	N/A	N/A
BR	0.963	0.955	0.947	N/A
ZM	0.974	0.948	0.977	0.952

All p-values for all correlations were found to be $p < 0.001$

4.8.2 Common Volume Inter Rater Correlation

Of the 5 raters that calculated the WVSS, 4 then went to calculate the CVSS for the patients with multiple scans. The raters were responsible for determining which slices corresponded to the common volume in these scans using the methods described earlier. Each rater would first calculate the WVSS over the entire volume and then individually choose the common volume between the scans. Once the common volume was selected, the average sound speed over this volume was calculated. The ability to identify common landmarks between scans was the greatest source of uncertainty between each rater. The raters examined the images for 15 patients with multiple scans, giving a total of 36 scans. Spearman coefficients for the different pairs were calculated

and are shown below in Table 4-15. The average correlation coefficient was found to be $r_s = 0.970$. The correlation between the different raters for the common volume is just as strong as the correlation for the whole volume despite the additional uncertainty of selecting the common volume between raters. The Intraclass correlation coefficient between the three raters was found to be $ICC = 0.962$, which indicates a very strong correlation.

Table 4-15 – Correlation Coefficients for Inter-Rater CVSS Measurements

Raters	MS	SJ	BH
SJ	0.986	N/A	N/A
BH	0.979	0.971	N/A
BR	0.964	0.963	0.958

All p-values for all correlations were found to be $p < 0.001$

4.8.3 Artifact Removed Inter Rater Correlation

Two different raters then went on to remove the ring artifacts for the whole volume calculations (DRWVSS). Choosing the slices with the artifact and the removal of the artifact introduce a new potential source of error. The measurements were made on a total of 13 patients that received 31 separate scans. The Spearman coefficient was found to be $r_s = 0.948$. The Intraclass correlation coefficient between the three raters was found to be $ICC = 0.907$, which indicates a very strong correlation.

Three raters then also measured the common volume sound speed with the artifact removed. A total of 31 scans were compared over 13 patients. The Spearman correlation coefficient for each pairing was calculated and shown below in Table 4-16. The average coefficient was $r_s = 0.921$. The intraclass correlation coefficient was calculated to be ICC

= 0.921. These strong correlations indicate that the removal of the artifact could be done in a similar fashion by different raters.

Table 4-16 – Correlation Coefficients for Inter-Rater DRCVSS Measurements

Raters	MS	SJ
SJ	0.940	N/A
BH	0.907	0.917

All p-values for all correlations were found to be $p < 0.001$

Table 4-17 summarizes the calculated ICC values from the different inter-rater measurements.

Table 4-17 – Intraclass Correlation Coefficients

Measurement	# of Raters	# of Scans	ICC
WVSS	5	64	0.966
CVSS	4	36	0.962
DRWVSS	2	31	0.907
DRCVSS	3	31	0.921

4.9 Estimating the Uncertainty in the Sound Speed Measurements

Estimating the uncertainty in the sound speed measurements requires careful consideration. The average sound speed is on the order of 1.4 – 1.5 km/s. Since the sound speed is the average of a distribution of values, the standard error of the mean, a value calculated from the statistics of the distribution, should describe the uncertainty adequately. However, the standard error was calculated by taking the standard deviation of the distribution, which for any single measurement was on the order of 15 – 40 m/s, and dividing by the square root of the number of counts, which was between a hundred thousand and one million. This gave a standard error that was usually less than 10 cm/s. However, this value underestimates the true uncertainty in the measurement.

A more accurate estimate of the uncertainty was obtained from the inter-rater measurements. The different readers will provide a range of values for each individual measurement. These differences arise from the subjective decisions made by each reader to choose the start/end slices and to separate the breast tissue from the water bath. By averaging the deviations in each of these measurements, an estimate of the rater uncertainty can be made. The 5 raters that were used to assess the 64 WVSS measurements caused an average deviation in the measured value of 1.8 m/s. With an effective range of potential sound speed measurements of about 100 m/s, this calculated uncertainty is a much more reasonable estimate of the actual uncertainty associated with an individual sound speed measurement.

To estimate the uncertainty in values that average several individual sound speed measurements involves simply calculating the standard error. This uncertainty applies to the average sound speed grouped by response type and grouped by baseline sound speed. Since there are a limited number of patients enrolled in the study, grouping the data into further subsets causes this uncertainty to vary strongly based on the actual number of patients in each group. Depending on which group is being examined, it contains between 5 and 20 averaged values. The uncertainty in these values ranges on the order of 3-4 m/s. The uncertainty will decrease with the inverse of the square root of the number of values. Upon completion of the study, these groups may contain up to 10 times the current number of patients. This will cause the uncertainty to fall below that of the individual measurement, making smaller changes more readily apparent and statistically meaningful.

4.10 Future Studies

The data presented here are only preliminary based on approximately 50 total patients. The study is not a completed study yet. The proposed study called for a total of 300 patients to be examined, 150 case and 150 comparison patients. The next course of action would be to continue the study and collect the full set of results from the entire cohort of patients. This includes collecting the full set of four scans from the case group (baseline, 1-3 month scan, 3-6 month scan and 12 month scan) and the pair of scans from the comparison group (baseline, 12 month scan). Collecting this entire set of data will allow for trends involving the effects of tamoxifen and VASS to be fully understood and analyzed. Despite the incomplete data set, these preliminary results are promising. Although the full 12-month measurements are necessary to draw complete conclusions of the effects of tamoxifen, large changes in breast density can be measured after only 1-3 months of treatment. The change after 1-3 months may also be indicative of the overall effectiveness of the treatment, but this cannot be concluded for certainty from this study as patient outcomes will not be followed. The percentage of women who have shown a decrease in breast density falls in line with the results of other studies. UST therefore shows promise to be an effective tool to track changes in breast density. It can be used to frequently and accurately monitor breast density in women with higher densities and greater risk. The degree of its effectiveness is still yet to be fully determined, but the preliminary results shown here reflect that there is some value to UST breast density measurements.

CHAPTER 5

DISCUSSION

The inclusion of mammography, menopausal, race, family history and parity data allows for the unique opportunity to compare and analyze differences in breast density measurements relative to each group and relative to the sound speed measurements.

5.1 Factors that Affect Breast Density

Table 3-2 summarizes the characteristics of the digital and film data sets. The statistically significant differences between the two groups include the mean values of mammographic percent density, dense area on the mammogram, age, weight and BMI. There is no reason why the average weight and BMI should be higher for the women who received a film mammogram, so the differences are likely due to random chance. One possible explanation for the lower age of the digital group is that younger women, who are more likely to have denser breasts, may be more likely to be referred to digital mammography. However, without knowing the exact reason for the choice of mammogram type, the difference could also simple be due to random chance.

Based on known correlations involving increased age and weight [Table 1-2], the breast density of the film group should therefore be lower than that of the digital group since the average age and weight in the film group is higher. However, the opposite is true. For the film group, the MPD and the dense area are actually greater than that of the digital group. When comparing the density measurements made on these two groups using UST, the density, as measured by the VASS, was higher for the group that received digital mammograms, yet statistically insignificant. Groups of women chosen randomly from a larger population should have a similar average breast density regardless of the

imaging modality used to measure the density. This should be true unless there is a systematic bias in patient referrals. Also, when comparing density measurements between the other groups, even when there was no statistical significance between them, the group with the higher VASS also had the larger MPD.

Therefore, these results suggest that the way digital and film mammography create images are fundamentally different. It appears that digital mammography underemphasizes dense tissue relative to film. Other studies have shown mixed results when comparing film and digital mammography. One study shows similar results presented here, that film mammograms give higher percent density measurements than digital mammograms¹⁸⁷. Another study shows comparable measurements, but between screen-film mammography and the digitized versions of the film¹⁸⁸. However, since the digital mammograms in this study were actually performed using digital detectors, the results of this study are not applicable here. Still, other studies show little to no difference between the two different modalities in regards to cancer detection rates^{63, 64, 189, 190}. Because of these inconsistencies, it is therefore justifiable to separate the two data sets for purposes of comparison with overall patient characteristics and with mammographic and UST-related imaging characteristics.

Menopausal status is a well known risk factor for breast cancer and the results shown in Table 3-3 indicate that it also has a great effect on breast density as well. Menopause is known to lead to a decrease in breast density. Density measurements made using both imaging modalities show higher breast densities in pre-menopausal women, exactly as expected. When using MPD, VASS or even USTPD, the results are consistent and statistically significant. Most other imaging characteristics show statistically

significant differences depending on menopausal status. In particular, the amount of fatty tissue is greater in post-menopausal women and while the amount of dense tissue is lower in post-menopausal women, the difference is not statistically significant. This seems to indicate that the amount of fatty tissue is the key change in breast anatomy as women proceed through menopause. However, this conclusion can not be definitively drawn since these women were drawn from two separate groups and not followed through the menopausal transition.

Boyd *et al*³⁶ did perform such a longitudinal study on the effect of menopause on mammographic density and concluded that menopause has effects on mammographic properties that are greater than those due to age alone. In line with the results shown here for mammography and UST, it was determined that breast density decreased and the amount of non-dense tissue increased as women passed through menopause. In addition, Boyd *et al* also found that the amount of dense tissue shows a statistically significant decrease during menopause, which conflicts with the behavior observed here. This can likely be explained because in the data presented here, the average size of the breast of the post-menopausal group is greater than the size in the pre-menopausal group. In the longitudinal study, the overall sizes of the different groups were very similar. Larger breasts are more likely to contain more dense and non-dense tissue which can potentially skew the results. If the measured areas in the data presented here are normalized, the decrease in dense tissue in post-menopausal women would be more apparent. Menopause is an important stage in a woman's life and has great effects on breast anatomy, breast cancer risk and even cancer treatment. However, even though the overall effects of menopause on breast density are well understood, UST can be a useful tool to

characterize the changes associated with menopause and effects of the menopausal transition on density.

Associations between race and breast density have been inconsistent. Previous results have found that breast density in African-American women can be higher or lower than breast density in white women⁴⁸⁻⁵⁰. The results presented here in Table 3-4 provide little consensus. There were few statistical significant differences in imaging or patient characteristics between the two different races. However, both mammographic and UST breast density were greater on average for African-American women. These differences were not statistically significant though. Age, weight and BMI are factors that are known to affect breast density and can cause discrepancies when comparing between two different groups. However, these variables are consistent between the two groups and should therefore not cause the breast density to appear greater in African-American women.

The only statistically significant differences between the two races involved the dense UST volume, dense mammographic area, total UST breast volume and non-dense UST volume. All were larger for the African-American women. Despite the average height and weight being similar, the average breast size was much larger for the African-American women. This caused a corresponding increase in the amount of dense and non-dense breast tissue. Had breast size been similar between the two groups, it is likely that the volume of the sub-regions of the breast would also have been similar. The effect this would have on breast density is uncertain. It is possible that the sub-regions would have decreased with in the same proportion, which likely would have left the percent density

and average sound speed measurements mostly unaffected. Therefore firm conclusions regarding differences in breast density among race can not be reached.

Family history of breast cancer is a well known risk factor for the disease. The results shown in Table 3-5 indicate that all measures of breast density, MPD and VASS, were higher for the higher risk group, which are those women with a family history of disease. However, these relationships were not statistically significant. There were also no other significant relationships when stratifying by family history. This suggests that family history does have some effect on breast density, but that it is not as pronounced as other factors, such as menopausal status. The elevated breast cancer risk as a result of family history of breast is likely not only caused by breast density. The additional risk is likely also due in part to genetic mutations, notably the *BRCA1* or *BRCA2* mutations, and lifestyle factors that may be shared by women within the same family.

Women who have not carried a full-term pregnancy do show an increased risk of developing breast cancer as well. The results shown in Table 3-6 do show an increased density measurement for nulliparous women, but once again, the relationship is not statistically significant. There are no other statistically relevant relationships involving parity and imaging or patient characteristics. Again, this suggests that the difference in hormones between these groups affect cancer risk by more than just affecting breast density.

UST has shown its ability to be able to potentially identify small changes in density among different subsets of women. However, in order to use UST to fully examine how these factors affect breast density, much larger studies are required. The results presented here show patterns similar to the ones observed when using

mammographic density measurements. These studies benefited from the widespread use of mammography which easily allowed for thousands of women to be examined. This large amount of data is required to be able to obtain statistically significant results. The small number of commercial UST devices means that acquiring enough data to draw firm conclusions will be time consuming. Yet, the results presented here show that UST density measurements have the potential to be as valid as mammographic density measurements. UST can easily be used to classify density according to known density-related risk factors in a safe and reliable way.

5.2 Correlations Involving Breast Density

The correlations between density measurements and many of the imaging and patient characteristics are strong. The results for all patients grouped together were shown in Table 3-7. The correlation between VASS and MPD was very strong with a Spearman coefficient of $r_s = 0.726$. This value was of similar strength to correlations found between other forms of volumetric density measurements and mammography. When the VASS versus MPD data was plotted in Figure 3-4, it appears to be slightly curvilinear. The MPD was then sorted by mammogram type to analyze the source of this curvilinear nature and Table 3-8 shows these correlations. The correlation is stronger for film than it is for digital, but in the plots shown in Figure 3-5, the film plot appears to be much more curvilinear than the digital plot. When using regression to fit equations to the data, the film plot showed a greater increase in the R^2 value when going from a linear fit to a polynomial fit. Other groups¹⁵² have suggested that this polynomial fit is more appropriate since VASS is a volumetric measurement of the breast while mammography is a two-dimensional analysis of the projected area. However, when examining the

USTPD, another three dimensional density measurement, versus mammography in Figure 3-13, the data appear more linear and less curvilinear. This once again suggests that the linear and sigmoidal detector response characteristics of digital and film mammography cause slight but fundamental differences in the measurement of breast density.

As expected, both the VASS and MPD were moderately and inversely correlated with age, weight and BMI. These results are consistent with the expectations that women develop fatter breasts naturally as they age (tissue replacement) and add fat content to breast tissue as they gain weight (obesity). The measurements made using VASS tend to be slightly stronger and more statistically relevant when compared to the MPD measurements. This is likely due to the fact that because of the differences between film and digital mammography, there is an additional variability in the MPD measurements that is not present in the VASS measurements.

When comparing the correlations involving the different imaging characteristics, the general trend was that the VASS correlated more strongly with UST characteristics than MPD and that mammographic characteristics correlated better with MPD than VASS. MPD showed strong to moderate associations with dense, non-dense and total areas on a mammogram whereas VASS only showed moderate to weak associations. The dense area showed a positive correlation with the density measurements while the non-dense and total areas showed a negative correlation. VASS showed strong and positive correlations with the average sound speed of the dense and non-dense tissues whereas MPD only showed moderate correlations. However, when comparing the volume of dense, non-dense and total tissue, the correlations were of a similar strength. In

particular, there was no statistically relevant correlation with the volume of dense tissue for either VASS or MPD. The lack of a correlation for dense volume indicates that the clustering algorithm used on the volumetric data experienced difficulty separating dense tissue. In mammography, dense tissue is separated based on its appearance on the detector and the threshold between dense and fat is subjective. Therefore, the density that is observed on the mammogram may not directly correspond to dense tissue in the breast. Because of the volumetric and quantitative nature of the UST device, dense tissue may be represented in a different way. Defining density based on a binary interpretation of tissue may not be the most ideal method. Two regions of the breast may be very close in density, but on a mammogram they are labeled as entirely dense or entirely fat. The density of breast tissue likely changes gradually across the breast and UST is sensitive to these subtle changes. Even if the breast volume cannot be easily separated into different categories, the information each voxel of tissue contains is still available in the VASS measurement. The lack of a correlation involving the dense volume is therefore not critical to the usefulness of UST measurements.

The correlations involving the density measurements with the non-dense and total areas and volumes behave just as expected. The correlations were negative which indicates that as the amount of non-dense and overall tissue increases, the density decreases. This can be explained by noting that larger breasts are more likely to be fattier than small breasts. This is reflected in the measurements. The non-dense and total areas on the mammogram have a range that is more than twice that of the dense area, while the non-dense and total volumes have a range that is 3-4 times that of the dense volume. In general, it appears that the larger the breast volume, the more fatty tissue it will contain

and therefore, the lower the density will be. This is consistent with the known negative correlation of MPD and VASS with weight and BMI. Obesity is a driver of breast size and breast fat content and likely accounts for the bulk of the observed negative association of VASS and breast volume.

All correlations that involved VASS show an interesting behavior. The sound speed measurements do not fall below a value of approximately 1.42 km/s, regardless of what the corresponding MPD is. This effect is more pronounced when MPD is measured using film. Conversely, there is no such limit for the higher densities which seems to indicate there is a gradation of sound speeds for the denser tissues. This observation suggests that the methods the two imaging systems use to determine density are fundamentally different. The quantitative nature of the UST system indicates that for women with low breast density, the difference in density is small. A change in the MPD or many of the other imaging characteristics is not likely to have a large effect on the measured VASS for women with low breast density. The UST device is much more sensitive to women with higher breast densities, where small changes in breast composition may have larger effects on the measured VASS. Since most of the breast volume is made up of fatty tissue, as previously discussed, small changes to the amount of dense tissue will have small effects on the overall UST density measurement. The amount of dense tissue in the breast relative to the total volume is smaller than the amount of dense area on a mammogram relative to the total area. It is therefore unsurprising that the average sound speed is similar for many patients while there is more variability in the mammography. Since most breasts are mostly composed of lower density fatty tissue, the overall UST density measurement will be much more dependent

on this tissue. This suggests that fatty tissue is of a similar average density and sound speed from woman to woman. The quantitative measurements obtained from UST imaging may in fact be better at identifying the subtle variations in breast anatomy, especially for those women with elevated densities.

Another difference between mammography and UST shows up in the plots involving the USTPD (Figure 3-12 and Figure 3-13). The range of USTPD does not exceed 50%, which is lower than the MPD, which ranges up to 80% in this population. Since the percent density is defined as the ratio of dense volume or area to total volume or area, this result implies that there is a difference in how both imaging modalities interpret density. The projected area of dense tissue on the mammogram should be closely related to the dense volume of the breast, since breast compression preserves breast volume. The same should be true for the total breast area and breast volume which should leave the ratio of the two relatively unaffected. Since the ratios do not span the same range, the two imaging modalities define dense breast tissue differently.

One possible explanation is that the algorithm used for either modality to separate between dense and non-dense regions is unable to accurately make this selection properly. Separation of the dense and non-dense tissue on the UST images was done using a k-means clustering algorithm. The ability to separate dense tissue from non-dense tissue is highly dependent on the algorithm used. It is possible that the algorithm was not efficient at delineating between the two tissue types. This would raise uncertainties in the associations measured using these sub regions. It may be difficult in general to separate breast tissue, which is composed of tissues with a wide spectrum of densities, into just two separate density categories. There is no universal standard that

defines the characteristics of dense tissue and fatty tissue. There is also no clear point that separates dense tissue from fatty tissue. Until such criteria are developed across multiple imaging modalities, if that is even possible, the separation of these tissue types will be a subjective process.

Alternately, the discrepancy may in fact be due to the differences in imaging 2-D projection images versus 3-D volumetric images. Depending on the amount of dense tissue present in the breast, the compression used in mammography can distort the distribution of the dense regions. This is thought to cause one of two effects: (i) regions of dense tissue can overlap each other on a mammogram, which shrinks the visible area of dense tissue and therefore underestimates the MPD or (ii) regions of dense tissue can overlap fatty tissue which increases the amount of visible dense tissue therefore leading to an overestimate of MPD. Although these two effects should effectively cancel each other out, they do introduce a greater variance in the measurement of the MPD. This likely explains why, in the association of VASS and MPD, the scatter is least at low values and increases steadily toward higher values. However, since breast compression, breast positioning and even the projection angle of the mammogram can be uncontrollable factors in mammography, there are some that argue⁸⁰ that density measurements made from mammography do not accurately reflect the amount of dense volume in the breast.

A study¹⁹¹ analyzed a group of UST sound speed images and applied a finite element model to deform the volumetric images into a form similar to that of a mammographic image. This allowed for a more direct comparison of UST imaging and mammographic imaging by directly registering them together. However, the study only

analyzed the displacement of visible lesions and did not attempt to measure density with this new sound speed image. Although the mean lesion displacement was 7.1 mm and the lesion overlap was 91%, these results suggest that the anatomy does align itself slightly differently when it is compressed in mammography. It is therefore possible, that dense regions in the breast are oversampled in mammography. This could lead to more white regions on the mammogram, which is then interpreted as higher density.

The plot of the dense mammographic area against the dense volume measured by UST shows a weak, but positive correlation, Figure 3-20. This could be a result of the discrepancies between the two different segmentation algorithms used in mammography and UST. However, it could also suggest that the methods used to measure density are fundamentally different and do not necessarily align between the two imaging modalities. Since the physics of ultrasound and x-ray interactions with breast tissue is fundamentally different, density, as measured by both imaging modalities, refers to separate physical characteristics. Without full knowledge of the x-ray technique that was used for the mammogram along with many other physical characteristics of the mammography system, the images that are produced provide a qualitative evaluation of the relative density throughout the breast. Also, the reconstruction algorithm used to create the sound speed images can produce uncertainties in identifying the sound speed of certain tissues. It is possible, especially for tissues with intermediate density values, that some fattier tissues are presented as denser than they actually are and that some denser tissues are shown as fattier than they are. This can lead to additional discrepancies when separating the tissues into the subregions. However, since measurement of the overall average sound speed of the breast does not depend on these separations, it is likely a more

accurate measure of the overall breast properties as the net effect of these uncertainties will likely cancel each other out. The quantitative nature of the UST system therefore provides a much more robust method of measuring and visualizing the distribution of densities within the breast.

The plots of the sub-region sound speeds in Figure 3-18 and Figure 3-19 give a further analysis of how density is manifested throughout the breast. By calculating the average sound speed of the sub-regions, a more in-depth inspection of breast tissue than is possible with mammography was performed. There were strong correlations between the average sound speed of the dense tissue and the average sound speed of the non-dense tissue and with the VASS and both sub-region sound speeds. This seems to indicate that density changes in the breast affect the entire breast somewhat uniformly. As the average sound speed and breast density increase, there is also an increase in the average speed of the dense and non-dense tissue as well. This result suggests that separating breast tissue into two categories, dense and fatty, is not straightforward representation of the anatomy. The tissue that is defined as either dense or fat may vary from patient to patient. The average sound speed of the fat regions in some of the denser breasts is actually higher than the dense regions in some of the fattier breasts. However, much like how there was a large peak in the distribution of VASS around 1.44 km/s, most of the non-dense and dense average sound speed show a similar distribution towards the lower values. Fatty breast tissue regions and dense breast tissue regions appear to be relatively uniform across most of the population, except for the minority of patients who show higher breast density. UST can be used as a tool to identify women with higher densities as this

suggests that UST imaging is more sensitive to small variations in density at higher sound speeds.

The analysis on the distribution of sound speeds on breasts of different densities give a visual interpretation of how dense tissue manifests itself throughout the breast. It appears that increases in breast density occur due to a combination of two reasons. First, increases in overall average breast density are due to a systematic increase in sound speed of all breast tissue. As the density of the breast increases, the distributions shift toward higher sound speeds systematically. All breast tissue increases its sound speed as the breast becomes denser. This is especially notable in Figure 3-24 as the mean, median and mode of the average distributions all shift toward higher sound speed values as the density of the group increases. Increases in density are therefore not solely due to an increase in the volume of dense tissue in the breast. The non-dense tissue in breast is not uniform in composition across different women. If non-dense tissue was uniform between women, then all the distributions would display a large peak in values near the same low sound speed value. This characteristic was not seen in these distributions, so the density of breast tissue does not act in this manner. As density increases, the average density of the dense tissue increases in much the same way as the density of the non-dense tissue. Since the sound speed increases systematically across the breast, it must also affect the sound speed of the dense tissue as well. From inspection of the distributions, it can be seen that dense breasts are uniformly denser than fatty breast. This suggests that it is possible for fatty tissue in dense breasts to be denser than the dense tissue in fatty breasts.

Although the dense and non-dense breast tissue changes in density as average breast density increases, it is not the only effect that is likely occurring. The other effect is that as density increases, the volume of dense breast tissue also increases. This can be seen by inspecting the shape of the distributions in each group. All distributions are positively skewed, which means that most sound speeds have low values, but there is a longer tail leading to the high sound speed values. However, as the overall density of each group is increased, the high sound speed tails become longer at the expense of the low sound speed majority. This can be seen the best in Figure 3-24. The mode of the low density group occurs at approximately 4% of the volume. However, as the density is increased, the mode decreases, which corresponds to a decrease in the amount of non-dense tissue. There is therefore an increase in the amount of dense tissue in the breast and this is visualized as the high sound speed tail growing longer and larger.

When the breast becomes significantly dense, it appears that this volume of dense tissue becomes comparable in size to the non-dense volume in the breast. For the high-density group, the dense-tissue occupies enough volume to cause a second peak to occur in the distribution. It is very clear in these patients that there are two distinct breast tissues with two distinct sets of tissue characteristics. These peaks are not as readily visible for the moderately dense breasts, although some individual patients do seem to show some small peaks. Women with dense breasts may therefore benefit the most from UST imaging as UST is able to identify dense breast tissue in a quantifiable fashion. This means that UST is likely much more sensitive to changes in their breast density as well. The differences in breast tissue in women with fatty or moderately dense breasts may be small. However, there appears to be much more variation in breast composition

among women with dense breasts. UST can be used to identify these variations and potentially quantify them.

When examining the small ROI's for the non-dense tissue in the different density patients, similar results were observed. It appears that as the overall density of the breast increases, the density of the non-dense tissue increases accordingly. The non-dense tissue of the heterogeneously dense breast does have a higher average sound speed than non-dense tissue in the fatty breast. When examining the values found in Table 3-22, the mean, median, mode and max values were all greater in the denser breast. This shows that density changes affect the entire breast. The distribution of density values also changes as the density increases. The skewness of the distribution was more positive for the denser breast than for the fatty breast and the standard deviation was larger as well. This indicates that there is a larger spread in sound speed values and that there are more high sound speed values for the denser breast. The wider range of values is likely why the minimum value is lower for the denser breast. In mammography, density is modeled a binary distribution of uniform dense and non-dense tissue. These results with UST show that the distribution of density in breast tissue is much more complex.

By examining the smaller regions, any averaging that was occurring when the entire breast was examined could be avoided. It allowed for potentially small differences in density to be examined on a more microscopic level and not be lost when macroscopically examining the whole breast. However, it was critical to be able to find regions of the breast that corresponded to mostly non-dense tissue. This is difficult as variations in the breast anatomy are likely subtle across the breast. The patients examined had no visible masses, so changes in density occur gradually across the volume

and not abruptly. Therefore each ROI still does contain tissue that is likely identified as both dense and non-dense. This is especially true for breasts that are very low or very high in density. However, despite the amount of tissue present in the breast, the regions are not necessarily well separated. This means that the non-dense ROI is simply more likely to contain non-dense tissue, but could still include dense tissue as well. This can be seen when comparing the mean value calculated within the ROI against the mean non-dense tissue sound speed that was measured using the k-means clustering algorithm. The values measured in the ROI were lower in sound speed than those measured using the clustering algorithm. This likely indicates that separating dense tissue from non-dense tissue is difficult and that the algorithm used will place some moderately dense tissue into the non-dense category. Doing this would cause the average value of each tissue type to be increased. There is no clear definition for what sound speed value should mark the transition from non-dense to dense tissue. These results, which show that density affects the entire breast volume instead of just certain tissues within the breast, indicate that more study is required to determine the true nature of UST breast density.

The dense tissue in the breast is not the sole driver of overall breast density. It is also affected by the fatty tissue. The association of VASS and non-dense sound speed is greater than the dense sound speed. Since the volume of fatty tissue is greater than the volume of dense tissue, it is not surprising that the larger volume has more of an effect on the whole breast's properties and characteristics. Mammographic density was originally determined using a visual inspection of the mammogram to gauge the relative amounts of dense tissue. Greater amounts of dense tissue lead to greater densities. However, these

results show that it may be important to include an analysis of the fatty tissue as well when discussing density.

5.3 Frequency Distributions

The frequency distributions of sound speed and mammographic percent density are significantly different, as shown in Figure 3-1. Although all the distributions are positively skewed, the VASS distributions are more heavily skewed than either the film-based or digital-based MPD measurements. There are several possible explanations for this behavior. Most likely, the most important factor is the fact that VASS is a volumetric measurement whereas MPD is an area measurement. Since MPD is essentially a projection of the volume, there is less intrinsic spread of the independent variable (MPD) compared to the VASS and therefore less stratification of density. It is important to recognize that MPD is a measurement of ratios of areas and is therefore subject to confounding effects such as the overlap of tissues. This overlap can act as a volume averaging phenomenon which can smooth density differences between subjects.

A secondary factor may be the need for setting thresholds in MPD measurements. This introduces subjective differences between measurements which adds to measurement error and also acts to smooth density differences. The difference in the distributions between film and digital density measurements is similar, but not as marked as the one between MPD and VASS. It suggests that digital MPDs peak somewhat more and to lower values compared to film MPDs. Due to film's sigmoidal response, it is plausible that for a given threshold, film measurements lead to higher estimates of MPD when compared to digital. This would cause a shift of the histogram peak to higher MPD values. It is likely the combination of the volumetric and threshold effects that cause the

significant difference between the VASS and MPD histograms. This difference is significant because it appears that the VASS measurements better isolate the highest densities, and therefore the women at highest risk, from the rest of the distribution. It is therefore possible that VASS may better stratify breast cancer risk in future risk studies.

The distributions for the mammographic factors of dense area, non-dense area and total area show slight differences when separated by type. The differences support the argument that the differences are attributable to the different ways in which digital and film images are created and analyzed. Once again, all distributions are positively skewed which leaves a greater percentage of lower values. The dense area is more skewed on film than it was for digital, which the non-dense and total areas are more skewed for digital mammograms. The dense volume measured by UST is much more strongly skewed. This suggests that the two different imaging modalities interpret density in different ways. The volumetric measures seem to indicate that more women tend to have a smaller amount of dense tissue while the mammographic measures seem to distribute the density more evenly. This may be due to the deformation of the anatomy that occurs during mammography as a result of compression. Mammography may therefore slightly overestimate the breast density relative to UST related density measurements.

5.4 The Ultrasound Study of Tamoxifen

The sample of patients involved in the Ultrasound Study of Tamoxifen is much smaller than the population involved in the sound speed study. However, even in this limited group, many of the same generalizations involving how density and other patient characteristics are associated with each other can be identified. In particular, the VASS measured in this population shows similar correlations to the previous results.

Associations between the VASS and age, weight and BMI are moderate and negative. Once again, these correlations behave exactly as expected. Breast density is expected to decrease with increasing age and increased weight causes breasts to become fattier. The relationships involving the mammographic quantities (MPD, dense, non-dense and total areas) behaved just as they did before. Once again, the relationship between VASS and MPD suggests that the x-ray response of digital detectors plays an important role. Since the digital detectors have a linear response to x-rays, a linear relationship between VASS and MPD also exists, as measured before. The mammographic area measurements correlate much more strongly with MPD than with VASS. This is unsurprising since MPD is determined by using the same area measurements. Measurement of the VASS is not dependent on the knowledge of the total amount of dense and non-dense tissue in the breast, so the subsequent correlations are therefore noisier and not as strong. Overall, although the correlations are not as strong as measured before in the VASS vs MPD study (Chapter 3), they are still statistically significant. This is likely due to the fact that the smaller number of patients in this cohort naturally leads to greater statistical uncertainty.

When comparing the differences in characteristics amongst the different groups, the first groups to compare are the case and comparison groups. There is no statistically significant difference between the two groups for almost all of the characteristics studied. The comparison population was specifically chosen to frequency match the cases on age, race and menopausal status. Doing so would allow for effects of tamoxifen for one patient be compared to the changes that occur naturally in a similar patient. Since there are no statistically relevant differences between the two groups, the patients enrolled so

far have been selected in a manner that will ultimately allow for the effects of tamoxifen to be studied.

Although the difference was not statistically significant, the UST and mammographically measured density was higher on average for the case group. The difference was much more pronounced for MPD measurements than for VASS measurements. This result is not unexpected as the case group is comprised of patients with confirmed breast cancers while the comparison group is comprised of healthy patients that have shown a screen negative mammogram. The women who were already diagnosed with breast cancer were more likely to be women with an already increased risk of developing breast cancer. Since increased breast density is one factor that leads to an increased risk, it is not surprising that, on average, the women in the case group show greater densities in the breast contralateral to the diagnosed breast than the women in the comparison group. The lack of statistical significance is likely due to the low statistics collected so far. As enrollment in the study grows, the statistical significance will likely appear. However, breast density is only one of many different factors that could have contributed to the diagnosed breast cancer, so the statistical uncertainty requires more data to overcome.

The only other group separation that provides meaningful differences is the separation by menopausal status. Once again, the average age and VASS show statistically significant differences between pre-menopausal and post-menopausal women. The average age is lower and the VASS is higher for pre-menopausal women while the average age is greater and the VASS is lower for post-menopausal women. This is the exact result that was observed before and it is exactly what is expected to

occur. All other groupings provide no statistically significant differences in any other patient characteristic.

A previous study¹⁸⁵ done on the effects of tamoxifen on breast density showed that after 12-18 months of tamoxifen treatment, 46% of women had a 10% or greater reduction in breast density as measured by mammogram. Since density in this study was measured by using VASS, there exists a difference in the scales used to describe the change. The VASS ranges from approximately 1.42 km/s to 1.52 km/s, giving a window of about 100 m/s to allow for relative variations in breast density. Therefore, a 10% change in mammographic breast density corresponds to a change in VASS of 10 m/s. Should similar results be seen in this study, approximately half of the patients undergoing tamoxifen treatment should show a decrease in VASS of at least 10 m/s after 18 months. When averaging the net change for all the patients in the trial, the average change in sound speed was found to be at most, approximately 1 m/s after 140 days (4-5 months). However, since this average includes the patients who have shown no change or even an increase in sound speed, it does not account for the effect of tamoxifen on those patients it is affecting. It may be more effective to track the changes in density for those patients who have shown a decrease in sound speed since the start of treatment. Figure 4-11 and Figure 4-12 show these results and when examining these results, the effect of tamoxifen is much more pronounced. The change in sound speed in these patients is on the order of approximately 4-5 m/s after 5 months.

The preliminary results presented here also show an interesting characteristic of the change in breast density. When the limited data are grouped according to the amount of change in density, the average change after approximately 50 days is almost identical

to the change in density after 3-6 months of treatment. Therefore, this may indicate that early screening of patients undergoing tamoxifen treatment can potentially predict with patients will respond positively and negatively to the treatment. Knowledge of this information early can then be used to optimize the treatment strategy for patients on a case by case basis. However, the full set of patients needs to be analyzed throughout the entire 12-month period before these conclusions can be fully developed, but the preliminary results are promising.

Weight is a factor that is known to be inversely related to breast density. This was also shown to be true for sound speed measurements (Table 3-7 and Figure 4-5). When attempting to measure changes in breast density over time, changes in the patient's weight must also be monitored as it is one factor that can fluctuate relatively easily. Should a patient show a large increase or decrease in weight between scans, this may result in a respective decrease or increase in breast density. This could mask or enhance the effect that tamoxifen is having on breast density. Therefore it is important to carefully monitor a patient's fluctuations in weight whenever density is measured and then account for the changes it produces. Fortunately, the results that were presented in Table 4-12 show that there was no statistically significant average change in weight during the course of treatment so far. Depending on how the patients are grouped, the average weight shows only a small decrease of a few pounds. Since weight and average sound speed show only a moderate correlation, it is very likely that the small decreases in weight between scans that were measured here have little effect on the measured breast densities.

When the baseline data is grouped into tertiles, it is apparent that the tertile with the greatest initial sound speed showed the greatest decrease in sound speed (Figure 4-13). This suggests that the density-decreasing effects of tamoxifen are most beneficial to women who initially have high density breasts. This makes logical sense as it is easier to lower a higher baseline sound speed than it is to lower a smaller baseline sound speed. This result may ultimately be useful in designing cancer treatments. Measuring breast density with UST is simple and fast. If women with higher UST breast densities respond better to tamoxifen treatment, these changes in these women can be better assessed by using UST. However, it should be noted that until all case and control patient data is collected, the true effect of tamoxifen cannot be inferred. The changes to the composition of the breast over the one year period being studied are a combination from the effects of tamoxifen and the natural changes expected due to aging along with other patient characteristics. Without the matched control data, it is therefore impossible to isolate the effects that tamoxifen has on its own. The results and conclusions presented here for this study are therefore preliminary. More data are necessary to be able to make fully formed conclusions about the true effects of tamoxifen. However, despite being unable to make full conclusions, UST imaging has shown its effectiveness in being able to measure small changes in breast density. It is an inexpensive and safe method that can be used to obtain repeated measurements of breast density over time.

5.5 Measurement Uncertainty

An advantage of measuring sound speed using UST is its high inter-rater agreement. Qualitative mammographic density measurements are highly subjective and significant differences between raters can be observed. The inherent quantitative nature

of the UST measurements is what provides the strong inter-rater agreement as it makes sound seed measurements less sensitive to the input of different raters. When examining a sound speed image, there are only two factors the rater has control over: i) the selection of the nipple and chest wall slices ii) the separation of the breast from the water bath in each slice. Once these two criteria are selected, the calculation of the average sound speed and average density is performed automatically on the remaining image pixels. The variation between each rater in their selection of these factors will be on the order of several thousand pixels. Since the UST device creates images of the breast with up to hundreds of thousands of pixels, even if different raters vary widely in their assessment of the two factors, it is still very likely that a large majority of the exact same data will be analyzed between the different raters. Therefore, the final measurement each rater makes will be far less subjective and this leads to a much stronger inter-rater agreement.

The calculation of standard error of the mean relies on the assumption that sound speed is normally distributed around a single value. This may not in fact be the case, especially for patients with visible tumors. Some voxel distributions seem to indicate there being a two-peaked distribution (Figure 2-9), with a large group of voxels distributed around one sound speed and a smaller group of voxels distributed around a higher mean sound speed. This seems to suggest that there may be more than one type of tissue present in the breast. A visible tumor or mass may be able to explain such results. Although, the results presented in Section 3.7 also seem to indicate that these two peaks may correspond to non-dense and dense tissue. Regardless of what is the cause, as a result, the calculation of the standard error may not be accurate. However, since UST generates images with a large number of pixels, the uncertainties calculated were on the

order of several cm/s. The measurement error between different users was on the order of approximately 1 m/s, so the standard error does not greatly impact the overall uncertainty of the final measurement. Further analysis of the individual distributions likely will not lead to better uncertainty estimates. However, it may lead to a greater understanding of density distribution throughout the entire breast.

5.6 Limitations and Future Direction

There are several limitations to the methods presented here that could not be overcome due to either time constraints or technological constraints. The measurement of the USTPD appeared to be weaker than all the other methods used to determine density. This is likely because only one k-means clustering algorithm was used to segment regions of dense and non-dense tissue from the UST images. The algorithm was not necessarily optimized for use with UST images and an improved segmentation may have produced better results. However, any modifications to the algorithm were limited to the amount of time and effort that could be devoted to creating it. The UST segmentation algorithm was likely less efficient than the segmentation used for the CUMULUS measurements made on the mammography. More time to develop a more robust segmentation algorithm for UST would likely have produced stronger associations with these subregions. However, the associations and trends that were seen here were promising and show that further investigation into the density structure of the breast may be required. Fortunately, the effectiveness of separating dense breast tissue from non-dense tissue has no consequence on determining the overall average breast density, unlike in mammography. The use of the volume average sound speed removes the need to segment the breast as the density is considered over the whole of the breast.

The dark ring artifacts that were present during the tamoxifen study also posed a limitation on the effectiveness on the results. Ideally, an imaging system will produce images that accurately depict the true anatomy with no artifacts. Realistically, this is an impossible technological task as sacrifices in image quality must be made in order to produce acceptable images in real time. Since the source of the artifact was identified as slow moving surface waves, the dark regions do not physically correspond to actual breast anatomy. The signal strength of the surface wave overwhelmed the normal transmission signal for the rays that correspond to the edge of the breast. The signal that corresponds to the ultrasound transmission through the center of each image was not affected by the surface wave. The algorithm was able to properly select the true transmission signals and distinguish them from the surface wave for these rays. This means that the portion of the image without the visible artifact should represent the true breast anatomy and the solution to manually remove the artifact is acceptable.

Due to the presence of the artifact, the calculation of the absolute average sound speed may be difficult and depend highly on how the artifact is handled. As expected, when the artifact was removed, the average sound speed of the breast increases. However, measuring relative changes in sound speed appear to be fairly accurate whether or not the artifact is removed as the different methods (WV, CV, DRWV, DRCV) showed similar changes in sound speed (Figure 4-11). As long as the same method is employed for all scans, the relative changes in density should be fairly accurate. While not the most elegant solution, manual removal of the artifact is required to obtain the most accurate measure of the breast density.

The hardware that was used to obtain the sound speed images was only a prototype and was limited by its technological constraints. While the images it provided were still acceptable, improvements to the UST device itself will lead to higher quality images and stronger data. SoftVue is the first UST commercial device that was designed using the clinical prototype discussed here¹⁹². It has recently been installed in place of the prototype and begun scanning patients. SoftVue is a massive upgrade over the prototype in terms of artifact suppression, image processing, image resolution and image quality. By using a ring transducer with more elements and transmit/receive channels, the SoftVue system produces images with much higher quality and resolution from the greater amounts of raw data that can be collected. The greater amount of information present in these images can potentially allow for the methods described here to produce better results without further modification. The better resolution may allow for dense and non-dense tissue to be defined more clearly, allowing the k-means clustering algorithm to segment them more effectively. Measurements of the average sound speed can improve with more well defined breast volume as well. The dark ring artifact is less prevalent when using SoftVue, which also improves the sound speed measurements. The technical limitations of the current prototype were addressed as well as possible, but they could only be addressed up to a certain point. As the hardware continues to improve and becomes more widespread, the analysis that can be done using UST will improve along with it.

CHAPTER 6

CONCLUSIONS

Ultrasound tomography imaging has been shown to be an effective tool for the measurement of breast density. Volume averaged sound speed, as measured by UST, was positively associated with mammographic percent density, as measured by mammography. The association between VASS and MPD was found to be very strong for both film ($p < 0.001$) and digital mammography ($p < 0.001$) which suggests that breast sound speed could be a viable marker of breast density. VASS was shown to associate with many other mammographic imaging properties such as the dense and non-dense areas for both film and digital mammography. Many other UST imaging properties also correlated with VASS. These included volume and sub-region sound speed measurements.

Factors that are known to affect breast density were tracked using VASS measurements made by UST imaging. Associations of VASS were measured that matched the expected negative correlations with age, weight and BMI. UST imaging was able to identify differences in density in groups of women that are the result of their menopausal status, which is a known factor of breast cancer risk. The distributions of the density measurements made by both UST and mammography indicate that the way film mammography measures density may be skewed toward overproducing higher densities. VASS may therefore be a more sensitive and accurate measure of density for women with higher densities. These results support the findings made previously¹⁹³ for UST that were based on smaller studies.

VASS measurements made using UST have also shown the ability to track small changes in density over time for women undergoing tamoxifen therapy. Changes on the order of several meters per second have been observed after only a few months of treatment. However, these are preliminary results as data relating to control patients was not yet collected and full information regarding the effects of tamoxifen on density could not be determined. Despite this, these preliminary results fall in line with results that were obtained using mammography in previous studies. Nevertheless, UST showed itself as capable of monitoring changes in breast density as early as 1-3 months post-tamoxifen initiation through the use of VASS as a marker.

Although the calculation of VASS is still user dependent and rather laborious, the results that are obtained by different users are strongly correlated to each other. Strong ICC's were calculated between different users on the same sets of patient images. The large breast volumes measured make the differences in calculations that each reader imposes very small. Therefore, VASS measurements made using UST are less subjective than MPD measurements.

Since sound speed is more directly linked to physical density of breast tissue than mammography, it has the potential to be more accurate and more relevant than MPD as a measure of breast density. Furthermore, since UST imaging does not require ionizing radiation or physical compression of the breast, it has the potential to become a safe and more accurate surrogate marker for breast cancer. Women with high breast densities are at an elevated risk of developing breast cancer; yet conventional screening mammography presents greater risks to this group of women. UST imaging can be used to safely and frequently screen this group and may in fact be more sensitive to changes in

their breast density. Future work will focus directly on testing the associations of VASS and breast cancer risk, but for now UST imaging shows promise as a safe and cost-effective imaging modality.

APPENDIX A

IMAGE J MACROS USED

A.1 Masked Sound Speed Image Creator

The code for the macro that was used in ImageJ to create the masks that removed the water background from the sound speed images is shown below.

```
//This macro is based on a macro originally written by Jason Shen
//This macro is used to manually create and save elliptical masks of the sound speed
images

//This prompts user to select the slice that corresponds to the nipple region
//Also obtains file names and directory names
path = File.openDialog("Select a File");
dir = File.getParent(path);
name = File.getName(path);
list_all = getFileList(dir);
L_name = lengthOf(name);

//Selects the patient number and slice number from the filename automatically
TAM=substring(name,3,6);
ind_end=indexOf(name, ".ss");
sli=substring(name,ind_end-3,ind_end);

//Filter out the files in the directory that are not sound speed images
temparray=newArray(list_all.length);
ki=0;
for (i=0;i<list_all.length; i++)
{
    if (endsWith(list_all[i], ".ss"))
    {
        temparray[ki]=list_all[i];
        ki=ki+1;
    }
}

list=newArray(ki);
for (i=0;i<ki; i++)
{
    list[i]=temparray[i]; //Only sound speed images remain now
}

newlist=newArray(ki);
//End selecting sound speed images

//Creation of elliptical mask begins now
nk=10; //Defines how many points for ellipse polygon.
xx=newArray(nk);
yy=newArray(nk);

k=0; //The first slice to be segmented.

do
{
    //Close unwanted windows
    if (k != 0)
    {
        selectWindow(name2);
        close();
        selectWindow(name1);
        close();
    }

    path1 = dir+"\\ "+name;
    run("ASC TextReader", "open="+path1); //Open first image
    setLocation(10,100);
    name1= "sound speed "+TAM+"_"+sli;
    rename(name1);
    //Check if working on the first image (k=0), if yes, then need an initial input
    for ellipse
}
```

```

//Don't need input if not working on first image (k>0)
if (k == 0)
{
    //Here is the first time segment, you need select some initial ROI points.
    waitForUser("Interactive Input Window", "For the first slice \n Select the
initial ROI points,\n then click OK");
    getSelectionCoordinates(x, y); //Ellipse points selected
    run("ASC TextReader", "open="+path1);
    setLocation(10,400);
    name2="ROI selection";
    rename(name2);

    //Adjust the initial input to have the same angle interval.
    //Find x,y mean of ROI.
    xmean=0.;
    ymean=0.;
    ni=x.length;
    for (i=0; i<ni; i++)
    {
        xmean=xmean+x[i];
        ymean=ymean+y[i];
    }
    xmean=xmean/ni;
    ymean=ymean/ni;
    //End find mean of ROI.

    radius=newArray(ni);
    angle=newArray(ni);

    for (i=0; i<ni; i++)
    {
        xpri=x[i]-xmean;
        ypri=y[i]-ymean;
        radius[i]=sqrt(xpri*xpri+ypri*ypri);
        angle[i]=atan2(ypri, xpri);
    }

    //Find max and min angle.
    kimin=0;
    kimax=0;
    anglemin=angle[kimin];
    anglemax=angle[kimax];
    for (ii=1; ii< ni; ii++)
    {
        if (anglemin > angle[ii])
        {
            anglemin=angle[ii];
            kimin=ii;
        }
        if (anglemax < angle[ii])
        {
            anglemax=angle[ii];
            kimax=ii;
        }
    }

    for (ik=0; ik<nk; ik++)
    {
        theta=3.1415926+2*3.1415926*((ik-nk)/nk);
        if ((theta < anglemax) && (theta > anglemin))
        {
            kamin=0;
            fmin=abs(theta-angle[kamin]);
            for (mi=1;mi<ni;mi++)
            {
                if (fmin > abs(theta-angle[mi]))
                {
                    kamin=mi;
                    fmin =abs(theta-angle[mi]);
                }
            }
            ra=radius[kamin];
        }
        else
        {
            ra=0.5*(radius[kimax]+radius[kimin]);
        }
        xx[ik]=round(xmean+ra*cos(theta));
        yy[ik]=round(ymean+ra*sin(theta));
    }
    //Polygon is fit to points selected, can still be adjusted if not good fit

```

```

        makeSelection("polygon",xx,yy);
        waitForUser("Interactive Input window","If Automatic selection is not
good,\n Adjust the ROI points, then click OK");
        getSelectionCoordinates(xx, yy); //Adjust still made here
        selectWindow(name1);
        makeSelection("polygon",xx,yy);
        run("Fit Ellipse"); //Ellipse is fit to selected points
    }
    //If not the first slice, not as many steps required.
    else
    {

        selectWindow(name1);
        makeSelection("points",xx,yy);

        run("ASC TextReader", "open="+path1);
        setLocation(10,400);
        name2="ROI selection";
        rename(name2);

        xmean=0.;
        ymean=0.;
        for (i=0; i<nk; i++)
        {
            xmean=xmean+xx[i];
            ymean=ymean+yy[i];
        }
        xmean=xmean/nk;
        ymean=ymean/nk;

        for (ik=0; ik<nk; ik++)
        {
            xpri=xx[ik]-xmean;
            ypri=yy[ik]-ymean;
            ra=0.8+sqrt(xpri*xpri+ypri*ypri);
            theta=atan2(ypri, xpri);
            xx[ik]=round(xmean+ra*cos(theta));
            yy[ik]=round(ymean+ra*sin(theta));
        }

        //Polygon can be adjusted to fit the image and ellipse will be fit to selecting
        makeSelection("polygon",xx,yy);
        waitForUser("Interactive Input window","If Automatic selection is not
good,\n Adjust the ROI points, then click OK");
        getSelectionCoordinates(xx, yy);
        selectWindow(name1);
        makeSelection("polygon",xx,yy);
        run("Fit Ellipse");
        //Ellipse has been fit to user selected data
    }

    //Sort the file, so the first file in the newlist is automatically the next slice
to be segmented.
    ki=0;
    while(name!=list[ki])
    {
        ki=ki+1;
    }
    kk=ki;
    for (ii=kk;ii<list.length;ii++)
    {
        newlist[ii]=list[ii];
    }
    nn=list.length-kk;
    for (ii=0;ii<kk;ii++)
    {
        newlist[kk-ii-1]=list[ii];
    }
    //End sort file.

    //Popup window asks for final judgement before creating mask
    Dialog.create("Final Judgement");
    Dialog.addChoice("Good and Continue", newArray("YES","NO"));
    Dialog.addChoice("SAVE MASK:", newArray("YES","NO"));
    Dialog.addString("The current slice:", TAM+"_"+sli);
    Dialog.addChoice("Input New Slice:", newlist);
    Dialog.show();
    Sta = Dialog.getChoice();

```

```

SAVE = Dialog.getChoice();
Cur = Dialog.getString();
run("Clear Outside");
//End window popup
//Make the appropriate directories only once to store image masks and masked sound
speed images
if (k==0)
{
    savedir="C:\\ROI_NoWater\\TAM"+TAM+"_ALLSLICES\\";
    File.makeDirectory(savedir);
    savedir1="C:\\ROI_NoWater\\TAM"+TAM+"_ALLSLICES\\Ascii\\";
    File.makeDirectory(savedir1);
    savedir2="C:\\ROI_NoWater\\TAM"+TAM+"_ALLSLICES\\Mask\\";
    File.makeDirectory(savedir2);
}
//End making directories
//Create and save masked sound speed images and masks
savepath1="save=C:\\ROI_NoWater\\TAM"+TAM+"_ALLSLICES\\Ascii\\TAM"+TAM+"_"+sli+".a
sc";
run("ASC Textwriter", savepath1); //Masked sound speed image created

savepath2="save=C:\\ROI_NoWater\\TAM"+TAM+"_ALLSLICES\\Mask\\TAM"+TAM+"_"+sli+"_ma
sk.asc";
run("ASC Maskwriter", savepath2); //Mask created
name = Dialog.getChoice();
sli=substring(name,ind_end-3,ind_end); //Increment to next slice number
k=k+1; //Increment slice counter
}
while (Sta == "YES");
//End Mask Creator

```

A.2 Sound Speed Statistics Calculator Macro

The code for the macro used in ImageJ to calculate the mean, standard deviation, total pixel count and standard error of the mean for the sound speed images is shown below.

```

// Macro to open and then find statistics for masked breast sound speed images

setBatchMode(1);
run("Clear Results");

//Select the first masked sound speed image
ASC_Path = File.openDialog("Select the Image");

//Obtains information about the file names and directory of the images
ASC_dir = File.getParent(ASC_Path);
ASC_files = getFileList(ASC_dir);
ASC_length = lengthOf(ASC_files);
ASC_Name = File.getName(ASC_Path);

setBatchMode(0);
//Open and stack the masked sound speed images
run ("ASC TextReader Stack NoBuffer", "open="+ASC_Path);
run("Images to Stack");

strt = ASC_length + 1; //Number of images

//Calculate the mean sound speed by summing over each pixel
mn=0;
cnt=0;
for (n=1; n< strt; n++)
{
    setSlice(n); //Set current slice
    h = getHeight();
    w = getWidth();
    //Measure over each pixel in image
    for (x=1; x<w+1; x++)
    {

```

```

for (y=1; y<h+1; y++)
{
    //Only measure pixels with sound speeds between 1.3 and 1.6 km/s
    //This ensures masked background, with values of 0, aren't included
    if (getPixel(x,y) > 1.3 && getPixel(x,y) < 1.6)
    {
        cnt++; //Running pixel count
        mn += getPixel(x,y); //Running sum
    }
}
}

//Mean calculated here
mean = mn/cnt;
avg = d2s(mean, 8);

//Calculate standard deviation by summing over each pixel
std = 0;
for (n=1; n< strt; n++)
{
    setSlice(n); //Set current slice
    h = getHeight();
    w = getWidth();
    //Measure over each pixel in image
    for (x=1; x<w+1; x++)
    {
        for (y=1; y<h+1; y++)
        {
            //Only measure pixels with sound speeds between 1.3 and 1.6 km/s
            //This ensures masked background, with values of 0, aren't included
            if (getPixel(x,y) > 1.3 && getPixel(x,y) < 1.6)
            {
                std += pow((getPixel(x,y)-mean),2);
            }
        }
    }
}

//Standard deviation calculated here
stdev = sqrt(std/(cnt-1))*1000;

//Calculate the error of the mean
eom=100*stdev/sqrt(cnt);

//Run a histogram to make sure values agree
run("Histogram", "bins=256 x_min=1.3 x_max=1.6 y_max=Auto stack");

//Close the images to not clutter up screen
selectWindow("Stack");
close();

setBatchMode("exit and display");

//Display final calculated values in form to allow them to easily be copied to
spreadsheet.
print (avg);
print (stdev);
print (cnt);
print (eom);
print (mn);

```

BIBLIOGRAPHY

1. American Cancer Society. *Cancer facts and figures 2013*. Atlanta: American Cancer Society, Inc. 2013.
2. Gail, M.H., et al., *Projecting Individualized Probabilities of Developing Breast Cancer for White Females Who Are Being Examined Annually*. Journal of the National Cancer Institute, 1989. **81**(24): p. 1879-1886.
3. Baker, L.H., *Breast cancer detection demonstration project: Five-year summary report*. CA: A Cancer Journal for Clinicians, 1982. **32**(4): p. 194-225.
4. Costantino, J.P., et al., *Validation Studies for Models Projecting the Risk of Invasive and Total Breast Cancer Incidence*. Journal of the National Cancer Institute, 1999. **91**(18): p. 1541-1548.
5. American Cancer Society. *Breast cancer facts and figures 2011-2012*. Atlanta: American Cancer Society, Inc. 2011.
6. Lerman, C., et al., *Effects of Individualized Breast Cancer Risk Counseling: a Randomized Trial*. Journal of the National Cancer Institute, 1995. **87**(4): p. 286-292.
7. Black, W.C., R.F. Nease, and A.N.A. Tosteson, *Perceptions of Breast Cancer Risk and Screening Effectiveness in Women Younger Than 50 Years of Age*. Journal of the National Cancer Institute, 1995. **87**(10): p. 720-731.
8. Tice, J., et al., *Mammographic Breast Density and the Gail Model for Breast Cancer Risk Prediction in a Screening Population*. Breast Cancer Research and Treatment, 2005. **94**(2): p. 115-122.

9. Barlow, W.E., et al., *Prospective Breast Cancer Risk Prediction Model for Women Undergoing Screening Mammography*. Journal of the National Cancer Institute, 2006 6 September. **98**(17): p. 1204-1214.
10. Chen, J., et al., *Projecting Absolute Invasive Breast Cancer Risk in White Women With a Model That Includes Mammographic Density*. Journal of the National Cancer Institute, 2006. **98**(17): p. 1215-1226.
11. Vachon, C.M., et al., *Mammographic density, breast cancer risk and risk prediction*. Breast Cancer Res, 2007. **9**(6): p. 217.
12. McCormack, V.A. and I. dos Santos Silva, *Breast Density and Parenchymal Patterns as Markers of Breast Cancer Risk: A Meta-analysis*. Cancer Epidemiology Biomarkers & Prevention, 2006. **15**(6): p. 1159-1169.
13. Byng, J.W., et al., *The quantitative analysis of mammographic densities*. Physics in Medicine and Biology, 1994. **39**(10): p. 1629.
14. Boyd, N.F., et al., *Quantitative Classification of Mammographic Densities and Breast Cancer Risk: Results From the Canadian National Breast Screening Study*. Journal of the National Cancer Institute, 1995. **87**(9): p. 670-675.
15. Boyd, N.F., et al., *Mammographic densities and breast cancer risk*. . Cancer Epidemiology Biomarkers & Prevention 1998 **7** (12): p. 1133-1144
16. Boyd, N.F., et al., *Mammographic Density and the Risk and Detection of Breast Cancer*. New England Journal of Medicine, 2007. **356**(3): p. 227-236.
17. Boyd, N., et al., *Mammographic Density and Breast Cancer Risk: Evaluation of a Novel Method of Measuring Breast Tissue Volumes*. Cancer Epidemiology Biomarkers & Prevention, 2009. **18**(6): p. 1754-1762.

18. Boyd, N.F., et al., *Breast Tissue Composition and Susceptibility to Breast Cancer*. Journal of the National Cancer Institute 2010 **102** (16): p. 1224-1237
19. Boyd, N.F., *Tamoxifen, Mammographic Density, and Breast Cancer Prevention*. Journal of the National Cancer Institute 2011 **103** (9): p. 704-705
20. Byrne, C., et al., *Mammographic Features and Breast Cancer Risk: Effects With Time, Age, and Menopause Status*. Journal of the National Cancer Institute 1995 **87** (21): p. 1622-1629
21. Byng, J.W., et al., *Automated analysis of mammographic densities and breast carcinoma risk*. Cancer, 1997. **80**(1): p. 66-74.
22. Byng, J.W., et al., *Analysis of mammographic density and breast cancer risk from digitized mammograms*. Radiographics, 1998. **18**(6): p. 1587-1598.
23. Wolfe, J.N., *Risk for breast cancer development determined by mammographic parenchymal pattern*. Cancer, 1976. **37**(5): p. 2486-2492.
24. Saftlas, A.F., et al., *Mammographic densities and risk of breast cancer*. Cancer, 1991. **67**(11): p. 2833-2838.
25. Sala, E., et al., *Mammographic parenchymal patterns and mode of detection: implications for the breast screening programme*. Journal of Medical Screening, 1998. **5**(4): p. 207-212.
26. Harvey, J.A. and V.E. Bovbjerg, *Quantitative Assessment of Mammographic Breast Density: Relationship with Breast Cancer Risk*. Radiology 2004 **230** (1): p. 29-41

27. Vachon, C.M., et al., *Mammographic Breast Density as a General Marker of Breast Cancer Risk*. *Cancer Epidemiology Biomarkers & Prevention* 2007 **16** (1): p. 43-49
28. El-Bastawissi, A., et al., *Reproductive and hormonal factors associated with mammographic breast density by age (United States)*. *Cancer Causes & Control*, 2000. **11**(10): p. 955-963.
29. Boyd, N., et al., *Mammographic densities as a marker of human breast cancer risk and their use in chemoprevention*. *Current Oncology Reports*, 2001. **3**(4): p. 314-321.
30. Kelemen, L.E., et al., *Age-specific Trends in Mammographic Density: The Minnesota Breast Cancer Family Study*. *American Journal of Epidemiology*, 2008. **167**(9): p. 1027-1036.
31. Stone, J., et al., *Determinants of Percentage and Area Measures of Mammographic Density*. *American Journal of Epidemiology*, 2009. **170**(12): p. 1571-1578.
32. Vachon, C., et al., *Association of mammographically defined percent breast density with epidemiologic risk factors for breast cancer (United States)*. *Cancer Causes & Control*, 2000. **11**(7): p. 653-662.
33. Pike, M.C., et al., *'Hormonal' risk factors, 'breast tissue age' and the age-incidence of breast cancer*. 1983.
34. Boyd, N.F., et al., *Effects at Two Years of a Low-Fat, High-Carbohydrate Diet on Radiologic Features of the Breast: Results From a Randomized Trial*. *Journal of the National Cancer Institute*, 1997. **89**(7): p. 488-496.

35. Grove, J.S., et al., *Factors associated with breast structure in breast cancer patients*. *Cancer*, 1979. **43**(5): p. 1895-1899.
36. Boyd, N., et al., *A Longitudinal Study of the Effects of Menopause on Mammographic Features*. *Cancer Epidemiology Biomarkers & Prevention*, 2002. **11**(10): p. 1048-1053.
37. Ziv, E., et al., *Mammographic Breast Density and Family History of Breast Cancer*. *Journal of the National Cancer Institute*, 2003. **95**(7): p. 556-558.
38. Tamimi, R.M., et al., *Birth weight and mammographic density among postmenopausal women in Sweden*. *International Journal of Cancer*, 2010. **126**(4): p. 985-991.
39. Lam, P.B., et al., *The association of increased weight, body mass index, and tissue density with the risk of breast carcinoma in Vermont*. *Cancer*, 2000. **89**(2): p. 369-375.
40. Irwin, M.L., et al., *Physical Activity, Body Mass Index, and Mammographic Density in Postmenopausal Breast Cancer Survivors*. *Journal of Clinical Oncology*, 2007. **25**(9): p. 1061-1066.
41. Boyd, N.F., et al., *Body Size, Mammographic Density, and Breast Cancer Risk*. *Cancer Epidemiology Biomarkers & Prevention*, 2006. **15**(11): p. 2086-2092.
42. Knight, J.A., et al., *Macronutrient Intake and Change in Mammographic Density at Menopause: Results from a Randomized Trial*. *Cancer Epidemiology Biomarkers & Prevention*, 1999. **8**(2): p. 123-128.
43. Bérubé, S., et al., *Vitamin D, Calcium, and Mammographic Breast Densities*. *Cancer Epidemiology Biomarkers & Prevention*, 2004. **13**(9): p. 1466-1472.

44. Tseng, M., et al., *Dietary intake and breast density in high-risk women: a cross-sectional study*. Breast Cancer Res, 2007. **9**(5): p. R72.
45. Sala, E., et al., *High risk mammographic parenchymal patterns and diet: a case-control study*. Br J Cancer, 2000. **83**(1): p. 121-6.
46. Vachon, C.M., et al., *Association of Diet and Mammographic Breast Density in the Minnesota Breast Cancer Family Cohort*. Cancer Epidemiology Biomarkers & Prevention, 2000. **9**(2): p. 151-160.
47. Bright, R.A., et al., *Relationship between mammographic and histologic features of breast tissue in women with benign biopsies*. Cancer, 1988. **61**(2): p. 266-271.
48. El-Bastawissi, A.Y., et al., *Variation in Mammographic Breast Density by Race*. Annals of Epidemiology, 2001. **11**(4): p. 257-263.
49. Carmen, M.G.d., et al., *Mammographic Breast Density and Race*. American Journal of Roentgenology, 2007. **188**(4): p. 1147-1150.
50. Razzaghi, H., et al., *Mammographic density and breast cancer risk in White and African American Women*. Breast Cancer Research and Treatment, 2012. **135**(2): p. 571-580.
51. Kaufman, Z., et al., *The mammographic parenchymal patterns of women on hormonal replacement therapy*. Clinical Radiology, 1991. **43**(6): p. 389-392.
52. Sterns, E.E. and B. Zee, *Mammographic density changes in perimenopausal and postmenopausal women: is effect of hormone replacement therapy predictable?* Breast Cancer Research and Treatment, 2000. **59**(2): p. 125-132.

53. Rutter, C.M., et al., *Changes in breast density associated with initiation, discontinuation, and continuing use of hormone replacement therapy*. JAMA: The Journal of the American Medical Association, 2001. **285**(2): p. 171-176.
54. McNicholas, M.M., et al., *Pain and increased mammographic density in women receiving hormone replacement therapy: a prospective study*. American Journal of Roentgenology, 1994. **163**(2): p. 311-5.
55. Stomper, P.C., et al., *Mammographic changes associated with postmenopausal hormone replacement therapy: a longitudinal study*. Radiology, 1990. **174**(2): p. 487-490.
56. Berkowitz, J.E., et al., *Hormonal replacement therapy: mammographic manifestations*. Radiology, 1990. **174**(1): p. 199-201.
57. Laya, M.B., et al., *Effect of postmenopausal hormonal replacement therapy on mammographic density and parenchymal pattern*. Radiology, 1995. **196**(2): p. 433-437.
58. Persson, I., E. Thurfjell, and L. Holmberg, *Effect of estrogen and estrogen-progestin replacement regimens on mammographic breast parenchymal density*. Journal of Clinical Oncology, 1997. **15**(10): p. 3201-7.
59. Greendale, G.A., et al., *Effects of estrogen and estrogen-progestin on mammographic parenchymal density*. Postmenopausal Estrogen/Progestin Interventions (PEPI) Investigators. Annals of internal medicine, 1999. **130**(4 Pt 1): p. 262-269.

60. Harvey, J.A., C.R. Herman, and J.V. Pinkerton, *Short-term Cessation of Hormone Replacement Therapy and Improvement of Mammographic Specificity*. Journal of the National Cancer Institute, 1997. **89**(21): p. 1623-1625.
61. Colacurci, N., et al., *Effects of a short-term suspension of hormone replacement therapy on mammographic density*. Fertility and Sterility, 2001. **76**(3): p. 451-455.
62. Fisher, B., et al., *Tamoxifen for Prevention of Breast Cancer: Report of the National Surgical Adjuvant Breast and Bowel Project P-1 Study*. Journal of the National Cancer Institute 1998 **90** (18): p. 1371-1388
63. Pisano, E.D., et al., *Diagnostic Performance of Digital versus Film Mammography for Breast-Cancer Screening*. New England Journal of Medicine, 2005. **353**(17): p. 1773-1783.
64. Pisano, E.D., et al., *Diagnostic Accuracy of Digital versus Film Mammography: Exploratory Analysis of Selected Population Subgroups in DMIST1*. Radiology, 2008. **246**(2): p. 376-383.
65. Nyström, L., *Breast cancer screening with mammography: overview of Swedish randomised trials*. The Lancet (British edition), 1993. **341**(8851): p. 973-978.
66. Whitehead, J., et al., *Wolfe mammographic parenchymal patterns. A study of the masking hypothesis of Egan and Mosteller*. Cancer, 1985. **56**(6): p. 1280-1286.
67. D'Orsi CJ, B.L., Berg WA, et al., *BI-RADS: Mammography, 4th edition in: Breast Imaging Reporting and Data System: ACR BI-RADS – Breast Imaging Atlas*. American College of Radiology, Reston, VA, 2003.

68. Ciatto, S., et al., *Categorizing breast mammographic density: intra- and interobserver reproducibility of BI-RADS density categories*. *The Breast*, 2005. **14**(4): p. 269-275.
69. Berg, W.A., et al., *Breast Imaging Reporting and Data System*. *American Journal of Roentgenology*, 2000. **174**(6): p. 1769-1777.
70. *Mammography Quality Standards Act (MQSA)*, 42 U.S.C. 263B - Certification of Mammography Facilities, 2011.
71. Grady, D. *New Laws Add a Divisive Component to Breast Screening*. *The New York Times*, October 24, 2012. Retrieved from <http://www.nytimes.com/2012/10/25/health/laws-tell-mammogram-clinics-to-address-breast-density.html?pagewanted=all&r=1&>.
72. American College of Radiology, *ACR Statement on Reporting Breast Density in Mammography Reports and Patient Summaries*, April 24, 2012, <http://www.acr.org/About-Us/Media-Center/Position-Statements/Position-Statements-Folder/Statement-on-Reporting-Breast-Density-in-Mammography-Reports-and-Patient-Summaries>.
73. Gao, J., et al., *Reproducibility of visual assessment on mammographic density*. *Breast Cancer Research and Treatment*, 2008. **108**(1): p. 121-127.
74. Egan, R.L. and R.C. Mosteller, *Breast cancer mammography patterns*. *Cancer*, 1977. **40**(5): p. 2087-2090.
75. de González, A.B. and S. Darby, *Risk of cancer from diagnostic X-rays: estimates for the UK and 14 other countries*. *The Lancet*, 2004. **363**(9406): p. 345-351.

76. Hubbard, R.A., et al., *Cumulative Probability of False-Positive Recall or Biopsy Recommendation After 10 Years of Screening Mammography: A Cohort Study*. *Annals of internal medicine*, 2011. **155**(8): p. 481-492.
77. Bushong, S.C., *Radiologic Science for Technologists: Physics, Biology and Protection, 9th Edition*. 2008, St. Louis, Missouri: Elsevier Inc.
78. van Gils, C., et al., *Mammographic breast density and risk of breast cancer: Masking bias or causality?* *European Journal of Epidemiology*, 1998. **14**(4): p. 315-320.
79. Elmore, J.G., et al., *Ten-Year Risk of False Positive Screening Mammograms and Clinical Breast Examinations*. *New England Journal of Medicine*, 1998. **338**(16): p. 1089-1096.
80. Kopans, D.B., *Basic Physics and Doubts about Relationship between Mammographically Determined Tissue Density and Breast Cancer Risk*. *Radiology*, 2008. **246**(2): p. 348-353.
81. Ducote, J.L. and S. Molloi, *Quantification of breast density with dual energy mammography: a simulation study*. *Med Phys*, 2008. **35**(12): p. 5411-8.
82. Laidevant, A.D., et al., *Compositional breast imaging using a dual-energy mammography protocol*. *Med Phys*, 2010. **37**(1): p. 164-74.
83. Highnam, R., M. Brady, and B. Shepstone, *A representation for mammographic image processing*. *Medical Image Analysis*, 1996. **1**(1): p. 1-18.
84. Highnam, R. and M. Brady, *Mammographic image analysis*. Vol. 14. 1999: Springer.

85. van Engeland, S., et al., *Volumetric breast density estimation from full-field digital mammograms*. Medical Imaging, IEEE Transactions on, 2006. **25**(3): p. 273-282.
86. Shepherd, J.A., et al., *Volume of Mammographic Density and Risk of Breast Cancer*. Cancer Epidemiology Biomarkers & Prevention, 2011. **20**(7): p. 1473-1482.
87. Shepherd, J.A., et al., *Novel use of single X-ray absorptiometry for measuring breast density*. Technology in cancer research & treatment, 2005. **4**(2): p. 173-182.
88. Maskarinec, G., et al., *Comparison of breast density measured by dual energy X-ray absorptiometry with mammographic density among adult women in Hawaii*. Cancer Epidemiology, 2011. **35**(2): p. 188-193.
89. Pawluczyk, O., et al., *A volumetric method for estimation of breast density on digitized screen-film mammograms*. Medical physics, 2003. **30**: p. 352.
90. Kaufhold, J., et al., *A calibration approach to glandular tissue composition estimation in digital mammography*. Medical Physics, 2002. **29**(8): p. 1867-1880.
91. Lokate, M., et al., *Volumetric Breast Density from Full-Field Digital Mammograms and Its Association with Breast Cancer Risk Factors: A Comparison with a Threshold Method*. Cancer Epidemiology Biomarkers & Prevention, 2010. **19**(12): p. 3096-3105.
92. Aitken, Z., et al., *Screen-Film Mammographic Density and Breast Cancer Risk: A Comparison of the Volumetric Standard Mammogram Form and the Interactive*

- Threshold Measurement Methods.* Cancer Epidemiology Biomarkers & Prevention, 2010. **19**(2): p. 418-428.
93. Ding, J., et al., *Evaluating the Effectiveness of Using Standard Mammogram Form to Predict Breast Cancer Risk: Case-Control Study.* Cancer Epidemiology Biomarkers & Prevention, 2008. **17**(5): p. 1074-1081.
94. Graham, S.J., et al., *Quantitative correlation of breast tissue parameters using magnetic resonance and X-ray mammography.* Br J Cancer, 1996. **73**(2): p. 162-8.
95. Lee, N.A., et al., *Fatty and fibroglandular tissue volumes in the breasts of women 20-83 years old: comparison of X-ray mammography and computer-assisted MR imaging.* American Journal of Roentgenology, 1997. **168**(2): p. 501-6.
96. Boston, R.C., et al., *Estimation of the content of fat and parenchyma in breast tissue using MRI T1 histograms and phantoms.* Magnetic resonance imaging, 2005. **23**(4): p. 591-599.
97. Nie, K., et al., *Development of a quantitative method for analysis of breast density based on three-dimensional breast MRI.* Med Phys, 2008. **35**(12): p. 5253-62.
98. Klifa, C., et al., *Magnetic resonance imaging for secondary assessment of breast density in a high-risk cohort.* Magnetic resonance imaging, 2010. **28**(1): p. 8-15.
99. Sutcliffe, J.F., *A review of in vivo experimental methods to determine the composition of the human body.* Physics in Medicine and Biology, 1996. **41**(5): p. 791.
100. Laskey, M.A., *Dual-energy X-ray absorptiometry and body composition.* Nutrition (Burbank, Los Angeles County, Calif.), 1996. **12**(1): p. 45-51.

101. Shepherd, J.A., et al., *Measurement of Breast Density with Dual X-ray Absorptiometry: Feasibility*. Radiology, 2002. **223**(2): p. 554-557.
102. Shepherd, J.A., et al., *Breast Density Assessment in Adolescent Girls Using Dual-Energy X-ray Absorptiometry: A Feasibility Study*. Cancer Epidemiology Biomarkers & Prevention, 2008. **17**(7): p. 1709-1713.
103. Novotny, R., et al., *Puberty, body fat, and breast density in girls of several ethnic groups*. American Journal of Human Biology, 2011. **23**(3): p. 359-365.
104. Boone, J.M., et al., *Dedicated Breast CT: Radiation Dose and Image Quality Evaluation*. Radiology, 2001. **221**(3): p. 657-667.
105. Boone, J., et al., *Computed Tomography for Imaging the Breast*. Journal of Mammary Gland Biology and Neoplasia, 2006. **11**(2): p. 103-111.
106. Lindfors, K.K., et al., *Dedicated Breast CT: Initial Clinical Experience*. Radiology, 2008. **246**(3): p. 725-733.
107. Alonzo-Proulx, O., et al., *Validation of a method for measuring the volumetric breast density from digital mammograms*. Physics in Medicine and Biology, 2010. **55**(11): p. 3027.
108. Murthy, K., et al., *Results of Preliminary Clinical Trials of the Positron Emission Mammography System PEM-I: A Dedicated Breast Imaging System Producing Glucose Metabolic Images Using FDG*. Journal of Nuclear Medicine, 2000. **41**(11): p. 1851-1858.
109. Vranjesevic, D., et al., *Relationship Between ¹⁸F-FDG Uptake and Breast Density in Women with Normal Breast Tissue*. Journal of Nuclear Medicine, 2003. **44**(8): p. 1238-1242.

110. Rosen, E.L., et al., *Detection of Primary Breast Carcinoma with a Dedicated, Large-Field-of-View FDG PET Mammography Device: Initial Experience*. Radiology, 2005. **234**(2): p. 527-534.
111. Abreu, M.C., et al., *Design and evaluation of the Clear-PEM scanner for positron emission mammography*. Nuclear Science, IEEE Transactions on, 2006. **53**(1): p. 71-77.
112. Berg, W.A., et al., *High-Resolution Fluorodeoxyglucose Positron Emission Tomography with Compression ("Positron Emission Mammography") is Highly Accurate in Depicting Primary Breast Cancer*. The Breast Journal, 2006. **12**(4): p. 309-323.
113. Rousseau, C., et al., *Monitoring of Early Response to Neoadjuvant Chemotherapy in Stage II and III Breast Cancer by [18F]Fluorodeoxyglucose Positron Emission Tomography*. Journal of Clinical Oncology, 2006. **24**(34): p. 5366-5372.
114. Bowen, S.L., et al., *Initial Characterization of a Dedicated Breast PET/CT Scanner During Human Imaging*. Journal of Nuclear Medicine, 2009. **50**(9): p. 1401-1408.
115. Duric, N., et al., *Development of ultrasound tomography for breast imaging: Technical assessment*. Medical Physics, 2005. **32**(5): p. 1375-1386.
116. Duric, N., et al., *Detection of breast cancer with ultrasound tomography: First results with the Computed Ultrasound Risk Evaluation (CURE) prototype*. Medical Physics, 2007. **34**(2): p. 773-785.

117. Duric, N., et al. *Detection and characterization of breast masses with ultrasound tomography: clinical results*. Proc. SPIE7265, Medical Imaging 2009: Ultrasonic Imaging and Signal Processing, 72651G (March 20, 2009).
118. Duric, N., et al. *In-vivo imaging results with ultrasound tomography: report on an ongoing study at the Karmanos Cancer Institute*. Proc. SPIE7629, Medical Imaging 2010: Ultrasonic Imaging, Tomography, and Therapy, 76290M (March 12, 2010).
119. Glide, C., N. Duric, and P. Littrup, *Novel approach to evaluating breast density utilizing ultrasound tomography*. Medical Physics, 2007. **34**(2): p. 744-753.
120. Glide-Hurst, C.K., N. Duric, and P. Littrup, *Volumetric breast density evaluation from ultrasound tomography images*. Medical Physics, 2008. **35**(9): p. 3988-3997.
121. Li, C., et al., *In vivo Breast Sound-Speed Imaging with Ultrasound Tomography*. Ultrasound in Medicine & Biology, 2009. **35**(10): p. 1615-1628.
122. Li, C., N. Duric, and L. Huang. *Clinical breast imaging using sound-speed reconstructions of ultrasound tomography data*. Proc. SPIE6920, Medical Imaging 2008: Ultrasonic Imaging and Signal Processing, 692009 (March 10, 2008).
123. Li, C., N. Duric, and L. Huang. *Breast ultrasound tomography with total-variation regularization*. Proc. SPIE7265, Medical Imaging 2009: Ultrasonic Imaging and Signal Processing, 726506 (March 13, 2009).
124. Gisvold, J., D. Reese, and P. Karsell, *Computed tomographic mammography (CTM)*. American Journal of Roentgenology, 1979. **133**(6): p. 1143-1149.

125. Chang, C., et al., *Computed tomographic mammography using a conventional body scanner*. American Journal of Roentgenology, 1982. **138**(3): p. 553-558.
126. Kolb, T.M., J. Lichy, and J.H. Newhouse, *Comparison of the Performance of Screening Mammography, Physical Examination, and Breast US and Evaluation of Factors that Influence Them: An Analysis of 27,825 Patient Evaluations*. Radiology, 2002. **225**(1): p. 165-175.
127. Stavros, A.T., et al., *Solid breast nodules: use of sonography to distinguish between benign and malignant lesions*. Radiology, 1995. **196**(1): p. 123-134.
128. Entekin, R.R., et al., *Real-time spatial compound imaging: Application to breast, vascular, and musculoskeletal ultrasound*. Seminars in Ultrasound, CT and MRI, 2001. **22**(1): p. 50-64.
129. Shapiro, R.S., et al., *Compound Spatial Sonography of the Thyroid Gland*. American Journal of Roentgenology, 2001. **177**(5): p. 1195-1198.
130. Greenleaf, J.F., S.A. Johnson, and R.C. Bahn. *Quantitative Cross-Sectional Imaging of Ultrasound Parameters*. Ultrasonics Symposium, 989-995 (1977).
131. Carson, P.L., et al., *Breast imaging in coronal planes with simultaneous pulse echo and transmission ultrasound*. Science (New York, NY), 1981. **214**(4525): p. 1141.
132. André, M.P., et al., *High-speed data acquisition in a diffraction tomography system employing large-scale toroidal arrays*. International Journal of Imaging Systems and Technology, 1997. **8**(1): p. 137-147.
133. Johnson, S.A., et al., *Apparatus and method for imaging with wavefields using inverse scattering techniques*, 1999, Google Patents.

134. Marmarelis, V.Z., T.-S. Kim, and R.E.N. Shehada, *High-resolution ultrasound transmission tomography*. 2003: p. 33-40.
135. Dong-Lai, L. and R.C. Waag, *Propagation and backpropagation for ultrasonic wavefront design*. Ultrasonics, Ferroelectrics and Frequency Control, IEEE Transactions on, 1997. **44**(1): p. 1-13.
136. Masugata, H., et al., *Relationship between myocardial tissue density measured by microgravimetry and sound speed measured by acoustic microscopy*. Ultrasound in Medicine & Biology, 1999. **25**(9): p. 1459-1463.
137. Mast, T.D., *Empirical relationships between acoustic parameters in human soft tissues*. Acoustics Research Letters Online, 2000. **1**(2): p. 37-42.
138. Weiwad, W., et al., *Direct Measurement of Sound Velocity in Various Specimens of Breast Tissue*. Investigative Radiology, 2000. **35**(12): p. 721-726.
139. Devaney, A., *Inverse-scattering theory within the Rytov approximation*. Optics letters, 1981. **6**(8): p. 374-376.
140. Devaney, A., *Inversion formula for inverse scattering within the Born approximation*. Optics letters, 1982. **7**(3): p. 111-112.
141. Johnson, S.A. and M.L. Tracy, *Inverse scattering solutions by a sing basis, multiple source, moment method—Part I: Theory*. Ultrasonic Imaging, 1983. **5**(4): p. 361-375.
142. Norton, S.J., *Computing Ray trajectories between two points: A solution to the ray-linking problem*. JOSA A, 1987. **4**(10): p. 1919-1922.

143. Andersen, A.H., *Ray linking for computed tomography by rebinning of projection data*. The Journal of the Acoustical Society of America, 1987. **81**(4): p. 1190-1192.
144. Andersen, A.H., *A ray tracing approach to restoration and resolution enhancement in experimental ultrasound tomography*. Ultrasonic Imaging, 1990. **12**(4): p. 268-291.
145. Gauss, R.C., M. Soo, and G. Trahey. *Wavefront distortion measurements in the human breast*. IEEE, Ultrasonics Symposium, 1997. Proceedings, 1547-1551
146. Klimeš, L., *Grid travel-time tracing: Second-order method for the first arrivals in smooth media*. pure and applied geophysics, 1996. **148**(3-4): p. 539-563.
147. Hansen, P.C., *The L-curve and its use in the numerical treatment of inverse problems*. 1999: IMM, Department of Mathematical Modelling, Technical University of Denmark.
148. Rasband, W.S., *ImageJ*, US National Institutes of Health, Bethesda, Maryland, USA, <http://imagej.nih.gov/ij/>, 1997-2012.
149. Wikipedia: The Free Encyclopedia, *Spearman's rank correlation coefficient*. Available from: http://en.wikipedia.org/wiki/Spearman's_rank_correlation_coefficient.
150. Harris, J.A., *On the calculation of intra-class and inter-class coefficients of correlation from class moments when the number of possible combinations is large*. Biometrika, 1913. **9**(3/4): p. 446-472.
151. Wikipedia: The Free Encyclopedia, *Skewness*. Available from: <http://en.wikipedia.org/wiki/Skewness>.

152. Kontos, D., et al., *A Comparative Study of Volumetric and Area-Based Breast Density Estimation in Digital Mammography: Results from a Screening Population Digital Mammography*, J. MartÃ, et al., Editors. 2010, Springer Berlin / Heidelberg. p. 378-385.
153. Faiz, M., *Inter-rater reliability of ultrasound tomography as a means to measure breast density*, 2012, Wayne State University.
154. Brisson, J., et al., *Tamoxifen and Mammographic Breast Densities* *Cancer Epidemiology Biomarkers & Prevention* 2000 **9** (9): p. 911-915
155. Early Breast Cancer Trialists' Collaborative Group, *Tamoxifen for early breast cancer: an overview of the randomised trials*. *The Lancet*, 1998. **351**(9114): p. 1451-1467.
156. Heuson, J.C., *Current overview of EORTC clinical trials with tamoxifen*. *Cancer treatment reports*, 1976. **60**(10): p. 1463-1466.
157. Mouridsen, H., et al., *Tamoxifen in advanced breast cancer*. *Cancer Treatment Reviews*, 1978. **5**(3): p. 131-141.
158. Legha, S.S., et al., *Tamoxifen: Use in treatment of metastatic breast cancer refractory to combination chemotherapy*. *JAMA: The Journal of the American Medical Association*, 1979. **242**(1): p. 49-52.
159. Margreiter, R. and J. Wiegele, *Tamoxifen (Nolvadex) for premenopausal patients with advanced breast cancer*. *Breast Cancer Research and Treatment*, 1984. **4**(1): p. 45-48.

160. Baum, M., D. Brinkley, and J. Dossett, *Controlled trial of tamoxifen as adjuvant agent in management of Early Breast Cancer: Interim analysis at four years by the Novaldex Adjuvant Trial Organisation*. The Lancet, 1983: p. 257-261.
161. Fisher, B., et al., *Adjuvant chemotherapy with and without tamoxifen in the treatment of primary breast cancer: 5-year results from the National Surgical Adjuvant Breast and Bowel Project Trial*. Journal of Clinical Oncology, 1986. **4**(4): p. 459-71.
162. Fisher, B., et al., *A Randomized Clinical Trial Evaluating Tamoxifen in the Treatment of Patients with Node-Negative Breast Cancer Who Have Estrogen-Receptor-Positive Tumors*. New England Journal of Medicine, 1989. **320**(8): p. 479-484.
163. Fisher, B. and C. Redmond, *New perspective on cancer of the contralateral breast: a marker for assessing tamoxifen as a preventive agent*. Journal of the National Cancer Institute, 1991. **83**(18): p. 1278-1281.
164. Hackshaw, A., et al., *Long-Term Benefits of 5 Years of Tamoxifen: 10-Year Follow-Up of a Large Randomized Trial in Women at Least 50 Years of Age With Early Breast Cancer*. Journal of Clinical Oncology, 2011. **29**(13): p. 1657-1663.
165. Lorizio, W., et al., *Clinical and biomarker predictors of side effects from tamoxifen*. Breast Cancer Research and Treatment, 2012. **132**(3): p. 1107-1118.
166. Allred, D.C., et al., *Adjuvant Tamoxifen Reduces Subsequent Breast Cancer in Women With Estrogen Receptor-Positive Ductal Carcinoma in Situ: A Study Based on NSABP Protocol B-24*. Journal of Clinical Oncology, 2012. **30**(12): p. 1268-1273.

167. Osborne, C.K., *Tamoxifen in the Treatment of Breast Cancer*. New England Journal of Medicine, 1998. **339**(22): p. 1609-1618.
168. Atkinson, C., et al., *Mammographic Patterns as a Predictive Biomarker of Breast Cancer Risk: Effect of Tamoxifen* Cancer Epidemiology Biomarkers & Prevention 1999 **8** (10): p. 863-866
169. Chen, J.-H., et al., *Reduction of breast density following tamoxifen treatment evaluated by 3-D MRI: preliminary study*. Magnetic resonance imaging, 2011. **29**(1): p. 91-98.
170. Chow, C.K., et al., *Effect of Tamoxifen on Mammographic Density* Cancer Epidemiology Biomarkers & Prevention 2000 **9** (9): p. 917-921
171. Fahey, S.M.L., et al., *Clinical pharmacology and endocrinology of long-term tamoxifen therapy*. 1994: The University of Wisconsin Press, Madison, WI.
172. Buckley, M.M. and K.L. Goa, *Tamoxifen. A reappraisal of its pharmacodynamic and pharmacokinetic properties, and therapeutic use*. Drugs, 1989. **37**(4): p. 451-490.
173. Lien, E.A., E. Solheim, and P.M. Ueland, *Distribution of Tamoxifen and Its Metabolites in Rat and Human Tissues during Steady-State Treatment*. Cancer Research, 1991. **51**(18): p. 4837-4844.
174. Arteaga, C.L. and C.K. Osborne, *Growth factors as mediators of estrogen/antiestrogen action in human breast cancer cells*. Cancer treatment and research, 1991. **53**: p. 289-304.
175. Cuzick, J., et al., *Overview of the main outcomes in breast-cancer prevention trials*. The Lancet, 2003. **361**(9354): p. 296-300.

176. Cuzick, J., et al., *Tamoxifen and Breast Density in Women at Increased Risk of Breast Cancer*. Journal of the National Cancer Institute, 2004. **96**(8): p. 621-628.
177. Warner, E., et al., *The risk of breast cancer associated with mammographic parenchymal patterns: a meta-analysis of the published literature to examine the effect of method of classification*. Cancer detection and prevention, 1992. **16**(1): p. 67-72.
178. Hemminki, K., C. Granström, and K. Czene, *Attributable risks for familial breast cancer by proband status and morphology: A nationwide epidemiologic study from Sweden*. International Journal of Cancer, 2002. **100**(2): p. 214-219.
179. Atkinson, C. and S. Bingham, *Mammographic breast density as a biomarker of effects of isoflavones on the female breast*. Breast Cancer Res, 2002. **4**(1): p. 1 - 4.
180. Chen, J.-H., et al., *Decrease in Breast Density in the Contralateral Normal Breast of Patients Receiving Neoadjuvant Chemotherapy: MR Imaging Evaluation I*. 2010.
181. Eng-Wong, J., et al., *Effect of Raloxifene on Mammographic Density and Breast Magnetic Resonance Imaging in Premenopausal Women at Increased Risk for Breast Cancer*. Cancer Epidemiology Biomarkers & Prevention, 2008. **17**(7): p. 1696-1701.
182. Warren, R., *Hormones and mammographic breast density*. Maturitas, 2004. **49**(1): p. 67-78.
183. Martin, L.J., S. Minkin, and N.F. Boyd, *Hormone therapy, mammographic density, and breast cancer risk*. Maturitas, 2009. **64**(1): p. 20-26.

184. Son, H.J. and K.K. Oh, *Significance of follow-up mammography in estimating the effect of tamoxifen in breast cancer patients who have undergone surgery*. American Journal of Roentgenology, 1999. **173**(4): p. 905-9.
185. Cuzick, J., et al., *Tamoxifen-Induced Reduction in Mammographic Density and Breast Cancer Risk Reduction: A Nested Case-Control Study*. Journal of the National Cancer Institute 2011 **103** (9): p. 744-752
186. Decensi, A., et al., *Randomized Double-Blind 2 × 2 Trial of Low-Dose Tamoxifen and Fenretinide for Breast Cancer Prevention in High-Risk Premenopausal Women*. Journal of Clinical Oncology, 2009. **27**(23): p. 3749-3756.
187. Harvey, J.A., *Quantitative assessment of percent breast density: analog versus digital acquisition*. Technology in cancer research & treatment, 2004. **3**(6): p. 611-616.
188. Jeffreys, M., et al., *Breast density: agreement of measures from film and digital image*. British Journal of Radiology, 2003. **76**(908): p. 561-563.
189. Skaane, P., K. Young, and A. Skjennald, *Population-based Mammography Screening: Comparison of Screen-Film and Full-Field Digital Mammography with Soft-Copy Reading—Oslo I Study*. Radiology, 2003. **229**(3): p. 877-884.
190. Skaane, P. and A. Skjennald, *Screen-Film Mammography versus Full-Field Digital Mammography with Soft-Copy Reading: Randomized Trial in a Population-based Screening Program—The Oslo II Study*. Radiology, 2004. **232**(1): p. 197-204.

191. Hopp, T., et al. *2D/3D image fusion of x-ray mammograms with speed of sound images: evaluation and visualization*. Proc. SPIE7968, Medical Imaging 2011: Ultrasonic Imaging, Tomography, and Therapy, 79680L (March 25, 2011).
192. Duric, N., et al. *Breast Imaging with the SoftVue Imaging system: First results*. Proc. SPIE8675, Medical Imaging 2013: Ultrasonic Imaging, Tomography, and Therapy, 8675-19
193. Sak, M., et al. *Breast tissue composition and breast density measurements from ultrasound tomography*. Proc. SPIE8320, Medical Imaging 2012: Ultrasonic Imaging, Tomography, and Therapy, 83200Q (February 23, 2012).

ABSTRACT**THE ROLE OF TISSUE SOUND SPEED AS A SURROGATE MARKER OF BREAST DENSITY**

by

MARK A. SAK**May 2013****Advisor:** Dr. Neb Duric**Major:** Medical Physics**Degree:** Doctor of Philosophy

Breast density is one of the strongest predictors of breast cancer risk as women with the densest breasts have a three- to five-fold increase in risk compared to women with the least dense breasts. Breast density is currently measured by using mammography, the current gold standard for breast imaging. There are many shortcomings to using mammography to measure breast density, including the use of ionizing radiation. Ultrasound tomography (UST) does not use ionizing radiation and can create tomographic breast sound speed images. These sound speed images are useful because breast density is proportional to sound speed. The purpose of this work was to assess the ability of UST to measure breast density and its ability to measure changes in breast density over short periods of time.

A cohort of 251 patients was examined using both UST and mammography. Many different associations were found between the UST density measurement, the volume averaged sound speed, and the mammographic percent density. Additional associations were found between many other UST and mammographic imaging characteristics. UST density was found to correlate with various patient characteristics in

a similar manner to mammographic density. Additionally, UST was used to examine the effects of tamoxifen on breast density. Tamoxifen has been shown to reduce mammographic density and breast cancer risk for some women. Preliminary data for 52 patients has shown promising results so far. UST density has decreased for approximately a similar percentage of patients as has been measured for mammographic density. These changes have been measured over short time frames that could not be achieved using mammography.

These results show that UST's ability to measure breast density is consistent with mammography, the current standard of care. UST has the potential to become a safe and effective device that can be used to reliably assess breast density and serial changes in breast density.

AUTOBIOGRAPHICAL STATEMENT

Mark A Sak

EDUCATION

2002-2006 Bachelor of Applied Science, Queen's University, Kingston, Ontario

TEACHING EXPERIENCE

2007-2009 Graduate Teaching Assistant, Medical Physics Department, Wayne State University
 2009-2010 Teacher, RT 3010, Department of Radiation Therapy Technology, College of Pharmacy and Health Sciences, Wayne State University

RESEARCH EXPERIENCE

2007-2009 Research Assistant, Windsor Regional Cancer Centre
 2009-2013 Graduate Research Assistant, Wayne State University, Karmanos Cancer Institute

PUBLICATIONS

Sak, M., et al. *Breast density measurements using ultrasound tomography for patients undergoing tamoxifen treatment*. Proc. SPIE8675, Medical Imaging 2013: Ultrasonic Imaging, Tomography, and Therapy, 8675.

Sak, M., et al. *Breast tissue composition and breast density measurements from ultrasound tomography*. Proc. SPIE8320, Medical Imaging 2012: Ultrasonic Imaging, Tomography, and Therapy, 83200Q (February 23, 2012).

Sak, M., et al. *Relationship between breast sound speed and mammographic percent density*. Proc. SPIE7968, Medical Imaging 2011: Ultrasonic Imaging, Tomography, and Therapy, 79680N (March 25, 2011).

Duric, N., Boyd, N., Littrup, P., Sak, M et al., *Breast density measurements with ultrasound tomography: A comparison with film and digital mammography*. Medical Physics, 2013. **40**(1): p. 013501-12.

Hopp, T., Bonn, J., Ruiter, N. Sak, M., et al. *2D/3D image fusion of x-ray mammograms with speed of sound images: evaluation and visualization*. Proc. SPIE7968, Medical Imaging 2011: Ultrasonic Imaging, Tomography, and Therapy, 79680L (March 25, 2011).